Baltic Astronomy, vol. 15, 1–4, 2006.

THE 2ND MEETING ON HOT SUBDWARF STARS AND RELATED OBJECTS

R. H. Østensen
Isaac Newton Group, Apartado 321, E-38700 Santa Cruz de La Palma, Spain

1. INTRODUCTION

The first meeting dedicated to hot subdwarf stars was held in Keele, U.K. on 2003 June 16–20. The idea of such a meeting was conceived by Pierre Maxted, and in his report in the proceedings of that meeting the full background is given (Maxted 2004). When I went to that meeting, I had just started a new three-year contract as a PPARC research fellow at the Isaac Newton Group of Telescopes (ING) on La Palma, Canary Islands. Since it has been a tradition for the research fellows at ING to organize a conference or workshop during their contract period, the possibility of hosting a follow-up meeting to the Keele event was on my mind. When several people suggested La Palma as a good option for the next meeting, I was not slow to accept, and on the last day of the Keele meeting, the offer to hold another meeting on La Palma in 2005 was presented.

The title of the first meeting was Extreme Horizontal Branch Stars and Related Objects. After a lengthy discussion in the SOC it was decided to change that to Hot Subdwarf Stars and Related Objects instead. The terms EHB stars and sdB/sdO stars are often used interchangeably, but the EHB term implies a specific evolutionary history. Recently, evidence has accumulated that many of the stars that appear similar to EHB stars in spectroscopic studies may have completely different evolutionary histories. From the beginning, the intention of the meeting was to keep it open to all these similar stars, falling under the extension *and related objects*. The term *hot subdwarf stars*, however, has no evolutionary implications, but is a classical term used in spectral classifications of blue stars. This term encompasses the sdB, sdOB and sdO stars as well as the helium rich varieties usually referred to as He-sdB or He-sdO stars. With *hot subdwarf stars* we include all objects that appear in the HR diagram below the main sequence and above the white dwarf cooling track, regardless of how they got there. The *related objects* extension was kept in order to make sure that objects such as the extreme helium (EHe) stars were not left out. (Technically they are subluminous, but due to their low gravities they are not classified as He-sdB stars.)

2. THE MEETING

The meeting took place in Santa Cruz de La Palma between the 6th and the 10th of 2005 June. 58 participants arrived from all over the world, almost half again as many as at the first meeting. The organization of the meeting was carried out in a collaboration between the Isaac Newton Group (ING) and the

Nordic Optical Telescope (NOT), both which contributed a considerable amount toward the budget of the meeting. Support for specific social events was provided by the local government (Excmo. Cabildo Insular de La Palma) and the tourist board (Patronato de Turismo de La Palma). Additionally, the Real Club Náutico de Santa Cruz de La Palma has been extremely helpful by making their excellent locales available to us at no cost. Thanks to all this financial support we were able to keep a very reasonable registration fee, and even waive it completely for about a third of the participants who were students or without financial support at the time. On behalf of all the participants who enjoyed the hospitality of La Palma, I would like to thank all the organizations involved.

The meeting room at the Real Club Náutico provided an excellent environment for the event. The Club's restaurant also managed to provide excellent coffee breaks with delicious and varied snacks, as well as a very impressive conference dinner. Being in the center of the city allowed people to use the extended lunch break to explore the old city and find their own places to eat.

Fig. 1. At the meeting.

3. THE SESSIONS

The meeting was divided into sessions that covered a broad range of topics related to the hot subdwarf stars. They were:

- Evolutionary models and the UV-upturn phenomenon;
- Hot subdwarfs and hot HB stars in the field, clusters and galaxies;
- Atmospheric properties of hot subdwarf stars;
- Hot subdwarfs in binary systems;
- Asteroseismology of sdB stars.

Eight half-day sessions were completed during the meeting, with three sessions dedicated to asteroseismology, two sessions for atmospheric properties and the remaining topics filling one session each. The contributions in these proceedings are arranged roughly along the order of the listed sessions. All the talks were limited to 30 minutes, with 5 minutes extra for discussions. Interleaved with the talks were short oral presentations with discussions of the posters.

4. THE ISLAND

The island of La Palma is one of the smaller Canary Islands, with a surface area of 706 km^2 and a population of only 80 000. It is unusual in that it rises exceptionally steeply from the ocean floor (from a depth of 4000 m) to a volcanic crater rim at an altitude of between 2000 and 2500 meters. The Observatory is located around the highest point, the Roque de los Muchacos (2426 m).

Fig. 2. At the William Herschel Telescope.

The participants of the meeting were invited to tour the observatory area and visit the 4.2 m William Herschel Telescope (WHT, see Fig. 2), the 2.5 m Nordic Optical Telescope (NOT) and the 10 m Gran Telescopio Canarias (GTC) which is currently being assembled in its enormous dome.

Fig. 3. Exploring the volcanoes.

On Friday evening, after the end of the meeting, a farewell party was held at the swimming-pool resort of the Real Club Náutico, in the harbor of Santa Cruz de La Palma. Most of the participants also enjoyed the entertainment provided by the local observatory band *Manifold*, and some even braved the dance floor.

On Saturday after the end of the meeting, the participants who had the opportunity to stay another day were invited to a tour around the island, including a visit to some recent volcanoes (Fig. 3).

5. THE PROCEEDINGS

For the first meeting it was decided by the SOC to submit all contributions to a thorough refereeing process, and the participants were called to assist with the reviewing of the papers (Maxted 2004). For this second meeting we have even called upon experts not present at the meeting, in order to ensure that all papers have been refereed by qualified researchers. This process has gone exceptionally smoothly thanks to the prompt response of (almost) all the referees.

An issue that the SOC was not happy with from the proceedings of the first meeting was the long printing time. The SOC felt that the purpose of publishing results from work in progress was somewhat defeated if the time between the original presentation and the printed version was more than a year. For this reason we sought to find a publisher who could promise us quick printing and freely accessible on-line versions at an affordable price. Baltic Astronomy was quick to promise us the first issue of 2006 for our purposes. In addition to the regular journal issues, we could obtain special hard-back copies for the participants at a very reasonable price.

Oral presentations from the meeting have been given a page limit of eight pages (although a few participants has been allowed to exceed this), and short "poster" presentations were limited to four pages. Three contributions are published in other journals, and for this reason only an abstract version is presented at the end of the proceedings book, with reference to the journal paper.

6. OTHER REMARKS

The LOC put a lot of effort into designing useful web-pages to assist the participants with information about the meeting, registration and manuscript submission. (`http://www.ing.iac.es/conferences/subdwarf/`). All the pages are written in PHP[1] and changes dynamically according to what information is available. A registration system was made using a PHP interface to a MySQL[2] database. The on-line registration form allowed participants to enter their registration data, update information such as talk titles and abstracts, and the database allowed automatic update of the conference program. An automatic interface for submission of the proceedings which also did some basic checks on the manuscripts, was also provided. The pages will remain accessible for the foreseeable future, and anybody interested in reworking this system for other events can contact the author.

The SOC wishes to thank the members of the LOC for their work in managing the event. Special thanks goes to Javier Méndez of the Isaac Newton Group for his excellent work in managing the venue and all the social events, as well as the design of the poster and the photos for the meeting.

After the success of this second meeting, the group in Bamberg has offered to host the 3rd meeting in 2007. It is clear that a new tradition for a biennial series of meetings on hot subdwarf stars has been established.

REFERENCES

Maxted P. F. L. 2004, Ap&SS, 291, 193

[1] PHP (`www.php.net`) is a script language that generates HTML documents.
[2] MySQL (`www.mysql.com`) is an open source database system.

Baltic Astronomy, vol. 15, 5–12, 2006.

THE LOOK-BACK TIME EVOLUTION OF THE UV UPTURN PHENOMENON

C. H. Ree[1], Y.-W. Lee[1], Y.-J. Sohn[1], S. K. Yi[1,2], S.-J. Yoon[1,2]
and the GALEX Science Team

[1] *Center for Space Astrophysics and Department of Astronomy, Yonsei University, 134 Shinchon, Seoul 120-749, Korea*

[2] *Department of Physics, University of Oxford, Keble Road, Oxford OX1 3RH, U.K.*

Submitted 2005 August 1

Abstract. In order to investigate the origin of the far-UV (FUV) flux from early-type galaxies, *Galaxy Evolution Explorer* (GALEX) is collecting the UV data for the elliptical-rich clusters at moderate redshifts ($z < 0.25$) where the dominant FUV source is predicted to be hot horizontal-branch (HB) stars and their post-HB progeny. The early results show that the FUV flux of quiescent early-type galaxies *does* evolve substantially during the last 1–2 Gyr of look-back time, and the observed UV fading is consistent with the variation predicted by the population synthesis models where the mean temperature of HB stars declines rapidly with increasing look-back time.

Key words: galaxies: elliptical – galaxies: evolution – galaxies: stellar content – ultraviolet: galaxies

1. INTRODUCTION

It is now well established that the far-UV (FUV) flux ("UV upturn") of nearby early-type galaxies originates from a minority population of old hot helium-burning horizontal-branch (HB) stars (O'Connell 1999; Brown et al. 2000b). Stellar evolution models of HB predict that the mean temperature of HB distribution declines rapidly with decreasing age (e.g., Lee et al. 1994), and therefore the FUV flux from ellipticals should fade rapidly with look-back time (Greggio & Renzini 1990; Tantalo et al. 1996). Population synthesis models of Yi et al. (1999) also indicate that careful observations for the UV look-back time evolution could also discriminate two alternative HB solutions on the origin of UV flux, i.e., "metal-poor" and "metal-rich" HB models, which predict different ages for giant ellipticals.

The *Hubble Space Telescope* (HST) has obtained FUV images for several elliptical-rich clusters in the redshift range of $0.3 < z < 0.6$ (Brown et al. 2000a, 2003), but stellar evolution models (Lee et al. 1999; Yi et al. 1999) predict that hot HB stars must be absent at these relatively high redshifts, as no stars of low enough mass have yet evolved. Therefore, UV observations covering a lower redshift range ($z < 0.25$) are still required, in order to test the look-back time evolution effect of HB stars in giant ellipticals. Here we present the early results from the *Galaxy Evolution Explorer* (GALEX) UV observations for the Abell clusters in this redshift range, and also for the Fornax cluster as a local calibrator.

2. GALEX UV OBSERVATIONS

GALEX UV deep imaging survey for the UV upturn early-type galaxies aims at the elliptical-rich Abell clusters at $z < 0.25$. The first deep imaging target for this study was Abell 2670 at $z = 0.076$. Figure 1 shows the GALEX FUV and optical images of the early-type galaxies successfully identified within 25 arcmin^2 field of view centered on the brightest giant elliptical galaxy, a19 (Lee et al. 2005a). From a subsequent observation, we also successfully detected several early-type galaxies in Abell 951 at $z = 0.143$ in the GALEX UV images (see Figure 2; Ree et al. 2005). In most cases, their FUV lights are concentrated in the central region of the red galaxies without recent massive star formation, which is analogous to the smooth UV profiles of the quiescent UV upturn galaxies in the local Universe (Ohl et al. 1998; O'Connell 1999), with a few exceptions discussed below. The multi-orbit deep imaging UV observations with GALEX dedicated for more other elliptical-rich clusters at moderate redshifts are ongoing.

In order to compare the remote targets at various redshifts with the local samples without any systematic effect that may arise from the different aperture sizes used in the photometry, we should measure the total luminosities with sufficiently large, variable apertures. The total luminosities of those cross-matched early-type galaxies in remote clusters were measured by the elliptical aperture photometry (MAG_AUTO) with SExtractor image analysis package (Bertin & Arnouts 1996) in both FUV and optical passbands. The Galactic foreground extinctions were then corrected with $R_V = 3.1$, $R_{FUV} = 8.16$ (Cardelli et al. 1989). We do *not* convert the observed values into the restframe ones, as the *empirical* k-corrections may cause uncertainties in the comparison between the data samples at different redshifts. Instead, we will compare the apparent values with the model synthetic spectra redshifted to the target distances.

Nearby clusters of galaxies, e.g., Fornax, Virgo and Coma, are the best places to find the local early-type galaxies with various UV strengths, and they provide constraints to the model parameters in the local Universe. GALEX observations for the early-type galaxies in the Fornax cluster are presented in Figure 3. Their FUV magnitudes were measured from the surface photometry using ellipse fitting. The FUV surface brightness profiles extend smoothly, out to $r > 80''$ in the case of NGC 1399 and NGC 1404. In order to minimize the aperture effect induced by UV/optical radial gradient (Ohl et al. 1998), we estimated the FUV total magnitudes by integration of the radial profiles. We have also corrected for the Galactic foreground extinctions ($A_{FUV} = 0.09 - 0.14$), and their total magnitudes in V-band were adopted from the Third Reference Catalog of Bright Galaxies (RC3; de Vaucouleurs et al. 1991). Our FUV photometry for the elliptical galaxies in the Fornax cluster, when measured within the *International Ultraviolet Explorer satellite* (IUE) aperture ($20'' \times 10''$), agrees well with the IUE measurements (Burstein et al. 1988) to within 0.01–0.06 mag.

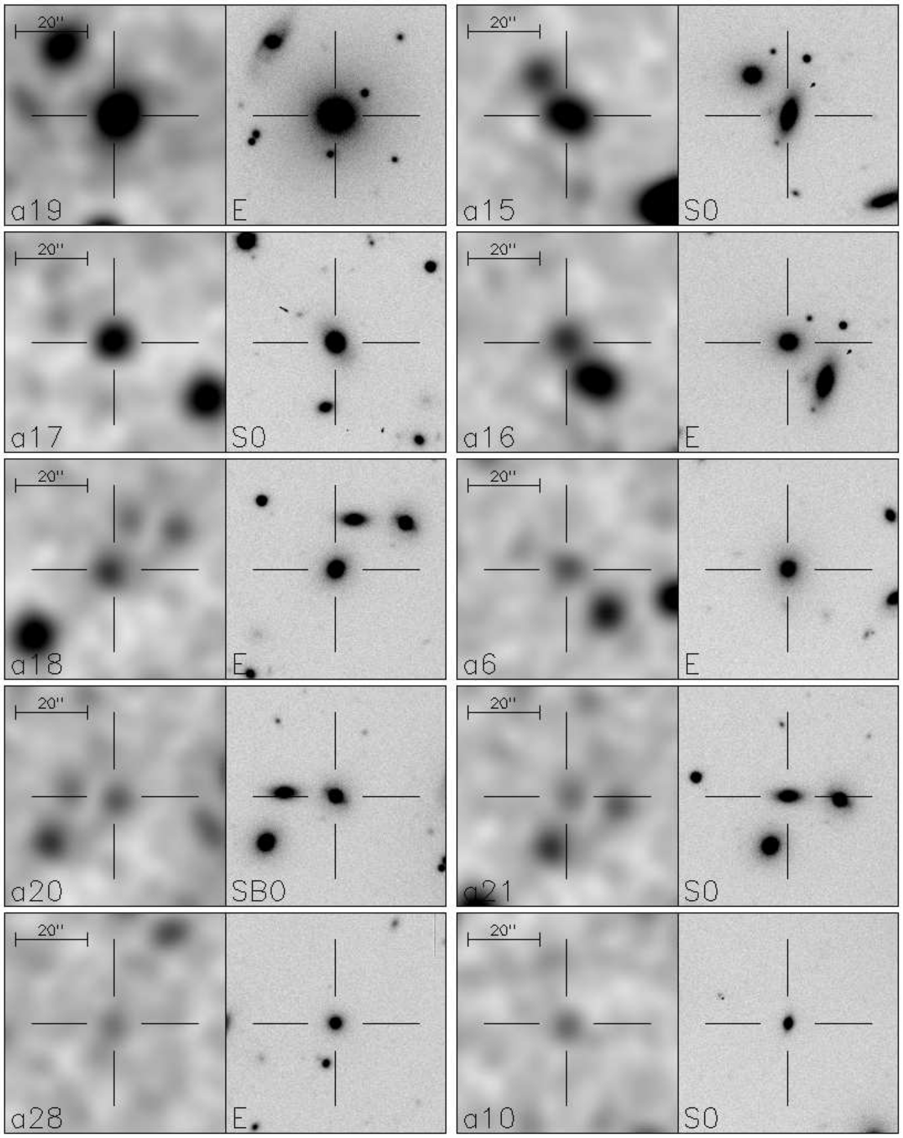

Fig. 1. GALEX FUV (*left panels*) and optical r-band (*right panels*) images ($1' \times 1'$) of the early-type galaxies in Abell 2670 ($z = 0.076$). The optical images are from Fasano et al. (2002). For some of UV-strong galaxies here, a15 and a16, there are strong evidences of young populations based on strong near-UV flux or Hα emission feature due to the residual star formation (Lee et al. 2005a).

3. MORE DISTANT CLUSTERS

Even the most massive giant elliptical galaxies ($M_V \leq -22$) should be fainter than 25th magnitude (AB) in FUV at $z > 0.3$. It would be very difficult to detect such faint *red* galaxies at high redshift with a small telescope like GALEX.

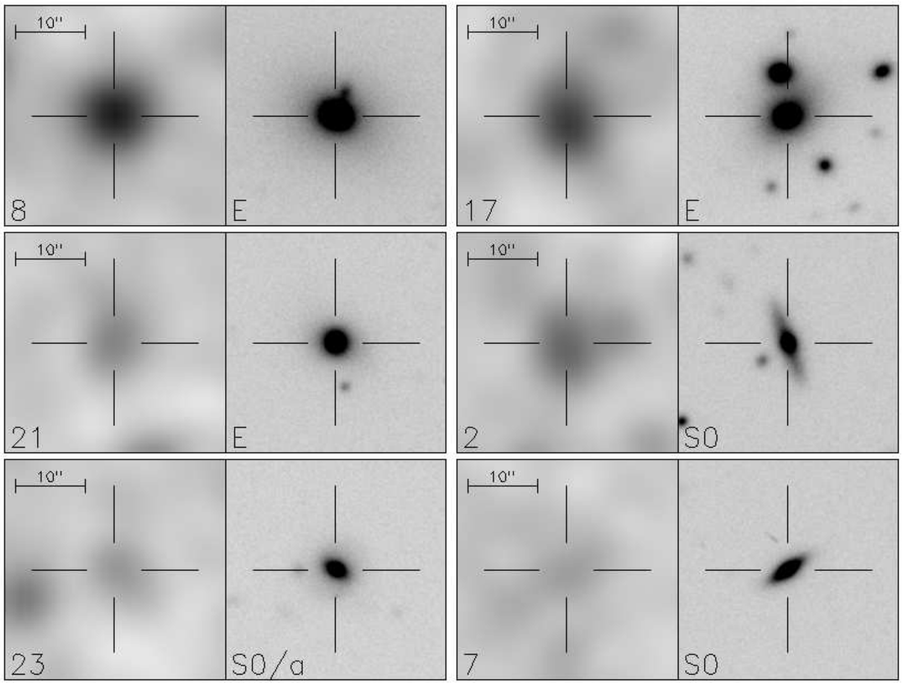

Fig. 2. GALEX FUV (*left panels*) and optical r-band (*right panels*) images ($30'' \times 30''$) of early-type galaxies in Abell 951 ($z = 0.143$). The optical images are from Fasano et al. (2000). Optical spectroscopic follow-ups are underway searching for the recent star formation signatures, if any, in these galaxies.

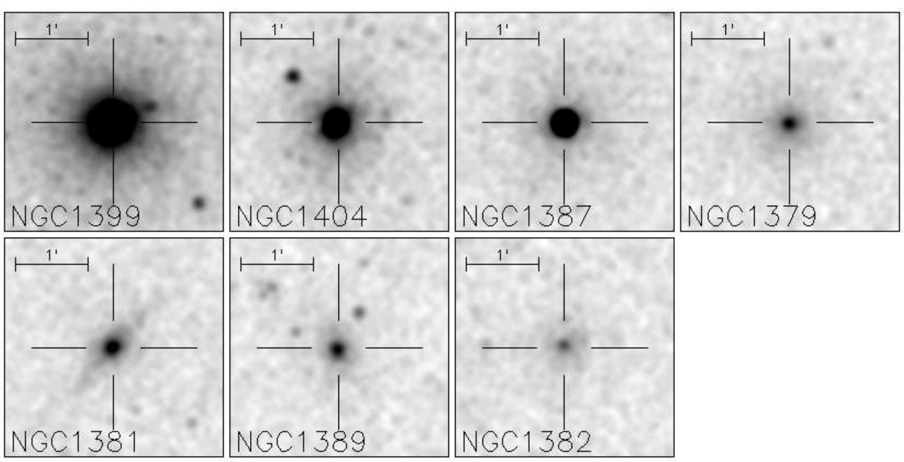

Fig. 3. GALEX FUV images ($3' \times 3'$) of the early-type galaxies in the Fornax cluster as a local calibrator. Their FUV lights are concentrated in the central region, and the radial profiles extend smoothly to $r > 1'$ for UV-strong galaxies.

However, there are several HST UV observations for the distant galaxy clusters at $0.3 < z < 0.6$ with the *Space Telescope Imaging Spectrograph* (STIS). From the literatures, we have taken the photometric measurements for the early-type galaxies in two distant clusters, Cl 1358+62 at $z = 0.33$ and Cl 0016+16 at $z = 0.55$, observed in UV by Brown et al. (2000a, 2003) and in optical passbands by van Dokkum et al. (1998) and Smail et al. (1997), respectively. The HST *Faint Object Camera* data for Abell 370 at $z = 0.375$ (Brown et al. 1998) are not included here, as they may have significant systematic errors according to Brown et al. (2003).

For the comparison with GALEX data, we converted those HST measurements to the AB magnitude system using the photometric zero-points and pivot wavelengths defined in the HST image headers ($m_{\rm AB} = m_{\rm ST} - 5\,log\,\lambda_p + 18.6921$). Model spectral energy distributions (SEDs) redshifted to $z = 0.33$ and 0.55 were then used to estimate the systematic difference between the HST and GALEX filter systems. Since the aperture radii in their analyses ($0.4''$ in FUV for both clusters, and $1.5''$ in V for CL 1358+62) are not large enough to represent total magnitudes, we applied appropriate aperture corrections, –0.32 (FUV) and –0.22 (V) for CL 1358+62. For the galaxies in CL 0016+16, we applied a correction only in FUV (–0.17 mag), as we adopted the total V magnitude from the catalog in Smail et al. (1997). The aperture correction values were obtained by utilizing the FUV (Lee et al. 2005a) and V (Marcum et al. 2001) radial profiles of NGC 1399, assuming that these clusters are at 75 (CL 1358+62) and 117 (CL 0016+16) times the distance of the Fornax cluster adopting the currently favored cosmological parameters (Ω_M, Ω_Λ, H_0) = (0.3, 0.7, 70). Finally, foreground extinction corrections are applied.

4. DISCUSSION

From the extinction-corrected apparent total magnitudes in both FUV and V passbands, we have derived the $FUV - V$ colors of the early-type galaxies in clusters, measured by GALEX (Fornax, Abell 2670 and *preliminary* analysis of Abell 951) and by HST (CL 1358+62 and CL 0016+16). The apparent redshift evolution of the observed $FUV - V$ colors is then presented in Figure 4, along with the two alternative model predictions. The "metal-poor HB model" suggests that the dominant FUV sources are very old ($t > 12$ Gyr) hot metal-poor HB stars and their post-HB progeny, and the FUV flux is expected to increase with age due to the smaller main-sequence turnoff and HB envelop masses. In the "metal-rich HB model", on the other hand, the dominant sources are old (t = 10–12 Gyr) hot super metal-rich HB and post-HB stars, and the FUV flux is predicted to increase with metallicity due to the enhanced helium enrichment and mass-loss. Even if these two alternative models are almost equally capable of reproducing the observed $FUV - V$ colors in present-epoch giant ellipticals, their evolutionary predictions are quite different from one another (see Yi et al. 1999).

The models in Figure 4 are specifically constructed to match the $FUV - V$ color of the local giant elliptical galaxy NGC 1399, the brightest galaxy in the Fornax cluster, and then passively evolved with look-back time. The model spectra and colors are then redshifted and the look-back times are converted to the equivalent redshift values, with the cosmological parameters above. Therefore, the foreground extinction-corrected observed data can be directly compared with the models. Since the NGC 1399 is a typical FUV-strong giant elliptical galaxy in the local

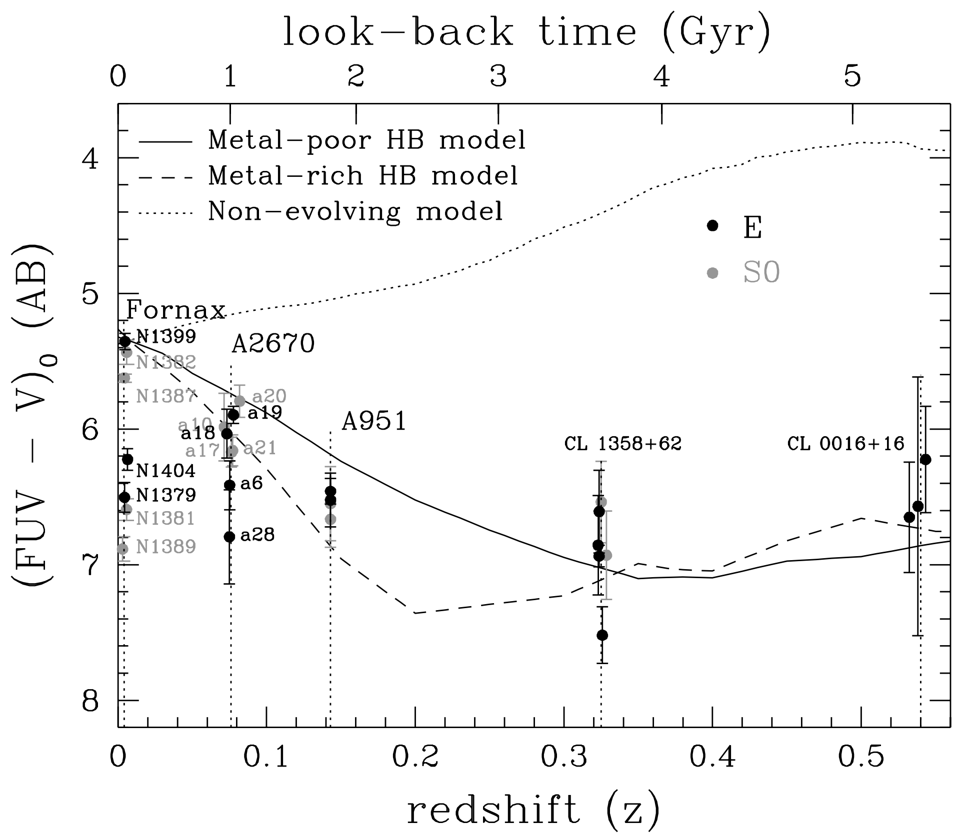

Fig. 4. Evolution of the UV upturn as a function of redshift. The observed apparent $FUV - V$ colors of the early-type galaxies in clusters at various redshifts are compared with the "metal-poor" (*solid*) and "metal-rich" (*dashed*) HB evolutionary models. The *dotted* line is for the case that the model spectrum of NGC 1399 is redshifted with no stellar evolution considered. Only the *quiescent* type of galaxy samples, without any strong star-formation signatures, are plotted (see text).

Universe, the model lines would represent the redshift (look-back time) evolution of giant ellipticals, and hence should be compared with the brightest ellipticals in each cluster. Note that there is a distinguishable amount of difference between the two alternative evolutionary models, up to ~ 1 mag. in $FUV - V$ color at $z \approx 0.2$, for the massive giant elliptical galaxies ($M_V \approx -22$).

It is clear from Figure 4 that we have detected the fading of the UV upturn expected at moderate redshifts. Compared to NGC 1399, the nearby giant elliptical galaxy in the Fornax cluster, an apparent extinction-corrected $FUV - V$ color of the giant elliptical galaxy (a19) in Abell 2670 gets redder by ~ 0.55 mag at $z = 0.076$ (look-back time ~ 1.0 Gyr). For the restframe $FUV - V$ color, this corresponds to 0.70 mag, which is consistent with the variation predicted by the models (Lee et al. 2005a). A preliminary analysis for Abell 951 ($z = 0.143$) confirms this by showing a similar amount of evolution again in the $FUV - V$ color of UV-strong giant elliptical galaxies between the look-back time of 1 and 2 Gyr. In these models, the dominant FUV source is hot HB stars for $z < 0.25$, and therefore the FUV flux fades rapidly with look-back time (redshift) as the HB temperature distribution becomes cooler with decreasing age (increasing look-back time).

For $z > 0.3$, the HST data also appear to be in reasonable agreement with our model predictions, to within the errors. Note, however, that the models become more uncertain at these relatively higher redshifts, as the dominant FUV source changes from hot HB stars to post-asymptotic giant branch (PAGB) stars for $z > 0.25$. In particular, Lee et al. (1999, see their Fig. 1) predict that the HB contribution to the total FUV flux becomes almost negligible for $z > 0.4$. At relatively higher redshifts, the total FUV flux would therefore increase as the mass of PAGB stars decreases because their lifetimes correlate inversely with their mass. Consequently, the available HST data may provide no direct test of HB evolution effect. Nevertheless, they provide a useful test on the adopted mass (0.565 $M_\odot$) of PAGB stars in our models.

Although we are witnessing the growing body of evidence indicating the FUV flux of quiescent early-type galaxies evolves substantially at moderate redshifts ($z < 0.25$) as the deep imaging survey with GALEX UV telescope continues, there are some issues to be solved. On the observational side of this study, UV blending and contamination by young stars are serious issues. With the given spatial resolution of GALEX (1.5 ″/pixel), it becomes difficult to de-blend properly the UV lights purely from the old stellar population in elliptical galaxies and the possible UV contaminations by neighboring dwarf galaxies, as we reach out to $z \sim 0.2$. Furthermore, some early-type galaxies show contamination from the residual star formation in their UV spectra (Burstein et al. 1988; Yi et al. 2005), and therefore it is important to check whether our sample galaxies are not affected by a minority population of young stars. As described in Lee et al. (2005a), we found two of the UV-strong early-type galaxies in Abell 2670, a15 (S0) and a16 (E), show the evidence of young populations inferred by unusually strong near-UV flux or by strong Hα emission. Some of HST data samples also show unexpectedly strong UV flux. All of these abnormal galaxies with recent star-forming signatures are excluded in Figure 4. The optical follow-up spectroscopy continues for the other GALEX target clusters in order to discriminate such star-forming red galaxies.

On the theoretical side, the nature of extreme HB (EHB) stars and their contribution to the UV flux should be understood. The effect of EHB stars are *not* fully included in the current population synthesis models presented here. Particularly, the excessively large age (up to 30 % older than the Galactic globular clusters) required for the local giant ellipticals in the "metal-poor" HB model would be reduced significantly, if the EHB stars are explained as the minority population of super helium-rich stars (Lee et al. 2005b). In any case, the observed rapid evolution of FUV flux with look-back time at moderate redshifts, if confirmed by further observations, would infer the strong age dependency in the evolution of UV sources in old stellar systems (Lee et al. 1994; Yi et al. 1999).

ACKNOWLEDGMENTS. GALEX is a NASA Small Explorer, launched in April of 2003. We gratefully acknowledge NASA's support for construction, operation and science analysis for the GALEX mission, developed in cooperation with the Centre National d'Etudes Spatiales of France and th e Korean Ministry of Science and Technology. Yonsei University participation is funded by the Korean Ministry of Science & Technology, for which we are grateful.

REFERENCES

Bertin E., Arnouts S. 1996, A&A, 117, 393

Brown T. M., Ferguson H. C., Deharveng J.-M., Jedrzejewski R. I. 1998, ApJ, 508, L139

Brown T. M., Bowers C. W., Kimble R. A., Ferguson H. C. 2000a, ApJ, 529, L89

Brown T. M., Bowers C. W., Kimble R. A., Sweigart A. V., Ferguson H. C. 2000b, ApJ, 532, 308

Brown T. M., Ferguson H. C., Smith E., Bowers C. W., Kimble R. A., Renzini A., Rich R. M. 2003, ApJ, 584, L69

Burstein D., Bertola F., Buson L. M., Faber S. M., Lauer T. R. 1988, ApJ, 328, 440

Cardelli J. A., Calyton G. C., Mathis J. S. 1989, ApJ, 345, 245

de Vaucouleurs G., de Vaucouleurs A., Corwin H. G., Buta R. J., Paturel G., Fouque P. 1991, *Third Reference Catalog of Bright Galaxies*, Springer (RC3)

Fasano G., Bettoni D., D'Onofrio M., Kjærgaard P., Moles M. 2002, A&A, 387, 26

Fasano G., Poggianti B. M., Couch W. J., Betoni D., Kjærgaard P., Moles M. 2000, ApJ, 542, 673

Greggio L., Renzini A. 1990, ApJ, 364, 35

Lee Y.-W., Demarque P., Zinn R. 1994, ApJ, 423, 248

Lee Y.-W. et al. 2005a, ApJ, 619, L103

Lee Y.-W. et al. 2005b, ApJ, 621, L57

Lee Y.-W., Woo J.-H., Yi S., Park J.-H. 1999, in *Spectrophotometric Dating of Stars and Galaxies*, eds. I. Hubeny, S. Heap & R. Cornett, ASP Conf. Ser., 192, 307

O'Connell R. W. 1999, ARA&A, 37, 603

Ohl R. G. et al. 1998, ApJ, 505, L11

Ree C. H. et al. 2005, in preparation

Smail I., Dressler A., Couch W. J., Ellis R. S., Oemler A. 1997, ApJS, 110, 213

Tantalo R., Chiosi C., Bressan A., Fagotto F. 1996, A&A, 311, 361

van Dokkum P. G., Franx M., Kelson D. D., Illingworth G. D., Fisher D., Fabricant D. 1998, ApJ, 500, 714

Yi S., Lee Y.-W., Woo J.-H., Park J.-H., Demarque P., Oemler A. 1999, ApJ, 513, 128

Yi S. et al. 2005, ApJ, 619, L111

Baltic Astronomy, vol. 15, 13–16, 2006.

BINARY POPULATION SYNTHESIS, SDB STARS AND THE UV UPTURN

D. Brown[1], S. Yi[2], Z. Han[3] and S.-J. Yoon[2]

[1] *Department of Physics and Astrophysics, University of Oxford, Oxford, OX1 3RH, U.K.*

[2] *Department of Astronomy, Yonsei University, Sinchon 134, Seoul 120-749, Korea*

[3] *Yunnan Observatory, National Astronomical Observatories, Chinese Academy of Sciences, P.O. Box 110, Kunming, 650011, China*

Received 2005 September 19

Abstract. We aim to use the methods of binary population synthesis (BPS) to study the ultraviolet upturn (UVX) in the spectra of giant elliptical galaxies with emphasis being placed on those binary channels which could lead to the formation of stars that can account for it. This project will combine Sukyoung Yi's single star population synthesis methodology with that of Zhanwen Han's binary population synthesis methods in order to provide a more coherent study of the origin of the UV upturn, the focus being on sdB stars as the possible source of the UV upturn. The primary approach of the project will be to explore the UV upturn, with sdBs included, for several different metallicities in order to examine the UVX in composite populations.

Key words: stars: hot subdwarfs – stars: binaries: general – galaxies: elliptical – galaxies: stellar content

1. THE UV UPTURN (UVX)

At present, a moderate consensus suggests that low-mass core helium burning stars, which are in the HB phase of their evolution, serve as the strongest candidates for sources of the UVX in stellar populations. The UVX is characterized by a high increase in rest-frame UV flux (in the range of $\lambda \sim 1000$–2500 Å) in the spectra of elliptical (E) galaxies, S0 galaxies and in the bulges of spiral galaxies.

2. UVX HYPOTHESES

Most population synthesis studies of the UVX, including those of Yi (1997, 1998), assume that it arises from the evolution of single HB stars. However, others, such as Han and Podsiadlowski (HP), having conducted an extensive binary population synthesis study of the origin of sdB stars (Han et al. 2002, 2003) formed via binary channels, note that sdB stars could help account for a significant portion of UV radiation in galaxies; in fact, HP have also conducted an extensive study of the UVX at solar metallicity. In the single star scenario, two hypotheses make contradictory claims as to how the UVX originates from low-mass HB stars. The metal-rich hypothesis (Yi et al. 1997, 1998) claims that the UVX originates in metal-rich stars characterized by a high He abundance, and, hence, high mass-loss. In contrast, the metal-poor hypothesis (Park & Lee 1997) claims that the UVX is the natural consequence of the oldest, metal-poor stars in a GE having evolved into the HB phase of their lives. In the binary scenario, the UVX originates from EHB stars in the form of sdBs which result from several different types of binary evolution channels: (1) common envelope (CE) ejection; (2) RLOF in one binary component and (3) merger of two WDs.

3. INPUT MODELS

EPS models for single star evolution are here combined with the products of binary population synthesis models to produce a combined population synthesis. The EPS models and methods employed are those of Sukyoung Yi and Seok-Jin Yoon. In these, data from the Y^2 isochrones and realistic synthetic HB constructions have been reduced and processed into synthetic CMD and SED models by Seok-Jin Yoon. The sdB models are products of Han (1995) binary population synthesis code, which uses an input grid generated by an updated version of Eggleton's original stellar evolution code (Eggleton 1971, 1972, 1973). The spectral library employed is that assembled by Lejeune et al. (1997). Tables 1 and 2 list the model input parameters.

Table 1. General input parameters.

Stellar population:	10^7 single stars; 10^7 binaries
IMF:	Miller-Scalo
Age range:	1 − 20 Gyr
Metallicity:	$Z = 0.02$ (single abundance population)
Stellar mass range:	$0.1\,M_{\odot} < m < 100\,M_{\odot}$
Binary input parameters:	
Binary fraction:	67%
Flat distribution in q:	$n(q) = 1$
Critical mass ratio:	$q_{\rm crit} = 1.5$
Reimers mass-loss coefficient:	$\eta = 0.25$
Common ejection frequency:	$\alpha_{\rm CE} = 0.75$
Thermal energy conversion efficiency:	$\alpha_{\rm TH} = 0.75$

Table 2. Model input parameters.

Parameter	Yi	Han
Convective core overshoot:	$0.20H_p$	$0.25H_p$
Mixing length parameter (l/H_p)	1.7431	2.0
Helium abundance (Y):	0.27	0.28
He enrichment parameter ($\Delta Y/\Delta Z$):	2.0	2.0

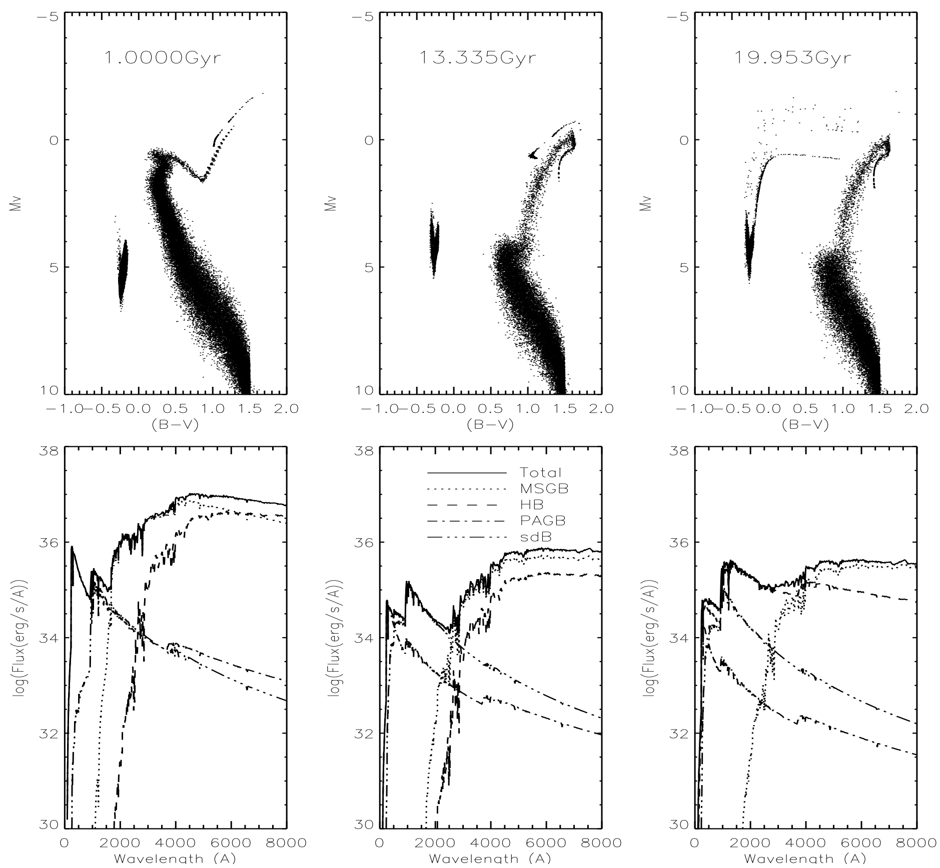

Fig. 1. Time evolution of the SSP as shown in the given CMDs and SEDs.

4. PRELIMINARY RESULTS

As a prelude to studying the UVX in composite systems (GEs), the first step of this inquiry has been to examine the UVX in a simple stellar population (SSP) for a single abundance of $Z = 0.02$. Both single and binary stars have been included in the population synthesis study. Figure 1 shows the CMD and SED time evolution of the population, respectively, for the given ages. With sdBs included, the total FUV flux decreases with increasing age until the trend is reversed by a contribution from single HB stars for late ages. The corresponding color evolution of *1500–V* with redshift z is given in Figure 2 (the solid line) along with two other models for composite systems obtained by Yi et Yoon (Lee et al. 2005). As seen, there is an increase of *1500–V* for the redshift range $0.0 < z < 0.2$ in contrast to that suggested by the other two models and empirical data points of NGC 1399 and Abell 2670. Incidentally, the cosmological parameters are $\Omega = 0.15$, $\Lambda = 0.85$, $z_F = 4.9$ and $H_o = 64.0$.

5. SUMMARY AND FUTURE PROSPECTS

Since the parameter space over which this study has been conducted is very limited ($Z = 0.02$ and $\eta = 0.25$), the results presented here are inconclusive in regard to the UVX hypotheses discussed earlier. Interestingly though, the given SSP does exhibit a UVX due to the presence of sdBs at early ages and later. However, the downward trend in *1500–V* for lower redshifts is not reversed, which differs from an increase in *1500–V* near low redshifts in GEs. The difference in results can stem from the fact that the SSP is a single abundance population whereas giant elliptical galaxies are composite metal-rich systems. Much is still to be learned from a study of Population II and super-solar stellar populations. Both abundance domains are the primary aims of this project in the future through an adaptation of Han's BPS code for different metallicities, mass-loss prescriptions and binary input parameters to see how the UV contribution from sdBs is affected.

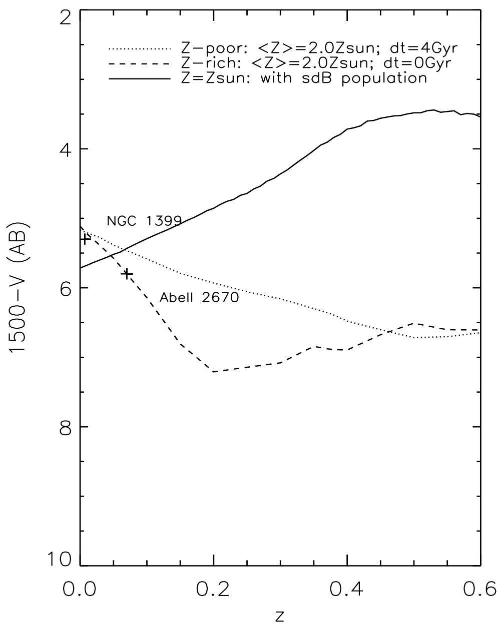

Fig. 2. Evolution of *1500–V* with z. Data points for NGC 1399 and Abell 2670 are from the GALEX survey (Lee et al. 2005).

REFERENCES

Eggleton P. P. 1971, MNRAS, 151, 351

Eggleton P. P. 1972, MNRAS, 156, 361

Eggleton P. P. 1973, MNRAS, 163, 179

Han Z. 1995, PhD thesis, Cambridge University

Han Z., Podsiadlowski P., Maxted P. F. L., Marsh T. R., Ivanova N. 2002, MNRAS, 336, 449

Han Z., Podsiadlowski P., Maxted P. F. L., Marsh T. R., Ivanova N. 2003, MNRAS, 341, 669

Lee Y. W., Ree C. H. et al. 2005, ApJ, 619, L103

Lejeune T., Cuisinier F., Buser R. 1997, A&AS, 125, 229

Park J. H., Lee Y. W. L. 1997, ApJ, 476, 28

Yi S., Demarque P., Oemler A. 1997, ApJ, 486, 201

Yi S., Demarque P., Oemler A. 1998, ApJ, 492, 480

Yi S., Lee Y. W., Woo J. H., Park J. H., Demarque P., Oemler A. 1999, ApJ, 513, 128

Baltic Astronomy, vol. 15, 17–24, 2006.

UV UPTURN OF ELLIPTICAL GALAXIES

Z. Han[1], Ph. Podsiadlowski[2] and A. Lynas-Gray[2]

[1] *National Astronomical Observatories, Yunnan Observatory, Chinese Academy of Sciences, PO Box 110, Kunming 650011, China*

[2] *University of Oxford, Department of Astrophysics, Keble Road, Oxford OX1 3RH, U.K.*

Received 2005 August 1

Abstract. We investigate the UV upturn phenomenon of elliptical galaxies by applying the binary model of hot subdwarfs of Han et al. (2002, 2003). Preliminary results show that the model provides a natural explanation for the UV upturn phenomenon and that the model could be used to detect low level recent star formation.

Key words: galaxies: elliptical – ultraviolet: galaxies – stars: binaries: close – stars: subdwarfs

1. INTRODUCTION

For old stellar populations, such as giant elliptical galaxies, far-UV radiation was expected to be almost completely dark. However, this is not the case. As surprisingly discovered by *Orbiting Astronomical Observatory 2* (OAO-2) mission in 1969, there exists a flux increase in spectral energy distributions of early-type galaxies from 2000 to 1200 Å, known as UV upturn (also referred as UV excess, UV rising-branch, UV rising flux, UVX) (see the review by O'Connell 1999). The origin of the UV upturn remained a mystery for many years ever since (see, e.g., Kjærgaard 1987). Ferguson et al. (1991), Dorman et al. (1995) and Brown et al. (1995, 1997) identified that UV upturn is mainly from extreme horizontal branch (EHB) stars. Brown et al. (2000) resolved hot HB stars for the first time in an elliptical galaxy (the core of M 32).

EHB stars are core-helium burning stars with very thin hydrogen envelopes ($M_{\rm env} \leq 0.02 M_\odot$). They are the major source of far UV radiation in the evolutionary population synthesis study of giant elliptical galaxies. There are two schools of thought about the UV upturn, metal-poor school (Lee 1994; Park & Lee 1997) and metal-rich school (Bressan et al. 1994, 1996; Tantalo et al. 1996; Yi et al. 1995, 1997a, 1997b, 1998). Both schools adopt the formation channel of EHB stars from single stellar evolution, in which stellar wind mass-loss near the tip of the first giant branch (FGB) may strip off a giant's envelope and leave an almost bare helium core (e.g., D'Cruz et al. 1996).

The metal-poor school ascribes the UV-upturn to an old metal-poor population (the metal-poor tail of the wide metallicity distribution). An uncomfortably large age (~ 20 Gyr) is required to explain observations. In the metal-rich school, the UV-upturn results from the metal-rich population of giant elliptical galaxies. In order to fit observations, some assumptions need to be made, i.e., helium enrichment parameter $\Delta Y/\Delta Z > 2.5$, a fine-tuning of Reimer's mass-loss coefficient and its dependence on metallicity, a metallicity of 1–3 $Z_\odot$ and an age usually larger than 10 Gyr. Some of the assumptions are not justified.

In both schools, the formation of EHB stars is due to stellar wind mass-loss near the tip of the FGB, and therefore there is a sudden onset of the formation of EHB stars when a stellar population evolves. In other words, the UV upturn of elliptical galaxies declines rapidly with redshift. However, this is not the case, as shown by HST observations of Brown et al. (1998, 2000, 2003).

However, more than half of hot subdwarfs are found in binaries observationally (e.g., Maxted et al. 2001). Han et al. (2002, 2003) therefore proposed a binary model for the formation of EHB stars (or hot subdwarfs). In the model, there are three channels for the formation of hot subdwarfs, i.e., common envelope ejection for hot subdwarf binaries with short orbital periods, stable Roche lobe overflow for hot subdwarfs with long orbital periods, and merger of helium white dwarfs to form single hot subdwarfs. The model can explain the main observational characteristics of hot subdwarfs, in particular their distributions in the orbital period vs. minimum companion mass diagram and in the effective temperature vs. surface gravity diagram, their distributions of orbital period and mass function, their binary fraction and the fraction of hot subdwarf binaries with white dwarf (WD) companions, their birth rates and their space density.

In this paper we apply the binary model of Han et al. (2002, 2003) to the study of UV upturn and give the preliminary results. A more systematic and comprehensive study will be published elsewhere.

2. THE APPROACH

Han et al. (1994, 1995a, 1995b, 1998, 2003) developed a binary population synthesis (BPS) code, with which millions of stars (including binaries) can be evolved simultaneously from the zero-age main sequence (ZAMS) to white dwarfs or supernova explosion. The code can simulate in a Monte Carlo way the formation of many interesting stellar objects, such as type Ia supernovae, cataclysmic variables, double degenerates, barium stars, etc.

We incorporate the binary hot subdwarf model of Han et al. (2002, 2003) into the BPS code so that we can carry out Monte Carlo simulations and obtain the hot subdwarf population and its evolution. In the simulations, we adopt a metallicity of $Z = 0.02$, the critical mass ratio $q_{\rm crit} = 1.5$ for stable Roche lobe overflow on first giant branch (FGB) or asymptotic giant branch (AGB), common envelope ejection efficiency $\alpha_{\rm CE} = 0.75$ and thermal contribution to the ejection $\alpha_{\rm th} = 0.75$ (see section 7.4 of Han et al. 2003 for details). In addition, the simulations also require as input the star formation rate (SFR), the initial mass function (IMF) of the primary, the initial mass-ratio distribution and the distribution of initial orbital separations as follows.

(1) The SFR is taken to be a single burst.

(2) A simple approximation to the IMF of Miller & Scalo (1979) is used; the primary mass is generated with the formula of Eggleton, Fitchett & Tout (1989)

$$M_1 = \frac{0.19X}{(1-X)^{0.75} + 0.032(1-X)^{0.25}}, \tag{1}$$

where X is a random number uniformly distributed between 0 and 1. The adopted ranges of primary masses are 0.8 to $100.0\,M_\odot$. The studies by Kroupa, Tout & Gilmore (1993) and Zoccali et al. (2000) support this IMF.

(3) We take a constant mass-ratio distribution in the current study,

$$n(1/q) = 1, \qquad 0 \le 1/q \le 1, \tag{2}$$

where $q = M_1/M_2$.

(4) We assume that all stars are members of binary systems and that the distribution of separations is constant in $\log a$ (a is the separation) for wide binaries and falls off smoothly at close separations:

$$an(a) = \begin{cases} \alpha_{\rm sep}(\frac{a}{a_0})^m, & a \le a_0; \\ \alpha_{\rm sep}, & a_0 < a < a_1, \end{cases} \tag{3}$$

where $\alpha_{\rm sep} \approx 0.070$, $a_0 = 10\,R_\odot$, $a_1 = 5.75 \times 10^6\,R_\odot = 0.13\,{\rm pc}$ and $m \approx 1.2$. This distribution implies that there is an equal number of wide binary systems per logarithmic interval and that approximately 50 per cent of stellar systems are binary systems with orbital periods less than 100 yr.

In order to convolve the simulation result into colors or spectral energy distribution (SED), we adopt the latest version of BaSeL library (see Lejeune et al 1997, 1998 for a description), which gives the colors and SEDs of stars with a wide range of metallicity Z, surface gravity $\log g$ and effective temperature $T_{\rm eff}$. The library does not cover the surface gravity range for hot subdwarfs, and we therefore calculated emergent fluxes for solar metallicity hot subdwarfs using plane-parallel static model stellar atmospheres computed with ATLAS9 (Kurucz 1992) and adopting the assumption of local thermodynamic equilibrium, and the range for $\log g$ is 5.0 to 7.0 with a spacing of $\Delta \log g = 0.2$, the range for $T_{\rm eff}$ is 10 000 K to 40 000 K with $\Delta T = 1000$ K.

3. RESULTS AND DISCUSSION

In our investigation, we evolve a simple stellar population (SSP), in which all the stars have the same metallicity and the same age, or a mixed stellar population (MSP) which consists of two SSPs, a major one and a minor one. The major population has solar metallicity and an age of 10 Gyr, while the minor one has a solar metallicity and an age t. The minor population fraction f is the ratio of minor population mass to the total mass of the MSP, and $f = 100\,\%$ means the MSP is actually a SSP with an age t.

Figure 1 is a comparison between the UV spectrum from our model and that of M 49 from the Hopkins Ultraviolet Telescope (HUT) (from Brown et al. 1997). The model is a solar metallicity MSP with a total stellar mass of $4.7 \times 10^{10} M_\odot$ and a major population age of 10 Gyr. The minor population fraction is $f = 0.28\,\%$, and the minor population has an age of 0.5 Gyr. Actually we fixed the age of the major population according to local galaxy ages derived by Terlevich & Forbes (2002) and the minor population fraction, and obtained the best fit when the minor population age is 0.5 Gyr (the details of the fitting process will be described in another publication). The fraction of $f = 0.28\,\%$ is below the detecting limit for recent star formation. We see that the fit is satisfactory.

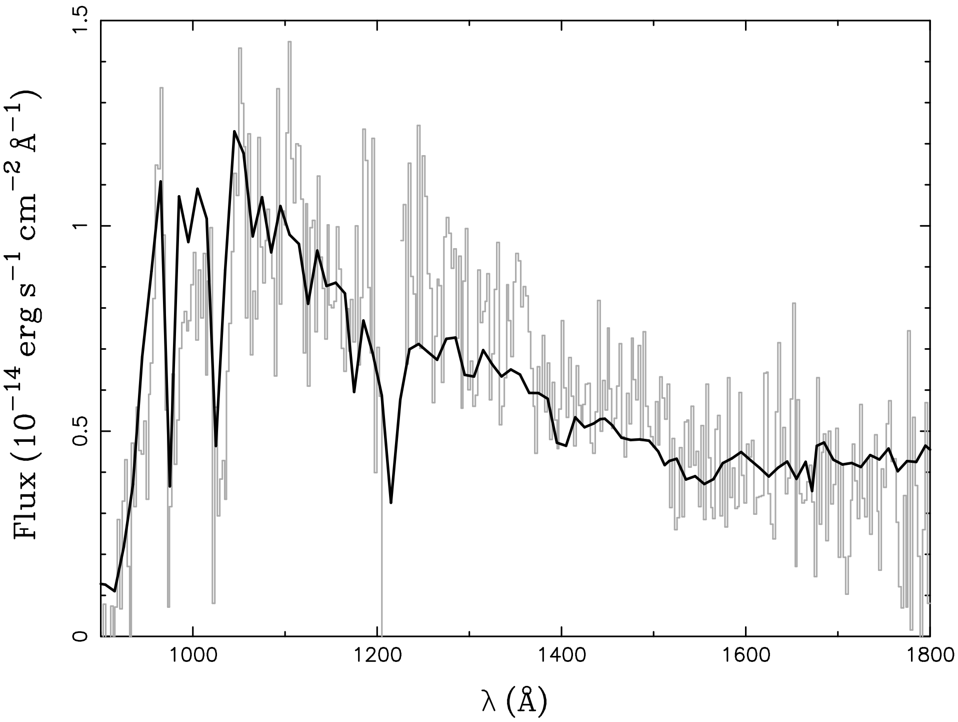

Fig. 1. A fit to the UV spectrum of elliptical galaxy M 49 obtained using the Hopkins Ultraviolet Telescope (HUT) (taken from Brown et al. 1997). The HUT data are shown by the grey histogram, while the thick solid line is from our model.

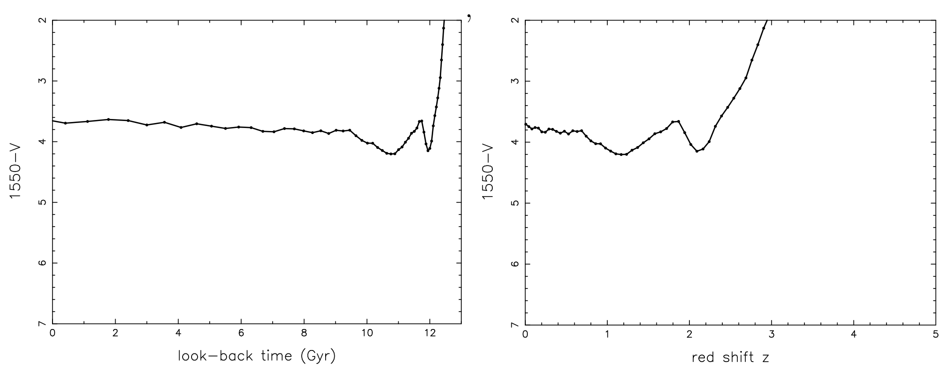

Fig. 2. The UV-upturn vs. look-back time (the left panel) and the UV-upturn vs. redshift (the right panel) from our model.

The magnitude of UV-upturn is defined by Burstein et al. (1988) as *1550–V* = –2.5 $\log(f_{1550}/f_V)$, where f_{1550} is the energy flux at 1550 Å and f_V – the flux in the V passband. Figure 2 is the UV-upturn versus the look-back time or the redshift for a SSP. The look-back time is defined as $t_{\rm L} = 13\,{\rm Gyr} - t_{\rm SSP}$, where $t_{\rm SSP}$

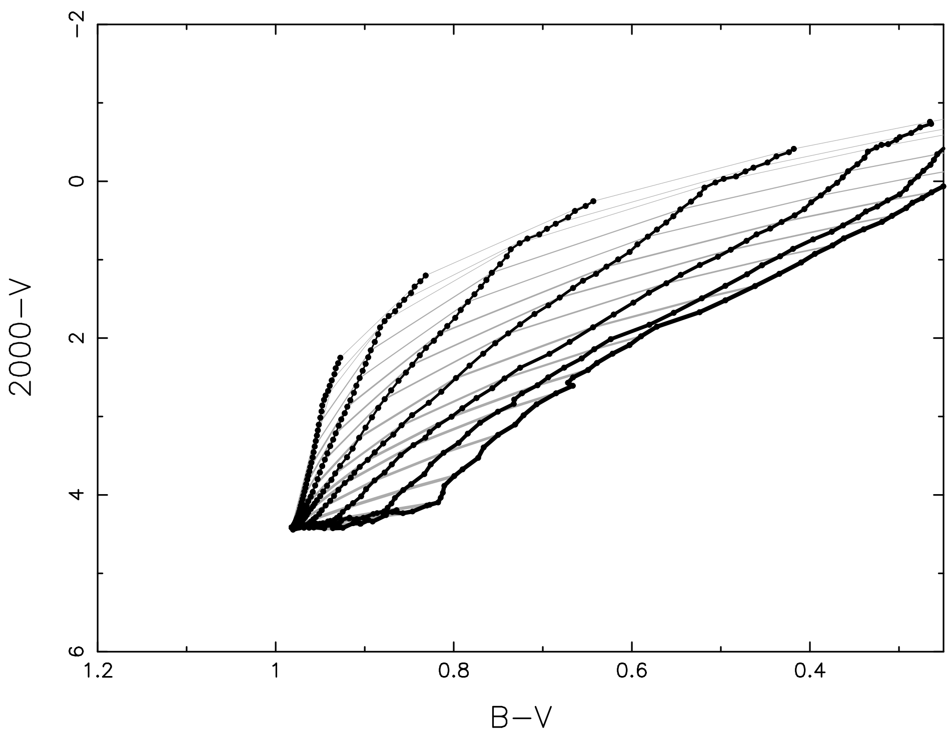

Fig. 3. *2000–V* vs. *B–V* for a mixed stellar population composed of a major and a minor population. The major population is with solar metallicity and with an age of 10 Gyr. The grey lines from top to bottom are for minor population age of $\log(t/\mathrm{Gyr}) = -1.0, -0.9, -0.8, -0.7 \ldots$, the dark solid lines from left to right are for minor population fractions of 0.1 %, 0.32 %, 1 %, 3.2 %, 10 %, 32 % and 100 %, while 100 % means that the mixed population is actually a single population (i.e., minor population only).

is the age of the SSP. We also convert the look-back time to redshift by adopting a flat universe and a Hubble time of 13.7 Gyr. As we see from Brown et al. (2003), UV-upturn does not depend much on redshift, and Figure 2 is consistent with the observations. Lee et al. (2005) tried to explain UV upturn-redshift relation by assuming that the post AGB (PAGB) mass decreases with redshift. However, the mass should increase with redshift from standard stellar evolution theory.

Figure 3 is the diagram of *2000* − *V* vs. $B - V$ for a solar metallicity MSP with a major population of 10 Gyr and a minor population of varying age and fraction. The figure can be used to explain the observation of far-ultraviolet emission of early-type galaxies (see Fig. 2 of Deharveng et al. 2002).

Figure 4 is the diagram of *FUV* − *NUV* vs. *FUV* − *r*, where *FUV* and *NUV* are magnitudes in the FUV and NUV passbands of the *Galaxy Evolution Explorer* (GALEX) and r is the magnitude in the r passband of the Sloan Digital Sky Survey (SDSS). If we compare our result to the systematics of the UV-upturn in a GALEX/SDSS sample of early-type galaxies (Fig. 3 of Rich et al. 2005), we find that the red-quiescent early-type galaxies in their sample have low level recent star formation.

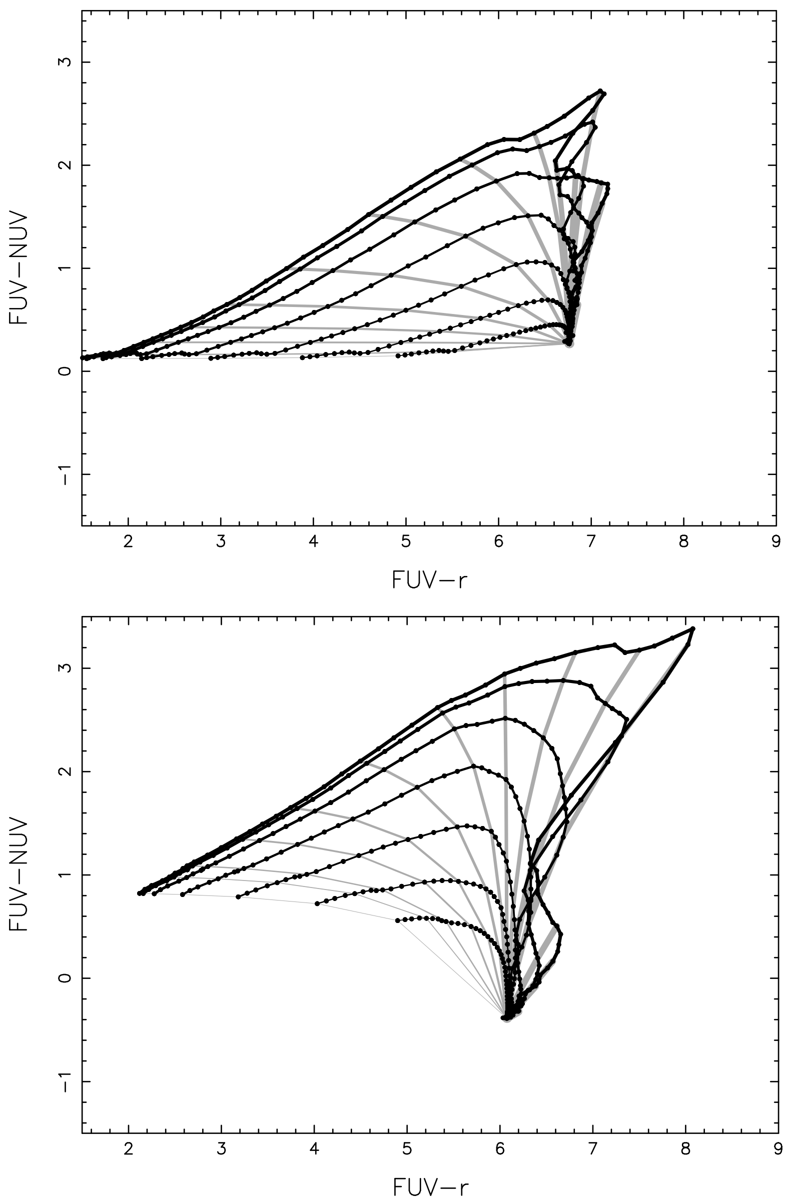

Fig. 4. $FUV-NUV$ vs. $FUV-r$ for a mixed stellar population composed of a major and a minor population. The major population is with solar metallicity and with an age of 10 Gyr. The grey lines from bottom-left to top-right are for minor population age of $\log(t/\mathrm{Gyr}) = -1.0$, -0.9, -0.8, -0.7 ..., the dark solid lines from bottom to top are for minor population fractions of 0.1 %, 0.32 %, 1 %, 3.2 %, 10 %, 32 % and 100 %, while 100 % means that the mixed population is actually a single population (i.e., minor population only). The top panel is for population at redshift $z = 0$, while the bottom panel is for $z = 0.2$.

4. CONCLUSIONS

We conclude that the binary model of hot subdwarfs of Han et al. (2002, 2003) is needed to understand the UV-upturn phenomenon of elliptical galaxies. Our model could be a useful tool in finding low level recent star formation.

REFERENCES

Bressan A., Chiosi C., Fagotto F. 1994, ApJS, 94, 63

Brown T. M., Bowers C. W., Kimble R. A., Ferguson H. C. 2000, ApJ, 529, L89

Brown T. M., Bowers C. W., Kimble R. A., Sweigart A. V. 2000, ApJ, 532, 308

Brown T. M., Ferguson H. C., Davidsen A. F. 1995, ApJ, 454, L15

Brown T. M., Ferguson H. C., Davidsen A. F., Dorman B. 1997, ApJ, 482, 685

Brown T. M., Ferguson H. C., Deharveng J. M., Jedrzejewski R. I. 1998, ApJ, 508, L139

Brown T. M. et al. 2003, ApJ, 584, L69

Burstein D., Bertola F., Buson L. M., Faber S. M., Lauer T. R. 1988, ApJ, 328, 440

D'Cruz N. L., Dorman B., Rood R. T., O'Connell R. W. 1996, ApJ, 466, 359

Deharveng J.-M., Boselli A., Donas J. 2002, A&A, 393, 843

Dorman B., O'Connell R. W., Rood R. T. 1995, ApJ, 442, 105

Eggleton P. P., Tout C. A., 1989, in *Algols*, ed. A. H. Batten, Kluwer Academic Publishers, Dordrecht, p. 164

Ferguson H. C. et al. 1991, ApJ, 382, L69

Han Z. 1998, MNRAS, 296, 1019

Han Z., Podsiadlowski Ph., Eggleton P. P. 1994, MNRAS, 270, 121

Han Z., Podsiadlowski Ph., Eggleton P. P. 1995a, MNRAS, 272, 800

Han Z., Eggleton P. P., Podsiadlowski Ph., Tout C. A. 1995b, MNRAS, 277, 1443

Han Z., Podsiadlowski Ph., Maxted P. F. L., Marsh T. R., Ivanova N. 2002, MNRAS, 336, 449

Han Z., Podsiadlowski Ph., Maxted P. F. L., Marsh T. R. 2003, MNRAS, 341, 669

Kjærgaard P. 1987, A&A, 176, 210

Kurucz R. L. 1992, in *The Stellar Populations in Galaxies*, IAU Symp. 149, eds. B. Barbuy & A. Renzini, Kluwer Academic Publishers, Dordrecht, p. 225

Lee Y. W. 1994, ApJ, 430, L113

Lee Y. W. et al. 2005, ApJ, 619, L103

Lejune T., Cuisinier F., Buser R. 1997, A&AS, 125, 229

Lejune T., Cuisinier F., Buser R. 1998, A&AS, 130, 65

Maxted P. F. L., Heber U., Marsh T. R., North R. C. 2001, MNRAS, 326, 1391

Miller G. E., Scalo J. M. 1979, ApJS, 41, 513

O'Connell R. W. 1999, ARA&A, 37, 603
Park J. H., Lee, Y. W. 1997, ApJ, 476, 28
Rich R. M. et al. 2005, ApJ, 619, L107
Tantalo R., Chiosi C., Bressan A., Fagotto F. 1996, A&A, 311, 361
Terlevich A. I., Forbes D. A. 2002, MNRAS, 330, 547
Yi S. K., Demarque P., Kim Y. C. 1997a, ApJ, 482, 677
Yi S. K., Afshari E., Demarque P., Oemler Jr. A. 1995, ApJ, 453, L69
Yi S. K., Demarque P., Oemler Jr. A. 1997b, ApJ, 486, 201
Yi S. K., Demarque P., Oemler Jr. A. 1998, ApJ, 492, 480

Baltic Astronomy, vol. 15, 25–31, 2006.

HOT SUBDWARFS IN THE GALACTIC BULGE

G. Busso[1], S. Moehler[1], M. Zoccali[2], U. Heber[3] and S. K. Yi[4]

[1] *Institut für Theoretische Physik und Astrophysik der Universität Kiel, Leibnizstrasse 12, D-24098 Kiel, Germany*

[2] *Departamento de Astronomia y Astrofisica, Pontificia Universidad Catolica de Chile, Avenida Vucuna Mackenna 4860, 782-0436 Macul, Santiago, Chile*

[3] *Remeis-Sternwarte, Astronommisches Institut der Universität Erlangen-Nürnberg, Sternwartstrasse 7, 96049 Bamberg, Germany*

[4] *Department of Physics, University of Oxford, Keble Road, Oxford OX1 3RH, U.K.*

Received 2005 August 1

Abstract. Recent observations and theories suggest that extreme horizontal branch (EHB) stars and their progeny should be the cause of the UV excess that many elliptical galaxies show in their spectra. Since the Galactic bulge is the closest representation of an old, metal-rich spheroid in which we are able to study the EHB scenario in detail, we obtained spectra of bulge EHB star candidates and we confirm their status as hot evolved stars. It is the first time that such stars are unambiguously observed in the Galactic bulge.

Key words: galaxies: elliptical – Galaxy: bulge – stars: hot subdwarfs

1. INTRODUCTION

The spectra of elliptical galaxies and bulge regions of spiral galaxies in many cases show a strong and unexpected increase in flux at wavelength shorter than 2500 Å. This feature, called "UV excess", was one of the most important discoveries of satellite-based UV astronomy (Code & Welch 1969) but also a puzzle, since it required the existence of hot stars in these old metal-rich systems (see Burstein et al. 1988 and references therein). After a long debate, most people agree that the observed UV radiation is mainly produced by very hot extreme horizontal branch stars (burning helium in their core) and their progeny, as Post-EarlyAGB and AGB-manqué stars (O'Connell 1999; Greggio & Renzini 1990, 1999; Dorman et al. 1995; Yi et al. 1998). This view is supported by spectroscopic (Ferguson et al. 1991; Brown et al. 1997, 2002) and photometric (Brown et al. 2002) UV observations of extragalactic systems. Near-UV HST observations of Brown et al. (2000) in M 32 detected for the first time individual EHB star candidates in an elliptical galaxy. The best fit to the observations is achieved with evolutionary tracks for helium- and metal-rich populations, since in this case EHB stars have the longest lifetimes in the temperature range required to reproduce the UV excess (cf. Bressan et al. 1994).

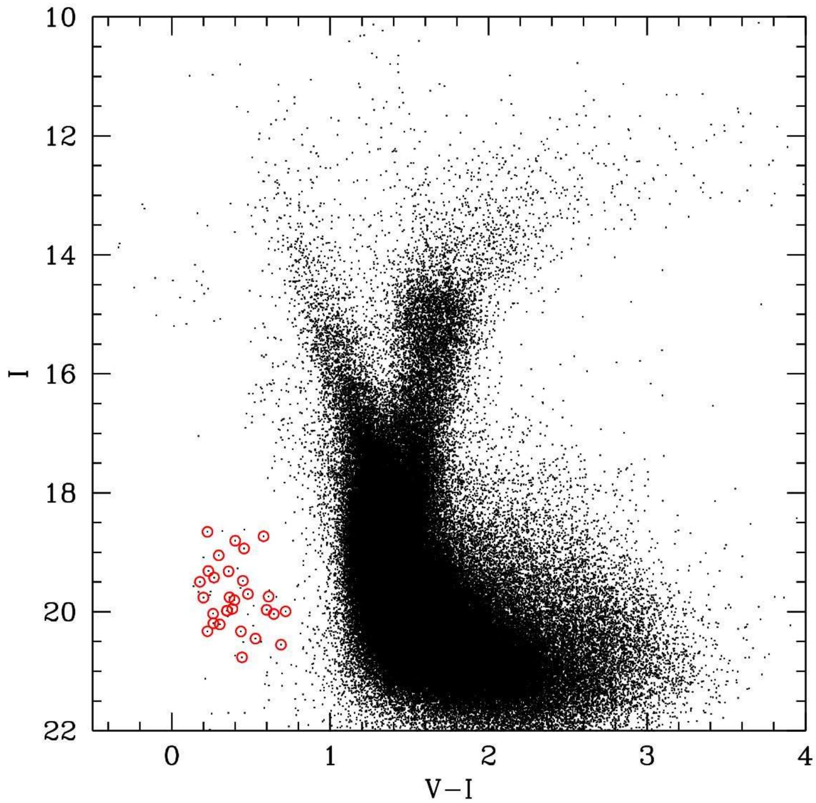

Fig. 1. Color-magnitude diagram of the Galactic bulge. Our targets are marked by circles.

The closest system similar to an elliptical galaxy with respect to age and metallicity for which it is possible to resolve stars is the Galactic bulge. The vast majority of EHB stars known in the Milky Way belongs however, to the metal-poor spheroid or to the disk population (where they show up as so-called subdwarf B (sdB) stars).

The only sdB candidates known in the bulge were found in the two massive globular cluster NGC 6388 and NGC 6441 (Rich et al. 1997; Busso et al. 2004), which are anyway not typical for the bulge population. The situation changed recently: Terndrup et al. (2004) found candidates in their survey for EHB stars in the Galactic bulge, and Wide Field Imager observations of a field toward the Galactic bulge (Zoccali et al. 2003) show a sequence of hot stars that are good candidates for EHB stars (see Figure 1). Using the values of Villeneuve et al. (1995) for scale height and space density of local field sdB stars, along a distance of 4.5 to 11 kpc within the field of view of WFI only less than 10 sdB stars are expected, while in our case about 140 candidates are found. Since they could be cool foreground stars (instead of reddened hot stars), we obtained spectroscopy of 29 candidates in order to derive effective temperatures and surface gravities and then, by means of comparison with HB models, to check their evolutionary status.

2. OBSERVATIONS

2.1. Target selection

Our spectroscopic targets were selected from the photometric catalogue of bulge stars obtained from Zoccali et al. 2003 (see Figure 1). We have chosen the stars with magnitude $18 < I < 21$ and color $0 < V - I < 0.8$ and among them we selected the most isolated ones.

2.2. VLT observations

We obtained medium-resolution spectra ($R \sim 1200$) of 29 candidates EHB stars at the VLT-UT1 (Antu) with FORS2. We used the multi-object spectroscopy (MXU) mode of FORS2 with the standard collimator, a slit width of $0.7''$ and grism B600, which allows to obtain spectra in the range between 3650 and 5200 Å(not all candidates though have spectra so extended because of the different positions on the CCD).

2.3. Data reduction

The data reduction was performed as described in Moehler et al. (2004) except for the following points. Due to the long exposure times (from 2700 s to 5400 s) the scientific observations contained a large number of cosmic rays and were therefore corrected with the algorithm described in Pych (2004). Regarding the subtraction of the sky background, we used two different methods depending on whether the target star in the slitlet was isolated or not. If the star was isolated, meaning any other stars in the slitlets were well enough separated from our target to identify regions uncontaminated by any stellar source, we approximated the spatial distribution of the sky background by a constant. If the slitlet showed severe crowding, meaning that the spectra of different stars were overlapping, we fitted each stellar profile with a Lorentzian function so that the whole spatial profile was reproduced by the sum of all the profiles; all the profiles but that one of the target were then subtracted (for details see Moehler & Sweigart 2006). With the extraction of the spectra, we saw that some (5 of 29) of our targets were actually cool stars. Therefore we did not proceed further with the reduction for these stars. The spectra were flux calibrated using standard stars spectra and corrected for any Doppler shifts determined from Balmer lines, as in Moehler et al. (2004).

3. ANALYSIS

Some examples of the spectra are shown in Figure 2. To fit the spectra (except for one He-rich one) we used ATLAS9 model atmospheres for solar metallicity (Kurucz 1993) to account for effects of radiative levitation (see Moehler et al. 2000 for details), from which we calculated spectra with Lemke's version of the LINFOR program (developed originally by Holweger, Steffen and Steenbock at Kiel University). The use of NLTE models or of LTE models with higher metallicity does not significantly change the results.

To establish the best fit, we used the routines developed by Bergeron et al. (1992) and Saffer et al. (1994), as modified by Napiwotzki et al. (1999), which employ a χ^2 test. The 1σ error necessary for the calculation of χ^2 is estimated from the noise in the continuum regions of the spectra. The fit program normalizes model spectra and observed spectra using the same points for the continuum definition.

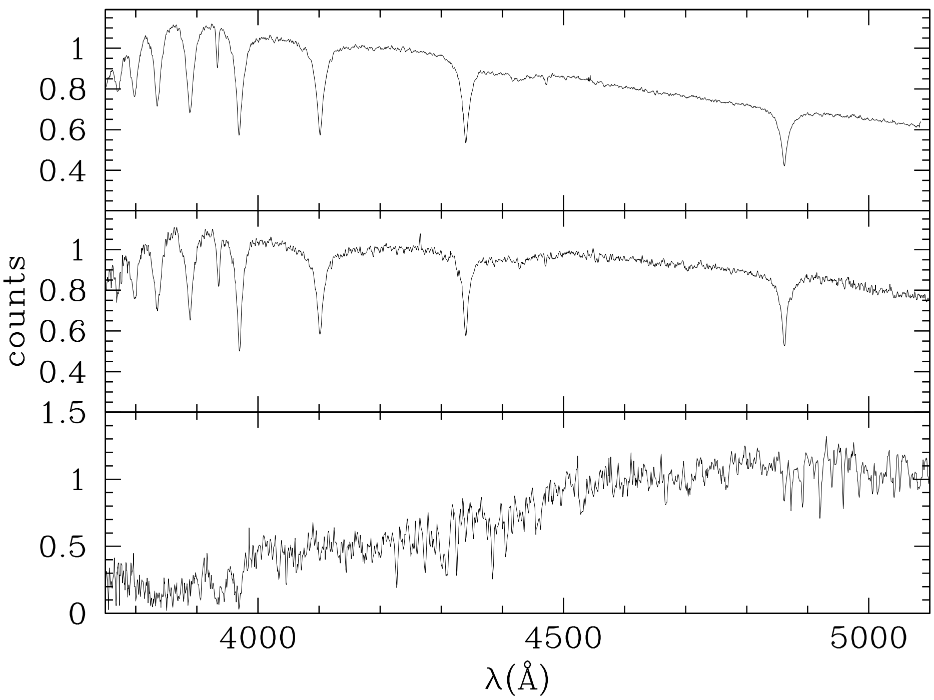

Fig. 2. Spectra of a few sdB star candidates. Top and central panel: typical spectra of newly detected hot stars with strong Balmer lines. Bottom panel: for comparison the totally different spectrum of a cool star.

We used the Balmer lines Hβ to H10 (excluding Hϵ to avoid the Ca II H line), the He I lines at 4026, 4388, 4471, 4921 Åand the He II lines at 4542 and 4686 Å.

We obtained the atmospheric parameters $T_{\rm eff}$, $\log g$ and helium abundances, and we calculated the absolute V and I magnitudes expected for these values, assuming $M_\star = 0.5\,M_\odot$. We left out one star because the fit was really bad. Considering a distance from the Galactic center of $\sim$ 8.5 kpc and a bulge radius of $\sim$1.5 kpc, we found that most of these objects are indeed bulge stars: of 23 hot stars, 13 stars are in the bulge within 1σ and 3 are in the bulge within 3σ.

This is also confirmed by the radial velocities found from the Doppler shift. The field we explored is centered at Galactic coordinates $\ell = 0°$, $b = -6°$, toward the Galactic center, so that the expected radial velocities for disk stars are around 0 km s^{-1}. Our velocities are distributed in a range between -200 and $+300$ km s^{-1}, in agreement with Terndrup et al. (1995).

Finally we compared our results with horizontal branch theoretical tracks: in Figure 3 we plotted in the $T_{\rm eff}$ vs. $\log g$ diagram the values found for those stars which belong to the bulge. The error bars are the formal errors from the fit procedure, but we are aware that the formal errors are underestimates (Napiwotzki, priv. comm.). The evolutionary tracks are from Yi et al. (1997) with metallicity $Z = 0.004$ and helium abundance $Y = 0.2416$. The Zero Age Horizontal Branch

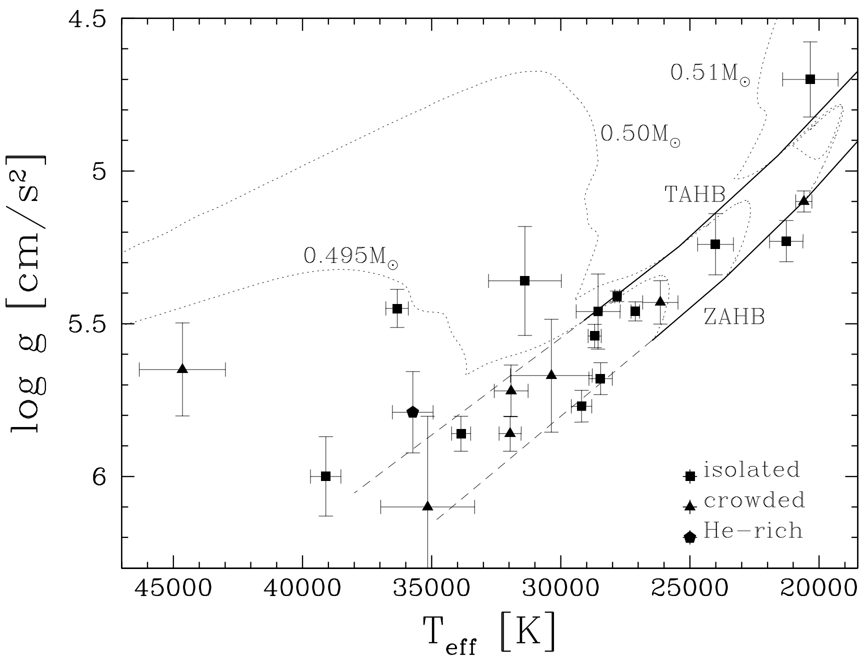

Fig. 3. $T_{\rm eff}$ vs. $\log g$) diagram. The squared symbols indicate the isolated stars; the triangles indicate the crowded stars and the pentagon is the He-rich star. The ZAHB and TAHB (Yi et al. 1997) and evolutionary tracks with metallicity $Z = 0.004$ and helium abundance $Y = 0.2416$ for 0.495, 0.50 and 0.51 $M_{\odot}$ are plotted. The dashed lines are extrapolated from the ZAHB and TAHB tracks.

(ZAHB), where the star starts to burn helium in its core quietly, and the Terminal Age Horizontal Branch, where the star burned the 99 % of the helium, are shown together with evolutionary tracks for stars with total masses of 0.495, 0.50 and 0.51 $M_{\odot}$. Since the theoretical lower limit for the mass of an EHB star is the core mass of the progenitor on the red giant branch ($\sim 0.45\,M_{\odot}$) while our tracks end at 0.495 $M_{\odot}$, we extrapolated the ZAHB and TAHB to lower masses (dashed curves in Figure 3). Proper models for lower masses will be calculated and used in a later paper. The observed points agree quite well with the theoretical tracks, therefore these objects are indeed EHB stars; some objects are above the TAHB meaning that they are in the post-HB phase and then evolving as AGB-manqué stars.

Finally we want to mention that all stars except one (which is helium-rich) are helium deficient as expected from diffusion.

5. CONCLUSIONS

We observed spectra of EHB star candidates in the Galactic bulge, from which we estimated the atmospherical parameters $T_{\rm eff}$ and $\log g$, confirming their evolutionary status. From the calculated radial velocities and distances we verified their membership to the bulge. This is the first time that such kind of stars are observed in the bulge, and with their spectra we are going to construct the integrated spectrum of the Galactic bulge from the UV to the optical, following the method described in Santos et al. (1995). The method consists in the construction of the integrated spectrum using a spectral library (in our case it will have to be a library extended to the UV) and the information contained in the spectroscopic and photometric observations. Regarding the spectral library, we will group the similar spectra, obtaining various groups of different spectral type, luminosity class and metallicity. For each group the average spectrum will be calculated, in order to obtain a better S/N. We will divide the color-magnitude diagram of the bulge in boxes, and each box will be associated to one of the library average spectra by means of the color index. The integrated spectrum will be the sum of the average spectra, scaling the contribute of each component keeping in account how many stars there are in each box.

This study will verify the role, so far only predicted, of EHB stars regarding the UV excess in elliptical galaxies.

ACKNOWLEDGMENTS. We are grateful to the ESO staff, especially those at the Paranal Observatory, for all their help during the observations. G.B. acknowledges support from the Deutsche Forschungsgemeinschaft via grant Mo 602/8.

REFERENCES

Bergeron P., Saffer R. A., Liebert J. 1992, ApJ, 394, 228

Bressan A., Chiosi C., Fagotto F. 1994, ApJS, 94, 63

Brown T. M., Ferguson H. C., Davidsen A. F., Dorman B. 1997, ApJ, 482, 685

Brown T. M., Bowers C. W., Kimble R. A., Sweigart A. V., Ferguson H. C. 2000, ApJ, 532, 308

Brown T. M., Ferguson H. C., O'Connell R. W., Ohl R. G. 2002, ApJ, 568, 19

Burstein D., Bertola F., Buson L. M., Faber S. M., Lauer T. R. 1988, ApJ, 328, 440

Busso G., Piotto G., Cassisi S. 2004, in *Stars in Galaxies*, eds. M Bellazzini, A. Buzzoni & S. Cassisi, Mem. Soc. Astron. Italiana, 75, 46

Code A. D., Welch G. A. 1969, ApJ, 228, 95

Dorman B., O'Connell R. W., Rood R. T. 1995, ApJ, 442, 105

Ferguson H. C., Davidsen A. F., Kriss G. A. et al. 1991, ApJ, 382, L69

Greggio L., Renzini A. 1990, ApJ, 364, 35

Greggio L., Renzini A. 1999, in *UV Astronomy in Italy*, eds. L. M. Buson & D. de Martino, Mem. Soc. Astron. Italiana, 70, 691

Kurucz R. L. 1993 in *ATLAS9 Stellar Atmospheric Program*, http://kurucz.harvard.edu

Moehler S., Sweigart A. V., Landsman W. B., Heber U. 2000, A&A, 360, 120

Moehler S., Sweigart A. V., Landsman W. B., Hammer N. J., Dreizler S. 2004, A&A, 415, 313

Moehler S., Sweigart A. V. 2006, Baltic Astronomy, 15, 41 (these proceedings)

Napiwotzki R., Green P. J., Saffer R. A. 1999, ApJ, 517, 399

O'Connell R. W. 1999, ARA&A, 37, 603

Pych W. 2004, PASP, 116, 148

Rich R. M., Sosin C., Djorgovski S. G. et al. 1997, ApJ, 484, L25
Saffer R. A., Bergeron P., Koester D., Liebert J. 1994, ApJ, 432, 351
Santos J. F. C., Bica E., Dottori H., Ortolani S., Barbuy B. 1995, A&A, 303, 753
Terndrup D. M., Sadler E. M., Rich R. M. 1995, ApJ, 110, 1774
Terndrup D. M., An D., Hansen A. et al. 2004, Ap&SS, 291, 247
Villeneuve B., Wesemael F., Fontaine G., Carignan C., Green R. F. 1995, ApJ, 446, 646
Yi S. K., Demarque P., Oemler A. J. 1997, ApJ, 486, 201
Yi S. K., Demarque P., Oemler A. J. 1998, ApJ, 492, 480
Zoccali M., Renzini A., Ortolani S. et al. 2003, A&A, 399, 931

Baltic Astronomy, vol. 15, 33–39, 2006.

SUPER-HELIUM-RICH STARS IN GLOBULAR CLUSTERS: THE ORIGIN OF EXTREME HORIZONTAL-BRANCH

S.-J. Joo[1], Y.-W. Lee[1], S.-J. Yoon[1,2], S.-I. Han[1], C. Chung[1], C. H. Ree[1], Y.-C. Kim[1], Y.-J. Sohn[1] and S. K. Yi[1,2]

[1] *Center for Space Astrophysics and Department of Astronomy, Yonsei University, Seoul 120-749, Korea*

[2] *Department of Physics, University of Oxford, Keble Road, Oxford OX1 3RH, U.K.*

Received 2005 August 1

Abstract. Recent observations of the globular cluster ω Centauri have shown that it has a double main sequence (MS), with a minority population of bluer and fainter MS well separated from a majority population of MS stars. Here we confirm that this special feature can only be reproduced by assuming a large range of helium abundance among several distinct populations in this cluster. We further show that the same helium enhancement required to reproduce this special feature on the MS can by itself reproduce the extreme horizontal-branch (EHB) stars observed in ω Cen, which are hotter than and separated from the majority population of normal HB stars. We also discuss the possibility that similar phenomena observed in the HB of other globular clusters are also due to the helium enhancement. If confirmed by further observations, this would establish that the third parameter that influences globular cluster color-magnitude diagram (CMD) morphology, in addition to metallicity and age, is indeed helium abundance.

Key words: globular clusters: individual (ω Centauri) – stars: abundances – stars: evolution – stars: horizontal-branch

1. INTRODUCTION

The Hubble Space Telescope snapshot survey of Galactic globular clusters has shown that the presence of extreme horizontal-branch (EHB) stars is not an unusual phenomenon among relatively massive globular clusters, which suggests that a third parameter, in addition to metallicity and age, is needed in order to explain the peculiar features observed on the HBs of these clusters (Piotto et al. 2002). It has been suggested for some time that more than one epoch of star formation and the accompanying helium and other elements enhancements in some globular clusters might be responsible for the presence of bimodal HBs and the EHB stars (D'Antona et al. 2002; D'Antona & Caloi 2004). While it has already been known that the HB morphology is very sensitive to helium abundance (see, e.g., Lee et

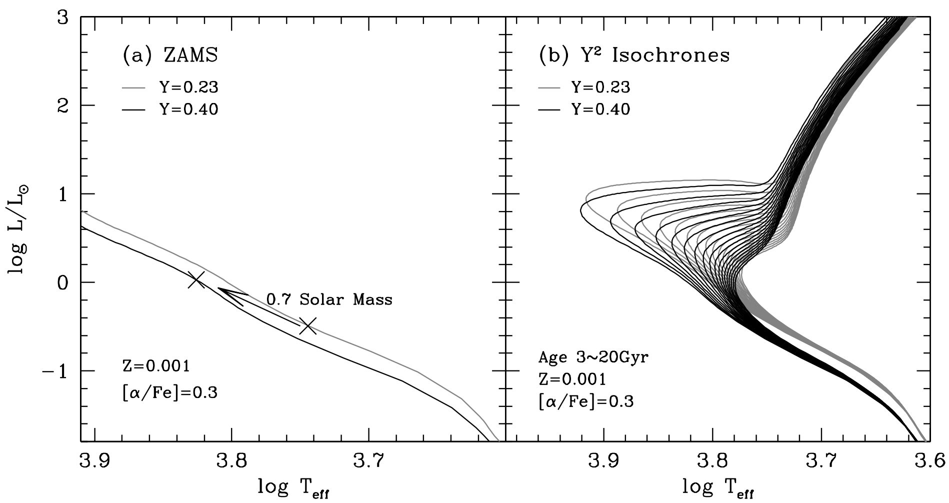

Fig. 1. New sets of Y^2 isochrones with helium enhancement. Panel (a) demonstrates the effect of helium enhancement on the zero-age main sequence for a given mass, while panel (b) illustrates the effect on the isochrones.

al. 1994), what is needed is a firm evidence that such a special helium enrichment indeed occurs in some globular clusters. This is because a star cluster is widely believed to be a coeval and chemically homogeneous system, and also the required helium enrichment is far more than that expected from standard chemical evolution models in galactic scales (i.e., $\Delta Y/\Delta Z = 1{\sim}2$).

The first good evidence that some stars in a globular cluster are actually enhanced in helium came from the recent observations of ω Cen. In particular, recent analyses with isochrones (Norris 2004) and spectroscopy (Piotto et al. 2005) of the MS stars in ω Cen have shown that a large helium abundance variation is needed to reproduce the double MS (Bedin et al. 2004) observed in this cluster. Although more work is needed for a specific chemical evolution model devoted for ω Cen to understand the origin of this unusually strong helium enrichment, these observations and analyses have nevertheless provided a compelling evidence that a minority population of stars at least in one globular cluster are indeed enhanced in helium. In this paper, we report our progress in constructing population models with the super-helium-rich scenario.

2. EFFECT OF HELIUM ENHANCEMENT

In order to investigate the effect of helium abundance on the observed features in the CMD, we have first calculated new sets of Yonsei-Yale (Y^2) stellar evolutionary tracks and isochrones with helium enhancements (Kim et al. 2002; Kim et al. 2005). These tracks adopted most up-to-date input physics including a new equation of state for the low mass stars. Figure 1 demonstrates the effect of helium enrichment on the HR diagram. Helium-rich stars, in general, are brighter and bluer for a given mass because of their higher core temperature (Fig. 1a), however, since they evolve faster than helium-poor stars, they would have smaller masses for a given age, and therefore the helium-rich MS appears both bluer and

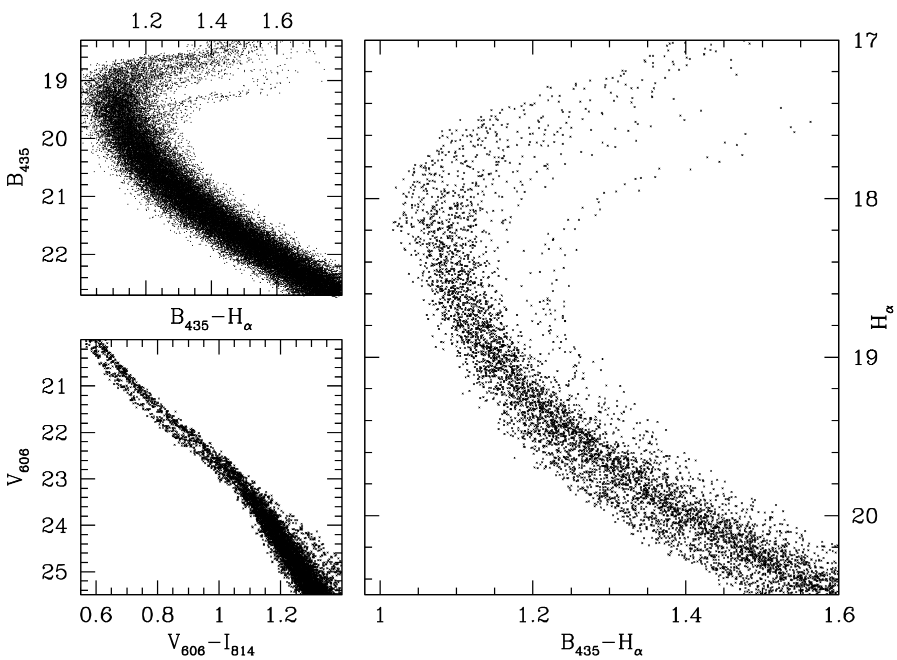

Fig. 2. Model CMDs for the main-sequence and subgiant-branch parts of ω Cen. These figures are to be directly compared with the observations by Bedin et al. (2004; see their Fig. 1).

fainter than the helium-poor MS on the isochrone (Fig. 1b). For the same reason, the mass at the tip of the red-giant-branch (RGB) of a helium-rich population is smaller than that of a helium-poor one, so that helium-rich HB stars have smaller total masses than helium-poor stars, which shifts their positions to the blue in the CMD (Lee et al. 1994).

3. POPULATION MODELS

Based on our new isochrones and the HB evolutionary tracks of Sweigart (1987) extrapolated to $Y \sim 0.4$,[1] population synthesis models are constructed following the techniques developed by Lee et al. (1990) and Park & Lee (1997). In Figure 2 we present the model CMDs for the MS and subgiant-branch (SGB) parts, based on the assumption that the helium abundances for the three most metal-rich populations are significantly enhanced among five populations with different metallicities in ω Cen (Sollima et al. 2005). These CMDs were specifically constructed with the passbands, photometric errors and total numbers of stars comparable to the observed ones of Bedin et al. (2004; see their Fig. 1), so that they can be directly compared with each other. The values of helium abundance and age are

[1] We are now in the process of constructing new sets of helium enhanced HB tracks fully consistent with our isochrones. Based on our preliminary models for ZAHB, we have confirmed that there is no serious systematic difference between our HB models and those of Sweigart (1987). We also verified that the extrapolation in Y does not produce a critical problem, by using the Sweigart & Gross (1976) HB tracks where the helium abundance is extended to $Y = 0.4$.

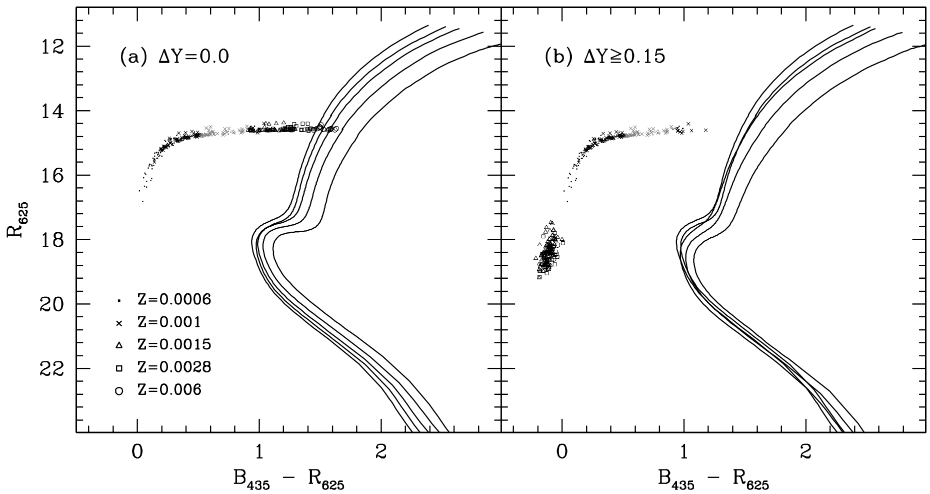

Fig. 3. Model CMDs for ω Cen. Panel (a) is for the case in which all five populations in ω Cen have the same helium abundance, while panel (b) is for the case in which the helium abundances for the metal-rich populations are significantly enhanced as in Table 1. Only the case of $\Delta Y \geq 0.15$ can reproduce the observed features on the MS and HB simultaneously. We adopted $(m-M)_R = 14.3$ and $E_{B-R} = 0.19$ in our models.

adjusted until the best matches between the models and the observed CMDs are obtained, while those for the metallicity are mostly fixed by the RGBs. Table 1 lists the input parameters used in our best model simulations. Similarly, in Figure 3, we compare two models constructed under different assumptions regarding the helium enhancement. As is clear from Figures 2 and 3, we confirm the conclusion from previous works that a large variation in helium abundance is indeed needed to reproduce the observed features on the MS to RGB, including the double MS, where the minority population of the bluer and fainter MS is both more metal-rich and super-helium-rich ($\Delta Y = 0.15$) compared to the majority population of the metal poor redder one.

In Figure 3 we have also presented corresponding synthetic HB models, which should be compared with the observed CMD by Ferraro et al. (2004; see their

Table 1. Input parameters in our best simulation of ω Cen. We adopted [α/Fe]=0.3 and η=0.46 for the mean mass-loss on the RGB. Population ratios were from Sollima et al. (2005).

Population	Z	Y	Age (Gyr)	Mass Loss ($M_\odot$)	Fraction
1	0.0006	0.231	13	0.168	0.42
2	0.001	0.232	13	0.178	0.27
3	0.0015	0.38	12	0.172	0.17
4	0.0028	0.40	11.5	0.177	0.08
5	0.006	0.42	11.5	0.201	0.05

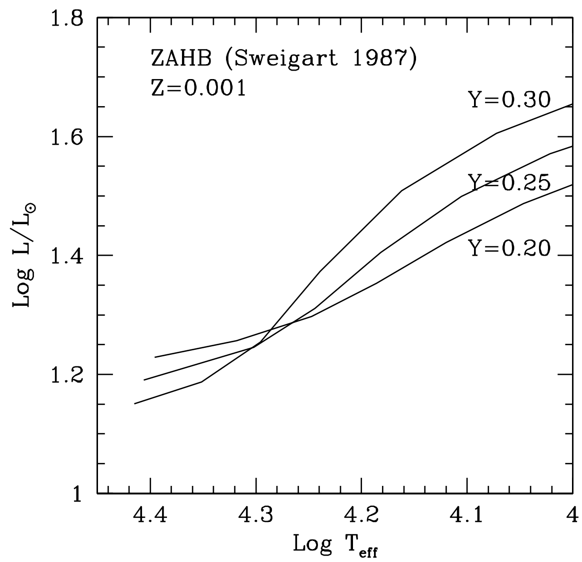

Fig. 4. The zero-age HB sequences with different helium abundances (Sweigart 1987).

Fig. 2, also see Fig. 1 of Lee et al. 2005). From models in Fig. 3a, we can see that the HB morphology generally gets redder with increasing metallicity, and the models fail to reproduce the EHB population. However, the models in Fig. 3b naturally reproduce the EHB stars observed in ω Cen with the same helium enhancements needed to reproduce the unique features on the MS. The fact that the three most metal-rich populations, including progeny of the bluer and fainter MS, all piled up on the extremely blue HB in Fig. 3b is a consequence of the large difference in helium abundance that easily overcomes the metallicity effect. In our model calculations, nothing other than the standard Reimers (1977) empirical relation was employed to estimate the amount of mass-loss on the RGB as a function of the input parameters adopted, and therefore the presence of extreme HB stars is solely the effect of helium enhancement. Under the same scenario, the complex features on the HBs of other globular clusters, such as NGC 2808, can be also explained by large internal variations of helium abundance (Lee et al. 2005; see also D'Antona et al. 2005).

An independent test for the helium-rich scenario might be provided from the FUV photometry of extreme HB stars, because the zero-age HB (ZAHB) locus is very sensitive to helium abundance. As Figure 4 illustrates, in general, helium-rich HB stars are brighter than helium-poor ones, but this trend is reversed when the effective temperature reaches $\sim$19 000 K. This is because extremely hot HB stars have very thin envelopes, with an almost negligible energy output from the hydrogen-burning shell. The total energy output is then mostly sustained by the helium-burning core, and since helium rich stars have a smaller core mass, they have a lower surface luminosity (Sweigart 1987). According to Sweigart (1987), EHB stars, therefore, would be fainter than HB stars as a result of the helium enhancement. The observed trends in UV CMD of EHB and blue HB stars in NGC 2808 (Brown et al. 2001) and ω Cen (Whitney et al. 1994) support our prediction (see Fig. 4 of Lee et al. 2005). It is important to note that spectroscopic analyses of the EHB stars in ω Cen and NGC 2808 (Moehler et al. 2002; Moehler et al. 2004) have shown anomalously high helium abundances up to about 0.3–1.0. While Moehler et al. interpreted this with the late hot flasher scenario (Brown et al. 2001), we believe that at least some of this helium enrichment might be also understood from our scenario.

4. DISCUSSION

The good agreements between the models and the observations for the appearance and population ratio of EHB stars in ω Cen suggest that the third parameter that controls HB morphology, in addition to metallicity and age, might be helium abundance. This in turn suggests that whenever the relative age is estimated from the HB morphology (Lee et al. 1994; Rey et al. 2001), a better result would be obtained by ignoring extreme HB stars or similar peculiar features on the HB. Fortunately, the effect of helium abundance on the MS and RGB is relatively small, and in most globular clusters with EHB stars, the expected helium-rich populations are a minority in terms of the population ratio. Therefore, the age dating from MS and RGB is likely to be less affected by the minority populations of helium-rich stars in these clusters. However, when one infers the relative age or other physical parameters from the integrated-light colors and spectra of globular clusters and early-type galaxies, the possible contamination from helium-rich populations should still be carefully considered, as they would make the observed colors bluer, especially in the UV. Further observations and modeling of globular clusters with peculiar features on their HBs will undoubtedly help us to establish the super-helium-rich scenario as the origin of EHB stars found in globular clusters.

ACKNOWLEDGMENTS. Support for this work was provided by the creative research initiative program of the Korean ministry of science and technology, for which we are grateful.

REFERENCES

Bedin L. R., Piotto G., Anderson J., Cassisi S. et al. 2004, ApJ, 605, L125

Brown T. M., Sweigart A. V., Lanz T., Landsman W. B., Hubeny I. 2001, ApJ, 562, 368

D'Antona F., Bellazzini M., Caloi V., Fusi Fecci F., Galleti S., Rood R. T. 2005, ApJ, in press

D'Antona F., Caloi V. 2004, ApJ, 611, 871

D'Antona F., Caloi V., Montalban J., Ventura P., Gratton R. 2002, A&A, 395, 69

Ferraro F. R., Sollima A., Pancino E., Bellazzini M. et al. 2004, ApJ, 603, L81

Kim Y.-C., Demarque P., Yi S. K., Alexander D. R. 2002, ApJS, 143, 499

Kim Y.-C. et al. 2005, in preperation

Lee Y.-W., Demarque P., Zinn R. 1990, ApJ, 350, 155

Lee Y.-W., Demarque P., Zinn R. 1994, ApJ, 423, 248

Lee Y.-W., Joo S.-J., Han S.-I., Chung C. et al. 2005, ApJ, 621, L57

Moehler S., Sweigart A. V., Landsman W. B., Dreizler S. 2002, A&A, 395, 37
Moehler S., Sweigart A. V., Landsman W. B., Hammer N. J., Dreizler S. 2004, A&A, 415, 313
Norris J. E. 2004, ApJ, 612, L25
Park J.-H., Lee Y.-W. 1997, ApJ, 476, 28
Piotto G., King I. R. Djorgovski S. G., Sosin C. et al. 2002, A&A, 391, 945
Piotto G., Villanova S., Bedin L. R., Momany Y. et al. 2005, ApJ, 621, 777
Reimers D. 1977, A&A, 57, 395
Rey S.-C., Yoon S.-J., Lee Y.-W., Chaboyer B., Sarajedini A. 2001, AJ, 122, 3219
Sollima A., Ferraro F. R., Pancino E., Bellazzini M. 2005, MNRAS, 357, 265
Sweigart A. V. 1987, ApJS, 65, 95
Sweigart A. V., Gross P. G. 1976, ApJS, 32, 367
Whitney J. H., O'Connell R. W., Rood R. T. et al. 1994, AJ, 108, 1350

Baltic Astronomy, vol. 15, 41–48, 2006.

THE NATURE OF THE HOT STARS IN THE BULGE OF GLOBULAR CLUSTER NGC 6388 †

S. Moehler[1] and A. V. Sweigart[2]

[1] *Institut für Theoretische Physik und Astrophysik, Christian-Albrechts-Universität zu Kiel, D-24098 Kiel, Germany*

[2] *NASA Goddard Space Flight Center, Code 681, Greenbelt, MD 20771, U.S.A.*

Received 2005 August 1

Abstract. The metal-rich bulge globular clusters NGC 6388 and NGC 6441 show distinct blue horizontal-branch tails in their color-magnitude diagrams. They are thus strong cases of the well known *Second Parameter Problem.* In addition, the horizontal branches in these globular clusters show an upward tilt toward bluer colors, which cannot be explained by canonical evolutionary models. We will discuss several scenarios which have been proposed to explain these two features and present observations obtained to test these scenarios.

Key words: stars: horizontal branch, stars: evolution, globular clusters: individual: NGC 6388

1. INTRODUCTION

Ever since its discovery over 30 years ago (Sandage & Wildey 1967; van den Bergh 1967), the 2nd parameter effect has stood as one of the major unsolved challenges in the study of the Galactic globular clusters. While it was recognized quite early that the horizontal branch (HB) becomes redder on average with increasing metallicity, many pairs of globular clusters are known with identical metallicities but markedly different HB morphologies, e.g., M 3 versus M 13. Thus some parameter(s) besides metallicity (the 1st parameter) must affect the evolution of the HB stars in these globular clusters. Possible 2nd parameter candidates include the globular cluster age, mass-loss along the red giant branch (RGB), helium abundance Y, α-element abundance, cluster dynamics, stellar rotation, deep mixing, etc.

HST observations by Rich et al. (1997) have found that the metal-rich globular clusters NGC 6388 and NGC 6441 ([Fe/H] ≈ -0.5) contain an unexpected population of hot HB stars and therefore show a prominent 2nd parameter effect. Ordinarily metal-rich globular clusters have only a red HB clump. However, NGC 6388 and NGC 6441 possess extended blue HB tails containing $\sim 15\,\%$ of the total HB population. Quite remarkably, the HBs in both clusters slope upward with decreasing B–V with the stars at the top of the blue tail being nearly 0.5 mag brighter in V than the well-populated red HB clump. Moreover, the RR Lyrae variables in these clusters have unusually long periods for the cluster metallicity,

† Based on observations from the European Southern Observatory, Chile (prop. 69.D-0231)

leading Pritzl et al. (2000) to suggest that NGC 6388 and NGC 6441 may represent a new Oosterhoff group. For all of these reasons the HBs of NGC 6388 and NGC 6441 are truly exceptional.

In the next section we will discuss the implications of NGC 6388 and NGC 6441 for the 2nd parameter effect and will review a number of scenarios for explaining the HB morphology of these clusters. The following sections will then describe the high and medium resolution spectra that we have obtained to test these scenarios.

2. HB MORPHOLOGY: PROBLEMS AND SCENARIOS

The presence of hot HB stars in globular clusters as metal-rich as NGC 6388 and NGC 6441 may provide an important diagnostic for understanding the 2nd parameter effect for the following reason. In intermediate-metallicity globular clusters such as M 3 the HB spans a wide range in color that extends both blueward and redward of the instability strip. The location of a star along the HB is then quite sensitive to changes in the stellar parameters. In fact, this is why the HB is "horizontal". In metal-rich globular clusters, however, the situation is quite different. Due to their high envelope opacity, metal-rich HB stars are normally confined to a red clump. To move such stars blueward requires a larger change in the stellar structure. Thus any 2nd parameter candidate capable of producing hot HB stars in a metal-rich globular cluster might also have other observational consequences. Indeed, the upward sloping HBs in NGC 6388 and NGC 6441 suggest that the 2nd parameter in these globular clusters is affecting both the temperature and luminosity of the HB stars.

Can canonical models explain the upward sloping HBs in NGC 6388 and NGC 6441? In principle, one could produce hot HB stars in these globular clusters by increasing the cluster age or by enhancing the amount of mass-loss along the RGB. Rich et al. (1997) considered both of these possibilities but found neither of them to be satisfactory because the required increase in the cluster age is quite large and because the frequency of stellar interactions within the cores of these clusters seems too low to produce the additional RGB mass-loss. This conclusion was further supported by the theoretical HB simulations of Sweigart & Catelan (1998, hereafter SC98). They found that the HB morphology predicted by canonical HB models is flat in the (M_V vs. B–V) plane. Increasing the cluster age or the RGB mass-loss simply moves the models blueward in B–V without increasing their luminosity. Thus canonical HB models cannot account for the HB morphology of NGC 6388 and NGC 6441. In particular, two of the most prominent 2nd parameter candidates – age and RGB mass-loss – do not work.

This failure of canonical HB models to produce upward sloping HBs has prompted the study of other noncanonical solutions. Theoretical models show that the HB luminosity at a fixed metallicity depends on two parameters: the helium abundance Y and the core mass M_c. This fact led SC98 to suggest three noncanonical scenarios involving increases in either Y or M_c which might potentially produce upward sloping HBs.

The first ("high-Y") scenario assumes that the stars in NGC 6388 and NGC 6441 formed with a high primordial helium abundance due to a peculiar chemical enrichment history in these clusters. From theoretical models we know that HB tracks at high helium abundances have very long blue loops which deviate considerably from the zero-age HB (ZAHB). The HB simulations of SC98 show that such high-Y tracks can indeed produce upward sloping HBs as seen in NGC 6388 and NGC 6441 provided Y is very large ($\gtrsim 0.4$). However, this scenario can be ruled out because it predicts too large a value for the number ratio R of HB stars to RGB stars brighter than the HB (Layden et al. 1999) as well as too bright a luminosity for the RGB bump (Raimondo et al. 2002).

The second ("rotation") scenario is based on the fact that internal rotation within an RGB star can delay the helium flash, thereby leading to a larger core mass and to greater mass-loss near the tip of the RGB. This increase in M_c together with the corresponding decrease in M will shift a star's HB location towards higher effective temperatures and luminosities. HB simulations show that this scenario can also produce upward sloping HBs similar to those observed in NGC 6388 and NGC 6441. The problem, however, is to understand how the blue HB stars could have the high rotation rates required by this scenario.

The third ("helium-mixing") scenario is motivated by the large star-to-star abundance variations which are found among the red-giant stars within individual globular clusters and which are sometimes attributed to the mixing of nuclearly processed material from the vicinity of the hydrogen shell out to the stellar surface (Kraft 1994). The observed enhancements in Al are particularly important because they indicate that the mixing is able to penetrate deeply into the hydrogen shell (Cavallo et al. 1998). Such mixing would dredge up fresh helium together with Al, thereby enhancing the envelope helium abundance and leading to a brighter RGB tip luminosity and hence greater mass-loss. Thus a helium-mixed star would arrive on the HB with both a higher envelope helium abundance and a lower mass and would therefore be both bluer and brighter than its canonical counterpart - just what is needed to produce an upward sloping HB. Indeed, the HB simulations of SC98 confirm that helium mixing can produce HB morphologies similar to those in NGC 6388 and NGC 6441. However, the existence of helium mixing can be questioned on several grounds. The O-Na and Mg-Al anticorrelations observed in turnoff stars of NGC 6752 by Gratton et al. (2001) indicate that the Al enhancements are more likely due to primordial pollution from an earlier generation of asymptotic-giant-branch (AGB) stars than to deep mixing on the RGB. It is also questionable whether the mixing currents could overcome the large gradient in the mean molecular weight within the hydrogen shell of a RGB star. Thus helium mixing seems unlikely.

A number of additional solutions have been offered to explain the HB morphologies of NGC 6388 and NGC 6441. One of the earliest solutions, suggested by Piotto et al. (1997), was a spread in metallicity. In this case the blue HB stars would be metal-poor compared to the stars in the red HB clump. Because the HB becomes brighter in V with decreasing metallicity, the blue HB stars would also be brighter. Thus a metallicity spread might also produce an upward sloping HB. This possibility was studied by Sweigart (2002), who showed that upward sloping HBs similar to those in NGC 6388 and NGC 6441 would require the stars at the top of the blue HB tail to be approximately 2 dex more metal-poor than the stars in the red HB clump. However, Raimondo et al. (2002) have noted that the progenitors of the blue HB stars should appear as a population of metal-poor giants lying well to the blue of the metal-rich RGB. Since such metal-poor giants are not seen in the color-magnitude diagrams of NGC 6388 and NGC 6441, Raimondo et al. (2002) conclude that any metallicity spread must be small.

Piotto et al. (1997) also suggested that NGC 6388 and NGC 6441 might contain two stellar populations with different ages. This possibility has been further explored by Ree et al. (2002). Their population models for NGC 6388 and NGC 6441 are able to produce blue HB stars provided these stars are older by 1.2 Gyr and metal-poor by 0.15 dex compared to the stars in the red HB clump. Such a small difference in metallicity between the blue and red HB stars avoids the problem with the missing metal-poor giants discussed above. However, while such models might produce bimodal HBs, they do not produce an upward sloping HB. As shown by SC98, differences in age merely move an HB star horizontally along the HB, and, as shown by Sweigart (2002), a metallicity difference of 0.15 dex is too small to produce a significant HB slope. Thus the Ree et al. (2002) models do not account for a key property of the HBs in NGC 6388 and NGC 6441. Ree et al. (2002) also suggest that the long RR Lyrae periods might be explained if these stars are highly evolved from the blue HB. While such stars would have long periods, they would also evolve rapidly across the instability strip on their way to the AGB. Explaining the observed number of RR Lyrae stars under such a scenario would therefore be very difficult (Pritzl et al. 2002).

A more promising possibility is based on the suggestion by D'Antona & Caloi (2004) that the stars in globular clusters with blue HB tails are born in two events: a first generation of helium-normal stars and a second generation of helium-rich stars which subsequently form from the ejecta of the intermediate-mass AGB stars of the first generation. Since a helium-rich star has a lower turnoff mass at a given age, it will be bluer on the HB than a helium-normal star. It will also be brighter due to the increased energy output of the hydrogen-burning shell. Thus the spread in the internal helium abundance predicted by this scenario will lead to a spread in color along the HB, with the red clump stars corresponding to the helium-normal, first generation stars and the blue tail stars being progressively more helium-rich as the effective temperature increases. An upward sloping HB is a natural consequence of this spread in helium. The fact that the HB slope is more prominent in NGC 6388 and NGC 6441 than in other blue tail globular clusters may be simply due to their higher metallicity which requires a larger increase in helium in order to force a star blueward of the red clump. We emphasize that this scenario differs from the high-Y scenario, mentioned above, in which all of the stars are helium-rich and the helium-mixing scenario in which the spread in helium arises from deep mixing on the RGB.

All of the above scenarios which can produce an upward sloping HB predict that the gravities of the blue HB stars should be lower than the gravities of canonical blue HB stars. In 1998 we observed some of the brighter objects in both clusters ($B < 18$; four stars in NGC 6388, three in NGC 6441) to test this prediction. Unfortunately the results only added to the confusion as most of the stars had *higher gravities* than predicted by canonical evolution (Moehler et al. 1999). It took us four years and three rejected proposals to convince the ESO TAC to give us observing time for another test of the above described scenarios: With proposal 69.D-0231 we obtained high resolution spectra of four cool blue HB stars in NGC 6388 to determine their metallicities and rotation velocities. In addition, we observed medium resolution spectra of about a dozen blue HB stars along the blue tail to determine their effective temperatures and surface gravities. By comparing the observed values to those predicted by the various scenarios, we hope to distinguish among the scenarios.

3. HIGH RESOLUTION SPECTROSCOPY

The high resolution spectra were obtained with the UVES spectrograph at the ESO VLT with the standard setting DIC1 (390+564) and a slit width of 1″. This setting covers the wavelength ranges 3720–4520 Å in the blue arm and 4605–5585 Å and 5674–6610 Å in the red arm (2 CCDs) at a resolution of 45 000 (blue) and 37 000 (red). This is the same setting as used by the SPY project (Karl et al., these proceedings). We therefore reduced the data with the UVES context within MIDAS, with the additional correction by a flat field shifted in wavelength direction as done by the SPY consortium to avoid ripples in the resulting one-dimensional spectrum. The details will be described in a forthcoming paper.

3.1. Analysis and results

To analyze the high resolution spectra, we first estimated effective temperatures from *B–V* colors corrected for a reddening of 0.37 mag. Keeping these temperatures fixed, we estimated the surface gravities by fitting the Balmer line profiles as described in Moehler et al. (2004). Using these values we did a first abundance determination by spectrum synthesis, using the LINFOR program*. Then we changed the effective temperature until the abundances from Fe I and Fe II agreed to within 0.15 dex. The surface gravity was again determined by fitting the Balmer line profiles. Figure 1 shows a section of the spectra of three HB stars together with the synthesized spectrum (the fourth star is the coolest one and therefore most difficult to analyze due to severe line blending). We find no significant deviations from the overall metallicity of NGC 6388 in these spectra and therefore no supporting evidence for a possible metal deficiency in these blue HB stars. We also do not find rotation velocities in excess of 10 km s^{-1}, which is in good agreement with the values found for blue HB stars in other globular clusters. We do find a *very tentative* evidence for a possible helium enrichment. In this temperature range, however, the helium lines are very weak and extremely sensitive to temperature variations, so that we so not want to place much emphasis on this *possible* result.

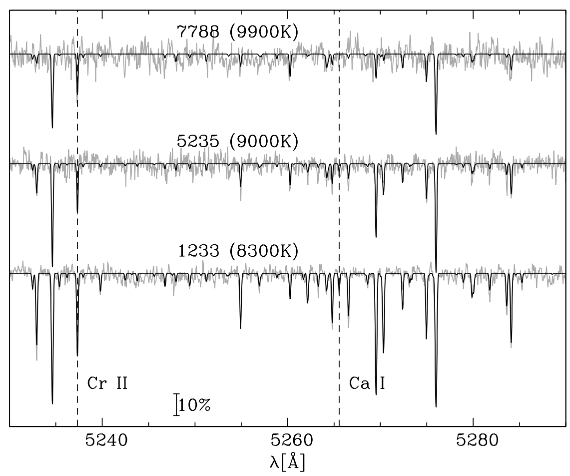

Fig. 1. Small section of the UVES spectra for the three hotter stars. The black line is the synthetic spectrum for each star and the unmarked lines are all iron lines.

4. MEDIUM RESOLUTION SPECTROSCOPY

The medium resolution spectra of stars along the blue tail were obtained with the multi-object spectroscopy mode MOS of FORS2, again at the ESO VLT.

---

* For a description see http://a400.sternwarte.uni-erlangen.de/∼ai26/linfit/linfor.html

We used the grism 600B with a slit width of 0.6″, corresponding to a resolution of 1200 and a wavelength range of 3700 Å to 5200 Å for all spectra. The wavelength range extended to blue or redder regions depending on the position of the slitlet on the CCD. The data were reduced as described in Moehler et al. (2004), except for the sky subtraction.

The MOS observations were obtained in very crowded fields, and due to the fact that several stars were observed simultaneously, we could not orient the individual slitlets in a way to avoid nearby stars. Therefore most slitlets contain spectra of several stars, in many cases overlapping so strongly that it is impossible to directly extract the spectrum of our intended target (see Figure 2). In order to account for this overlap we proceeded as follows.

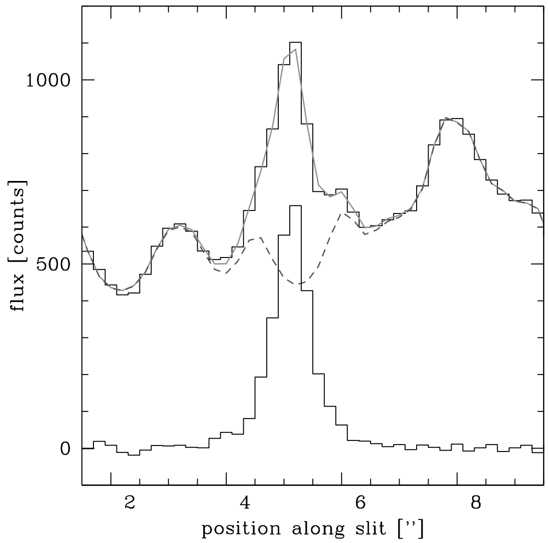

Fig. 2. The spatial light distribution along one slitlet. The upper histogram is the observed light distribution, the light continuous line gives the fit of all sources, the light dashed line marks the subtracted sky background. The lower histogram is the spatial profile of the sky subtracted image.

- We corrected the curvature of the FORS2 spectra.
- We averaged the wavelength-calibrated two-dimensional spectra along their dispersion axis between 3500 and 5200 Å (roughly the range which is later used for fitting the line profiles), thereby producing a one-dimensional spatial profile along the slitlet (cf. Figure 2, upper histogram).
- The one-dimensional spatial distribution of light was fitted with a combination of Moffat functions, i.e.,

$$I_{(x)} = bck + \sum_{j=1}^{n} I_{j(x)}$$

$$\text{with} \qquad I_{j(x)} = a_j \left(1 + \frac{4(x-b_j)^2}{c^2}\right)^{-d}.$$

For each profile the parameters a_j (amplitude) and b_j (position) were fitted individually, whereas the parameters c and d, which determine the profile width and shape (and should depend only on the seeing and instrumental broadening), had to be the same for all objects within one slitlet. We used up to 13 individual profiles to fit the full spatial light distribution along one slitlet (see Figure 2, light solid line).

- After achieving a good fit to the observed spatial profiles we kept the parameters b_j, c and d fixed and used these profiles to fit the spatial profile now at

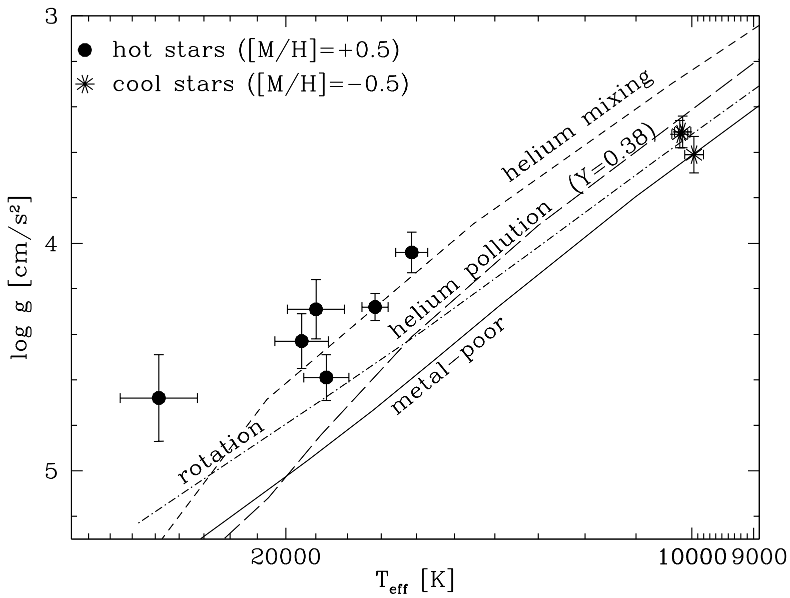

Fig. 3. Effective temperatures and surface gravities for our target stars as derived from line profile fits. Three stars have temperatures below 8000 K, where we do not trust the fit procedure, and one star showed a prominent G-band in its spectrum after the sky subtraction and was therefore not analyzed. For comparison we show the tracks discussed in Section 2.

every wavelength step. The amplitudes a_j and the spatial constant bck (for the true sky background) were allowed to vary with wavelength, in order to describe the various spectra.

- The sum of all profiles *minus the target profile* were then used as sky background (cf. Figure 2, dashed line) and subtracted from the wavelength calibrated two-dimensional image. The resulting image – containing only the target spectrum – was again averaged over the same wavelength range as above to verify the quality of the sky correction (see Figure 2, lower histogram).

4.1. Analysis and results

We then fitted the Balmer and helium line profiles to determine effective temperatures, surface gravities and helium abundances as described in Moehler et al. (2004), using a solar metallicity model grid to account for the effects of radiative levitation. The resulting values of $T_{\rm eff}$ and log g are shown in Figure 3, together with tracks describing the scenarios mentioned in Section 2. Obviously the hot stars show significantly lower gravities than expected. To verify if this is a luminosity effect or rather a reduction and/or analysis artifact, we used these values to estimate masses for the stars. While the three stars around 10 000 K show an average mass of 0.52 $M_\odot$, the hot stars have an average mass of 0.28 $M_\odot$, which is too low by almost a factor of 2. We therefore suspect that the sky subtraction did not work sufficiently well to really isolate the light from the hot stars. Tests with the spectra indicate that sky subtraction problems may also be the cause for the unexpectedly high gravities found previously by Moehler et al. (1999).

5. CONCLUSIONS

From our high resolution data (which include two of the three stars at 10 000 K in Figure 3) we find no supporting evidence for the low metallicity scenario. The atmospheric parameters of the stars at about 10 000 K also do not support the helium mixing scenario. The medium resolution data of the hotter and visually fainter stars unfortunately yield results that are apparently affected by systematic errors. As the hotter stars are fainter by at least 1.2 mag in B compared to the stars at about 10 000 K, the systematic problems are most probably due to crowding problems, which are more severe for fainter stars. Despite our best efforts, which yielded spectra without obvious evidence for contamination in all but one case, we apparently did not succeed in extracting from the observed data the information related *only* to the intended target. This should serve as a warning that observations in crowded regions are difficult, especially, if the targets are selected from HST observations (as was the case here).

ACKNOWLEDGMENTS. We want to thank the staff at the Paranal Observatory for obtaining the observations for us.

REFERENCES

Cavallo R. M., Sweigart A. V., Bell R. A. 1998, ApJ, 492, 575

D'Antona F., Caloi V. 2004, ApJ, 611, 871

Gratton R. G., Bonifacio P., Bragaglia A. et al. 2001, A&A, 369, 87

Kraft R. P. 1994, PASP, 106, 553

Layden A. C., Ritter L. A., Welch D. L., Webb T. M. A. 1999, AJ, 117, 1313

Moehler S., Sweigart A. V., Catelan M. 1999, A&A, 351, 519

Moehler S., Sweigart A. V., Landsman W. B., Hammer N. J., Dreizler S. 2004, A&A, 415, 313

Piotto G., Sosin C., King I. R. et al. 1997, in *Advances in Stellar Evolution*, eds. R. T. Rood & A. Renzini, Cambridge University Press, Cambridge, p. 84

Pritzl B. J., Smith H. A., Catelan M., Sweigart A. V. 2000, ApJ, 530, L41

Pritzl B. J., Smith H. A., Catelan M., Sweigart A. V. 2002, AJ, 124, 949

Raimondo G., Castellani V., Cassisi S., Brocato E., Piotto G. 2002, ApJ, 569, 975

Ree C. H., Yoon S.-J., Rey S.-C., Lee Y.-W. 2002, in *Omega Centauri, a Unique Window into Astrophysics*, eds. F. van Leeuwen, J. D. Hughes & G. Piotto, ASP Conf. Ser., 265, 101

Rich R. M., Sosin C., Djorgovski S. G. et al. 1997, ApJ, 484, L25

Sandage A., Wildey R. 1967, ApJ, 150, 469

Sweigart A. V. 2002, in *Highlights of Astronomy*, ed. H. Rickman, ASP, San Francisco, p. 292

Sweigart A. V., Catelan M. 1998, ApJ, 501, L63 (SC98)

van den Bergh S. 1967, AJ, 72, 70

Baltic Astronomy, vol. 15, 049–052, 2006.

NEW CANDIDATE EHB STARS IN THE OPEN CLUSTER NGC 6791: LOOKING LOCALLY INTO THE UV-UPTURN PHENOMENON

L.M. Buson[1], E. Bertone[2], A. Buzzoni[3] and G. Carraro[4,5,6]

[1] *INAF - Osservatorio di Padova, Italy*

[2] *INAOE, Puebla, Mexico*

[3] *INAF - Osservatorio di Bologna, Italy*

[4] *Dept. de Astron. Univ. de Chile, Santiago. Chile*

[5] *Astronomy Dept., Yale Univ., USA*

[6] *Dip. di Astronomia, Univ. di Padova, Italy*

Received 2005 August 1

Abstract. Relying on U and B imagery at the Italian Telescopio Nazionale Galileo (TNG), we report here the discovery of a sample of 13 new UV-bright post-HB candidate stars in the field of the Galactic open cluster NGC 6791. Owing to its super-solar metal content ([Fe/H] $\gtrsim$ 0.2 dex) and estimated age ($t \gtrsim 8$ Gyr), this cluster represents the nearest and ideal stellar aggregate to match the distinctive properties of the evolved stellar populations possibly ruling the UV-upturn phenomenon in elliptical galaxies and bulges of spirals. Our ongoing spectroscopic follow-up of this unique UV-bright sample will allow us to assess – once cluster membership of the candidates is properly checked – the real nature (e.g., sdB, sdO, AGB-manqué or EHB stars) of these hot sources and their link with the ultraviolet excess emerging from low-mass, metal-rich evolutionary environments of external galaxies.

Key words: stars: sudwarfs – stars: horizontal-branch – ultraviolet: stars

1. INTRODUCTION

Since its early discovery (Code 1969), the so-called UV-upturn phenomenon in old stellar populations of ellipticals and spiral bulges (namely the abrupt rise in the UV continuum emission shortward of $\lambda \sim 2000$ Å) has been the subject of growing theoretical analyses intended to establish its origin and evolution (see, e.g., Greggio & Renzini 1990 and O'Connell 1999, for reviews).

Both theory and observations currently seem to converge towards the "Extreme Horizontal Branch" (EHB) scenario as the main factor responsible for the phenomenon (Dorman et al. 1995; Brown 2004). If this is the case, models show that hot HB stars with helium core mass $M_{\rm core} \lesssim 0.52\ M_\odot$ can escape the standard post-HB evolution (that would culminate with the planetary-nebula event at the end of the asymptotic giant branch evolution), and directly reach the high-temperature region of the HR diagram ($T_{\rm eff} \gtrsim 30\,000$ K) to fade then along the white-dwarf cooling sequence (Dorman et al. 1993).

In this framework, the role of metallicity cannot yet be confidently assessed, however, as we face two conflicting scenarios relying either on a metal-poor evolution (naturally giving rise to a blue HB morphology, see Park & Lee 1997) or a metal-rich case, where the onset of UV emission needs at least a fraction of stars to exceed some critical threshold in [Fe/H] (Greggio & Renzini 1990; Bressan et al. 1994; Buzzoni 1995; Dorman et al. 1995). In this regard, one should be aware that even the high-resolution UV spectroscopy provided by FUSE for the UV-brightest elliptical NGC 1399 turned out to be inadequate to solve the problem, as it mainly probes the photospheric abundance of hot stars, likely perturbed by diffusion effects and therefore not fully indicative of the true metallicity of the whole galaxy stellar population (Brown et al. 2002).

2. NGC 6791: THE UNEXPECTED SHORTCUT

Photometric observations of evolved UV-bright stars in external galaxies are still confined to the relevant case of M 31 and its satellite system (e.g., Bertola et al. 1995; Brown et al. 1998, 2000), and no suitable spectroscopy for single stars is available to date.

Surprisingly enough, the close Galactic open cluster NGC 6791, less than 5 kpc away (Friel 1995; Carraro et al. 1999), turned out to be a highly valuable candidate to address the issue of the EHB UV-bright stars, standing out as a sort of backyard “Rosetta Stone” to assess the UV emission of spheroids much farther away. This cluster is actually one of the brightest ($L_V \sim 6.3\,10^3\ L_\odot$), oldest ($t \gtrsim 8$ Gyr) and metal-rich ([Fe/H]$\gtrsim +0.2$) ones (King et al. 2005; Stetson et al. 2003; Carraro et al. 1999), and hosts a significant fraction of sdB/O stars (Kaluzny & Rucinski 1995; Kaluzny & Udalski 1992, see Fig. 1) interpreted by Yong et al. (2000) as EHB stars with $T_{\rm eff}$ in the range 24–32 000 K, as confirmed by ground and space-borne (UIT and HST) observations (Liebert et al. 1994; Landsman et al. 1998).

3. OBSERVATIONS AND REDUCTIONS

In 2003 we started a specific observing program aiming at imaging a large field of NGC 6791 in the Johnson U and B passbands with the LRS FOSC camera at the 3.5 m Italian Telescopio Nazionale Galileo (TNG) at La Palma. Taking advantage of its 0.275 arcsec/px scale and its wide (9.4 × 9.4 arcmin) field of view, this imager allowed us to carry out a suitable (16×16 arcmin) and accurate (± 0.01 mag) survey of the cluster region. Resulting CMDs, based on 330 s B and 1200 s U exposures, are shown in Fig. 2. Data have been reduced with IRAF packages CCDRED, DAOPHOT, ALLSTAR and PHOTCAL, making use of the point spread function method (Stetson 1987).

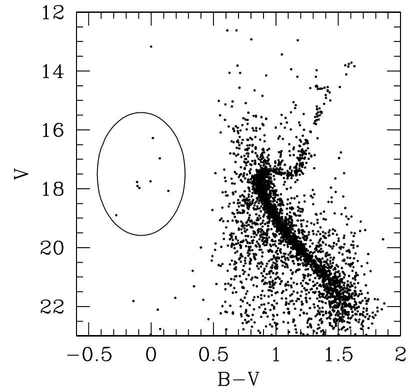

Fig. 1. The Kaluzny & Rucinski (1995) C-M diagram of NGC 6791, based on CCD photometry at the ESO 2.1 m telescope (only best photometric sample plotted here). Yong et al. (2000) provided a good fit to these data with a ([Fe/H], t) = (0.33 dex, 8 Gyr) model, predicting however a red HB morphology clumped about $(B - V) \simeq 1.3$, and clearly missing the eight hot (supposedly EHB) stars singled out in the plot.

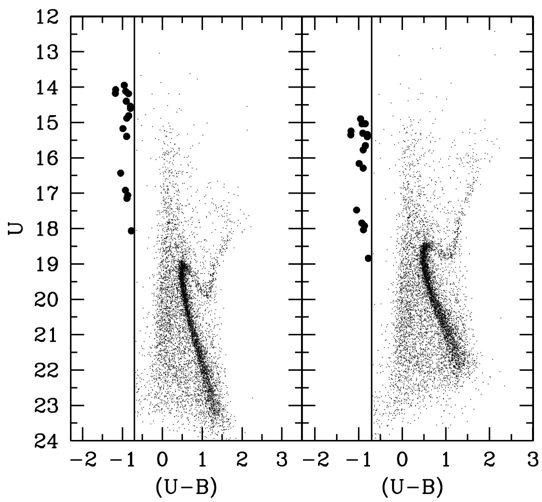

Fig. 2. Combined U vs. U–B and B vs. U–B diagrams of the field of NGC 6791 explored with TNG LRS. Big solid dots mark our 13 newly discovered UV-bright sources with U–B < −0.7 (vertical line) together with four objects (the clump about $U \sim 17$) including three member sdB and one sdO from the sample of faint blue stars by Kaluzny & Udalski (1992).

4. TOWARDS THE FUTURE

The analysis of Fig. 2 shows a cleanly detected sample of 13 new UV-bright objects, bluer than U–$B < -0.7$, and consistent with sdB/O stars, that sums up to the four EHB candidates (the clump of stars around $U \sim 17$) previously found in this color range by Kaluzny & Udalski (1992).*

Our current observational campaign, making use of several spectroscopic facilities at TNG and other telescopes, will provide us with both low- (∼ 10 Å FWHM) and mid- (∼ 6 Å) resolution spectra along the full optical range (3500–8000 Å) for these newly identified targets, assessing their cluster membership and, for those positive cases, allowing us to settle the effective temperature and surface gravity of each star by fitting the observed spectral energy distribution with the new

* Although about 2 mag brighter than the Kaluzny & Udalski (1992) candidates, our targets might still be consistent with an sdB/O classification, recalling the large spread in the bolometric correction to U and B magnitudes and the allowed temperature range compatible with the observed scatter in the U–B color (see Johnson 1966).

UVBLUE and BLUERED synthetic spectral libraries (Rodriguez-Merino et al. 2005; Bertone et al. 2003) of appropriate metallicity. Among others, such a complete sample of *bona fide* EHB stars will also provide a first reliable estimate of the lifetime and global UV energetic budget associated to the EHB evolution relying on the so-called "Fuel Consumption Theorem" of Renzini & Buzzoni (1986).

REFERENCES

Bertola F., Bressan A., Burstein D., Buson L. M., Chiosi C., di Serego Alighieri S. 1995, ApJ, 438, 680

Bertone E., Buzzoni A., Rodriguez-Merino L. H., Chavez M. 2003, in *Modelling of Stellar Atmospheres*, IAU Symp. 210, eds. N. E. Piskunov, W. W. Weiss & D. F. Gray, ASP, San Francisco

Bressan A., Chiosi C., Fagotto F. 1994, ApJS, 94, 63

Brown T. M. 2004, Ap&SS, 291, 215

Brown T. M., Ferguson H. C., Deharveng J.-M., Jedrzejewski R. I. 1998, ApJ, 508, L139

Brown T. M., Bowers C. W., Kimble R. A., Sweigart A. V., Ferguson H. C. 2000, ApJ, 532, 308

Brown T. M., Ferguson H. C., O'Connell R. W., Ohl R. G. 2002, ApJ, 568, L19

Buzzoni A. 1995, ApJS, 98, 69

Carraro G., Girardi L., Chiosi C. 1999, MNRAS, 309, 430

Code A. D. 1969, PASP, 81, 475

Dorman B., Rood R. T., O'Connell R. W. 1993, ApJ, 419, 596

Dorman B., O'Connell R. W., Rood R. T. 1995, ApJ, 442, 105

Friel E. D. 1995, ARA&A, 33, 381

Greggio L., Renzini A. 1990, ApJ, 364, 35

Johnson H. L. 1966, ARA&A, 4, 193

Kaluzny J., Rucinski S. M. 1995, A&AS, 114, 1

Kaluzny J., Udalski A. 1992, Acta Astron., 42, 29

King I. R., Bedin L. R., Piotto G., Cassisi S., Anderson J. 2005, AJ, 130, 626

Landsman W. Bohlin R. C., Neff S. G., O'Connell R. W., Roberts M. S., Smith A. M., Stecher T. P. 1998, AJ, 116, 789

Liebert J., Saffer R. A., Green E. M. 1994, ApJ, 107, 1408

O'Connell R. W. 1999, ARA&A, 37, 603

Park J.-H., Lee Y.-W. 1997, ApJ, 476, 28

Renzini A., Buzzoni A. 1986 in *Spectral Evolution of Galaxies*, eds. C. Chiosi & A. Renzini, Reidel, Dordrecht, p. 195

Rodriguez-Merino L. H., Chavez M., Bertone E., Buzzoni A. 2005, ApJ, 626, 411

Stetson P. B. 1987, PASP, 99, 191

Stetson P. B., Bruntt H., Grundahl F. 2003, PASP, 115, 413

Yong H., Demarque P., Yi S. 2000, ApJ, 539, 928

Baltic Astronomy, vol. 15, 53–60, 2006.

SPECTROSCOPIC SEARCH FOR BINARIES AMONG EHB STARS IN GLOBULAR CLUSTERS *

C. Moni Bidin[1,2], R.A. Mendez[2], S. Moehler[3], G. Piotto[1], A. Recio-Blanco[1,4] and Y. Momany[1]

[1] *Dipartimento di Astronomia, Universtitá di Padova, Vicolo dell'Osservatorio 2, 35122 Padova, Italy*

[2] *Departamento de Astronomía, Universidad de Chile, Casilla 36-D, Santiago, Chile*

[3] *Institut für Theoretische Physik und Astrophysik, Christan-Albrechts-Universität zu Kiel, D-24098 Kiel, Germany*

[4] *Observatoire de la Côte d'Azur, Dpt. Cassiopée, CNRS UMR 6202, B.P. 4229, F-06304 Nice, Cedex 04, France*

Received 2005 August 1

Abstract. We performed a spectroscopic search for binaries among hot horizontal branch stars in globular clusters. We present final results for a sample of 51 stars in NGC 6752 and preliminary results for the first 15 stars analyzed in M 80. The observed stars are distributed along all the HBs in the range $8000 \leq T_{\rm eff} \leq 32\,000$ K, and have been observed during four nights. Radial velocity variations were measured with the cross-correlation technique. We analyzed the statistical and systematic errors associated with the measurements in order to evaluate the statistical significance of the observed variations. No close binary system has been detected, neither among cooler stars nor among the sample of hot EHB stars (18 stars with $T_{\rm eff} \geq 22\,000$ K in NGC 6752). The data corrected for instrumental effects indicate that the radial velocity variations are always below the 3σ level of ~ 15 km s^{-1}. These results are in sharp contrast with those found for field hot subdwarfs, and open new questions about the formation of EHB stars in globular clusters and possibly of the field subdwarfs.

Key words: stars: horizontal branch – hot subdwarfs – binaries: spectroscopic – globular clusters: individual (NGC 6752, M 80)

1. INTRODUCTION

Although stellar evolution theory has successfully identified horizontal branch (HB) stars as post-core helium flash stars of low initial mass (Hoyle & Schwarzschild 1955; Faulkner 1966), we still lack a comprehensive understanding of their nature. There is a general agreement that the hottest HB stars (EHB) must have suffered a heavy mass-loss during their evolution, keeping only a thin envelope ($\sim 0.02\ M_\odot$), but their specific formation mechanism remains unclear. The bi-

---

* Based on observations with the ESO Very Large Telescope at Paranal Observatory, Chile (proposal ID 69.D-0682).

narity of EHB stars, as proposed by many authors (Mengel et al. 1976; Heber et al. 2002) can provide an explanation, since in a close binary system the mass-loss can be enhanced through a number of different binary evolution channels (Han et al. 2002). Binaries have been found to be very common among field subdwarf B-type stars (sdBs), considered to be the counterparts of the cluster EHB stars. Maxted et al. (2001) estimated that 69±9 % of sdB stars are close binaries with periods $P \leq 10$ days, and Han et al. (2003) by binary population synthesis techniques predicted a 76–89 % binary fraction. From the recent investigation of Morales-Rueda et al. (2003) it appears clear that close binaries with periods $P \leq 5$ days and semiamplitudes of the radial velocity variation $K \geq 50$ km s^{-1} are very common among sdBs. Nevertheless the binary scenarios, extensively investigated by Han et al. (2002), are not free from problems as shown by Lisker et al. (2005). Moreover a more recent survey of Napiwotzki et al. (2004) found a significantly lower binary fraction among the sdB sample (42 %), showing that we are still far from a full understanding of this kind of stars. With this contribution we investigate a sample of EHB stars in globular clusters, searching for evidence of the presence of close binaries among them.

2. OBSERVATIONS AND DATA REDUCTION

In the globular cluster NGC 6752 we selected 51 target stars from the photometric data of Momany et al. (2002). We chose to perform a more complete investigation distributing the sample along the entire HB, from cooler stars ($T_{\mathrm{eff}} \approx 8000$ K) to hot EHB stars ($T_{\mathrm{eff}} \geq 20\,000$ K), although our attention was focused toward the EHB sample among which we expected to find a high fraction of close binary systems. The targets were divided into three stellar fields for multiobject spectroscopy. The positions of the targets in the color-magnitude diagram of the cluster are shown in Figure 1. In Figure 2 we indicate their radial distribution with respect to the cluster center. The spectra were collected during four nights of observation (2002 June 12–15) at the VLT-UT4 telescope with the FORS2 spectrograph in MXU mode. During each night, up to two pairs of 1800 s exposures were obtained in each field with a grism 1400V+18 (0.5″ wide slits, 1.2 Å resolution), except in the third night in field A, where only one single exposure was acquired, and the first night in field C, where no observations were performed. In Table 1, the UT of the start of the pair of 1800 s exposures is shown.

Table 1. UT of the start of the exposures (hours and minutes).

Field	Night			
	12	13	14	15
A	8:43	2:44 3:56	9:34	7:47
B	5:55 6:59	5:08	8:33	8:58
C	–	8:04	6:39 7:33	6:36

Due to different positions of the slits on the mask, the spectra covered slightly different spectral ranges, but in each spectrum the Hβ line was always present, except for star 14 in field C, that has been excluded from our analysis.

The data reduction has been performed with standard MIDAS procedures, as described in detail in Moehler et al. (2004) and Moni Bidin et al. (2005). During the same observing run similar data were acquired also for 32 HB stars in M 80.

3. MEASUREMENTS

Radial velocity (RV) variations have been measured with the cross-correlation (CC) technique (Tonry & Davis 1979) with the *fxcor* IRAF task. Before coadding the single 1800 s exposures in pairs we performed a CC between them in order to verify that no significant RV variation had occurred. For every star each spectrum has been cross-correlated with all the others, performing 10 CCs for each star in fields A and B, and 6 in field C, covering different temporal intervals from one hour to 3.1 days.

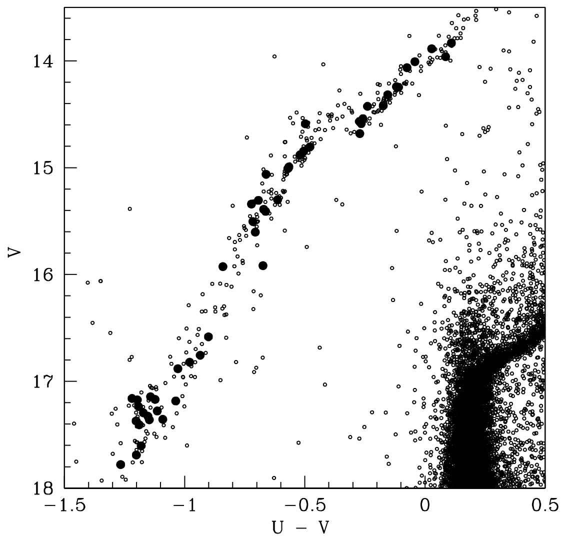

Fig. 1. Positions of the observed stars in the color-magnitude diagram of NGC 6752. Data from Momany et al. (2002).

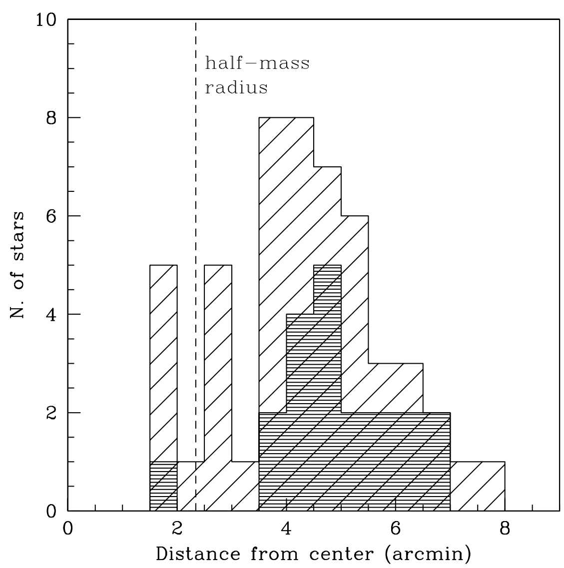

Fig. 2. Radial distribution of the observed stars. The dark shaded area indicates hot stars ($T_{\rm eff} \geq 20\,000$ K). The half-mass radius from Harris (1996) is also indicated.

Our analysis was focused on the Hβ line, cross-correlating the 4830–4890 Å spectral range. Nevertheless, all the measurements have been repeated also at other wavelengths, cross-correlating the entire spectra, with and without Hβ and Hγ when present in the spectral range. In each CC the position of the center of the cross-correlation function (CCF) has been determined with a Gaussian fit (for example, see Recio-Blanco et al. 2004 for a description of the procedure). In the measurements of hot stars it has been often impossible to cross-correlate the entire spectra without the Hβ line, and we selected spectral intervals with the strongest He lines instead, in order to minimize the noise included in the CC procedure and obtain a CCF with a clear peak. We also applied a Fourier filter of various shapes (Brault & White 1971) to the noisy spectra, obtaining always better CCFs but substantially unchanged results.

The [OI] 5577 Å sky line has been used as zero-point in order to correct the spectral shifts due to differences between lamp and star spectra.

We have been forced to correct the data for a systematic effect due to different positions of stars inside the slits in different nights. The effect was up to 10–12 $\mathrm{km\,s^{-1}}$. On the slit images (without grism), acquired just before each pair of exposures, we measured the position of the stars with respect to the center of the slit with a Gaussian fit of the stellar profile parallel to the dispersion direction. Then we translated the displacements between the frames to $\mathrm{km\,s^{-1}}$ with the instrumental relation 1 pixel = 38.2 $\mathrm{km\,s^{-1}}$ and applied them as corrections to the RV variations. A trend with Y position was evident, but with a certain scatter due to random errors, and we opted to derive the final corrections from the values obtained from the least-square solution of this relation, in order to avoid to introduce additional noise to the results.

This procedure gave corrections very similar to the RV variations measured, indicating both that the removal of the systematic effect had been successful and that the RV variations observed were due only to it.

We measured absolute RVs in order to check the cluster membership of our targets, by means of CCs with the template star HD 188112, a binary sdB star with known ephemeris (Heber et al. 2003). These RVs have undergone similar correction procedures as described before. The errors (1σ) of these measures are 6–10 $\mathrm{km\,s^{-1}}$. All the stars show an absolute RV in agreement with that of the cluster (–27.9 $\mathrm{km\,s^{-1}}$, Harris 1996) within 2σ and can be considered RV cluster members.

4. ERROR ANALYSIS

The detection of binary systems in our survey is strongly dependent on a proper estimate of the error budget. We performed an accurate analysis of all the sources of errors and estimated their values (σ). Finally, all the error sources have been combined in quadrature. The resulting errors are about 3–5 km $\mathrm{s^{-1}}$, with the exception of some measurements for hotter stars, where the low S/N sometimes increased the total error up to 7.5 km $\mathrm{s^{-1}}$. In Table 2 we summarize the contribution of each error source and the corresponding ranges (1σ). The CC error is evaluated directly from the CC theory (Tonry & Davis 1979).

Table 2. Estimates of errors.

Error	Range of values (km $\mathrm{s^{-1}}$)
$\sigma_{\rm CC}$	0.5-2 (Hβ) 1-5 (weak lines)
$\sigma_{\rm wlc}$	1.4-1.6
$\sigma_{\rm sky}$	1.5
$\sigma_{\rm disp}$	0.7-1.4
$\sigma_{\rm fit+ext}$	0.7-1.5 (cooler stars) 2.1-3.5 (hotter stars)

The wavelength calibration (wlc) error has been measured on the lamp images calibrated with the coefficients obtained in the wlc procedure, analyzing the position of nine bright lamp lines.

The errors introduced by the corrections for the sky line position, $\sigma_{\rm sky}$, and for the displacement of the star inside the slits, $\sigma_{\rm disp}$, have been estimated from the dispersion of the corrections around the least-square solution when plotted against the Y positions.

We identified two additional sources of errors: the choice of the "best fit" of CCF peak and the extraction of the spectra. In fact a different extraction can

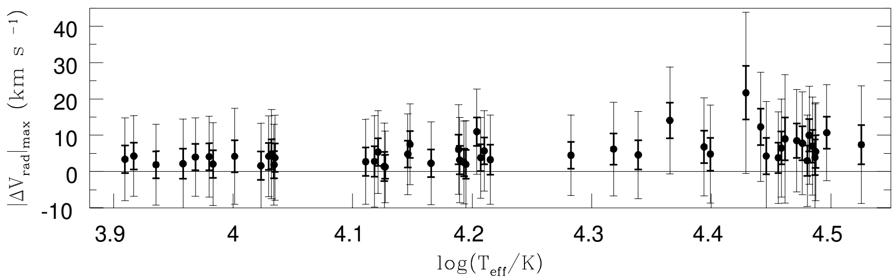

Fig. 3. Maxima of RV variations (in absolute value) measured in Hβ as a function of the temperature of the stars. The thick error bar indicates the 1σ interval, the thin one – 3σ.

cause a slightly different line profile; the CC procedure is sensitive enough to reveal it. In measurements on hot stars these have been identified as the main source of error. We evaluated them together extracting all the spectra a second time in a different manner and performing new measures in Hβ with different fits and, finally, measuring the dispersion $\sigma_{\rm fit+ext}$ of the differences between these new data and the previous ones. This error was strongly dependent on the S/N of the spectra. Then we divided the targets into two groups (stars cooler and hotter than $\sim 20\,000$ K).

5. RESULTS

5.1. Results from Hβ

In Figure 3 we summarize the results obtained from measurements in the Hβ wavelength range, where we obtained the most reliable data. All the RV variations are small, lower than 15 km s^{-1}, except for one star, and are never greater than the estimated 3σ interval. They are only slightly higher for hotter stars, but with larger errors due to decreasing S/N in the spectra. We therefore conclude that *none of the observed RV variations can be considered statistically significant*.

Star 15 in field A exhibited higher RV variations in the third night, and the higher datum plotted in the figure (21.7 km s^{-1}) refers to these measurements. We consider this result interesting but particularly dubious, because it was obtained in the only not-summed spectrum (a single 1800 s exposure, as mentioned before), where all the stars tended to show higher RV variations due to the increased noise, and a comparable variation is never seen in any of the other observing nights.

5.2. Results from other lines

The results from CCs involving the entire spectral range did not provide additional information, because they always repeated the results already obtained with Hβ. This is due to the sensitivity of CC technique to the stronger line, and the extreme difference in strength between Balmer and others lines in our spectra.

The results obtained with Hγ, when present in the spectra, always confirm the ones obtained in Hβ wavelength range. The differences are always lower than 10 km s^{-1}, with just a handful of exceptions in agreement with a Gaussian distribution given the evaluated σ value.

None of the variations measured with weak lines ever exceeds the evaluated

3σ value, confirming the previous conclusions. The measurements with weak metallic lines have given very good results for cooler stars, mainly in the range $11\,500 \leq T_{\rm eff} \leq 18\,000$ K due to the presence of many lines induced by radiative levitation of heavy elements (Glaspey et al. 1989; Behr 2003). In these cases the differences between the measured variations and the ones in Hβ are really small, always below 4 km s^{-1}. For hotter stars the low S/N and the lack of lines complicated the measurements, and the results are less reliable. Occasionally the difference reaches 30 km s^{-1}, but always in the sense of limiting the highest RV variations measured in Hβ and never emphasizing them. In fact, the stars, that show the highest variations in Figure 3, do not show great variation in these measurements.

5.3. Detection probability

In order to better understand our results, we calculated the probability of detecting a binary in our observations as a function of the period P. We assumed circular orbits and a mass of 0.5 $M_\odot$ for each component, in order to relate the semiamplitude of the RV variation to the period. These assumptions are representative of typical binary systems observed among field sdBs. We repeated the calculations assuming a companion of 0.1 $M_\odot$. Systems with a low-mass companion are a minority among field sdBs, but their presence is well established. Our survey is not sensitive enough for this kind of systems, except for the shortest periods, and from our results we cannot draw interesting conclusions about them. The probabilities are shown in Figure 4 (the solid line for a 0.5 $M_\odot$ companion and the dotted line – for 0.1 $M_\odot$).

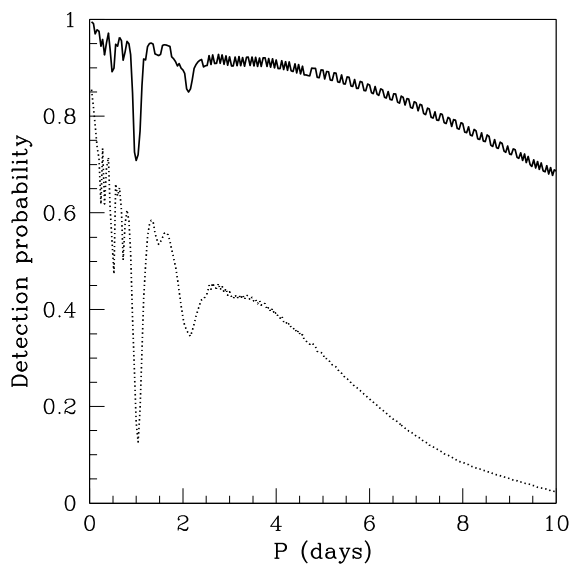

Fig. 4. Probability of detecting a binary in our observations.

5.4. Results for M 80

Since this is a work in progress we are still unable to show a plot similar to Figure 3 for the stars observed in M 80. Nevertheless we can point out that the preliminary analysis of the first 15 stars in this cluster gives the results similar to what obtained in NGC 6752. The variations are small, the highest values being around 20 km s^{-1}. Only two RV variations exceed 15 km s^{-1}, similarly to what was observed in NGC 6752. It must be emphasized that the results on M 80 are going to be less significant than in the case of NGC 6752 both because the stars are much fainter and the errors are larger, and because strong wind from north during the observing run prevented us from observing this cluster in the first two nights, so that the detection probability is reduced. We evaluated a loss of sensitivity of about 20–25 % for periods up to 5 days (compared to that in NGC 6752), which, for longer periods, drops rapidly to very low values.

6. CONCLUSIONS

The results shown in Figure 3 indicate that there is no close binary system in our sample, neither among cooler stars, nor among EHB targets. All the RV variations are within the estimated errors and are significantly lower than what expected. In the compilation of Morales-Rueda et al. (2003) for all field binary sdB stars with known periods, the RV semi-amplitudes are always greater than 30 km s^{-1}. These binary systems would be easily detectable in our survey. If the binary fraction of EHB stars in NGC 6752 were 69 %, as found by Maxted et al. (2001) in the field, we would expect that 13±2 of our 18 stars with $T_{\rm eff} \geq 22\,000$ K should be binaries. According to the period distribution found by Morales-Rueda et al. (2003) 80 % of them should have $P \leq 5$ days, and thus 9±2 binary systems should have been detected in our sample. The absence of evidence of their presence is in sharp contrast with these previous results, and can indicate a significant difference between sdB stars in and outside globular clusters.

In conclusion, most of the EHB stars in NGC 6752, and possibly in M 80, are not close binaries. These results pose a number of problems. First of all, we are forced to conclude that the dominant mechanism for the formation of these stars in globular clusters does not involve the interactions within a close binary system. Although the high close binary fraction among field sdBs indicates that binary interactions can play an important role, our results on the EHB stars in NGC 6752 indicate that there must be other mechanisms at work.

It is possible that in GCs there are different formation channels of EHB stars with respect to the main ones in the field. For example, dynamical evolution of GCs could remove the primordial binaries able to produce sdB stars, at least in the inner part of the cluster. This is an interesting possibility, which has already been proposed also to explain why the frequency of blue stragglers (BSs) in GCs is significantly smaller than the frequency of field BSs (Piotto et al. 2004), and the anticorrelation between the frequency of BSs in GC cores and the GC total mass (Davies et al. 2004). At the same time, the GC environment can favor different formation mechanisms for the EHB stars, like close encounters and collisions among stars (at least in the cluster cores), or even more complex scenarios like the ones proposed to explain the anomalous double main sequence population in Omega Centauri (Bedin et al. 2004 and Piotto et al. 2005) and in NGC 2808 (D'Antona et al. 2005). Apparently, in these two clusters, a second generation of stars could have formed from material polluted by SNe and/or intermediate mass AGB star ejecta. These stars have an enhanced He content and could explain the presence of the EHB in both clusters.

An extended survey of the presence of close binaries among cluster EHB stars, from the inner core to the outskirts of NGC 6752, and of the presence of binaries with low companions or with longer (100 days or so) periods in NGC 6752 and other clusters with EHBs, is absolutely needed in order to test the hypothesis of the environment effects on the main production channels of these stars.

We note also that Peterson et al. (2002) reported a high fraction of binaries among the same type of stars in the same cluster, but Peterson (priv. comm.) also pointed out that their sample is mainly located in the outer regions of the cluster.

In concluding this brief discussion, we note that Napiwotzki et al. (2004) suggested that the low binary fraction among field sdBs found in their survey could be due to contamination of the sample by halo and thick disk stars, absent in Maxted et al. (2001) sample since it included only bright (thin disk) stars. On average, our cluster EHB stars are expected to be older and possibly more metal-poor than the Napiwotzki et al. sample, and apparently, the fraction of binaries among them is even smaller than among thick disk-halo sdBs, suggesting a possible dependence on ages or metallicities or on a combination of these parameters.

ACKNOWLEDGMENTS. C.M.B. and R.A.M. acknowledge support by the Chilean Centro de Astrofísica FONDAP (No. 15010003). G.P. acknowledges support by MIUR, under the program PRIN03.

REFERENCES

Bedin L. R., Piotto G., Anderson J. et al. 2004, ApJ, 605, L125

Behr B. B. 2003, ApJS, 149, 67

Brault J. W., White O. R. 1971, A&A, 13, 169

D'Antona F., Bellazzini M., Caloi V. et al. 2005, ApJ, 631, 868

Davies M. B., Piotto G., De Angeli F. 2004, MNRAS, 349, 129

Faulkner J. 1966, ApJ, 144, 978

Glaspey J. W., Michaud G., Moffat A. F. J., Demers S. 1989, ApJ, 339, 926

Han Z., Podsiadlowski P., Maxted P. F. L., Marsh T. R., Ivanova N. 2002, MNRAS, 336, 449

Han Z., Podsiadlowski P., Maxted P. F. L., Marsh T. R. 2003, MNRAS, 341, 669

Harris W. E. 1996, AJ, 112, 1487

Heber U., Edelmann H., Lisker T., Napiwotzki R. 2003, A&A, 411, L477

Heber U., Moehler S., Napiwotzki R., Thejll P., Green E. M. 2002, A&A, 383, 938

Hoyle F., Schwarzschild M. 1955, ApJS, 2, 1

Lisker T., Heber U., Napiwotzki R. et al. 2005, A&A, 430, 223

Maxted P. F. L., Heber U., Marsh T. R., North R. C. 2001, MNRAS, 326, 1391

Mengel J. G., Norris J., Gross P. G. 1976, ApJ, 204, 488

Moehler S., Sweigart A. V., Landsman W. B., Hammer N. J., Dreizler S. 2004, A&A, 415, 313

Momany Y., Piotto G., Recio-Blanco A. et al. 2002, ApJ, 576, L65

Moni Bidin C., Moehler S., Piotto G. et al. 2005, A&A, submitted

Morales-Rueda L., Maxted P. F. L., Marsh T. R., North R. C., Heber U. 2003, MNRAS, 338, 752

Napiwotzki R., Karl C. A., Lisker T. et al. 2004, Ap&SS, 291, 321

Peterson R. C., Green E. M., Rood R. T., Crocker D. A., Kraft R. P. 2002, in *Omega Centauri, a Unique Window into Astrophysics*, ASP Conf. Ser., 265, 255

Piotto G., De Angeli F., King I. R. et al. 2004, ApJ, 604, L109

Piotto G., Villanova S., Bedin L. R. et al. 2005, ApJ, 621, 777

Recio-Blanco A., Piotto G., Aparicio A., Renzini A. 2004, A&A, 417, 597

Tonry J., Davis M. 1979, AJ, 84, 1511

Baltic Astronomy, vol. 15, 61–64, 2006.

NGC 6121-V46: A LOW-MASS DOUBLE DEGENERATE ELLIPSOIDAL VARIABLE IN A GLOBULAR CLUSTER

S. J. O'Toole[1], R. Napiwotzki[2], U. Heber[1], H. Drechsel[1], S. Frandsen[3], F. Grundahl[3] and H. Bruntt[4]

[1] *Remeis-Sternwarte Bamberg, Astronomisches Institut der Universität Erlangen-Nürnberg, Sternwartstrasse 7, D-96049 Bamberg, Germany*

[2] *Centre for Astrophysics Research, University of Hertfordshire, Hatfield AL10 9AB, U.K.*

[3] *Department of Physics and Astronomy, University of Aarhus, Ny Munkegade, DK-8000 Aarhus C, Denmark*

[4] *Niels Bohr Institute, Juliane Maries Vej 30, DK-2100 Copenhagen Ø, Denmark*

Received 2005 August 1

Abstract. The variable sdB known as V46 in the globular cluster M 4 has remained enigmatic since its discovery almost 10 years ago. We present here radial velocity measurements obtained from medium-resolution VLT/FORS2 spectra that show variations at twice the period of the luminosity changes. This implies that the system is an ellipsoidal variable. Unlike the other sdB binaries of this nature, the fundamental parameters of this star we derive suggest that it lies below the Zero Age Extreme Horizontal Branch. From the cluster distance and the gravity we determine the mass of V46 to be $\sim$0.19 $M_\odot$. This is too low to sustain core helium burning. From the mass function we derive a lower limit for the companion of only 0.26 $M_\odot$. We discuss the star's origin in the context of close binary evolution in the field and globular clusters.

Key words: stars: variable: general – stars: individual (NGC 6121-V46)

1. HISTORY AND MOTIVATION

It is now known that while the mass distribution of DA white dwarfs peaks at $\sim$0.6 $M_\odot$, there is also a subset of objects with masses $\leq$0.46 $M_\odot$ (Bergeron et al. 1992). Their low mass implies that they cannot ignite helium in their cores, and must have lost most of their envelope mass before reaching the tip of the red giant branch. The implication of this is that the stars must be in close binary systems, although recent results suggest that fewer than 50 % show radial velocity variations (Napiwotzki et al. 2005).

There are two kinds of known binaries containing helium-core white dwarfs (HeWDs): double degenerate systems, typically containing two low-mass white dwarfs (e.g., Nelemans & Tout 2005) and millisecond pulsar (MSP) systems. In the former case the lowest mass HeWD companion known has 0.31 $M_\odot$ (Marsh et al. 1995), while in the latter the masses are $\leq$0.2 $M_\odot$ (e.g., Callanan et al. 1998).

Recent discoveries suggest a link between HeWDs and a small subset of sdB stars. As part of a program to measure radial velocities of sdBs, Heber et al. (2003)

discovered that the apparently normal sdB HD 188112 lies below the Zero-Age Extreme Horizontal Branch (ZAEHB). The star's mass, determined from its trigonometric parallax, $T_{\rm eff}$ and $\log g$, to be only 0.24 $M_\odot$, is inconsistent with the lowest mass for the common envelope ejection model of Han et al. (2003). HD 188112 is a radial velocity variable with a minimum companion mass of 0.73 $M_\odot$, suggesting the primary is the progenitor of a helium core white dwarf, while the unseen companion is most likely a C/O white dwarf. Comparison with the evolutionary tracks of Driebe et al. (1998) supports this conclusion.

Since then, Liebert et al. (2004) have discovered another object lying below the ZAEHB. Comparison of the parameters of SDSS J123410.37-022802.9 (hereafter SDSS J1234) with the evolution tracks of Althaus et al. (2001) shows that this star has a mass in the range 0.18–0.19 $M_\odot$. Note that the mass is dependent on the evolution models adopted. A higher mass is found ($\sim$0.23 $M_\odot$) for SDSS J1234 when it is compared to the Driebe et al. tracks.

Kaluzny et al. (1997) discovered intensity variations with amplitude $\sim$1.9 % and period 1.045 h in the star now known as V46 in NGC 6121 (= M 4). The system was a puzzle from the beginning, with colors consistent with those of a cataclysmic variable, but no emission lines present in its spectrum. Mochejska et al. (2002) found that the spectrum is consistent with an sdB star. With the discovery of pulsations in sdB stars with periods of 0.75–2 hours (Green et al. 2003), it seemed possible that V46 was a member of this class. We therefore set out to clarify the object's nature.

2. IS IT AN EHB STAR?

A low resolution spectrum of V46 taken with the MMT was kindly provided by Janus Kaluzny. By means of Balmer line profile fitting we find $T_{\rm eff} = 16197 \pm 546$ K and $\log g = 5.75 \pm 0.108$; the star shows no helium lines. We used Detlev Koester's DA white dwarf grid (Finley et al. 1997) to derive these parameters. When we examine the position of V46 in the $T_{\rm eff}$ vs. $\log g$ plane (Figure 1), we find that it, like HD 188112 and SDSS J1234, lies below the ZAEHB. This means the star has not evolved via the EHB and strongly suggests that it too is the progenitor of a HeWD (similar to HD 188112).

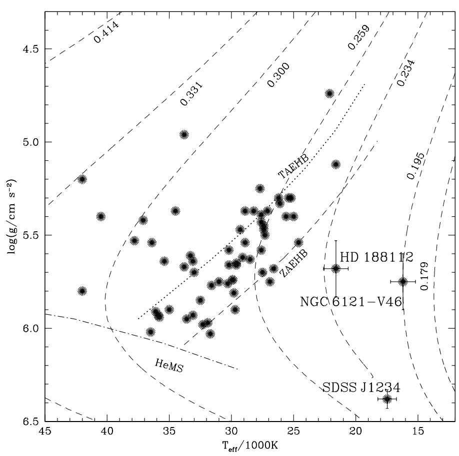

Fig. 1. Position of V46 in the $T_{\rm eff}$ vs. $\log g$ diagram.

If we consider the distance to the cluster M 4 (2.2 kpc, Rosenberg et al. 2000) and the surface gravity of V46, we find that it should have a mass of $\sim$0.19 $M_\odot$. In Figure 1 we show the post-RGB evolutionary tracks of Driebe et al. (1998) which suggest that V46 should have a mass of $\sim$0.195 $M_\odot$. This is very good agreement considering the uncertainties of the model physics, and is strong evidence that the star is a member of the cluster and not a foreground object. Using the VLT we have determined the nature of this system by measuring the radial velocity of V46.

3. THE NATURE OF NGC 6121-V46

We obtained 81 spectra with resolution ~2100 using VLT/FORS2 with the 1400V grating in service mode. The only line visible in the spectra is Hβ, and the resulting S/N per 4 min exposure was 10–15. We measured the radial velocity of Hβ by cross correlation with a model spectrum at the temperature and gravity derived above. The velocity curve is shown at the top of Figure 2, while the power spectrum is shown at the bottom. It was calculated by fitting the curve with a range of periods using χ^2 minimization. Based on this method, we measure the period and ephemeris to be HJD(T_0) = 2453134.496797+0.087159$\times E$, while the system velocity and semi-amplitude of the system are $\gamma = 31.3 \pm 1.6$ km/s and $K = 211.6 \pm 2.3$ km/s, respectively. Using this period and semi-amplitude we derive the mass function of the system to be $f(m) = 0.0855 \pm 0.0028\ M_\odot$. Taking the mass of the sdB to be 0.195 $M_\odot$, the minimum mass of the secondary is 0.26 $M_\odot$. We note that the period of the radial velocity variation is exactly twice that of the intensity variation, indicating that V46 is an ellipsoidal variable, similar to the previously known systems KPD 0422+5421 (Koen et al. 1998) and KPD 1930+2752 (Billéres et al. 2000; Maxted et al. 2000).

4. LIGHT CURVES

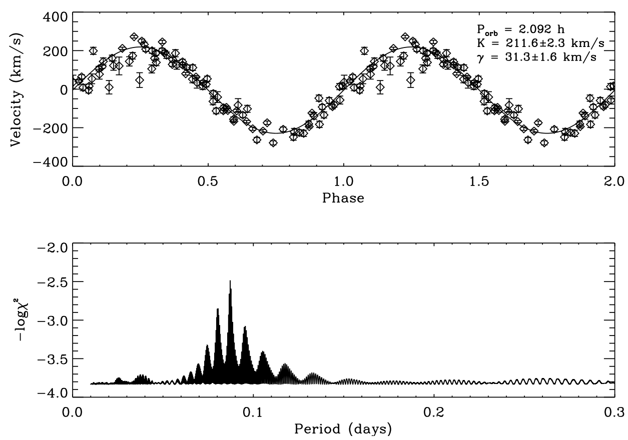

Fig. 2. Radial velocity curve and corresponding power spectrum of V46.

As well as a velocity curve, we have also obtained BVR light curves. These observations were made over April–June of 2001 to search for oscillations in red giants in M 4 (Bruntt 2003). They were obtained at the Danish 1.54 m at La Silla, Chile with DFOSC. We have attempted to determine the inclination angle of the system using a light curve analysis similar to that used for the sdB HS 2333+3927 (Heber et al. 2004). No eclipses have been detected. Due to the low amplitude of the ellipsoidal variations, the analysis is difficult. We kept the $T_{\rm eff}$ and mass of the sdB fixed at 16 200 K and 0.2 $M_\odot$, respectively, during the analysis, but could not find a unique solution. Even fixing the mass ratio arbitrarily at, e.g. $q = 3.0$, does not help. The fits from all solutions appear identical and have very similar χ^2 values. There must be a lower limit for the inclination since at some angle the deformation of the sdB will no longer be visible. To find this limit, we first set $q = 6.0$ and then decreased it in steps of 1.0. Again no unique solution could be found, meaning that unfortunately the light curves cannot place any constraints on the system. Nevertheless we can conclude that the companion must be a white dwarf, because the variations are ellipsoidal in nature and there is no sign of a reflection effect. The latter would be expected if it were a low-mass main-sequence star.

5. IMPLICATIONS

Despite not being able to constrain the inclination of the V46 system, we can still discuss the implications of its existence for close binary formation in globular clusters. Hansen et al. (2003) discussed low-mass HeWDs in globular clusters from a theoretical standpoint, and found that for the population of these stars in the core of NGC 6397 the companions are most likely C/O white dwarfs and not neutron stars. The likelihood of the companion of V46 being a neutron star is not high, since the inclination angle of the system would have to be $\leq 26°$, and there has been no detection at radio wavelengths of any neutron star in M 4 other than PSR B1620-26 (Lyne et al. 1988). We suggest therefore that V46's companion is either a C/O or HeWD. At the most probable inclination of 52° the mass of the companion is $\sim$0.40 $M_\odot$, making it an object with a helium core. We also point out that V46 lies outside the central part of M 4; more massive objects are expected to settle towards the core of a globular cluster.

REFERENCES

Althaus L. G., Serenelli A. M., Benvenuto O. G. 2001, MNRAS, 323, 471
Bergeron P., Saffer R. A., Liebert J. 1992, ApJ, 394, 228
Billéres M., Fontaine G., Brassard P. et al. 2000, ApJ, 530, 441
Bruntt H. 2003, PhD dissertation, University of Aarhus
Callanan P. J., Garnavich P. M., Koester D. 1998, MNRAS, 298, 207
Driebe T., Schönberner D., Blöcker T., Herwig F. 1998, A&A, 339, 123
Finley D. S., Koester D., Basri G. 1997, ApJ, 488, 375
Green E. M., Fontaine G., Reed M. D. et al. 2003, ApJ, 583, L31
Han Z., Podsiadlowski P., Maxted P. F. L., Marsh T. R. 2003, MNRAS, 341, 669
Hansen B. M. S., Kalogera V., Rasio F. A. 2003, ApJ, 586, 1364
Heber U., Drechsel H., Østensen R. et al. 2004, A&A, 420, 251
Heber U., Edelmann H., Lisker T., Napiwotzki R. 2003, A&A, 411, L477
Kaluzny J., Thompson I. B., Krzeminski W. 1997, AJ, 113, 2219
Koen C., Orosz J. A., Wade R. A. 1998, MNRAS, 300, 695
Liebert J., Bergeron P., Eisenstein D. et al. 2004, ApJ, 606, L147
Lyne A. G., Biggs J. D., Brinklow A., McKenna J., Ashworth M. 1988, Nature, 332, 45
Marsh T. R., Dhillon V. S., Duck S. R. 1995, MNRAS, 275, 828
Maxted P. F. L., Marsh T. R., North R. C. 2000, MNRAS, 317, L41
Mochejska B. J., Kaluzny J., Thompson I., Pych W. 2002, AJ, 124, 1486
Nelemans G., Tout C. A. 2005, MNRAS, 356, 753
Rosenberg A., Piotto G., Saviane I., Aparicio A. 2000, A&AS, 144, 5

Baltic Astronomy, vol. 15, 65–68, 2006.

DO EC 14026 STARS EXIST IN CLUSTERS?

M. D. Reed[1], D. Kilkenny[2] and D. M. Terndrup[3]

[1] *Missouri State University, Springfield, MO 65804, U.S.A.*

[2] *South African Astronomical Observatory, Cape Town, South Africa*

[3] *The Ohio State University, 140 W. 18th Avenue, Columbus, OH 43210, U.S.A.*

Received 2005 August 1

Abstract. We have began a program to search for pulsating sdB stars in open and globular clusters. Detection of pulsators in clusters would aid the understanding of their evolution, since the masses and metal content of the main-sequence progenitors would be known. Here we describe the beginning of our search during which we plan to observe about 100 sdB stars. A failure to detect any pulsators would suggest differences between sdB stars in clusters and in the field of the Milky Way (e.g., metallicity, binarity) which would need to be taken into account by any pulsation/evolution scenario.

Key words: stars: AGB and post-AGB, variable: general – clusters: individual (NGC 6791, NGC 188, NGC 6571, M 13, M 15, NGC 2808)

1. OBSERVATIONS AND ANALYSIS

To date we have observed more than 50 stars during 54 short data runs. Data were obtained for the open clusters using McDonald Observatory's 2.1 m telescope and for the globular clusters using the MDM Observatory's 2.4 m and the SAAO 1.9 m telescopes. All data were obtained using high-speed CCDs and processing was done using standard IRAF routines.

Differential light curves were produced using MOMF (Kjeldsen & Frandsen 1992). The accuracy of the photometry depended on several factors including the signal-to-noise (brightness) of the target and comparison stars, the number of available comparison stars, and of utmost importance for globular cluster fields, the seeing and how crowded the fields are compared to the resolution. A selection of some of the light curves and temporal spectra for sdB stars in NGC 6752 are provided in Figures 1 and 2. The dotted lines in Fig. 2 is the detection threshold discussed below.

Limits on time-series photometry can be a bit tricky as even noisy data can result in relatively flat temporal spectra (Howell 1992; Breger et al. 1994). To quantify the detection limits of our data, we used the 4σ approach of Breger et al. (1994). However, it is actually easier to detect pulsations than it might seem as during short data runs, the power can combine into unresolved peaks. (Likewise, unresolved pulsations can also cancel each other during a "beat.") For example, the highest amplitude mode of the known pulsator Feige 48 is about 5 mma when

Table 1. Detection limits for the target stars. Column 1 gives the star designation, column 2 the 4σ limit and column 3 indicates the percentage of (24) known pulsators that would be detectable at our threshold limit.

Target	Limit (mma)	%	Target	Limit (mma)	%	Target	Limit (mma)	%
				NGC 6791				
B3	3.9	92	B5	5.8	75	B9	4.6	92
B4	4.8	92	B6	3.0	92	B10	3.2	92
				NGC 188				
II-91	3.1	92	D702	1.9	96			
				NGC 1904				
Hill11	3.1	92	Hill34	3.1	92	Hill70	1.9	96
				NGC 2808				
6022	3.1	92	6816	1.9	96	6849	2	20
8750	3.1	92	9301	1.9	96	9863	2	20
14040	3.1	92	18899	1.9	96			
				ω Cen				
10123	3.1	92	C521	1.9	96	BC77702	4	20
D16003	3.1	92						
				NGC 6752				
S3616	3.0	92	S23768	2.2	92	S3936	2.0	96
S3422	2.5	92	S23665	2.0	96	S24268	2.0	96
S31695	3.0	92	S23407	5.0	75	S5610	4.5	92
S30963	3.2	92	S12087	7.0	58	S23975	25	8
S3008	2.8	92	S11517	3.9	92	S5719	14	25
S29988	3.0	92	S9135	3.0	92	S27622	3.8	92
S29704	2.2	92	S7935	3.0	92	S6224	3.3	92
S28234	3.5	92	S7860	4.3	92	S28073	2.0	92

resolved, but typically appears close to 8 mma in nightly runs that do not resolve the pulsations. Therefore, we examined our own observations of known sdBV stars, as well as those of the literature to estimate pulsation amplitudes of known sdBV stars from 2 hour data runs. This provides two detection limits:

(1) the 4σ limit, and

(2) a "likelihood" that we would detect pulsations. The percentage of known pulsators that would be detected at our 4σ limit from a 2 hour data run (of 24 known sdBV stars). These values are given in Table 1 and show that we are far more likely to have detected pulsations, were they occurring, than to have missed them for the majority of our targets.

2. RESULTS

Though this is a work-in-progress, we have already made significant progress and achieved some success. We have observed more than half of our goal of 100 stars, but have yet to ensure that all targets have appropriate temperatures and gravities for EC 14026-type pulsators. We have also not completed our photometry and analysis, yet are already aware that some stars will not have useful detection limits. During the 2004 January SAAO observing run, we became aware that

NGC 2808 was too faint for the seeing conditions and scampered for back-up targets. These stars were chosen on the basis of color, so should be EHB stars, but may not be sdB stars. In contrast, during our 2004 July SAAO observing run, the seeing was excellent and we obtained useful limits for nearly every target star on our list.

At this point in our analysis, we have not detected any pulsating stars, but it is too early to determine how significant our non-detection is. Yet we can state with some certainty that previously suspected open cluster pulsators B5 and D702 (Yong et al. 1998; Bailyn 1998) do not pulsate. We also examined our data for PG 1716-type pulsations. However, our observing runs were typically too short to discern, with any accuracy, whether or not such variations exist. In no case did we detect long period variations, even though the star B4 is known to vary with a period near 19 hours; far too long for us to detect. (However, for contrast we refer readers to the paper by Kilkenny et al. (2006) where a PG 1716-type pulsator *was* detected with just 2 hours of data!)

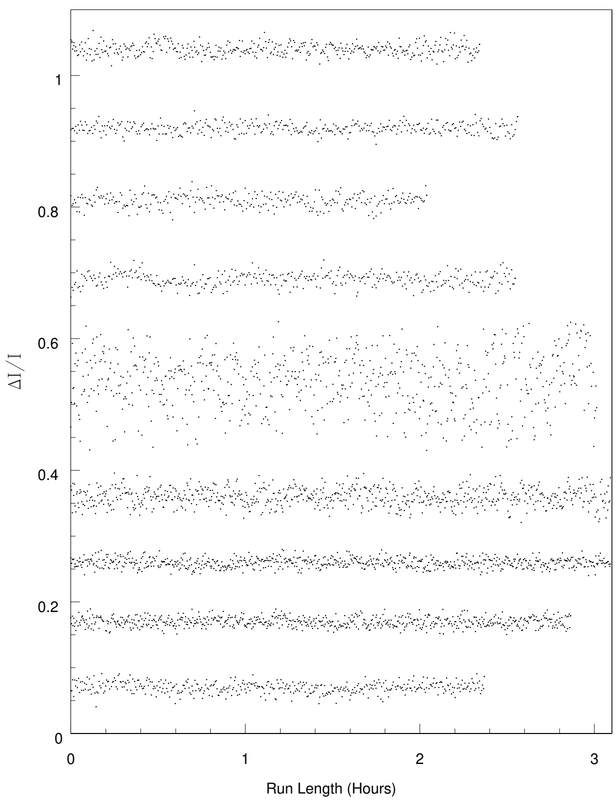

Fig. 1. Sample light curves for nine stars in NGC 6752 observed from SAAO.

Our efforts have been somewhat hampered by the fact that most of our targets are in the Southern Hemisphere, yet telescope time is very difficult to obtain there. The SAAO 1.9 m, though readily available and an excellent telescope, is a bit too small for most clusters while 4 m telescopes either lack appropriate instrumentation (CTIO) or are heavily constrained by queue schedules and allocation procedures (ESO).

ACKNOWLEDGMENTS. The Authors gratefully acknowledge Dr. Sabine Moehler for her finding charts for nearly all of our targets. This material is based upon work supported by the National Science Foundation under Grant No. 0307480. Any opinions, findings, and conclusions or recommendations expressed in this material are those of the author(s) and do not necessarily reflect the views of the National Science Foundation.

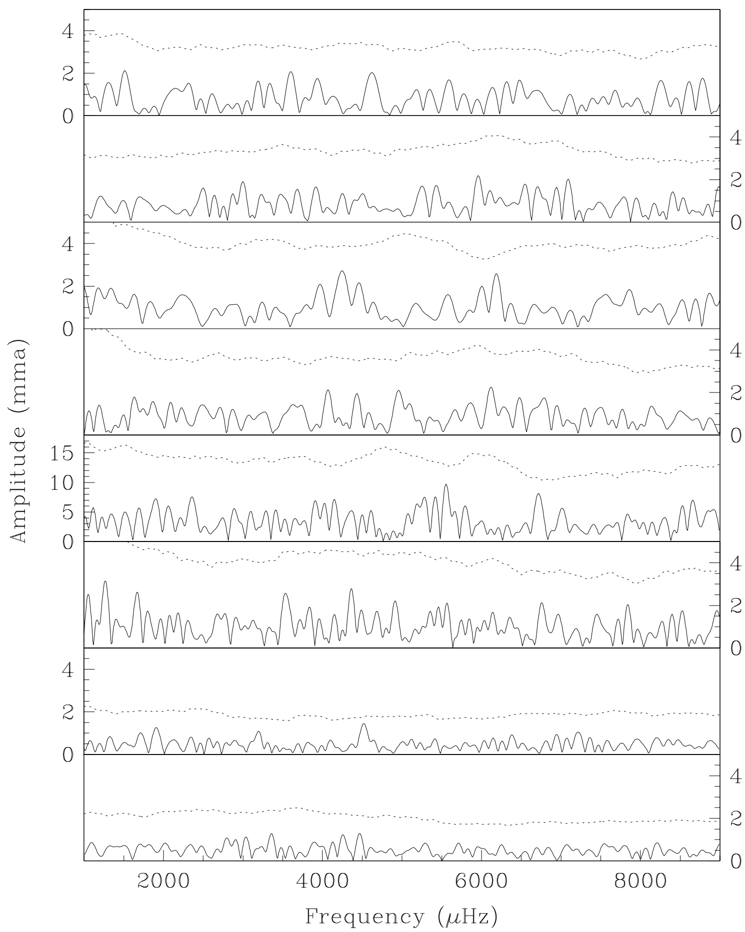

Fig. 2. Fourier transforms of the light curves in Fig. 1. Dashed lines are the 4σ detection limit.

REFERENCES

Bailyn C. D. 1998, private communication

Breger M., Ostermann W. M., Shi-Yang J. 1994, A&A, 289, 162

Howell S. B. 1992, in *Astronomical CCD Observing and Reduction Techniques*, ed. S. B. Howell, ASP Conf. Ser., 23, 105

Kilkenny D., O'Donoghue D., Reed M. D. et al. 2006, Baltic Astronomy, 15, 317 (these proceedings)

Kjeldsen H., Frandsen S. 1992, PASP, 104, 413

Yong H., Bailyn C. D., Demarque P. 1998, BAAS, 193.6403

Baltic Astronomy, vol. 15, 69–76, 2006.

HOT SUBDWARFS FROM LOW-DISPERSION SURVEYS – METHODS OF EXTRACTION AND AUTOMATIC ANALYSIS

C. Winter C. S. Jeffery A. Ahmad and D. R. Morgan
Armagh Observatory, College Hill, Armagh BT61 9DG, Northern Ireland

Received 2005 August 1

Abstract. We present our first attempts to construct an automatic system for extracting and analysing hot subdwarf spectra from a large set of unknown, low-resolution spectra. The first element in this system is a filtering technique, based on Principal Components Analysis (PCA), which is used to extract hot subdwarf candidates from the unknown data. We field-test the PCA filter on a test data set obtained from the SDSS, and initial results are illuminating. The second element in the system is an automatic pipeline for providing spectral classification and parameterisation of hot subdwarf candidates. Classification is carried out by an artificial neural network, and parameterisation by a χ^2 minimiser over a set of LTE model atmospheres. We combine both elements to extract and analyse a set of 282 hot subdwarf candidates obtained from the SDSS. As such, this work is the first step toward constructing a fully automated tool for analysing large data sets.

Key words: methods: data analysis – methods: numerical – stars: fundamental parameters – stars: subdwarfs – stars: Hertzsprung-Russell (HR) and C-M diagrams

1. INTRODUCTION

Modern digital sky surveys, such as the Sloan Digital Sky Survey (SDSS), are able to produce extremely large data sets which contain observations of millions of objects. To extract and process data of relevance to a particular line of research in a time-efficient manner requires the astronomer to employ automated methods to help sift through the soup of objects not necessarily of interest and then analyse any resulting candidate objects.

As such, we are attempting to construct an automated filtering tool to assist in locating hot subdwarf candidates from any set of low-dispersion spectra. These will then be submitted to an automated analysis pipeline from which classifications and physical parameterisations are derived.

The filtering tool is based around the multivariate statistical technique called Principal Components Analysis (PCA) which can be used to identify patterns in an N-dimensional data set. Our intention is to employ PCA as a coarse spectral classifier to distinguish between hot subdwarf-like objects, and objects/data of little interest, e.g., white dwarfs, QSOs, incomplete or low SNR exemplars. As a test, we apply the tool to a sample of spectra obtained from the SDSS.

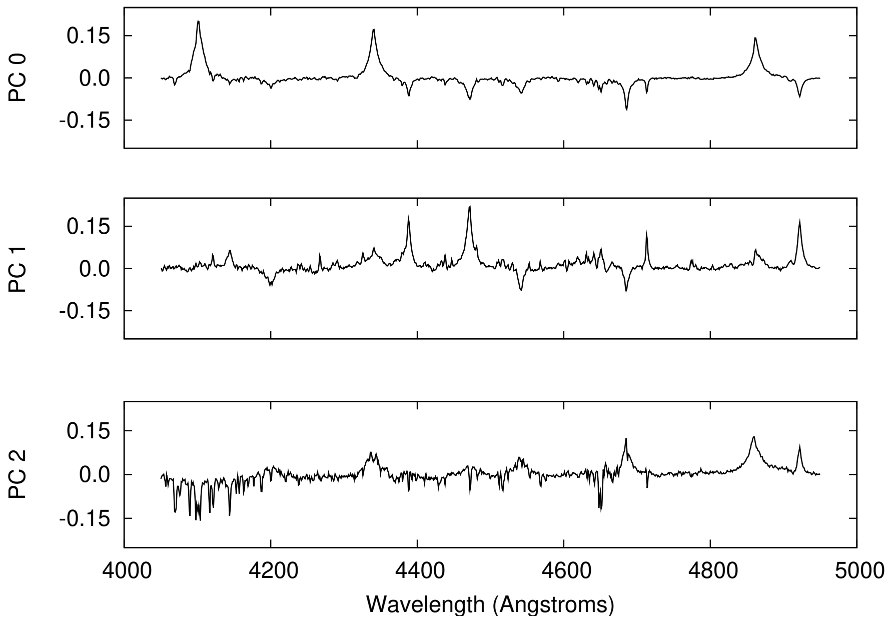

Fig. 2. First three principal components. Eigenfluxes are plotted against wavelength.

The automated analysis pipeline will allow us to gain insight into large volumes of spectra in a short amount of time. At present, the pipeline accepts a quantity of spectra, prepares them for analysis, and simultaneously feeds them to an artificial neural network (ANN), which has been trained to perform classifications using the Drilling et al. (2005) system, and a spectral optimisation toolkit which determines physical parameters by fitting each spectrum to a grid of LTE model atmospheres. Herein, we present the first application of the automated pipeline to a collection of 282 hot subdwarf candidates extracted from the SDSS with the aid of the PCA filter.

2. PRINCIPAL COMPONENTS ANALYSIS FILTER

2.1. Background

The basic idea behind PCA is to describe the variation of an N-dimensional data set in terms of a set of uncorrelated variables, each of which is a mutually-orthogonal linear combination of the original variables. Geometrically speaking, PCA is a rotation and scaling of a data set onto a new set of orthonormal vectors. The vectors (principal components) represent the directions of greatest variance in the data, and are a natural means for classifying the data set. If the first few vectors account for most of the variance in the original data, then they can be used to summarise the data with little loss of information – thus a reduction in dimensionality is achieved.

Technically, the principal components (PCs) are found by calculating the eigenvectors of the covariance matrix of an N-dimensional data set. A complete derivation of the technique can be found in, e.g., Murtagh & Heck (1987).

PCA has been applied on several occasions to the classification of astronomical spectra. Deeming (1964) applied the technique to stellar spectral classification, Connolly et al. (1995) used it to classify galaxy spectra, and Francis et al. (1992) applied it to the classification of quasar spectra. The dimensionality reduction capabilities of PCA have been used in conjunction with artificial neural networks, for example, Storrie-Lombardi et al. (1994).

2.2. Filter construction

We construct our PCA-based filter from the set of hot standards used in the classification system of Drilling et al. (2005). The spectra, which are at a resolution of 2.5 Å, were velocity corrected and resampled onto a uniform wavelength grid of 4050–4950 Å at a dispersion of 1 Å per pixel before performing the PCA. The first three of the derived PCs are shown in Figure 1. One can immediately notice that the first PC (PC 0) distinguishes between H and He lines. The second PC (PC 1) differentiates between He I and He II. This reification makes sense as it is the hydrogen and helium lines which vary most across all of the Drilling et al. (2005) spectra. Weaker lines, and uncorrelated features, such as noise, are distributed across the remaining less significant PCs. The first three derived PCs account for 69% of the variance present in the set of hot standards, and we use them to summarise the data set and to construct our filter.

If we consider the $(3 \times n)$ matrix, $\mathbf{E}$, of these eigenvectors, we can find the 3-dimensional projection vector, $\mathbf{p}$, of a spectrum projected onto the PCs by,

$$\mathbf{p} = \mathbf{x} \cdot \mathbf{E}, \tag{1}$$

where $\mathbf{x}$ is a vector of fluxes of dimension n.

Using the projection vector, we can then derive a reconstructed version of the original spectrum, $\mathbf{x_{rec}}$ by,

$$\mathbf{x_{rec}} = \sum_{k=1}^{k=3} p_k \mathbf{e}_k, \tag{2}$$

where p_k is the k^{th} element of the projection vector, $\mathbf{p}$, and $\mathbf{e}_k$ is the k^{th} eigenvector stored in matrix $\mathbf{E}$. The RMS error between $\mathbf{x}$ and $\mathbf{x_{rec}}$ can be used to differentiate between unknown stars which are most like the Drilling et al. (2005) hot standards, and those objects which we wish to discard.

2.3. Test application

We have applied the PCA filter to a test sample of ∼4600 spectra from the SDSS Data Release 3 database. Our selection criteria naively rely upon the classifications assigned automatically by the SDSS reduction pipeline. The SQL query used is as follows:

```
SELECT s.plate, s.mjd,s.fiberid
FROM BESTDR3..SpecPhotoAll as s
WHERE s.specClass = dbo.fSpecClass('STAR')
AND (s.primTarget & (dbo.fPrimTarget('TARGET_STAR_BHB')
     + dbo.fPrimTarget('TARGET_STAR_SUB_DWARF')) > 0)
AND (s.objType = 2)
```

Each spectrum was velocity corrected using the redshift as derived by the SDSS spectroscopic processing pipeline and stored in the FITS file header, and subsequently resampled onto the same wavelength grid as the Drilling et al. (2005) hot standards before being reconstructed by the PCA filter.

At present, the reconstruction filter is successful in filtering out objects with spectroscopic features that differ significantly from those of the hot subdwarfs, e.g., the white dwarfs in our test sample, or incomplete spectra.

The filter also allows a SNR threshold to be determined beyond which all samples can be discarded on the principle that they are too noisy for further analysis. Unfortunately, the filter does not readily allow the extraction of objects that are spectroscopically similar to subdwarfs but which contain small, yet important, differences that set them apart somehow. For instance, the test data sample, because it was selected based on the automatic classifications given by the SDSS (which are not very precise), contained many A- and F-type BHB stars which were clearly not subdwarfs because of very strong Balmer lines and the appearance of metal lines, and also other objects with weaker Balmer lines but containing the molecular G-band.

In calculating the reconstruction error of such spectra, the simple RMS error measure is not sensitive enough to allow small differences to influence the final error value in any meaningful way. The error calculation could be enhanced perhaps by introducing a weighting scheme, however, although these stars may have much in common with subdwarfs spectroscopically, they are very dissimilar photometrically and can be avoided easily by searching the SDSS by color.

3. AUTOMATED ANALYSIS PIPELINE

3.1. Outline

The input for our analysis pipeline comes from the PCA filter described in the previous section. The filter does still admit a number of false positives at this stage, so a manual inspection of the data is necessary.

Candidate spectra are subjected to a data preparation stage. The SDSS continuum fitting procedure does not do a great job in most cases, so we renormalise the calibrated spectra using a cubic spline fitting algorithm. The normalised spectra are then resampled onto a uniform wavelength grid of 4050–4950 Å, at a dispersion of 1 Å per pixel, ready for further analysis.

Classification is performed by an artificial neural network (ANN) which has been trained to classify onto the system defined by Drilling et al. (2005). This is an MK-like system which extends and refines the earlier work of Drilling (1996) and Jeffery et al. (1997) – it defines a spectral type (analogous to MK spectral classes), luminosity class and a helium class based on H, He I and He II line strengths. The ANN can classify onto this system with approximate errors (1σ) of ± 2 subtypes for spectral type, ± 1 subclass for luminosity class, and ± 4 subclasses for the helium class.

Physical parameters ($T_{\rm eff}$, $\log g$, $\log(n{\rm He}/n{\rm H})$) are derived from candidate spectra by χ^2 fitting to a grid of LTE model atmospheres. This is performed automatically by our spectrum optimisation toolkit, SFIT2 (Jeffery et al. 2001). To accommodate the physical diversity of the hot subdwarfs, our grid of model atmospheres coarsely covers the parameter space $T_{\rm eff}$: 15 000–50 000; $\log g$: 3–6; nHe:

0.001–0.999.

3.2. SDSS data samples

We selected two samples of spectra from the SDSS Data Release 3 database. The first sample consists of all the hot standard stars used for SDSS spectrophotometric calibrations.

Our second sample was selected based on photometric colors. Although the SDSS spectroscopic processing pipeline does make an attempt to classify stellar spectra, we learned in section 2.3 that it does not do so in any great detail, so we cannot rely upon the SDSS classifications to accurately extract a complete sample of subdwarf candidates from the database. Our selection criteria are summarised in the following SQL query:

```
SELECT s.fiberID,s.mjd,s.plate
FROM BESTDR3..SpecPhotoAll as s
WHERE s.psfMag_u < 21
AND (s.psfMag_u - s.psfMag_g) < 0.7
AND (s.psfMag_g - s.psfMag_r) < -0.1
AND s.specClass <> dbo.fSpecClass( QSO )
```

After passing all the retrieved spectra through our PCA filter, manually extracting any false positives and removing samples occurring in both data sets, we obtained a final sample of 282 hot subdwarf candidates. A summary of data set statistics is given in Table 1.

Table 1. With the combination of our PCA filter and visual selection, we were able to extract 282 unique subdwarf candidates from a total of 8171 spectra retrieved from the SDSS.

Data set	Spectra retrieved	Candidates extracted
Hot standards	1417	152
Color-color	6754	249
Total	8171	401 (282 Unqiue)

3.3. Results

Classification and parameterisation results for the 282 SDSS spectra are presented in Figure 2. The analogues between the classification parameters and physical parameters can be clearly seen by comparing the left-hand plots with the right-hand plots in Figure 2.

We note the patterns visible in the $\log g$ vs. $T_{\rm eff}$ plot: the gap at approximately $T_{\rm eff} \approx 20,000$K, $\log g \approx 4.5$; and the line extending leftwards at $\log g \approx 5.0$. We are unsure as to their nature, but the work of Green et al. (2006) discovered similar patterns from an analysis of an independent set of subdwarf stars.

An example of the model atmosphere fits and corresponding ANN classification of four stars from the sample are presented in Figure 3.

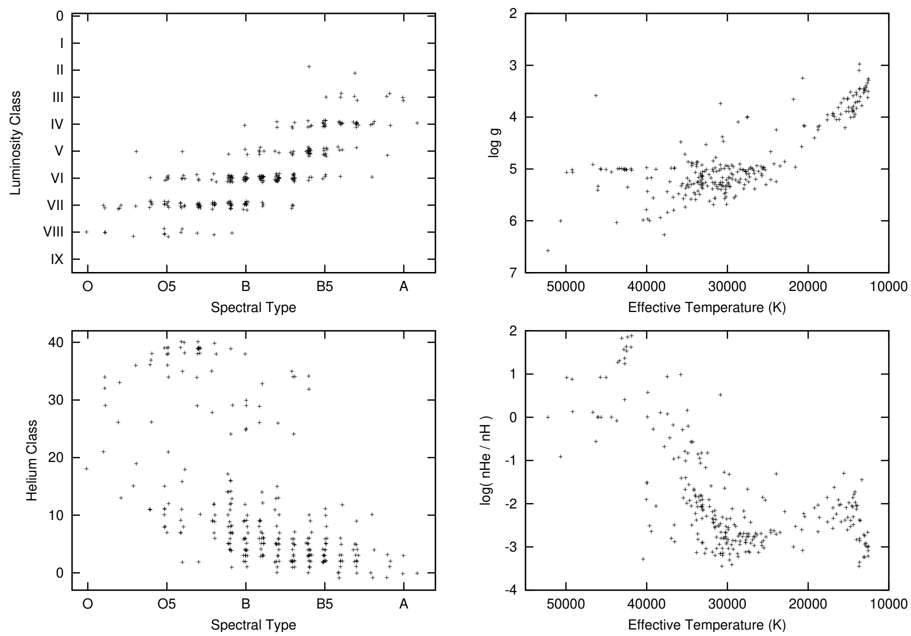

Fig. 2. Results of classifying and parameterising the 282 hot subdwarf candidates extracted from the SDSS. Classifications are presented in the two left-hand plots, with parameterisations presented in the two right-hand plots. The analogues between classification parameters and physical parameters is clearly evident.

4. FUTURE DIRECTIONS

The automatic filtering and analysis pipeline presented here is a part of what will be a more extensive system for automatic spectral analysis (see Jeffery 2003).

Given the nature of the hot subdwarfs, our use of LTE model atmospheres represents a problem for the analysis of very hot stars wherein NLTE effects become more apparent. However, our analysis pipeline can be easily extended to incorporate third-party model atmosphere codes that will allow us to address this issue in future work. We have used this study to help us refine our analysis pipeline and uncover the main hazards in dealing with large quantities of data. As we work to further improve the system, we must also tackle a number of issues, such as:

• **Data management.** Keeping track of different data sets, selection criteria, extracted candidates, their classifications and parameterisations, and maintaining general order when working with large quantities of spectra is an important task. Doing it manually is time-consuming, prone to user-forgetfulness, and can result in unfortunate industrial accidents (`rm -fr *`)[1].

• **Visualisation and interaction.** Analysing large data sets presents the problem of how to visualise thousands of spectra in a meaningful way. Also, when results have been obtained, the user must be able to produce plots and interact

[1] This is the Unix shell incantation which wipes clean the files in a user's current working directory and all its sub-directories.

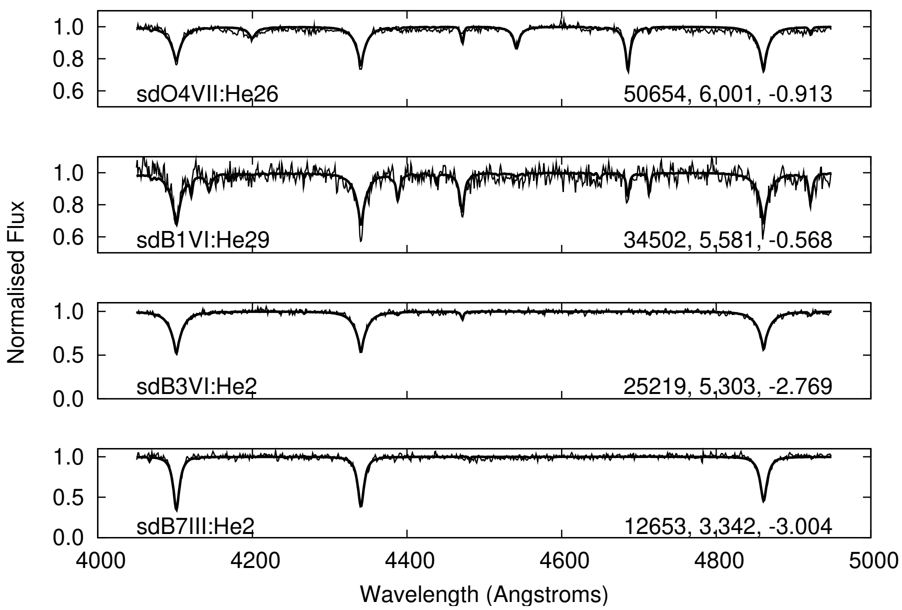

Fig. 3. A selection of stars from the set of 282 subdwarf candidates. The bottom-left of each plot details that star's spectral type as determined by the ANN, and the derived physical parameters are given at the bottom-right ($T_{\rm eff}$, $\log g$, $\log(n\mathrm{He}/n\mathrm{H})$). The thicker line in each plot is the best-fit model determined by SFIT2.

with them such that objects of interest can be displayed, allowing the data to be explored and connections to be made.

ACKNOWLEDGEMENTS. This work was carried out as part of the Cosmo-Grid project, funded under the Programme for Research in Third Level Institutions (PRTLI) administered by the Irish Higher Education Authority under the National Development Plan and with partial support from the European Regional Development Fund.

REFERENCES

Connolly A. J., Szalay A. S., Bershady M. A., Kinney A. L., Calzetti D. 1995, AJ, 110, 1071

Deeming T. J. 1964, MNRAS, 127, 493

Drilling J. S. 1996, in *Hydrogen Deficient Stars*, eds. C. S. Jeffery & U. Heber, ASP Conf. Ser., 96, 461

Drilling J. S., Jeffery C. S., Moehler S., Heber U., Napiwotzki R. 2005, in preparation

Francis P. J., Hewett P. C., Foltz C. B., Chaffee F. H. 1992, ApJ, 398, 476

Green E. M., Fontaine G., Hyde E. A., Charpinet S., Chayer P. 2006, Baltic

Astronomy, 15, 167

Jeffery C. S. 2003, in *Stellar Atmosphere Modeling*, eds. I. Hubeny, D. Mihalas & K. Werner, ASP Conf. Ser., 288, 137

Jeffery C. S., Drilling J. S., Harrison P. M., Heber U., Moehler S. 1997, A&AS, 125, 501

Jeffery C. S., Woolf V. M., Pollacco D. L. 2001, A&A, 376, 497

Murtagh F., Heck A., 1987, *Multivariate Data Analysis*, Reidel, Dordrecht

Storrie-Lombardi M. C., Irwin M. J., von Hippel T., Storrie-Lombardi L. J. 1994, Vistas in Astronomy, 38, 331

Baltic Astronomy, vol. 15, 77–80, 2006.

A SPECTROSCOPIC SEARCH FOR NEW SDB STARS FROM THE GALEX SURVEY

J. Rhee[1,2], M. Seibert[1], R. H. Østensen[3], S. K. Yi[4], S.-C. Rey[5], R. M. Rich[6], L. Bianchi[7] and Y.-W. Lee[2]

[1] *Space Astrophysics Laboratory, California Institute of Technology, MC 405-47, 1200 East California Boulevard, Pasadena, CA 91125, U.S.A.*

[2] *Center for Space Astrophysics, Yonsei University, Seoul 120-749, S. Korea*

[3] *Isaac Newton Group, E-37800 Santa Cruz de La Palma, Canary Islands, Spain*

[4] *Department of Physics, University of Oxford, Keble Road, Oxford OX1 3RH, U.K.*

[5] *Department of Astronomy and Space Sciences, Chungnam National University, Daejeon 305-764, S. Korea*

[6] *Department of Physics and Astronomy, University of California at Los Angeles, Los Angeles, CA 90095, U.S.A.*

[7] *Department of Physics and Astronomy, Johns Hopkins University, Baltimore, MD 21218, U.S.A.*

Received 2005 August 1

Abstract. We have recently initiated a systematic search for the UV-bright, subdwarf B (sdB) stars in the Milky Way. The sdB stars are core He-burning stars with very thin H envelopes and are known to be immediate progenitors of white dwarfs, but their formation mechanism is still enigmatic. For instance, it is not clear whether such objects are born as single stars or can form only in binary systems. The number ratio of sdB stars in each Galactic stellar population (i.e., thin disk, thick disk and halo) may give a clue to which of the suggested formation mechanisms dominates: the binary scenario or the RGB-peel-off scheme. This approach was hampered by the lack of identified sdB stars belonging to the thin disk and halo. Thus, it is of primary importance to find new sdB stars that are faint (halo) and lie at lower Galactic latitudes (thin disk). In this contribution, we will describe the motivation and plan for our spectroscopic survey and preliminary results based on pilot observations for 34 sdB star candidates from the GALEX All-sky Imaging Survey.

Key words: stars: early-type – stars: subdwarfs – surveys

1. INTRODUCTION

The UV bright, hot subdwarf B (sdB) stars are considered to be core He-burning stars of 0.5 $M_\odot$ with very thin H envelopes of $M_{\rm env} \leq 0.02 M_\odot$ (Heber 1986). In the Galactic field, they are characterized by H-dominated atmospheres with $T_{\rm eff} \approx 24\,000$–$30\,000$ K and $\log g > 5$. Their counterparts in globular clusters are generally recognized to be extended horizontal-branch (EHB) stars found as the faint and blue tail of the horizontal-branch (HB) in clusters such as NGC 6752 and M 13. These observations suggest that the UV-bright stars might be populous enough to account for much of the UV uptrun phenomenon observed in elliptical galaxies and spiral galaxy bulges (Greggio & Renzini 1990; O'Connell 1999; Yi et al. 1999). The sdB stars are known to be immediate progenitors of low mass white dwarfs (WDs), although they consist of only a small fraction of whole sample of WD progenitors (Saffer et al. 1994). In their past, sdB stars must have experienced a core He flash and substantial mass-loss during or after the red giant branch (RGB) phase. But, it is still a mystery how the mass-loss mechanism in the sdB star's progenitor manages to remove all but a tiny fraction of the H envelope exactly at the same time when the He core has attained the canonical sdB mass of 0.5 $M_{\odot}$ required for the He flash. This project aims to study the sdB population in the Galaxy, which may shed light on their still enigmatic formation process.

2. WHY LOOK FOR "NEW" SDB STARS?

Major formation channels of sdB stars can be divided into two scenarios: (1) single sdB stars are created from the enhancement of stellar wind near the RGB tip which strips off the H envelope (D'Cruz et al. 1996), and (2) sdB stars are formed from close binary evolution with strong mass transfer by a companion (Mengel et al. 1976). Previous observational results are not in contradiction with either scenario (Maxted et al. 2001; Altmann et al. 2004). The RGB-peel-off models predict a depletion of the HB stars in the middle temperature range (HBA stars) as metallicity increases, while stars at the hot and cold ends of HB (sdB and Red HB stars) should be abundant at all metallicities. Thus, as proposed by Altmann et al. (2004), the number ratio of sdB stars in each stellar population may provide a clue to answer which formation mechanism can be dominating. If the binary scenario is the most significant process, the number ratio of sdB stars in the thin disk, thick disk and halo would be similar to that of other evolved, low-mass stars. In the RGB-peel-off scheme, sdB stars would be more dominant over HBA stars in the thin disk. Unlike the known case of HBA stars (e.g., Altmann & de Boer 2000), this approach was hampered by the lack of identified sdB stars belonging to the thin disk and halo. Therefore, it is particularly important to increase the number of identified sdB stars with faint magnitudes (halo) and at lower Galactic latitudes (thin disk), and GALEX can provide useful targets for it.

It has lately been confirmed that large He abundance variations (ΔY) among stars can not only naturally reproduce the EHB stars in ω Cen, but can also explain the large spread of FUV magnitude for the EHB stars in NGC 2808 (Lee et al. 2005). They have suggested He abundance being a third parameter which influences HB morphology of such clusters, other than metallicity and age. Spectroscopic distances of these field sdB stars will be derived from stellar radii and angular diameters: the former is based on the surface gravity measured from the spectra and a canonical mass of 0.5 $M_{\odot}$, and the latter is obtained from comparing model atmosphere flux with dereddened NUV photometry. We then expect to be able to determine absolute $M_{\rm FUV}$ of sdB stars at an accuracy of 0.2 magnitude owing to the spectroscopic distances and GALEX FUV photometry, and thus reasonable ΔY among the sdB stars by the comparison of, if any, observed $M_{\rm FUV}$ spread and the predictions derived from isochrones. This would permit us to systematically obtain ΔY of sdB stars as a function of stellar population in order to study the global third parameter effect of the Galaxy.

It has been known that sdO stars have a larger scale height ($\geq$ 1.0 kpc, Thejll et al. 1994) than sdB stars ($\sim$ 0.5 kpc, Villeneuve et al. 1995), which is inconsistent

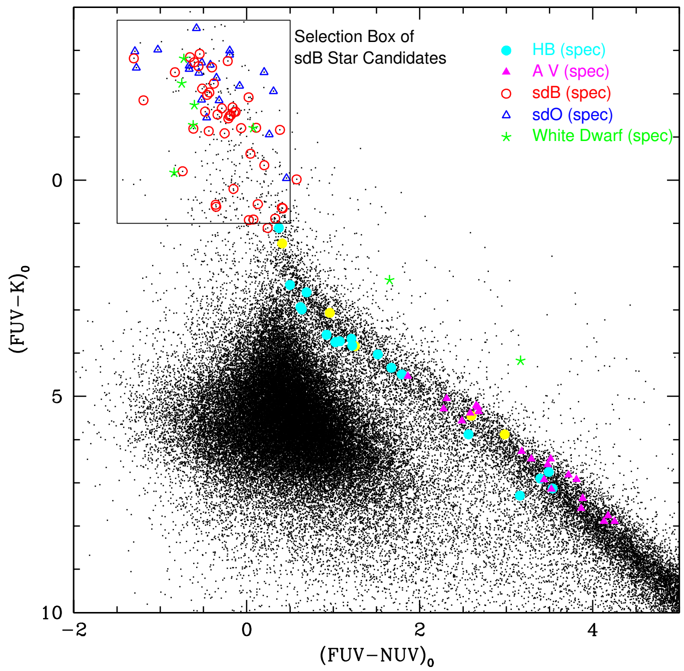

Fig. 1. GALEX AIS objects from about 1000 fields in GR1, also matched in 2MASS. Spectroscopically known sdB/O, WD, HB and A V stars are marked by different symbols. The sdB and sdO stars are clearly separated.

with an evolutionary connection between sdB and sdO stars. But, a larger scale height of 0.9 kpc has recently been obtained including "fainter" (but still $B \leq 16$) sdB stars (Altmann et al. 2004). This implies that a correct scale height can only be obtained with a sample without limiting magnitude bias.

3. CANDIDATE SELECTION

The public GALEX Release (GR1) of All-sky Imaging Survey (AIS) data was made in 2004 December. We performed cross-matching of the GALEX and 2MASS catalogs for some 3000 AIS fields ($\sim$3500 deg^2). As seen in Figure 1, two-color diagram efficiently separates sdB/O stars because the FUV–NUV color provides relatively long temperature baseline (spectral type) for hot stars, while the FUV–K_S color is useful for classification between stellar and non-stellar objects. Our empirical comparison with spectroscopically known sdB/O stars agrees well with the above expectation. It should be pointed out that replacing 2MASS K_S with SDSS i or USNO-B I gives a similar result, so our sdB candidate stars should reach apparent magnitude NUV ≈ 20 ($B \approx 20$), four magnitudes fainter than for the Palomar Green survey (Green et al. 1986) which was one of the most extensive surveys for sdB star in the past. Using this method, we have selected a sample of some 1000 sdB star candidates over a range of depths and sky-coverages.

4. OBSERVATIONS, RESULTS AND PLANS

We have performed pilot spectroscopic observations for 34 sdB star candidates with the KPNO 2.1 m telescope and GoldCam, McDonald 2.7 m telescope and LCS and Lick 3.0 m telescope and KAST between 2004 June and 2005 May. Based on the visual inspection of spectra and measurements of $D_{0.2}$ (average width of Hγ and Hδ lines at 20% below continuum) and R_c (average depth of Hγ and Hδ lines) employed in Beers et al. (1992), the medium-resolution (1–3 Å) spectroscopy has revealed that the sample consists of 14 sdB, 5 narrow-lined B, 8 WD, 4 HBB with He lines and 3 normal B stars. Based on the preliminary detection rate of sdB stars (14/34) and the number of our sdB star candidates ($N \geq 1000$), we expect to "newly" confirm more than 400 *bona fide* sdB stars in the halo and thin disk as well as in the thick disk. In the future, more sophisticated methods will be employed to determine stellar parameters (log g, $T_{\rm eff}$, and He abundance) accurately. Using observing time awarded at the CTIO 4.0 m, KPNO 2.1 m and Lick 3.0 m telescopes, we plan to complete a spectroscopic survey of some 1000 sdB star candidates by early 2006. Radial velocities determined from our spectroscopy, combined with proper motions from astrometric surveys such as UCAC2 (Zacharias et al. 2004), USNO-B (Monet et al. 2003) and future space missions (Gaia and SIM), will provide us with full space motions and thus allow us to assign population membership for the sdB stars. Indeed, this huge data set of GALEX sdB stars, which reach the entire UV visible Milky Way, will eventually help us broaden our understanding about their formation/evolution mechanism and Galactic structure.

ACKNOWLEDGMENTS. We are grateful to the referee, Sabine Moehler, for her careful review of the paper and a number of thoughtful suggestions. We gratefully acknowledge support for this work from NASA grant GALEX GI 04-0000-0096. J. R. and Y.-W. L. appreciate partial support by the Korean Ministry of Science and Technology through the Creative Research Initiative Program.

REFERENCES

Altmann M., de Boer K. S. 2000, A&A, 353, 135
Altmann M., Edelmann H., de Boer K. S. 2004, A&A, 414, 181
Beers T. C., Doinidis S. P., Griffin K. E., Preston G. W., Shectman S. A. 1992, AJ, 103, 267
D'Cruz N. L., Dorman B., Rood R. T., O'Connell R. W. 1996, ApJ, 466, 359
Green R. F., Schmidt M., Liebert J. 1986, ApJS, 61, 305
Greggio L., Renzini A. 1990, ApJ, 364, 35
Heber U. 1986, A&A, 155, 33
Lee Y.-W., Joo S.-J, Han S.-I. et al. 2005, ApJ, 621, L57
Maxted P. F. L., Heber U., Marsh T. R., North R. C. 2001, MNRAS, 326, 1391
Mengel J. G., Norris J., Gross P. G. 1976, ApJ, 204, 488
Monet D. G., Levine S. E., Canzian B. et al. 2003, AJ, 125, 984
O'Connell R. W. 1999, ARA&A, 37, 603
Saffer R. A., Bergeron P., Koester D., Liebert J. 1994, ApJ, 432, 351
Thejll P., Bauer F., Saffer R. et al. 1994, ApJ, 433, 819
Villeneuve B., Wesemael F., Fontaine G., Carignan C., Green R. F. 1995, ApJ, 446, 646
Yi S., Lee Y.-W., Woo J.-H. et al. 1999, ApJ, 513, 128
Zacharias N., Urban S. E., Zacharias M. I. et al. 2004, AJ, 127, 3043

Baltic Astronomy, vol. 15, 81–84, 2006.

SEARCHING FOR THE "MISSING" PG HOT SUBDWARFS IN SDSS AND GALEX DATA

R. A. Wade[1] M. A. Stark[1] R. F. Green[2] and P. R. Durrell[3]

[1] *Department of Astronomy & Astrophysics, Pennsylvania State University, 525 Davey Lab., University Park, PA 16802, U.S.A.*

[2] *NOAO, P.O. Box 26732, Tucson, AZ 85726-6732, U.S.A.*

[3] *Department of Physics and Astronomy, Youngstown State University, Youngstown, OH 44555-2001, U.S.A.*

Received 2005 July 28

Abstract. Many EHB stars have been found in short-period binaries, where the companions in these post-common envelope systems are either white dwarfs or dM stars; these systems are catalogued as hot subdwarfs because the subdwarf is the more luminous component. Hypothesized Roche-lobe overflow systems (with more massive companions) may largely be uncatalogued, since the G band or Ca II K line from the companion may have caused them to be overlooked or discarded. In particular, many candidate objects were excluded from the PG catalog because of such spectroscopic indicators. Could these rejects include large numbers of "missing" hot subdwarfs? We have examined 2MASS, SDSS and GALEX archival data for large subsets of these rejected stars and conclude that only a handful (about 3%) show indications of binarity; most are consistent with (single) metal-poor F stars, as was originally supposed.

Key words: binaries: close – stars: horizontal-branch – ultraviolet: stars

1. HYPOTHETICAL "MISSING sdB" STARS

Binary population synthesis (BPS) models suggest that many core-helium burning, thin hydrogen envelope objects ("sdB stars") are not yet discovered, hidden in binary systems with luminous (non-degenerate) relatively cool companions. The existing catalogs of sdB stars would therefore be significantly biased, and a clear picture of the true situation regarding formation and current population of sdB stars is lacking. It is desirable to learn whether these proposed hidden populations of sdB stars actually exist.

It has been suggested (Han et al. 2002, 2003) that the stars that were rejected from the Palomar-Green (PG: Green, Schmidt & Liebert 1986, GSL86) survey for ultraviolet-excess (UVX) objects are a potential rich source for some types of these. During the PG survey, candidate UVX objects were those with (transformed) $U–B < -0.46$. Because of the large errors in $U–B$, $\sigma \approx 0.38$, the color selection was supplemented by classification spectroscopy, for more accurate temperature information. Many candidate UVX targets were indeed excluded from the final

PG catalog, because their spectra showed the Ca II K line (or the G band) in absorption. These rejected K-line stars were inferred to be metal-poor subdwarf F or G stars that crept into the candidate list owing to a combination of low metal-line blanketing and photometric errors.

In the alternative BPS view, these "PG-rejects" could be binaries containing sdB or sdO stars. The cool star would contribute a K line and make the blended U–B color marginal for the PG color criterion, giving a result similar to a metal-poor subdwarf. In this interpretation, therefore, the PG-rejects actually belong in the PG catalog, and moreover would constitute important evidence in favor of certain binary formation channels for sdBs.

2. THE SAMPLE OF REJECTED (K-LINE) STARS

Here we use broad-band photometry over extended wavelength ranges to assess two large subsamples from the list of PG rejects. This allows the spectral energy distribution of a composite hot+cool system to be distinguished from that of a single star. From the master catalog of 1125 PG-rejects (RW & RFG, in preparation), we found 291 stars that are present in both the Two-Micron All-Sky Survey (2MASS) Point Source Catalog and the Sloan Digital Sky Survey (SDSS) DR2 survey region, and we identified 103 stars that have GALEX observations accessible in the first Data Release. These samples are almost completely non-overlapping.

3. THE SDSS/2MASS DATASET: COLOR-COLOR DIAGRAMS

Of the 291 K-line stars that overlap 2MASS/SDSS, we consider here the 173 stars with Sloan r magnitudes in the range 14.00 to 16.00 (median $r = 14.86$) that have non-flagged (unsaturated) magnitudes in at least 4 of the 5 passbands of the SDSS (*ugriz*) photometric system (136 have all 5 optical magnitudes). All of these 173 stars have detections in the 2MASS J, H and K_s bands.

We plotted the 173 K-line stars in both g–r vs. u–g and r–K_s vs. g–r diagrams, along with 199 PG stars that have been classified as hot subdwarfs. We compared these with loci for the Population I main sequence, metal-poor main sequence and metal-poor giants (representing horizontal branch stars). We also considered three sequences of composite (binary) models. These combine the light from a hot subdwarf star ($T_{\rm eff} = 25\,000$ K, $30\,000$ K and $35\,000$ K; M_V derived from the zero-age EHB calculations of Caloi 1972) with the light from a cool main-sequence (MS) companion. These sequences emerge from the hot end of the stellar locus (faintest, coolest companions at this end), loop away from the single-star locus, and then loop back to meet the stellar locus at a (single-star) $T_{\rm eff} \approx 10\,000$ K. At this end, the 'cool' (A or F star) companion dominates.

In these diagrams, the recognized PG hot subdwarfs and the K-line PG-rejects are very different groups of stars. In this sense, the spectroscopy carried out by GSL86 succeeded in improving on the photographic U–B color selection. Some catalogued PG hot subdwarfs clearly are composite objects (Stark & Wade 2003; Reed & Stiening 2004). Most PG-reject stars, however, are consistent with being single stars, just as they were interpreted to be by GSL86. Except for a few outliers, they are not EHB+MS binary systems.

4. FITTING THE PG-REJECT STARS AS SINGLE STARS

We fitted the observed magnitudes for the 173 stars with model magnitudes, derived from the synthetic photometry done by the Padova group (Girardi et al. 2002, 2004). We considered all Padova models with $T_{\rm eff}$ in the range 4000–50 000 K, $4.0 < \log g < 5.0$ and metallicities between solar and $[\mathrm{M/H}] = -2.5$.

For each of the 173 stars, we scaled each model in brightness to find the best fit. We chose as the best overall model, the one that gave the smallest reduced chi-square statistic, χ^2_ν. Seven outliers have either large χ^2_ν or unusual $T_{\rm eff}$ or $\log g$. All of the remaining 166 PG-rejects can be fitted as single stars with $T_{\rm eff}$ in the range 5000–7100 K. The χ^2_ν values for these 166 non-outliers are acceptably small, given our present understanding of the SDSS error estimates, our neglect of interstellar reddening, etc. Most of these stars (136 of 166) are preferably fitted with low-metallicity models, $[\mathrm{M/H}] = -1.0$ or below, consistent with the GSL86 interpretation that these are metal-poor F and G subdwarfs.

Two of the outliers have SDSS spectra. They show Mg Ib, Na D and Ca II infrared triplet absorption, but the continua are blue. Both stars lie among the composite models in the color-color diagrams. A plausible model for the first is a 30 000–35 000 K hot subdwarf plus a $T_{\rm eff} \approx 6000$ K MS star. A plausible model for the second outlier is a $\sim 30\,000$ K hot subdwarf plus a $T_{\rm eff} \sim 7500$ K MS star. The other outliers lie either close to the hot single-star locus or the sequences of composite models; one may be a blue horizontal branch star.

5. THE GALEX DATASET

The GALEX photometry is in two bands, far- and near-ultraviolet (F and N), with $\lambda_{\rm eff} = 1528$ Å and 2271 Å. Figure 1 is a two-color diagram, with models of single and composite stars shown (synthetic photometry from Kurucz models). At the hot (upper left) end we show the observed colors of six known EHB stars (three of these are in binary systems, based on their 2MASS colors). We also found GALEX observations for a number of well-observed ($V \sim 9$) metal-poor single stars near $T_{\rm eff} = 6000$ K, and thus determined that the locus for such stars actually lies higher than the model line shows, by about 1–2 mag in F–N.

Of the 103 PG-rejects that were observed by GALEX, only twelve were detected in both FUV and NUV bands. We derived limits on F–N for the rest (assuming $F > F_{\rm lim} = 19.9$). We plot 24 limits in Figure 1; the other 67 systems have similar locations in the figure and are omitted to reduce confusion. Only three of the 103 stars show far-UV flux consistent with the presence of a hot star; the rest are consistent, given the errors and limits, with single cool stars. All of the "hot" detections have red J–K_s colors from 2MASS, so these stars are composite. (One of the three "hot" cases, at N–$V \approx 5.1$ and F–$N = 3.0$ is not an EHB+MS binary but can be modeled as a $T_{\rm eff} \approx 30$ kK WD+dG system.)

6. SUMMARY

A few objects ($\sim 3\%$) in our sample of PG-reject stars may plausibly be binary systems that include a hot subdwarf star as a member. The vast majority of the PG-reject stars, however, are sufficiently modeled as single stars, consistent with their being the metal-poor sdF and sdG contaminants that GSL86 were guarding against. The color-color sequences of sdB + cool (MS) star binaries are well separated from the observed colors of the PG-reject stars in both the optical vs.infrared plane and the optical vs. ultraviolet plane. There is no compelling evidence for large numbers of additional hot subdwarf stars hiding in binaries that were rejected from the PG catalog.

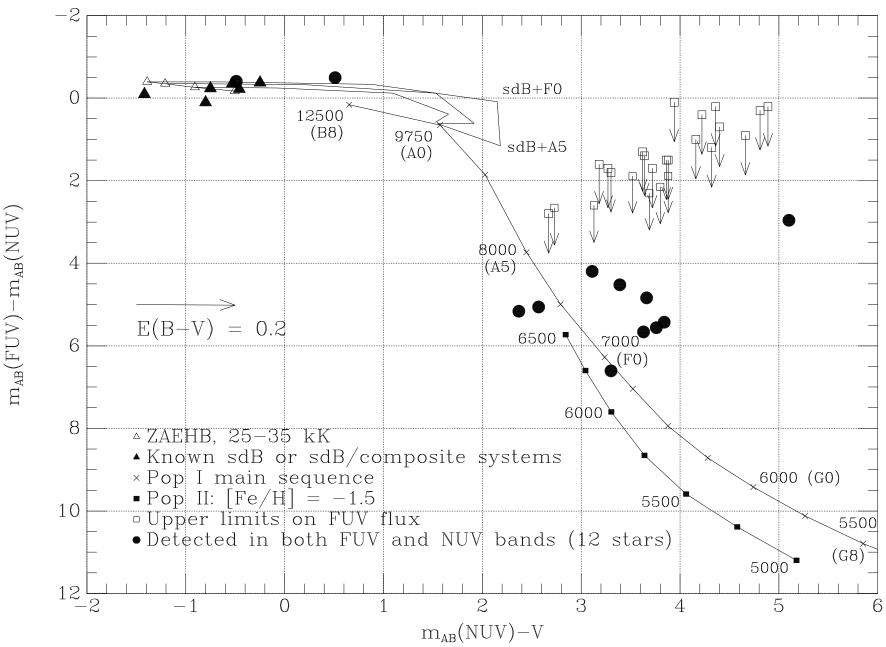

Fig. 1. GALEX and visible two-color diagram.

ACKNOWLEDGMENTS. We made use of SDSS Data Release 2, the 2MASS, GALEX Data Release 1, the USNO-A2 catalog, and SIMBAD. Supported in part by Sigma Xi, NASA grants NAG5-9586 and NGT5-50399, and the Pennsylvania Space Grant Consortium.

REFERENCES

Caloi V. 1972, A&A, 20, 357

Girardi L. et al. 2002, A&A, 391, 195

Girardi L, Grebel E. K., Odenkirchen M., Chiosi C. 2004, A&A, 422, 205

Green R. F., Schmidt M., Liebert J. 1986, ApJS, 61, 305 (GSL86)

Han Z., Podsiadlowski Ph., Maxted P. F. L., Marsh T. R., Ivanova N. 2002, MNRAS, 336, 448

Han Z., Podsiadlowski Ph., Maxted P. F. L., Marsh T. R. 2004, MNRAS, 341, 669

Reed M. D., Stiening R. 2004, PASP, 116, 506

Stark M. A., Wade R. A. 2003, AJ, 126, 1455

Baltic Astronomy, vol. 15, 85–90, 2006.

THE SUBDWARF DATABASE: RELEASED

R. H. Østensen
Isaac Newton Group, Apartado 321, E-38700 Santa Cruz de La Palma, Spain

Received 2005 August 15

Abstract. The work on the Subdwarf Database, presented at the previous meeting, has been completed, and the tool is now publicly available. The first release contains data from close to 240 different literature sources, but more still awaits entry. The database interface includes advanced search capabilities in coordinate, magnitude and color space. Output tables can be generated in HTML with hyperlinks to automatically generated finding charts, the Aladin viewer and a detailed data sheet that displays all registered data for each target, including physical data such as temperature, gravity and helium abundance, together with a finding chart. Search results can be visualized automatically as interactive position, magnitude or color diagrams.

Key words: stars: hot subdwarfs – catalogs – surveys

1. INTRODUCTION

As presented at the last subdwarf meeting (Østensen 2004) a database has been designed and implemented based on the data in The Catalogue of Spectroscopically Identified Hot Subdwarf Stars (or the Subdwarf Catalogue, for short: Kilkenny et al. 1988) and its updates. This list contains more than 2300 unique hot subdwarf stars.

The database runs under MySQL[1] with interfaces in Perl for uploading and linking together the database entries. The WWW interface uses HTML forms and PHP[2].

2. WHAT'S NEW

In the past year the whole database has been completely redesigned. The first implementation was merely a searchable version of the original electronic table, but it soon became evident that there was a major problem with this simple solution. For instance, the table allows space for a small number of different classifications and several photometry entries, but there was no way to distinguish between the quality of two measurements of the same object. This applies both to photometric data, classifications and physical data.

---

[1] MySQL (`www.mysql.com`) is an open source database.

[2] PHP (`www.php.net`) is a script language can produce HTML documents. The PHP code is interpreted when a page is requested, allowing the server to generate HTML in real time.

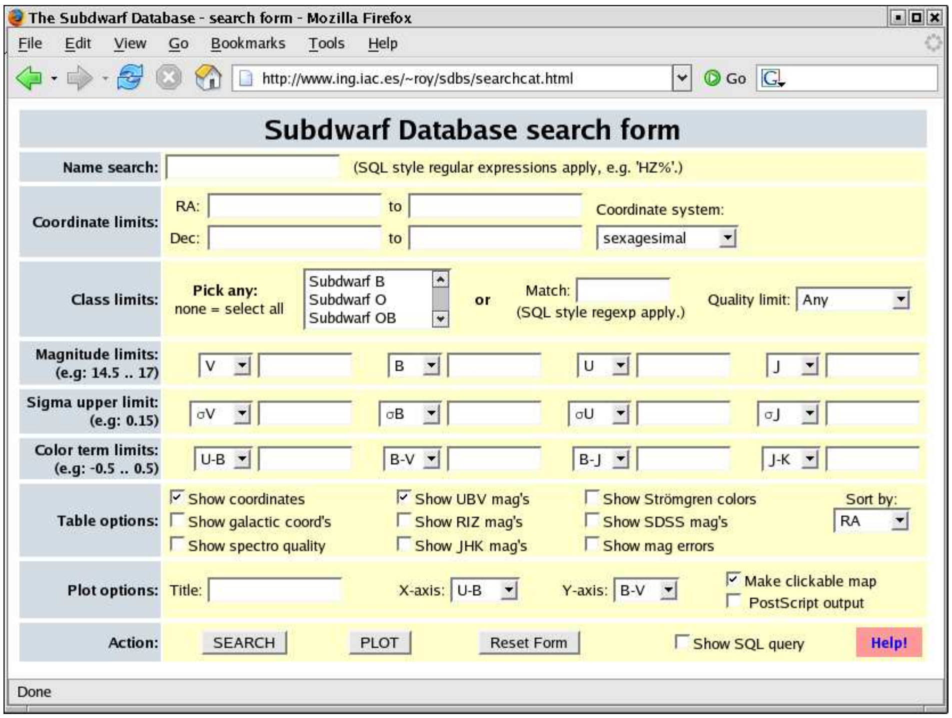

Fig. 1. The Subdwarf Database Search Form.

Obviously, if a particular object is observed and classified by several different authors, the reliability of the respective classifications will depend on the quality of the observations. If a classification entry was accompanied by a quality indicator, the system would be able to automatically adopt the classification with the highest quality flag, and thus vastly improve the reliability of the entries in the database. Thus, a scheme was implemented where a quality indicator of 1 signifies a photometric classification, a 2 signifies a classification based on a low resolution photographic spectrum, a 3 signifies a low to intermediate resolution spectrum (3–15 Å) – typically a photoelectric scan, a 4 signifies an intermediate resolution spectrum (1–3 Å) – typically a CCD observation in the blue part, and so on.

With this scheme in place it is easy to distinguish between reliably classified objects, and objects with dubious classifications. Also, for the photometric data in the database, it was decided that all entries must be accompanied by an error bar – either a one sigma error estimate provided by the observer, or at the very least a crude estimate based on the technique applied. Furthermore, the system is now able to convert magnitudes from photometric systems like the *Strömgren* system or *SDSS* magnitudes to Johnson *UVBRIZ* with reasonable precision and while maintaining realistic error estimates. It will then load the *UBVRIZ* magnitudes with the lowest error estimates available into the searchable database, regardless if this is an observed or derived magnitude. The database also contains *Strömgren, SDSS* and 2MASS *JHK* magnitudes, but these are never derived by conversion.

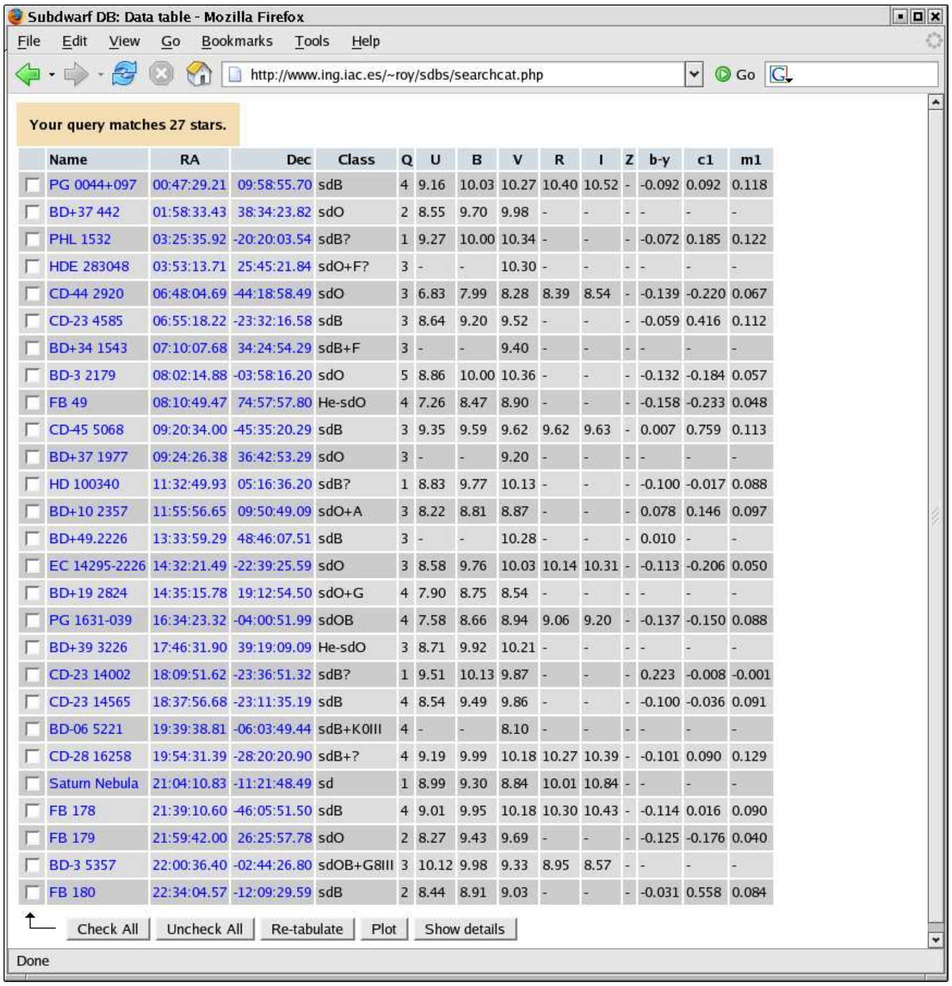

Name	RA	Dec	Class	Q	U	B	V	R	I	Z	b-y	c1	m1
PG 0044+097	00:47:29.21	09:58:55.70	sdB	4	9.16	10.03	10.27	10.40	10.52	-	-0.092	0.092	0.118
BD+37 442	01:58:33.43	38:34:23.82	sdO	2	8.55	9.70	9.98	-	-	-	-	-	-
PHL 1532	03:25:35.92	-20:20:03.54	sdB?	1	9.27	10.00	10.34	-	-	-	-0.072	0.185	0.122
HDE 283048	03:53:13.71	25:45:21.84	sdO+F?	3	-	-	10.30	-	-	-	-	-	-
CD-44 2920	06:48:04.69	-44:18:58.49	sdO	3	6.83	7.99	8.28	8.39	8.54	-	-0.139	-0.220	0.067
CD-23 4585	06:55:18.22	-23:32:16.58	sdB	3	8.64	9.20	9.52	-	-	-	-0.059	0.416	0.112
BD+34 1543	07:10:07.68	34:24:54.29	sdB+F	3	-	-	9.40	-	-	-	-	-	-
BD-3 2179	08:02:14.88	-03:58:16.20	sdO	5	8.86	10.00	10.36	-	-	-	-0.132	-0.184	0.057
FB 49	08:10:49.47	74:57:57.80	He-sdO	4	7.26	8.47	8.90	-	-	-	-0.158	-0.233	0.048
CD-45 5068	09:20:34.00	-45:35:20.29	sdB	3	9.35	9.59	9.62	9.62	9.63	-	0.007	0.759	0.113
BD+37 1977	09:24:26.38	36:42:53.29	sdO	3	-	-	9.20	-	-	-	-	-	-
HD 100340	11:32:49.93	05:16:36.20	sdB?	1	8.83	9.77	10.13	-	-	-	-0.100	-0.017	0.088
BD+10 2357	11:55:56.65	09:50:49.09	sdO+A	3	8.22	8.81	8.87	-	-	-	0.078	0.146	0.097
BD+49.2226	13:33:59.29	48:46:07.51	sdB	3	-	-	10.28	-	-	-	0.010	-	-
EC 14295-2226	14:32:21.49	-22:39:25.59	sdO	3	8.58	9.76	10.03	10.14	10.31	-	-0.113	-0.206	0.050
BD+19 2824	14:35:15.78	19:12:54.50	sdO+G	4	7.90	8.75	8.54	-	-	-	-	-	-
PG 1631-039	16:34:23.32	-04:00:51.99	sdOB	4	7.58	8.66	8.94	9.06	9.20	-	-0.137	-0.150	0.088
BD+39 3226	17:46:31.90	39:19:09.09	He-sdO	3	8.71	9.92	10.21	-	-	-	-	-	-
CD-23 14002	18:09:51.62	-23:36:51.32	sdB?	1	9.51	10.13	9.87	-	-	-	0.223	-0.008	-0.001
CD-23 14565	18:37:56.68	-23:11:35.19	sdB	4	8.54	9.49	9.86	-	-	-	-0.100	-0.036	0.091
BD-06 5221	19:39:38.81	-06:03:49.44	sdB+K0III	4	-	-	8.10	-	-	-	-	-	-
CD-28 16258	19:54:31.39	-28:20:20.90	sdB+?	4	9.19	9.99	10.18	10.27	10.39	-	-0.101	0.090	0.129
Saturn Nebula	21:04:10.83	-11:21:48.49	sd	1	8.99	9.30	8.84	10.01	10.84	-	-	-	-
FB 178	21:39:10.60	-46:05:51.50	sdB	4	9.01	9.95	10.18	10.30	10.43	-	-0.114	0.016	0.090
FB 179	21:59:42.00	26:25:57.78	sdO	2	8.27	9.43	9.69	-	-	-	-0.125	-0.176	0.040
BD-3 5357	22:00:36.40	-02:44:26.80	sdOB+G8III	3	10.12	9.98	9.33	8.95	8.57	-	-	-	-
FB 180	22:34:04.57	-12:09:29.59	sdB	2	8.44	8.91	9.03	-	-	-	-0.031	0.558	0.084

Fig. 2. Sample output from a magnitude limited search in the Subdwarf Database.

3. A FLEXIBLE INPUT FORMAT

Instead of the old system where the database merely reflected the entries in an electronic table with a fixed number of columns, the new system allows free format tables. Each data file under the new scheme contains information from one (or a related set of) publications with standardized tags to identify authors, title and a reference code. After a valid reference is given, each line contains data on one object in a format that specifies a list of names identifying the object followed by a colon and a list of data entries. The data entries are given in the form of a comma separated list of tag-value associations. Errors or quality flags are provided either on a separate line for all entries in the file, or as a number in brackets after each data value.

When the database is initialized, each data file is parsed and the data loaded

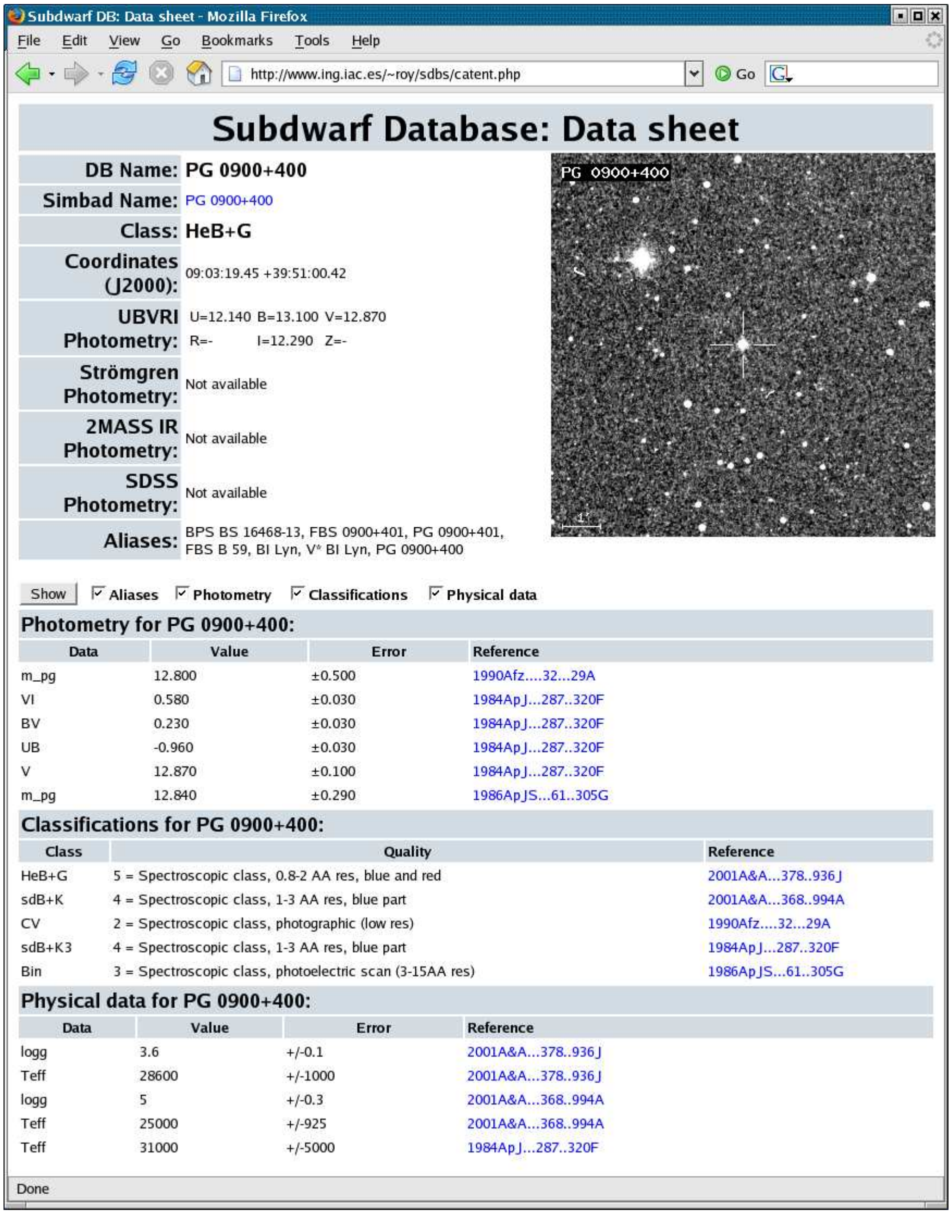

Subdwarf DB: Data sheet - Mozilla Firefox

File Edit View Go Bookmarks Tools Help

http://www.ing.iac.es/~roy/sdbs/catent.php Go

Subdwarf Database: Data sheet

DB Name:	PG 0900+400
Simbad Name:	PG 0900+400
Class:	HeB+G
Coordinates (J2000):	09:03:19.45 +39:51:00.42
UBVRI Photometry:	U=12.140 B=13.100 V=12.870 R=- I=12.290 Z=-
Strömgren Photometry:	Not available
2MASS IR Photometry:	Not available
SDSS Photometry:	Not available
Aliases:	BPS BS 16468-13, FBS 0900+401, PG 0900+401, FBS B 59, BI Lyn, V* BI Lyn, PG 0900+400

Show Aliases Photometry Classifications Physical data

Photometry for PG 0900+400:

Data	Value	Error	Reference
m_pg	12.800	±0.500	1990Afz....32...29A
VI	0.580	±0.030	1984ApJ...287..320F
BV	0.230	±0.030	1984ApJ...287..320F
UB	-0.960	±0.030	1984ApJ...287..320F
V	12.870	±0.100	1984ApJ...287..320F
m_pg	12.840	±0.290	1986ApJS...61..305G

Classifications for PG 0900+400:

Class	Quality	Reference
HeB+G	5 = Spectroscopic class, 0.8-2 AA res, blue and red	2001A&A...378..936J
sdB+K	4 = Spectroscopic class, 1-3 AA res, blue part	2001A&A...368..994A
CV	2 = Spectroscopic class, photographic (low res)	1990Afz....32...29A
sdB+K3	4 = Spectroscopic class, 1-3 AA res, blue part	1984ApJ...287..320F
Bin	3 = Spectroscopic class, photoelectric scan (3-15AA res)	1986ApJS...61..305G

Physical data for PG 0900+400:

Data	Value	Error	Reference
logg	3.6	+/-0.1	2001A&A...378..936J
Teff	28600	+/-1000	2001A&A...378..936J
logg	5	+/-0.3	2001A&A...368..994A
Teff	25000	+/-925	2001A&A...368..994A
Teff	31000	+/-5000	1984ApJ...287..320F

Done

Fig. 3. Sample data sheet from the Subdwarf Database. Different observers have given many different classifications for this composite system.

into a number of database tables. The list of object names are loaded into one table, and coordinates, classifications, references and physical data are loaded into separate tables. Each entry is associated with its reference code, and there is no longer any limit on the number of entries for the same object.

After all available data files have been loaded into the set of database tables,

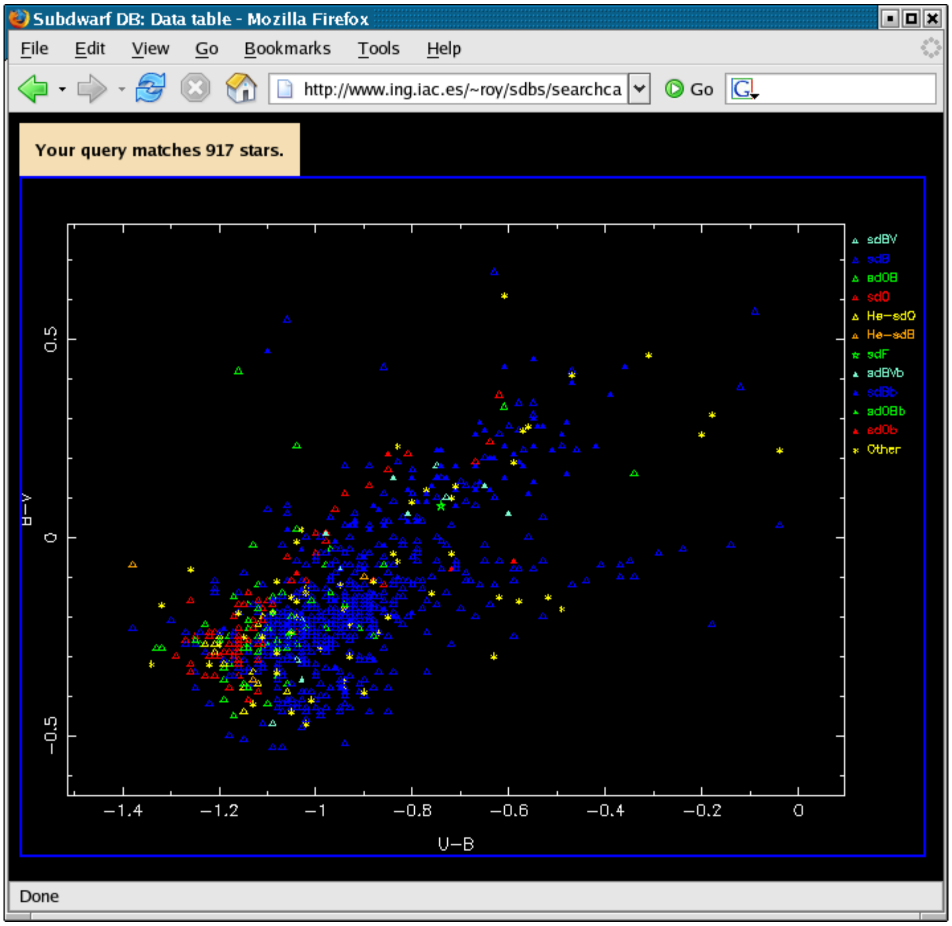

Fig. 4. A color-color plot auto-generated from the database with set limits on photometric quality. The plot is interactive in the sense that moving the pointer over a symbol will show the name of the star, and clicking on a symbol will produce the data sheet for that object.

a table containing compiled data is constructed. The script that does this job searches the table of classifications for entries of hot subdwarf stars. This list is then cross-checked so that each entry has a pair of valid coordinates associated with it. For each entry, all classifications and photometric data are loaded from the respective tables, derived magnitudes are computed, and only the best values are loaded into the compiled database. The entry that is created may actually not be that of a subdwarf star. All stars that have at one time been classified as a hot subdwarf star will be registered in the database, but the classification recognized is the one with the highest quality flag (e.g., Figure 3).

4. TO DO

The released database contains all the 146 references from the original Subdwarf Catalogue, with the exception of a few references that I have not been able to access. About 100 additional sources have been added to this collection, but this is still far away from exhausting the available sources. Many more papers still need to be recognized, and their data must be entered into tables. This is a work that can hardly ever be completed, and in order for the situation to improve, I will have to rely on people sending me notifications of old papers that have been missed as well as new papers being released. It would also be a great help if authors could provide electronic tables of their data that I can convert to the database format, thereby avoiding introducing further typing errors to the collection of discrepancies that already exist. If you spot any, please let me know.

The database is currently hosted at `http://www.ing.iac.es/~roy/sdbs/`. A more permanent home is being sought.

REFERENCES

Kilkenny D., Heber U., Drilling J. S. 1988, SAAOC, 12, 1, with updated electronic edition (1992)

Østensen R. H. 2004, Ap&SS, 291, 263

Baltic Astronomy, vol. 15, 91–98, 2006.

SUBLUMINOUS O STARS

U. Heber[1], H. Hirsch[1], A. Ströer[1], S. O'Toole[1], S. Haas[1] and S. Dreizler[2]

[1] *Remeis-Sternwarte Bamberg, Astronomisches Institut der Universität Erlangen-Nürnberg, Sternwartstrasse 7, D-96049 Bamberg, Germany*

[2] *Institut für Astrophysik, Georg-August-Universität Göttingen, Friedrich-Hund-Platz 1, D-37077 Göttingen, Germany*

Received 2005 August 1

Abstract. We report results of spectral analyses of sdO stars selected from the Supernova Ia Progenitor Survey, the Hamburg Quasar Survey and the Sloan Digital Sky Survey and based on state-of-the-art NLTE model atmospheres. By combining the sdO with the sdB samples we discuss trends of the atmospheric parameters in order to search for evidence for possible evolutionary linkage. The He-sdO stars are found to cluster near $T_{\rm eff} = 45\,000$ K, $\log g = 5.5$, whereas the number of sdO stars in this area is very small. The "cooler" sdO stars seem to form an extension to the sdB sequences. A couple of sdO stars are obviously evolved from the extended horizontal branch and reach temperatures as high as 80 000 K. We conjecture that the He-sdO stars and sdO/sdB stars have a different evolutionary origin. This is corroborated by the much lower binary frequency of the former. Strong enrichments of iron group elements are discovered for hydrogen-rich sdO stars as well as for sdB stars from high resolution UV spectra and have severe implications for the temperature scale. We finally highlight the discovery of a hyper-velocity He-sdO star with a radial velocity of 708 km s^{-1} unbound to the Galaxy.

Key words: stars: hot subdwarfs – stars: helium – stars: atmospheres

1. INTRODUCTION

Ever since the field has been introduced by Greenstein & Sargent (1974), the helium-rich sdO stars were believed to be linked to the evolution of the hydrogen-rich subluminous B stars. Any evolutionary link between subluminous B and O stars, however, is difficult to explain since the physical processes driving a transformation of a hydrogen-rich star into a helium-rich one remain obscure. The convective transformation has been explored by Wesemael et al. (1984) as well as by Groth, Kudritzki & Heber (1985). While the former found helium convection to occur even at subsolar helium abundances which mixes helium from deeper layers into the photosphere, the latter concluded that a helium driven convection zone develops only in helium-rich atmospheres. If the latter is true, convective transformation would not work.

Several evolutionary scenarios for subluminous O stars have been suggested: invoking either a delayed helium core flash or merging of white dwarfs. In the *late hot flasher scenario* the core helium flash occurs when the star has already left the RGB and is approaching the white dwarf cooling sequence (delayed He core flash). During the flash, He and C are dredged-up to the surface (Sweigart 1997).

The merger scenario is favored by binary population synthesis models and has met with some success to explain the origin of subluminous B stars. Merging of two helium core white dwarfs will result in helium main sequence stars with masses between 0.3 $M_\odot$ and 0.9 $M_\odot$. It has been proposed that some of the subluminous O and B stars may form through this channel (Webbink 1984). Recently detailed population synthesis models have been calculated by Han et al. (2003) which demonstrate, that a significant fraction of sdB stars can indeed form either through mass exchange or through merging of two Helium white dwarfs The first mass exchange episode (on the RGB) results in sdB stars with a main sequence companion, while after the second mass exchange a white dwarf companion forms. After correcting for selection effects birthrates are predicted. The models predict rather high birth rates for mergers, which in some case even exceed the birthrate of sdB-white dwarf binaries.

Whether or not the merger scenario is applicable to subluminous O stars as well is yet unclear. The situation is more complicated than for the sdB stars since the sdO stars form a much less homogenous class than the sdB stars (cf. Heber 1992). They have to be divided into at least three subclasses. Most of the sdO stars are enriched in helium, from mild cases (helium abundance slightly above solar) to extreme cases (no hydrogen detectable which translates into enrichments of at least several hundred times solar). The helium richness is accompanied by peculiar C and N line spectra. In addition the sdO stars have to be subdivided according to their luminosity. The most luminous sdO stars are very similar to some central stars of planetary nebulae and can be explained by post-AGB evolution which strongly suggest an evolutionary linkage to the helium giants (extreme helium stars and R CrB stars). Amongst the less luminous sdO stars again two spectroscopic subclasses differing in chemical composition must be distinguished. The first one, which we shall name He-sdO, does not show any trace of hydrogen but strong nitrogen and/or carbon lines. The second subclass, which we shall term simply sdO from now on, has hydrogen in quite different amounts. The evolutionary link between these two subgroups on the one hand and the sdB stars on the other is not yet clear.

Detailed quantitative spectral analyses are available for the subluminous B stars but only a few have been carried out for the sdO class because of the complexity of their spectra. In addition deviations from local thermodynamic equilibrium (NLTE) have to be taken into account, because of their high effective temperatures. However. only few quantitative spectral analyses have been published (Dreizler 1993; Dreizler et al. 1990; Thejll et al. 1994; Bauer & Husfeld 1995; Haas et al. 1996; Lanz et al. 1997), with some conflicting results becoming apparent. This is probably due to shortcomings in the early NLTE models used. Therefore we construct a new grid of atmospheric models and synthetic spectra using a state-of-the-art NLTE model atmosphere code.

2. MODEL ATMOSPHERES

An extensive grid of NLTE atmosphere models was calculated using the latest version of the PRO2 code (Werner & Dreizler 1999) that employs a new temperature correction technique (Dreizler 2003). A new detailed model atom for helium appropriate for the sdO temperature regime was constructed. 2700 partially line blanketed NLTE model atmospheres consisting of hydrogen and helium were calculated resulting in a grid of unprecedented coverage and resolution, extending

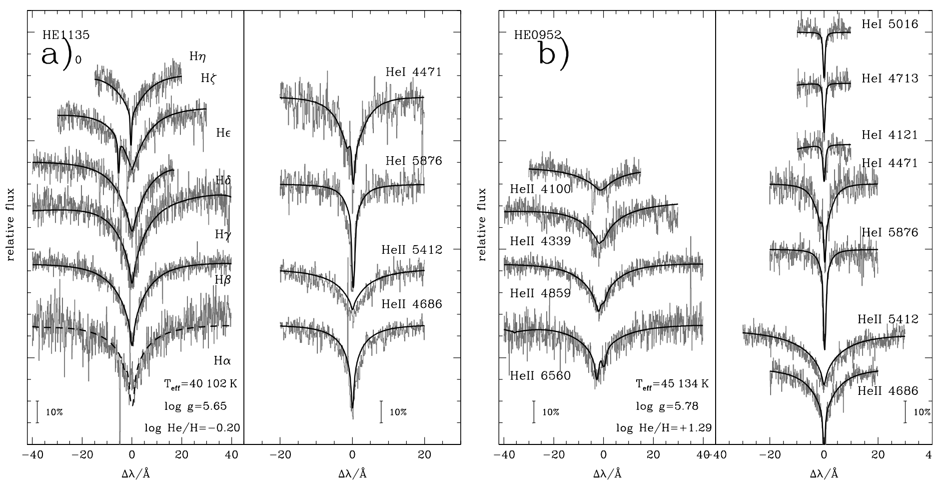

Fig. 1. Line profile fits for a H-sdO (left panel) and a He-sdO (right panel).

from 30 000 K to 100 000 K in $T_{\rm eff}$, from 4.0 to 6.4 in $\log g$ and from -4 to $+3$ in helium abundance, i.e., $\log{(N_{\rm He}/N_{\rm H})}$, in order to match the diversity of observed spectra (see Ströer et al. 2005).

We have used this model grid to analyze spectra of sdO stars from the ESO SPY-survey (Ströer et al. 2005), the Hamburg Quasar Survey (HQS, Ströer 2004) and the Sloan Digital Sky Survey (SDSS).

3. SDO STARS FROM THE SPY, HQS AND SDSS SURVEYS

SPY. The ESO Supernova Progenitor Survey (SPY) has identified 137 hot subluminous stars. 79 of them were classified as hydrogen rich subluminous B stars, 58 of them were classified as subluminous O stars. The spectra of the subluminous B/OB stars have been analyzed by Lisker et al. (2005).

High resolution spectra of sdO stars covering the spectral range from 3300 Å to 6650 Å at a resolution of 0.36 Å have been obtained with the UVES spectrograph at the ESO-VLT. In the course of spectral classification we distinguished He-sdO (30) from sdO stars (28) by the absence of Balmer line absorption in the former. Napiwotzki et al. (2004) searched for radial velocity variables amongst the SPY sdB and sdO stars and found a large fraction ($\sim 40\,\%$) amongst the sdB stars as well as amongst the sdO stars but only one He-sdO star turned out to be radial velocity variable. This star is unique amongst the SPY-subdwarfs as it turns out to be a double sdO (Lisker et al. 2004).

Effective temperatures ($T_{\rm eff}$), surface gravities ($\log g$), and helium abundances ($N_{\rm He}/N_{\rm H}$) for 49 stars were determined by fitting simultaneously hydrogen and helium lines to our synthetic model spectra, using a χ^2 procedure (Napiwotzki 1999). Resulting temperatures range from 36 000 K to 78 000 K, gravities from $\log g = 4.9$ to 6.4 and helium abundances from $\log{(N_{\rm He}/N_{\rm H})} = -3$ to $+3$. Four stars have temperatures in excess of 60 000 K and are probably post-AGB stars and will not be discussed further. Figure 1 gives two examples, one for each spectral subclass.

HQS. During our follow-up observations of blue stars from the Hamburg

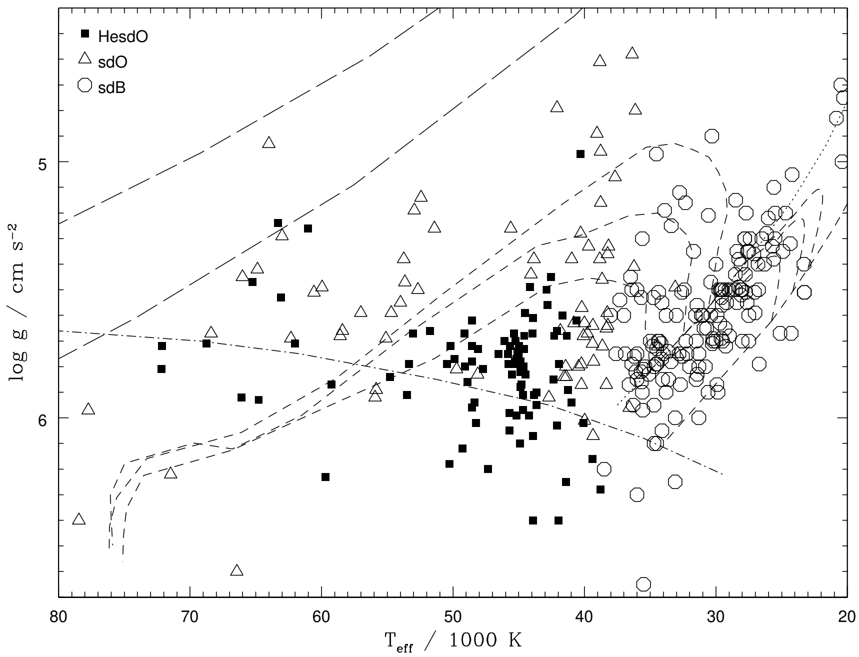

Fig. 2. Distribution of sdB, sdO and He-sdO stars (combined sample) in the $T_{\rm eff}$ vs. $\log g$ plane. Also shown are evolutionary tracks for post-EHB and post-AGB evolution.

Quasar Survey we have discovered many hot subdwarf stars. The analysis based on medium to low resolution spectra of the more than 100 HQS sdB stars has been presented by Edelmann et al. (2003).

In addition several sdO stars have been found. Due to insufficient S/N some of the spectra could not be analyzed. We also had to exclude the lowest resolution spectra because the results had errors too large to be useful. This left us with 14 hydrogen-rich sdO stars and 23 He-sdOs analyzed from spectra of 3.5 Å resolution.

SDSS. The ongoing Sloan Digital Sky Survey is a rich source of hot subluminous O stars. Candidates were found photometrically by selecting all stars with $u-g<0.2$, $g-r<0.1$. Inspection of their spectra yielded 40 sdO and 43 He-sdO stars, which were analyzed as described above.

Combined SPY, HQS & SDSS sample. In Figures 2 and 3 we combine the results of the spectral analyses of all three samples including the sdB stars. Figure 2 displays the distribution in the $T_{\rm eff}$ vs. $\log g$ plane. A strong concentration of the He-sdO stars near $T_{\rm eff}=45\,000$ K, $\log g=5.5$ is obvious. Some of the sdO stars lie in between the sdB star domain and the He-sdO stars, while others are of lower gravity than the sdB stars. It is worthwhile to note that a gap in the sdO sequence becomes apparent. There are very few sdO stars in the $T_{\rm eff}$ range from 40 000 to 50 000 K, where most of the He-sdOs are found.

Edelmann et al. (2003) noticed a trend of increasing helium abundances with increasing $T_{\rm eff}$ for sdB stars. They also pointed out that two distinct sequences exist. The "cooler" sdO stars nicely match the sdB sequences (see Figure 3) and extend the trend to higher $T_{\rm eff}$ ($\approx 40\,000$ K).

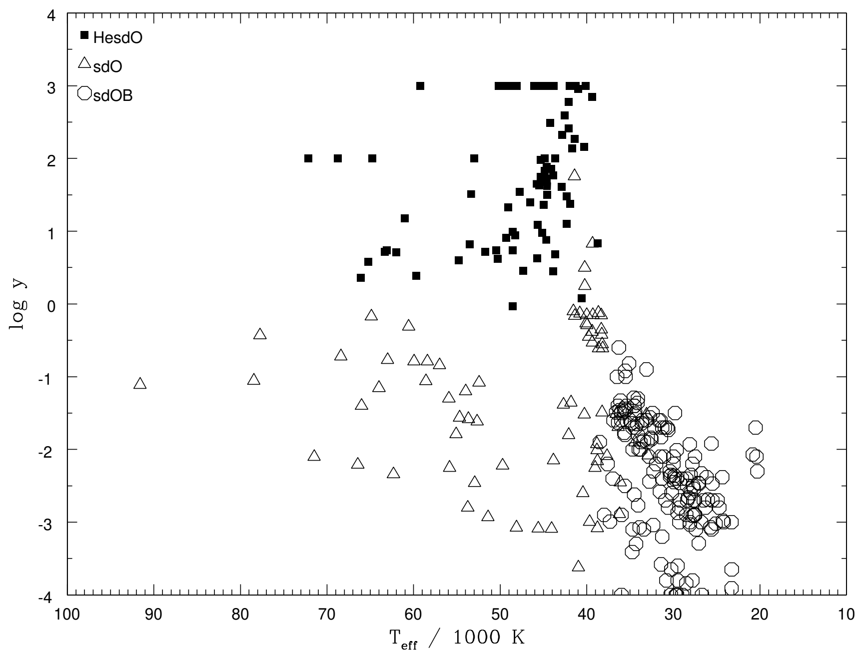

Fig. 3. Distribution of sdB, sdO and He-sdO stars (combined sample) in the $T_{\rm eff}$ vs. $\log y$plane ($y = N_{\rm He}/N_{\rm H}$). For stars with $\log y > +3$ lower limits are given.

4. METAL ABUNDANCES

While metal abundances of several dozens of sdB stars have been derived using LTE techniques from optical spectra (see Edelmann et al. 2006) very few detailed abundance analyses are available for sdO stars. A self-consistent spectral analysis is available for BD+75 325 only (Lanz et al. 1997). Abundances of Fe and Ni have been determined in a few sdO and He-sdO stars. Haas (1997) finds strong enrichments of Fe (10 times solar) and Ni (70 times solar) in the hot hydrogen-rich sdO stars Feige 34, Feige 67 and LS II+18 9. These high abundances cause strong backwarming and the temperatures derived from the Fe/Ni ionization equilibria (60 000 K) is much lower than the one (75 000 K) obtained from optical Balmer and He II lines using metal free NLTE model atmospheres.

Recently, O'Toole & Heber (2006) analyzed high resolution ultraviolet spectra of five sdB stars from HST/STIS. Many heavy elements (up to lead) become accessible to a detailed quantitative analysis. Abundance of 23 metals were derived. While the cooler sdB stars ($T_{\rm eff}$ <30 000 K) show abundances of the iron group elements similar to the sun. The hotter ones ($T_{\rm eff}$ ≈35 000 K) have near solar iron abundances as well, but strong enrichments (100 times) of other elements are found. The high Ni abundances are very similar to those found by Haas (1997) for the hydrogen-rich sdO stars.

As has been noted by Heber, Reid & Werner (2000) in their quantitative spectral analysis of pulsating sdB stars, there is a discrepancy between temperatures derived from Balmer line fitting and helium ionization equilibrium. For PG 1219+534, the difference in $T_{\rm eff}$ was found be as large as 2000 K.

After the initial discovery of strongly super-solar abundances of heavy metals in three sdB stars (Feige 66, CD $-24°731$ and PG 1219+534), we investigated how this affects the determination of the atmospheric parameters. Using LTE atmospheres with metals scaled by a factor of 10 ([M/H] = 1.0), we have recalculated both our abundances and stellar parameters ($T_{\rm eff}, \log g$). There are currently no opacity distribution functions with higher metallicities.

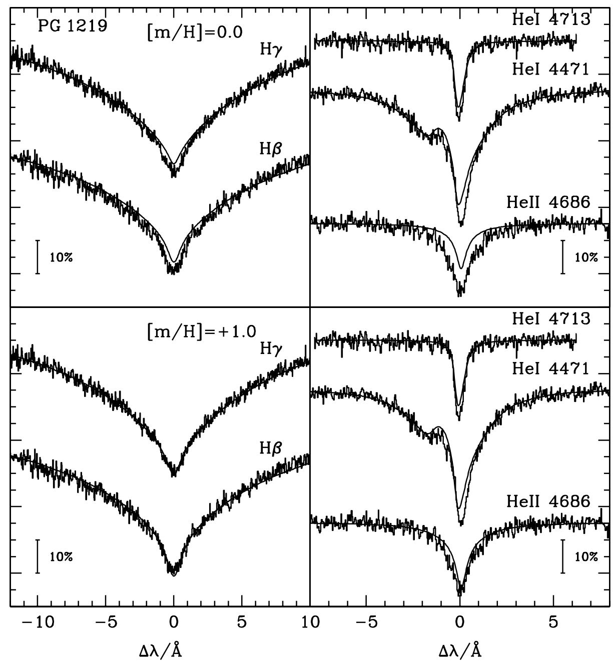

Fig. 4. Line profile fit for PG 1219+534 using solar metallicity models (top panel) and metal-rich models (10 times solar, bottom panels). The Balmer lines and He II at 4686 Å match simultaneously when using the metal-rich models.

In Figure 4 we show a fit with these models to the optical spectrum of the pulsating sdB star PG 1219+534. The Balmer lines and the He II can now be matched simultaneously. The parameters we derive with our metal-enhanced models is closest to those found by fitting the Balmer lines only with a solar-metallicity model. Hence the discrepancy between Balmer and He-ionization can be traced back to an metallicity effect. Unfortunately, however, the heavy metal abundances can be derived from UV spectra, only. Opacity sampling techniques (see Behara & Jeffery 2006) are required to account for the different enrichment of individual heavy elements.

5. A HYPER-VELOCITY SDO STAR

While all the hot subluminous stars studied by us have low radial velocities (system velocities in case of close binary stars), one object sticks out. In the sample of sdO stars selected from the SDDS we found the faint He-sdO US 708 ($g = 18.75$) to have a radial velocity of more than 700 km s^{-1}. To improve this measurement and to check for radial velocity variations, we observed the star with the Low Resolution Imaging Spectrometer LRIS at the KECK I telescope and obtained spectra of 5 Å and 4.4 Å resolution in the blue and red channels, respectively, with much better S/N than the SDSS spectrum (see Figure 5). The heliocentric radial velocity of 708±20 km s^{-1} is consistent with that from the SDSS spectrum, and we conclude that the high radial velocity is due to a very large space motion. Its radial velocity corresponds to a minimum Galactic rest frame velocity of 750 km s^{-1} exceeding the Galactic escape velocity at the position of the star. Hence the US 708 is unbound to the Galaxy. A spectral analysis of the LRIS spectrum is performed and the preliminary result is $T_{\rm eff} = 45\,500$ K, $\log g = 5.2$ and He/H = 10, typical for He-sdO stars. Assuming a mass of 0.5 $M_\odot$ this places US 708 at a distance of almost 20 kpc.

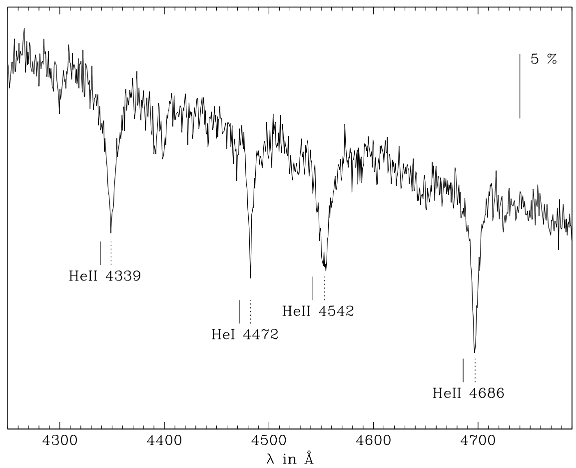

Fig. 5. Keck/LRIS spectrum of the He-sdO US 708 in the blue channel showing the typical He I and He II lines shifted by 708 $\mathrm{km\,s^{-1}}$.

Two so-called hyper-velocity stars have recently been discovered with radial velocities of 853 $\mathrm{km\,s^{-1}}$ (Brown et al. 2005) and 723 $\mathrm{km\,s^{-1}}$ (Edelmann el al. 2005). The corresponding minimum Galactic rest frame velocities are 709 $\mathrm{km\,s^{-1}}$ and 563 $\mathrm{km\,s^{-1}}$, respectively. Proper motions are unavailable but their measurement probably has to await future space missions, such as *Gaia* as they are probably very small given the large distances of the stars. Unlike US 708, the two hyper-velocity stars are young massive B stars at distances of 60 kpc. It is generally believed that interaction with the massive black hole in the Galactic center can accelerate stars to such high velocities. Hills (1988) investigated the tidal break-up of binary stars by a massive black hole and found ejection velocities, indeed, to be as high as 4000 $\mathrm{km\,s^{-1}}$. Some kinematical experiments are presently being carried out to check whether a Galactic center origin is feasible for US 708.

6. CONCLUSION

Recent spectral analyses of sdO stars have paved the way to discuss the evolutionary status of these stars as well as their linkage to sdB stars. The Supernova Ia Progenitor Survey has provided a set of high resolution spectra of sdO stars. The most important result is a separation of the subluminous O stars into at least two groups, the He-sdOs and the sdOs. The sdO stars form an extension of the sdB stars to higher temperatures and higher helium abundances. A couple of sdO stars are obviously evolved from the extended horizontal branch and reach temperatures as high as 80 000 K. The He-sdO stars, however, cluster near $T_{\rm eff} = 45\,000$ K, $\log g = 5.5$. The second important result from SPY is that the binary fraction of sdO stars is similar to that of the sdB stars, while it is very low for He-sdO stars. Therefore we conclude that the two types of subluminous stars have different evolutionary origin. Recently, many sdO stars have been analyzed from low-resolution spectra from the HQS follow-up project and the SDSS spectral database. The results strength the conclusions drawn from the SPY set substantially and suggest the presence of a gap in the distribution of sdO stars at the position of He-sdO cluster in the $T_{\rm eff}$ vs. $\log g$ plane.

From high resolution UV spectra strong enrichments of iron group elements are discovered for hydrogen-rich sdO stars as well as for sdB stars and have severe implications for the temperature scale.

We finally highlighted the discovery of a hyper-velocity (HVS) He-sdO star with a radial velocity of 708 $\mathrm{km\,s^{-1}}$ unbound to the galaxy. While the two known HVS stars are main-sequence stars, this is the first highly-evolved HVS. The star is probably ejected by the supermassive black hole in the Galactic center.

REFERENCES

Bauer F., Husfeld D. 1995, A&A, 300, 481

Behara N. T., Jeffery C. S. 2006, Baltic Astronomy, 15, 115 (these proceedings)

Brown W. R., Geller M. J., Kenyon S. J., Kurtz M. J., 2005, ApJ, 622, L33

Dreizler S. 1993, A&A, 273, 212

Dreizler S. 2003, in *Stellar Atmosphere Modeling*, eds. I. Hubeny et al., ASP Conf. Ser., 288, 69

Dreizler S., Heber U., Werner K., Moehler S., de Boer K. S. 1990, A&A, 235, 235

Edelmann H., Heber U., Hagen H.-J., Lemke M., Dreizler S., Napiwotzki R., Engels D. 2003, A&A, 400, 939

Edelmann H., Napiwotzki R., Heber U., Christlieb N., Reimers D. 2005, ApJ (submitted)

Edelmann H., Heber U., Napiwotzki R. 2006, Baltic Astronomy, 15, 103 (these proceedings)

Greenstein J. L., Sargent, A. I. 1974, ApJS, 28, 157

Groth H. G., Kudritzki R. P., Heber U. 1985, A&A, 152, 107

Haas S. 1997, PhD Thesis, Univerity of Erlangen-Nürnberg

Haas S., Dreizler S., Heber U., Jeffery C. S., Werner K. 1996, A&A, 311, 669

Han, Z., Podsiadlowski P., Maxted P. F. L., Marsh T. R. 2003, MNRAS, 341, 669

Heber U. 1992, in *The Atmospheres of Early-Type Stars*, Lecture Notes in Physics, Springer-Verlag, 401, 233

Heber U., Reid I. N., Werner K. 2000, A&A, 363, 198

Hills J. G. 1988, Nature, 331, 687

Lanz T., Hubeny I., Heap S. R. 1997, ApJ, 485, 843

Lisker T., Heber U., Napiwotzki R., Christlieb N., Reimers D., Homeier D. 2004, Ap&SS, 291, 351

Lisker T., Heber U., Napiwotzki R. et al. 2005, A&A, 430, 223

Maxted P. F. L., Heber U., Marsh T. R., North R. C. 2001, MNRAS, 326, 1391

Napiwotzki R., Karl C. A., Lisker T., Heber U. et al. 2004, Ap&SS, 291, 321

O'Toole S., Heber U. 2006, A&A (submitted)

Ströer A., Heber U., Lisker T., Napiwotzki R., Dreizler S. 2005, in *14th European Workshop on White Dwarfs*, eds. D. Koester & S. Moehler, ASP Conf. Ser., 334, 309

Ströer A. 2004, Diploma Thesis, University of Erlangen-Nürnberg

Sweigart A. 1997, in *Third Conference on Faint Blue Stars*, eds. A. G. D. Philip, J. Liebert & R. A. Saffer, L. Davis Press, Schenectady, NY, p. 3

Thejll P., Bauer F., Saffer R. et al. 2004, ApJ, 433, 819

Webbink R. F. 1984, ApJ, 277, 252

Wesemael F., Winget D. E., Cabot W., van Horn H. M., Fontaine G. 1981, ApJ, 254, 221

Werner K., Dreizler S. 1999, J. Comp. and Appl. Mathematics, 109, 65

Baltic Astronomy, vol. 15, 99–102, 2006.

ANALYSIS OF THE FUSE SPECTRA OF THE HE-POOR SDO STAR MCT 0019−2441

M. Fontaine[1], P. Chayer[2,3], F. Wesemael[1], G. Fontaine[1] and R. Lamontagne[1]

[1] *Département de Physique, Université de Montréal, Montréal, H3C 3J7, Canada*

[2] *Bloomberg Center for Physics and Astronomy, The Johns Hopkins University, Baltimore, MD 21218, U.S.A.*

[3] *Department of Physics and Astronomy, University of Victoria, Victoria, BC, V8W 3P6, Canada*

Received 2005 August 1

Abstract. We present a preliminary analysis of the FUSE spectra of MCT 0019−2441, a relatively He-poor sdO star. Among the handful of absorption features of photospheric origin present in the ultraviolet, we identify the O VI doublet at 1031.9 and 1037.6 Å, the S VI doublet at 933.4 and 944.5 Å, the Si IV triplet at 1122.5 and 1128.3 Å and some N IV lines. While synthetic spectra based on NLTE line blanketed model atmospheres can reproduce most line profiles, they fail to reproduce the O VI line profiles in a satisfactory manner. Possible solutions to this puzzle are considered.

Key words: stars: hot subdwarfs – stars: abundances – stars: individual (MCT 0019−2441)

1. INTRODUCTION

The hot subdwarf MCT 0019−2441 ($V = 14.48$) was observed with the FUSE Observatory as a part of an ongoing effort at mapping the atmospheric chemical composition of a relatively large sample of sdB and sdOB stars (see, e.g., Fontaine et al. 2005). The main objective of this work is to understand better the physical processes that determine the chemical composition of subdwarf atmospheres. However, at $T_{\rm eff} = 58\,350$ K and $\log g = 5.6$, MCT 0019−2441 turned out to be a "cool" sdO star with a low helium abundance ($n_{\rm He}/n_{\rm H} = 0.08$). Since its FUSE spectra do not show the myriad of lines that are present in the spectra of most other hot subdwarf stars, MCT 0019−2441 is well suited for a complete spectral analysis, as the continuum level is clearly defined and most photospheric absorption features can be identified. A first look at the unusual FUSE spectra of this object was provided by Lamontagne et al. (2003), and we present here the first quantitative analysis of its abundance pattern.

2. OBSERVATIONAL MATERIAL AND MODEL ATMOSPHERES

The FUSE data on MCT 0019−2441 (dataset B0541001) are similar to those presented by Lamontagne et al. (2003) and consist of four exposures, for a total of 9.2 ksec. In parallel, a medium-resolution optical spectrum of MCT 0019−2441 was secured by M. Billères at the NTT, while two IUE low-dispersion observations were recovered from the MAST archives (images SWP 26277 and LWP 06290).

To carry out our analysis of the spectra, we use TLUSTY 200 and SYNSPEC 48 (Hubeny 1988; Hubeny & Lanz 1995) respectively for the computation of model atmospheres and synthetic spectra. These codes are used to generate grids of NLTE, homogeneous, plane-parallel models that include blanketing by the hydrogen and helium lines. A first grid, used to derive the atmospheric parameters, is devoid of heavy elements. Our fits to the hydrogen and helium lines yield $T_{\rm eff} = 58\,350$ K, $\log g = 5.6$ and $n_{\rm He}/n_{\rm H} = 0.08$. The corresponding reddening-free energy distribution shows good agreement with the composite energy distribution built from FUSE, IUE and optical data.

With these atmospheric parameters, grids of model atmospheres were generated that include detailed atomic models for O III through O VI and for S IV through S VI. Not only does this allow line blanketing by O and S to be accounted for, but NLTE populations of O and S can also be calculated and used in the computation of synthetic spectra. For other heavy elements (C, N, Si, P and Fe), we currently use a line blanketed model with log(O/H)= −5 and log (S/H) = −7 for the computation of synthetic spectra in which these elements are added as traces and treated in LTE. The atomic data for the lines is taken from the compilations of Kurucz[1].

3. ABUNDANCE ANALYSES

The ultraviolet line spectrum of MCT 0019−2441, although far simpler than that of the vast majority of hot subdwarfs, provides interesting challenges when confronted to detailed abundance analyses. Some features, like the Si IV 1128 Å lines, can be fit with the help of a χ^2 minimizing procedure that simultaneously optimizes the abundance and the level of the continuum. For the O VI lines the procedure does not work well, because the lines appear too strong to be entirely photospheric. In many cases, the absence of absorption features in the FUSE spectra led to upper limits on the abun-

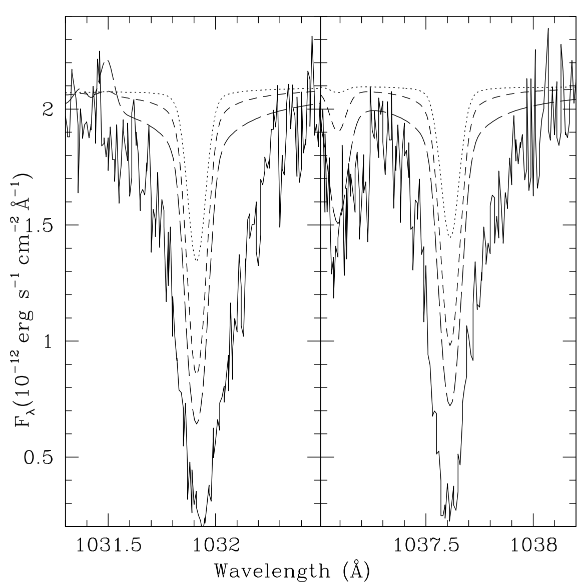

Fig. 1. Synthetic spectra with log (O/H) = –5 (dots), –4 (short dash) and –3 (long dash) compared to the FUSE data.

[1] see http://cfa-www.harvard.edu/amdata/ampdata/kurucz23/sekur.html

dance of the element considered. We now comment on specific elements.

Oxygen. We observe strong O VI resonance lines at 1031.9 and 1037.6 Å, with respective equivalent widths of ~ 275 and ~ 190 mÅ. They have the same velocity as the Lyman lines within the instrumental resolution (about 15 $\mathrm{km\,s^{-1}}$). At the same time, there is negligible absorption from O IV throughout the FUSE spectral range. The only O IV lines detected in the FUSE spectra (1067.768 and 1067.832 Å) indicate $\log(\mathrm{O/H}) < -4.8$, an abundance too low by orders of magnitude to reproduce the O VI equivalent widths, not to mention the line profiles (see Figure 1). This situation is addressed in the next section.

Sulfur. The S VI 933 and 944 Å lines are detected and have equivalent widths of 67.6 and 62.4 mÅ, respectively. The fit to the S VI 933 Å line yields an abundance of $\log(\mathrm{S/H}) = -7.9$, while the 944 Å line is best matched for $\log(\mathrm{S/H}) = -7.6$. In the latter case, the core of the line is still poorly matched.

Carbon. The C III 1175 Å multiplet is absent, while the C III 977 Å resonance line is strong. This indicates that C III absorption occurs in the ISM, as the 1175 Å multiplet arises from an excited state. Unfortunately, there are no additional constraints to be extracted from the IUE spectra, since the C IV resonance lines are absent. From the absence of absorption features near 1175 Å, we derive an upper limit to the photospheric carbon abundance of $\log(\mathrm{C/H}) < -7.0$.

Nitrogen. The N IV lines around 922–955 Å are all compatible with an abundance of $\log(\mathrm{N/H}) = -7.6 \pm 0.3$, but there are minor discrepancies between the shape of the observed continuum and the synthetic spectrum in this spectral interval. This may perhaps be due to small errors in the values of the atmospheric parameters we determined or to problems with the flux calibration of the FUSE data at such short wavelength.

Silicon. The Si IV 1128 Å lines are well matched by our automated χ^2 procedure, yielding $\log(\mathrm{Si/H}) = -7.4$. The 1122 Å line is blended with a Fe III ISM line, but the observed feature is compatible with the derived abundance.

Phosphorus. The absence of the P V resonance lines at 1118.0 and 1128.0 Å yields an upper limit of $\log(\mathrm{P/H}) < -9.6$. The atmosphere of MCT 0019−2441 appears to be completely devoid of phosphorus, an element observed in most hot subdwarfs.

Iron. The FUSE spectra have been inspected for evidence of Fe V or Fe VI lines or both. Their non-detection implies an upper limit of $\log(\mathrm{Fe/H}) < -5.0$ under LTE assumption. We stress that NLTE effects play an important role in the ionization and excitation balance of iron under such atmospheric conditions and are not accounted for in this preliminary analysis.

4. DISCUSSION

Many lines routinely seen in hot subdwarfs are absent from the ultraviolet spectrum of MCT 0019−2441; we nevertheless have some difficulty in accounting for the strongest features, those of O VI, observed in the spectrum. While small errors in the atmospheric parameters (T_{eff} and $\log g$) could play some role in explaining these difficulties, we note that the parameters we derive reproduce satisfactorily both the optical spectrum and the overall energy distribution; the only disagreement appears in the predicted continuum in the 910–950 Å region. We also remark that, while our calculations for the Stark broadening of the O VI and S VI lines make use of the latest semi-classical damping constants of Dimitrijević & Sahal-

Bréchot (1992, 1993), there are still no fully quantum-mechanical calculations of the broadening of these lines.

In addition to these obvious possibilities, other scenarios should perhaps also be considered to account for the strength of the O VI lines. The first possibility is that their strength reflects an inhomogeneous equilibrium distribution of heavy elements. A stratification of this type might be disrupted by a weak stellar wind, however. In MCT 0019−2441, the O VI lines do show asymmetric profiles that may be related to the presence of such a wind. It appears therefore unlikely that stratification can be invoked to solve the puzzle of the O VI lines.

Another possibility is a contribution to the observed profile from diffuse O VI absorption in the local ISM. This is considered unlikely, on the basis of the recent analysis by Oegerle et al. (2005) of 25 lines of sight to nearby ($d < 250$ pc) white dwarfs. They report equivalent widths of O VI lines less than 22 mÅ. Situated ~ 1.7 kpc away, however, MCT 0019−2441 is significantly beyond the distance sampled by Oegerle et al. On a much longer line of sight ($d = 10.2$ kpc), Howk et al. (2003) present an analysis of vZ 1128, a post-AGB star located in the globular cluster M 3, which shows an ultraviolet spectrum similar to that of MCT 0019−2441. They suggest that the O VI absorption, with equivalent widths of 260 mÅ and 150 mÅ respectively, arises at the interfaces between the hot and warm phases of the ISM. While the line strengths are compatible with those observed in MCT 0019−2441, the distance is significantly larger than that to our target.

A final possibility is that circumstellar material might contribute to the observed O VI absorption. In the case of vZ 1128, Howk et al. (2003) argue that this is unlikely given the absence of high-velocity material. The same argument could be made for MCT 0019−2441, but the issue could be settled by a direct observation of the surroundings of that star. For instance, Otte et al. (2004) report the detection of a O VI-emitting nebula around the hot white dwarf KPD 0005+5106 ($T_{\rm eff} = 120\,000$ K, $\log g = 7.0$), a hot PG 1159 star known to show O VI absorption in the optical (Sion et al. 1985).

ACKNOWLEDGMENTS: This work was supported in part by the NSERC Canada, by the Fund FQRNT (Québec) and by NASA contract NAS5-32985.

REFERENCES

Dimitrijević M. S., Sahal-Bréchot S. 1992, A&AS, 93, 359

Dimitrijević M. S., Sahal-Bréchot S. 1993, A&AS, 100, 91

Fontaine M., Chayer P., Wesemael F. et al. 2005, in *Astrophysics in the Ultraviolet*, eds. G. Sonneborn, H. W. Moos & B.-G. Andersson, in press

Howk J. C., Sembach K. R., Savage B. D. 2003, ApJ, 586, 249

Hubeny I. 1988, Computer Physics Comm., 52, 103

Hubeny I., Lanz T. 1995, ApJ, 439, 875

Lamontagne R., Chayer P. et al. 2003, in *White Dwarfs*, eds D. de Martino, R. Silvotti, J.-E. Solheim & R. Kalytis, NATO Science Series II, 105, 159

Oegerle W. R. et al. 2005, ApJ, 622, 377

Sion E.M., Liebert J., Starrfield S. G. 1985, ApJ, 292, 471

Baltic Astronomy, vol. 15, 103–106, 2006.

METAL ABUNDANCES OF SDB STARS

H. Edelmann[1], U. Heber[1] and R. Napiwotzki[2]

[1] *Remeis-Sternwarte Bamberg, Astronomisches Institut der Universität Erlangen-Nürnberg, Sternwartstrasse 7, D-96049 Bamberg, Germany*

[2] *Centre for Astrophysics Research, University of Hertfordshire, College Lane, Hatfield AL10 9AB, U. K.*

Received 2005 August 1

Abstract. The surface abundance patterns of four dozen bright sdB stars have been determined from high resolution, high S/N optical spectra. As typical in early B stars, the metal lines are few and weak. We searched for trends of the metal abundance patterns with the atmospheric parameters (effective temperature and gravity). It is remarkable that almost all metal abundances of sdBs with $T_{\rm eff} < 32\,000$ K stay at similar values, virtually independent of stellar parameters. The only exceptions are He and C which vary considerably from star to star. The hottest EHB stars lack O, Mg, Al and Si. Furthermore, all stars are rotating very slowly or not at all.

Key words: stars: abundances – stars: horizontal-branch – stars: rotation – hot subdwarfs

1. INTRODUCTION

The atmospheres of hot subdwarfs represent a huge puzzle in stellar physics: some chemical elements (such as helium) are highly depleted, whereas other elements (e.g., iron group elements) are enriched by factors up to a few 10 000 (Edelmann et al. 2001). Although these anomalies can probably be understood in terms of chemical layering processes in stellar envelopes (gravitational settling, radiative levitation and mass-loss), current models fail to explain the observed abundance patterns by orders of magnitudes. Also, the available sample of stars with well determined abundances is far too small to constrain diffusion theory. We present here the analysis for 49 sdB stars to determine their surface metal abundance patterns. This analysis has increased drastically (factor of ten) the number of detailed metal abundance analyses of sdB stars done so far.

2. OBSERVATIONS

Optical echelle spectra with high S/N were obtained at the German-Spanish Astronomical Center (DSAZ) on Calar Alto, Spain, with the 2.2 m telescope equipped with the FOCES spectrograph and at the ESO 1.5 m and 2.2 m telescopes equipped with the FEROS spectrograph. The observational dataset is homogeneous due to similar spectral resolutions (0.14Å at DSAZ and 0.09Å at ESO) and spectral coverage (3900 Å-6900 Å at DSAZ and 3600Å–8900Å at ESO) of all observed sdBs.

3. ANALYSIS

The atmospheric parameters (effective temperature, gravity and helium abundance) of all sdB's were derived simultaneously from the spectra by means of a χ^2 fit using fully line blanketed LTE model atmospheres (updated version of the code of Heber 1986). The results for all program stars are shown in Figure 1 in a theoretical ($T_{\rm eff}$ vs. log g) diagram.

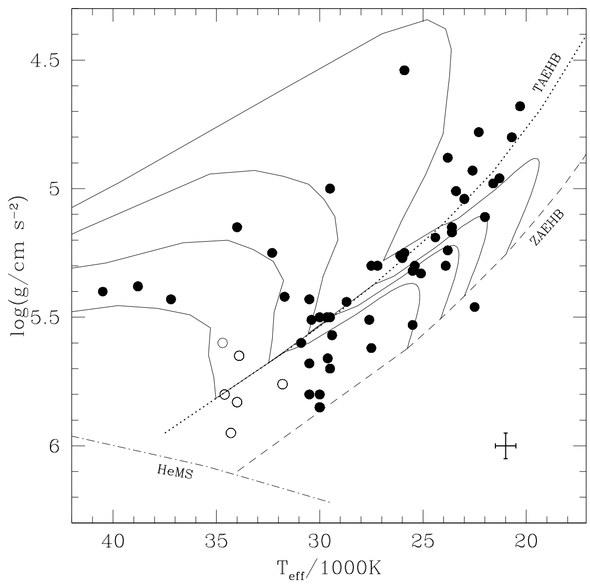

Fig. 1. Program stars in the $T_{\rm eff}$ vs.log(g) plane (stars denoted by open symbols lack of O, Mg, Al and Si).

LTE abundances were derived for all metals from measured equivalent widths using the classical curve-of-growth method. We generated model atmospheres, using the atmospheric parameters and solar metal abundances with the ATLAS9 code of Kurucz (1992). From these models we calculated curves-of-growth for the observed metal lines, from which abundances were derived. Blends from different ions were omitted from the analysis. Finally, the abundances were determined from a detailed spectrum synthesis for all lines measured before. The atomic data for the analysis were taken from the list of Wiese et al. (1996) for the CNO elements, from Kurucz (1992) and Ekberg (1993) for Fe and for all other elements from the table of Hirata & Horaguchi (1995).

4. TRENDS WITH ATMOSPHERIC PARAMETERS?

The chemical abundances observed in the atmospheres of sdB stars are very puzzling. There is now general consensus, that the peculiar abundance patterns are due to *diffusion.* Diffusion denotes the interplay between radiative acceleration (directly proportional to $T_{\rm eff}^4$) which levitates particles into upper regions, and the gravity which settles heavier particles into lower regions inside the envelope of stars. Therefore, we tried to identify possible trends of the chemical composition with $T_{\rm eff}$, log g and the luminosity (expressed in terms of the Eddington luminosity L_e).

Figure 2 shows the results for helium and for some (five) of the analyzed metal ions. Binarity and pulsations may influence the metal abundance patterns. Therefore we indicate known short period binaries (triangles) and pulsators (circles) in Figure 2. However, their metal abundance do not differ from those of apparently single, non-pulsating sdB stars (squares). Surprisingly, the abundances for most analyzed metal ions (especially for N II and Fe III) are constant irrespective of the stellar parameters. Only for S II and also for N III there seem to be a direct correlation with the stellar parameters: the larger the temperature and/or gravity, the larger the abundance for S II, and the lower the abundance for N III. However, this is most likely due to NLTE effects because the dominant ionization stages (N II and S III) do not show such trends.

For most of our program stars hotter than $\sim$32 000 K no absorption lines due to O, Mg, Al and Si can be detected in the optical wavelength range. This indicates that for the majority of sdB stars the abundances of O, Mg, Al and Si drop suddenly from a slightly subsolar value below $\sim$32 000 K to larger depletion for $T_{\rm eff}$ exceeding 32 000 K (see Figure 2). There are a few exceptions, though.

Those hot stars ($T_{\rm eff} > 32\,000$ K) that do show O, Mg, Al and Si are all of low gravity and, therefore, have evolved off the EHB. None of the hot sdB stars on or near the EHB show O, Mg, Al and Si lines (see Figure 1).

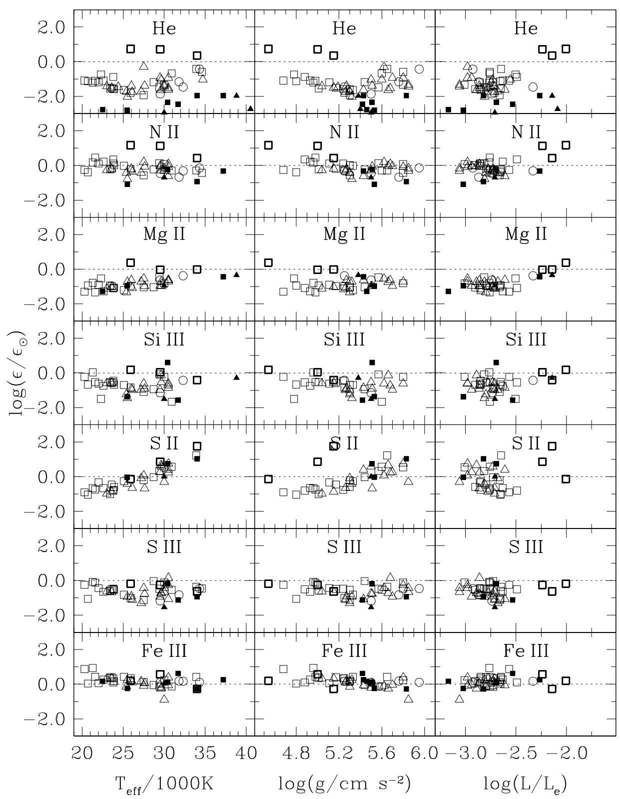

Fig. 2. Sample LTE abundances for all analyzed sdB stars relative to the solar values (dashed horizontal lines) versus $T_{\rm eff}$, log g and $L/L_{\rm e}$ (different symbols, see text).

Furthermore, three of those more luminous stars show a supersolar helium abundance (indicated by thick open symbols in Figure 2) and metal abundances which are almost solar or even higher in the case of N and Ar, which are enriched each by a factor or 3–10.

In a previous analysis of a large sample of low resolution spectra of sdB stars drawn from the Hamburg Quasar survey (Edelmann et al. 2003) we found a general trend of the helium abundances to increase with increasing $T_{\rm eff}$. Actually, sdB stars were found to separate into two distinct sequences. A small fraction (1/6) have much lower helium abundances at the same temperatures than the bulk of sdB stars. For the program stars presented here, we find also two distinct sequences with exactly the same fraction of stars (1/6) to show a helium "underabundancy" (indicated by filled symbols in Figure 2). The metal abundances of these helium underabundant sdB stars, however, do not differ from those of the others.

5. ROTATION

The projected rotational velocity can be measured by comparing synthetic line profiles, calculated for the given atmospheric parameters ($T_{\rm eff}$, log g, element abundance) of a star folded with an adopted rotational velocity, with the observed line profiles. The Mg II doublet at 4481.13 Åand 4481.33Åis most suitable for this purpose. The lines are very narrow and closely separated, and therefore very sensitive to rotational broadening. If the doublet is resolved into two components, the projected rotation velocity has to be very small. Only sdB stars that are known to be in short period binary systems show significant rotation. All others are slow rotators ($v_{\rm rot}$ $\sin(i) < 3$ km s^{-1}) or do not rotate at all (unless seen pole-on).

6. CONCLUSION

With this work, the number of detailed metal abundance analyses of sdB stars has increased drastically (by a factor of ten). We have selected sdB stars for the abundance analysis covering a wide range of parameter space, which allowed us to search for trends of the metal abundances with these parameters. It is remarkable that for all program stars the abundances for many metals which are common in the atmospheres of sdB stars (C, N, S, Ar and Fe), are similar all over the parameter space. The same holds for O, Mg, Al and Si, but, only for stars with $T_{\rm eff} < 32\,000$ K. These metals practically vanish from the surface of most sdB stars with higher temperatures. Only for luminous (i.e., post-EHB) sdB stars the abundances of O, Mg, Al and Si are "normal", or become even larger than in the cooler EHB stars. No obvious differences for the abundances of pulsating or non-pulsating, and radial velocity variable or non-variable sdB stars became apparent. Our results represent a challenge for a theoretical interpretation.

REFERENCES

Ekberg J. O. 1993, A&AS, 101, 1

Edelmann H., Heber U., Napiwotzki R. 2001, Astron. Nachr., 322, 401

Edelmann H., Heber U., Hagen H.-J., Lemke M., Dreizler S., Napiwotzki R., Engels D. 2003, A&A, 400, 939

Heber U. 1986, A&A, 155, 33

Hirata R., Horaguchi T. 1995, *Atomic Spectral Line List*, Department of Astronomy, Faculty of Science, Kyoto University, and National Science Museum, 3-23-1 Hyakunin-cho, Shinjuku-ku, Tokyo

Kurucz R. L. 1992, in *The Stellar Populations of Galaxies*, IAU Coll. 149, eds. B. Barbuy & A. Renzini, Kluwer Academic Publishers, Dordrecht, p. 225

Wiese W. L., Fuhr J. R., Deters T. M. 1996, in *Atomic Transition Probabilities of Carbon, Nitrogen and Oxygen: a Critical Data Compilation*, eds. W. L. Wiese, J. R. Fuhr & T. M. Deters, American Chemical Society ... for the National Institute of Standards and Technology (NIST), Washington, QC 453 W53

Baltic Astronomy, vol. 15, 107–114, 2006.

NLTE ANALYSES OF SDB STARS: PROGRESS AND PROSPECTS

N. Przybilla[1], M. F. Nieva[1,2] and H. Edelmann[1]

[1] *Remeis-Sternwarte Bamberg, Sternwartstrasse 7, D-96049 Bamberg, Germany*

[2] *Observatório Nacional, R. Gal. José Cristino 77, 20921-400, São Cristóvão, Rio de Janeiro, RJ, Brasil*

Received 2005 July 31

Abstract. We report on preliminary results of a hybrid non-LTE analysis of high-resolution, high-S/N spectra of the helium-rich subdwarf B star Feige 49 and the helium-poor sdB HD 205805. Non-LTE effects are found to have a notable impact on the stellar parameter and abundance determination. In particular the He I lines show significant deviations from detailed balance, with the computed equivalent widths strengthened by up to $\sim$35 %. Non-LTE abundance corrections for the metals (C, N, O, Mg, S) are of the order $\sim$0.05 – 0.25 dex on the mean, while corrections of up to $\sim$0.7 dex are derived for individual transitions. The non-LTE approach reduces systematic trends and the statistical uncertainties in the abundance determination. Consequently, non-LTE analyses of a larger sample of objects have the potential to put much tighter constraints on the formation history of the different sdB populations than currently discussed.

Key words: line: formation – stars: abundances – stars: atmospheres – stars: fundamental parameters – stars: evolution – hot subdwarfs

1. INTRODUCTION

Astrophysics faces the general difficulty that almost all relevant information cannot be directly inferred from observation. One has to rely on the interpretation of the radiation from a light-emitting plasma and its interaction with matter. Accurate physical modeling is crucial, with systematic uncertainties often dominating the error budget at present. In the case of subdwarf B (sdB) stars quantitative spectroscopy is well established, relying on grids of either line-blanketed LTE or metal-free non-LTE model atmospheres (e.g., Heber & Edelmann 2004 and references therein). Here we investigate what improvements on sdB analyses can be expected from a hybrid non-LTE method, which avoids the weaknesses of both traditional approaches by combining metal line-blanketed model atmospheres with non-LTE line formation. The impact on the stellar parameter determination is of special interest, as this provides the basis for all further interpretation. Then, in the second part, non-LTE metal abundances are determined from observations in the visual spectral range for the first time. More accurate stellar parameter and abundance determinations can be expected to shed further light on the formation mechanisms of sdB stars that have been debated over the last decades.

2. MODEL CALCULATIONS AND OBSERVATIONAL DATA

The model calculations are carried out in a hybrid approach, thus solving the (so-called) restricted non-LTE problem. Hydrostatic, plane-parallel and line-blanketed – via an opacity sampling (OS) technique – LTE model atmospheres are computed with the Atlas12 code (Kurucz 1996), which is in particular suited for the analysis of chemically peculiar stars. Then, non-LTE line formation is performed on the resulting model stratifications. The coupled radiative transfer and statistical equilibrium equations are solved, and spectrum synthesis with refined line-broadening theories is performed using Detail and Surface (Giddings 1981; Butler & Giddings 1985). Both codes have undergone major revisions and improvements over the past few years. State-of-the-art non-LTE model atoms (see Table 1) are utilized for the stellar parameter and abundance determination.

The model atoms are largely based on data from quantum-mechanical *ab-initio* computations using the R-matrix method in the close-coupling approximation, which typically have uncertainties of the order ∼10–20 %. Data sources comprise the astrophysically motivated Opacity and IRON Project, but also the vast physics literature, see the original publications for details. This allows for a realistic treatment not only of the (non-local) radiative processes, which drive the departures from detailed balance. Also the thermalizing collisions are accurately represented for the relevant transitions, in contrast to the usual approach of applying simple approximation formulae, which can be in error by orders of magnitude. Finally, state-of-the-art line-broadening theories are accounted for, like the data of Stehlé & Hutcheon (1999) for the Stark broadening of the hydrogen lines.

Spectra of HD 205805 and Feige 49 were taken with Feros (Kaufer et al. 1999) on the ESO 1.52 m and 2.2 m telescopes, respectively. The Echelle spectra were reduced using standard procedures, giving complete wavelength coverage of the entire visual spectral region at high S/N (>100) and high resolution ($R \simeq 48\,000$).

3. STELLAR PARAMETERS

Standard methods are used for the stellar parameter determination, by simultaneous fitting the hydrogen Balmer and helium line profiles, and when possible utilizing the He I/II ionization balance. We deviate from the usual approach based on χ^2-fitting on grids of synthetic spectra, because of the largely increased computational expenses for OS model atmospheres and non-LTE line formation. For

Table 1. Non-LTE model atoms.

Ion	Source
H	Przybilla & Butler (2004)
He I/II	Przybilla (2005)
C II/III	Nieva & Przybilla (in prep.)
N II/III	Przybilla & Butler (2001), with extensions
O II	Becker & Butler (1988)
Mg II	Przybilla et al. (2001)
S II/III	Vrancken et al. (1996), with updated atomic data

Table 2. Stellar parameters.

	HD 205805	Feige 49
$T_{\rm eff}$ (K)	25 000	35 000
$\log g$ (cgs)	5.00	5.25
ξ (km/s)	0	2
y	0.01	0.15
$v \sin i$ (km/s)	0	0

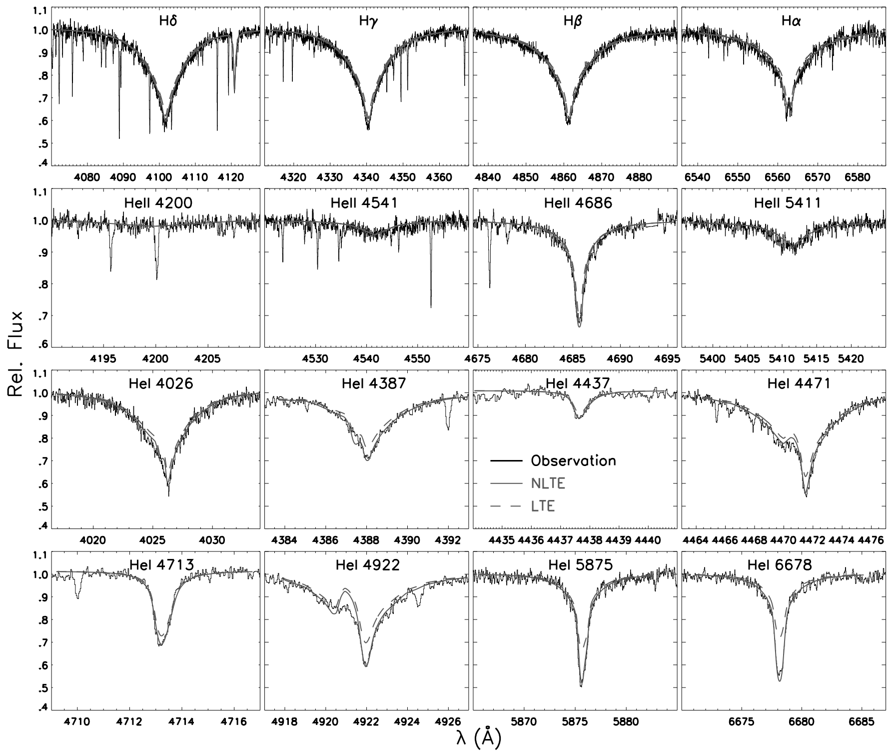

Fig. 1. Fits to H and He lines in the helium-rich sdB Feige 49.

the moment, the fits are done by eye. The resulting stellar parameters, effective temperature T_{eff}, surface gravity $\log g$, microturbulence ξ, helium abundance y (by number) and projected rotational velocity $v \sin i$, are summarized in Table 2.

Examples for the quality of the modeling achievements are displayed in Figures 1 and 2, where our spectrum synthesis for several diagnostic features (grey lines) is compared to observation (histogram) for the two sample stars. Obviously, non-LTE line formation (full lines) improves enormously on the LTE spectrum synthesis for identical stellar parameters (dashed lines), resulting in a practically perfect match of theory and observation (except for the forbidden component of He I at 4922 Å).

The largest discrepancies between non-LTE and LTE results occur for some He I lines. Non-LTE equivalent widths are larger by up to ∼35 % in particular for the strong features in the red. Both, line wings and cores can be affected. This is because the lower levels of the transitions (for principal quantum number $n = 2$) are overpopulated relative to states at higher excitation energy that couple closely to the He II ground state, which is in detailed balance. Among the He II lines only the He II 4686 Å line gets slightly strengthened by non-LTE effects. A similar situation as with the He I lines occurs with the hydrogen Balmer lines because of an analogous non-LTE overpopulation of the $n = 2$ level, which also can affect the line wings (most notable for Hα in Feige 49). The non-LTE effects get reduced with decreasing temperature. In HD 205805 only the line cores are affected.

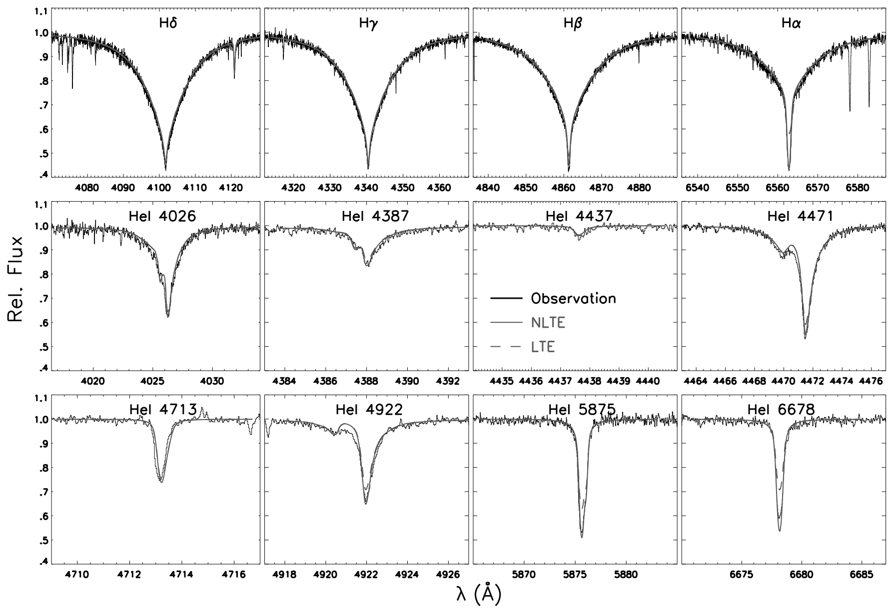

Fig. 2. Fits to H and He lines in the helium-poor sdB HD 205805.

It is obvious that the overall differences in the fitting process will impact the stellar parameter determination. In the present case this transfers into a $\Delta T_{\rm eff}$ of +1000 and +1200 K and a $\Delta \log g$ of +0.10 and +0.12 dex for Feige 49 and HD 205805 relative to the LTE results of Edelmann et al. (2006). These *systematic* shifts are slightly larger than the typically attributed uncertainties of sdB analyses. Further refinements can be expected from the use of (multiple) non-LTE ionization equilibria of metals which are even more sensitive to stellar parameter changes than the hydrogen and helium lines. So far, only the S II/III ionization equilibrium has been used to verify the parameter determination for HD 205805 from H and He line profile fits (see below).

4. ELEMENTAL ABUNDANCES

Besides unbiased stellar parameters, which are a prerequisite for meaningful comparisons with stellar evolution computations, also the surface abundances of the heavier elements bear important information. They allow to put observational constraints on formation/evolution scenarios of the stars and on transport processes (in particular diffusion for sdBs) in stellar atmospheres.

For the time being, non-LTE abundances are determined only for H, He, C, N, O and the α-elements Mg and S because we lack realistic non-LTE model atoms for the other chemical species. The lighter elements are of interest because of their involvement in fusion reactions, either as catalysts or as burning products, thus giving clues on the nature of the sdB progenitors. The α-process elements on the other hand can be used as tracers for the stellar metallicity. All the present-day abundances may be of course subject to diffusion. We intend to extend the study to Al, Si and Fe in the near future. Work on this is in progress.

Elemental abundances are derived from line-profile fits, using a χ^2-minimization

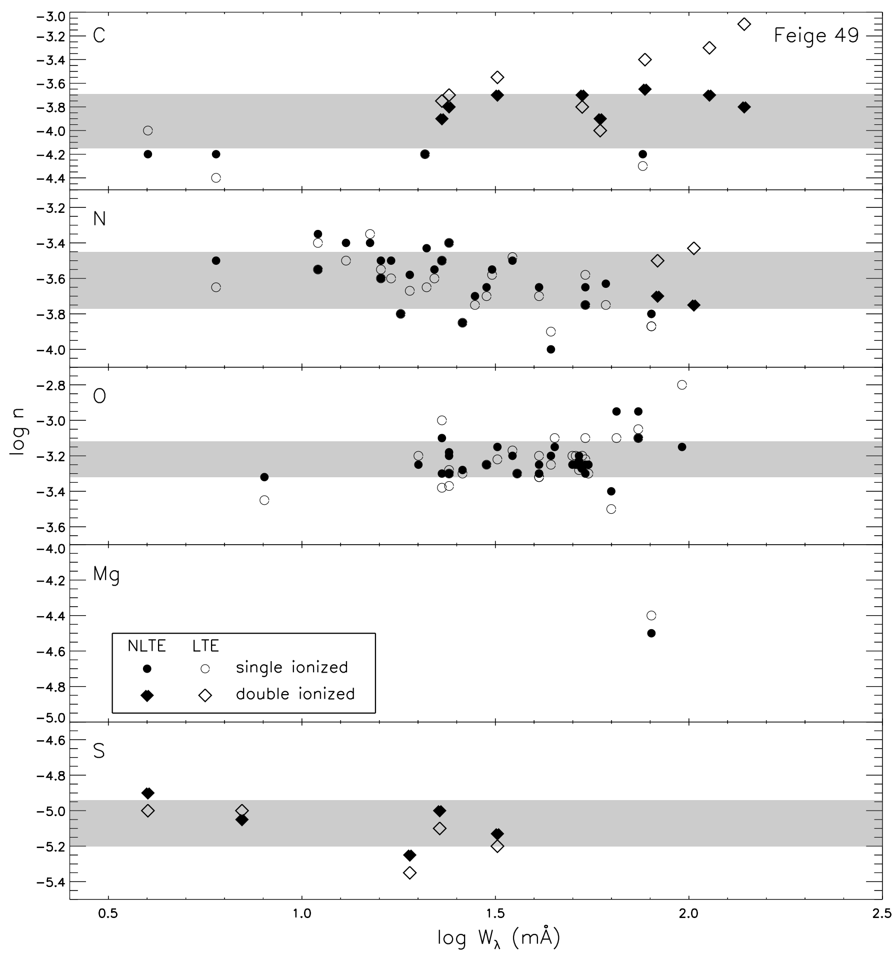

Fig. 3. Elemental abundances in Feige 49 from individual spectral lines.

technique based on small grids of synthetic spectra with varying abundances for given stellar parameters. This puts tighter constraints than the standard equivalent-width analysis. Abundances (by number) from individual spectral lines as a function of equivalent width are displayed in Figures 3 and 4. Non-LTE abundances are denoted by full and LTE results by open symbols; circles mark single-ionized and diamonds double-ionized species. The grey bands indicate the 1σ-uncertainty range of the resulting abundances for the chemical species.

The results have to be viewed as preliminary, as abundances from the different ionization stages of the elements – in particular C II/III and N II/III – indicate a need to improve on the stellar parameters. Metal ionization equilibria react much more sensitively to changes than the hydrogen and helium lines, such that the necessary fine-adjustments will barely impact the fit quality of the latter. However, already now the advantages of non-LTE computations become apparent: a tendency towards a reduced statistical scatter relative to LTE and a reduction of systematic trends, like for N II in HD 205805. The aim is to push the statistical 1σ-

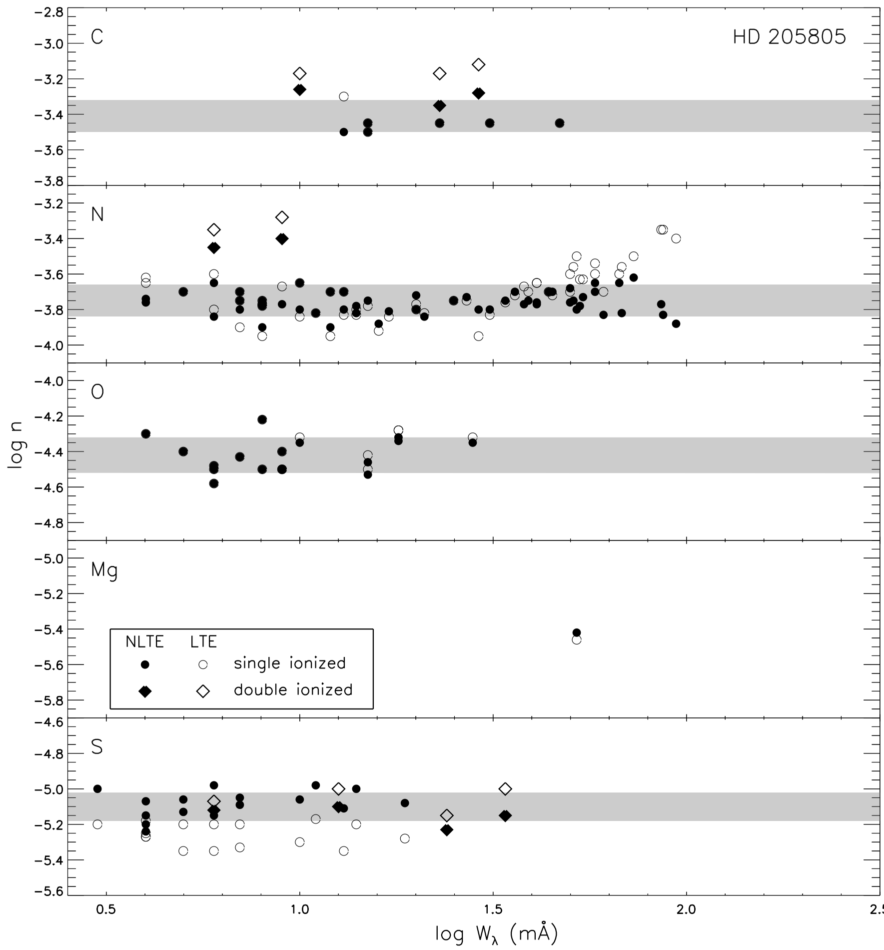

Fig. 4. Elemental abundances in HD 205805 from individual spectral lines.

Table 3. Metal abundances in the sample stars, relative to the solar standard (Grevesse & Sauval 1998): $[\log n] = \log n_\star - \log n_\odot$.

		C II	C III	N II	N III	O II	Mg II	S II	S III
Feige 49	NLTE	−0.72	−0.29	+0.48	+0.35	−0.05	−0.08	...	−0.27
		...	0.10	0.16	0.04	0.10	...	...	0.13
	LTE	−0.75	−0.10	+0.44	+0.61	−0.06	+0.02	...	−0.33
		0.17	0.30	0.15	0.05	0.14	...	...	0.15
HD 205805	NLTE	+0.01	+0.18	+0.32	+0.65	−1.25	−1.00	−0.28	−0.35
		0.03	0.05	0.06	0.04	0.10	...	0.08	0.06
	LTE	+0.05	+0.33	+0.38	+0.77	−1.24	−1.04	−0.46	−0.25
		0.07	0.03	0.14	0.05	0.10	...	0.07	0.07

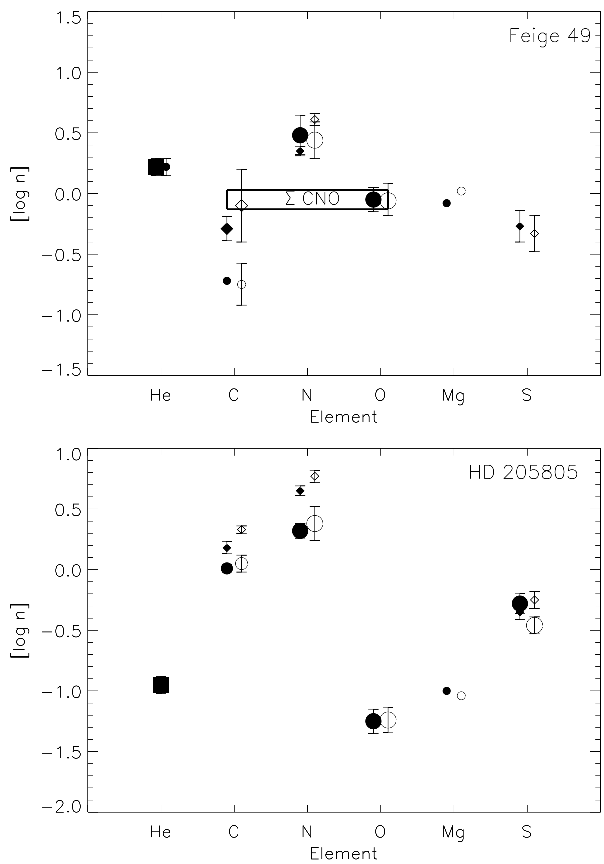

Fig. 5. Elemental abundances in the two sample sdBs (symbols as in Fig. 4).

uncertainties below 0.1 dex, like in similar computations for BA-type supergiants (Przybilla 2002) and B-type main-sequence stars (Nieva & Przybilla, in prep.). The systematic uncertainties need to be determined, but they can be expected to be of the order ∼0.1 dex on the mean, as in the other cases.

The metal abundances of the sample stars relative to the solar standard are summarized in Table 3. For each ionic species non-LTE and LTE results with uncertainties derived from the line-to-line scatter are given. The data is also displayed in Figure 5, using the same symbols as in the figures before, with the symbol size encoding the number of lines used for the abundance determination.

The abundance pattern for Feige 49 indicates mixing of the surface layers with CNO-processed material: He and N are enriched and C is depleted. Oxygen appears to be unchanged relative to the other α-elements, which indicate approximately solar metallicity for this star. Note that the sum of the CNO abundances also gives a value close to solar, emphasizing the catalyst role of these species. The pattern is unusual for a sdB star. On the other hand, HD 205805 shows an abundance pattern more typical for sdB stars, indicating that diffusion processes have been active.

5. CONCLUSIONS AND PROSPECTS

Hybrid non-LTE analyses of two sdB stars demonstrate that non-LTE effects have to be accounted for in the stellar parameter and abundance determination, resulting in excellent fits of *all* the diagnostic spectral features. Systematic shifts in the basic parameters $T_{\rm eff}$ and $\log g$ are implied and non-LTE abundance corrections on the order of $\sim$0.05–0.25 dex on the mean. The latter are similar to corrections of metal abundances in (less-luminous) BA-type *supergiants* (Przybilla 2002).

The next steps in the refinements of the method will include the necessary fine-adjustments in the stellar parameter determination in order to meet the constraints imposed by various metal ionization equilibria. The uncertainties in the metal abundances can then be expected to drop below 0.1 dex, as experience tells us from analyses of objects in other parts of the Hertzsprung-Russell diagram. Additional non-LTE model atoms are required for a few other important diagnostic chemical species, like aluminum (an element with odd neutron number), silicon (another α-element, highly valuable for stellar parameter estimations) and iron (to cover iron group abundances).

Similar analyses of a larger sample of sdB stars, and an extension towards the sdO regime, will allow for unbiased positioning in the $T_{\rm eff}$ vs. $\log g$ plane. This will help to delineate the different populations of subluminous stars with unprecedented accuracy and may provide the crucial clues for uncovering their formation history (single vs. binary star evolution channels). A stellar sample with highly accurate parameter and abundance determinations will hereby also put tight observational constraints on the stellar evolution computations. These can be used for an empirical calibration of the parametrization of complex (hydrodynamical) phenomena involved in the stellar evolution calculations, thus leading to an improved modeling.

REFERENCES

Becker S. R., Butler K. 1988, A&A, 201, 232
Butler K., Giddings J. R. 1985, in Newsletter on Analysis of Astronomical Spectra, No. 9, Univ. London
Edelmann H., Heber U., Napiwotzki R. 2006, Baltic Astronomy, 15, 103 (these proceedings)
Giddings J. R. 1981, Ph. D. thesis, Univ. London
Grevesse N., Sauval A. J. 1998, Space Sci. Rev., 85, 161
Heber U., Edelmann H. 2004, Ap&SS, 291, 341
Kaufer A., Stahl O., Tubbesing S. et al. 1999, ESO Messenger, 95, 8
Kurucz R. L. 1996, in *Model Atmospheres and Spectrum Synthesis*, eds. S. J. Adelman, F. Kupka & W. W. Weiss, ASP Conf. Ser., 108, 160
Przybilla N. 2002, Ph. D. thesis, Univ. Munich
Przybilla N. 2005, A&A, 443, 293
Przybilla N., Butler K. 2001, A&A, 379, 955
Przybilla N., Butler K. 2004, ApJ, 609, 1181
Przybilla N., Butler K., Becker S. R., Kudritzki R. P. 2001, A&A, 369, 1009
Stehlé C., Hutcheon R. 1999, A&AS, 140, 93
Vrancken M., Butler K., Becker S. R. 1996, A&A, 311, 661

Baltic Astronomy, vol. 15, 115–122, 2006.

NEW MODEL ATMOSPHERES FOR HYDROGEN-DEFICIENT STARS: CONTINUOUS AND LINE OPACITIES

N. T. Behara and C. S. Jeffery
Armagh Observatory, College Hill, Armagh BT61 9DG, N. Ireland

Received 2005 August 1

Abstract. The model atmosphere code STERNE has evolved considerably over the years. Most recently, attention has turned to revising the treatment of both continuous and line opacities. Opacity Project photoionization cross-sections have been incorporated and an opacity sampling technique has been implemented. The new opacities and methods are described, while the principal consequences for the models are presented. In studying the application of these new models to atmospheres with extreme chemical compositions, we find the new opacity treatment increases the temperature in the line forming region by 1000–3000 K for extremely hydrogen-poor stars with $T_{\rm eff}$ around 30 000 K. This implies cooler effective temperature measurements for stars of this type.

Key words: stars: atmospheres – stars: chemically peculiar

1. INTRODUCTION

Hydrogen deficiency is a wide spread phenomenon occurring in a variety of stellar objects such as extreme helium stars, hydrogen-deficient binaries, helium-rich subdwarfs, Wolf-Rayet stars, R CrB stars and helium white dwarfs. These hydrogen-deficient systems are believed to evolve by very different processes. R CrB and extreme helium stars evolve by binary merger or last thermal pulse evolution from the white dwarf phase, hydrogen-deficient binary stars through a sequence of mass exchange phases, and helium-rich subdwarfs evolve possibly through white dwarf mergers, late helium flash or common envelope evolution.

Stellar atmosphere models are an essential tool used in the derivation of fundamental stellar parameters, such as effective temperature, surface gravity and overall metallicity, as well as determining individual element abundances. The accuracy of the atmospheric structure obtained from our models is inherently dependent on the quality of the atomic data used and the methods by which they are incorporated into the models, especially in the case of hydrogen-deficient atmospheres.

Because neutral helium is a poor absorber, the effect of continuous and line opacity is of greater importance in hydrogen-deficient stars, shown in Figure 1. The figure on the left shows the emergent flux distribution of hydrogen-rich atmospheres and on the right for hydrogen-deficient atmospheres with ($T_{\rm eff}$, $\log g$) = (10 000, 1.0), (11 000, 1.0), (12 000, 1.0), (13 000, 1.5) and (14 000, 1.5). Continuum-only models are shown by dotted lines and line-blanketed models by

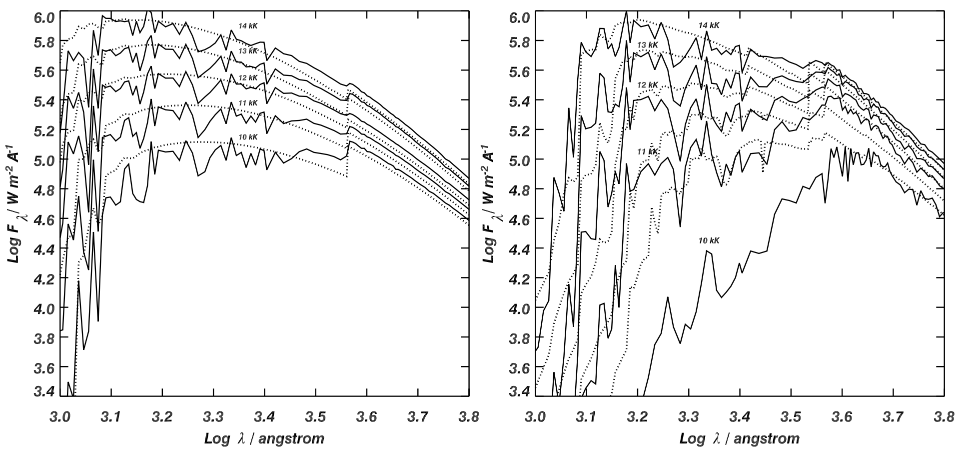

Fig. 1. Importance of line blanketing in hydrogen-rich atmosphere (left panel) and hydrogen-deficient atmospheres (right panel). The figure on the left is from Dudley & Jeffery (1993).

solid lines labeled with effective temperature. The effects of line blanketing on the flux distribution are extremely marked for stars with effective temperatures below 14 000 K.

The entire spectrum of hydrogen-deficient stars comprises an inhomogeneous mix of chemical abundances. For example, in the case of extreme helium stars the hydrogen abundance is roughly 1 part in 10^4, and carbon dominates the opacity at many wavelengths. As a consequence, the carbon abundance greatly influences the atmospheric structure. However, hydrogen-deficient binaries are carbon-poor and nitrogen-rich, while for a few hot R CrB stars $n_{\rm H}$ may be as high as 0.1. In order to model these atmospheres correctly, we should adapt the composition of our models to the composition of stars.

Theoretical work in recent years has provided superior calculations of continuous opacities, and the contribution of absorption lines to the overall opacity has also been an area of progress since STERNE was originally written. We discuss the recent revisions to STERNE and compare some results of the new updated version to the last published version of the code (Jeffery & Heber 1992).

1.1. STERNE – model atmosphere program

The LTE model atmosphere code STERNE was originally developed to study hydrogen-deficient stars. The code is optimized for stars with effective temperatures between 10 000 K and 35 000 K, and extreme compositions dominated by helium, carbon and nitrogen (Schönberner & Wolf 1974; Jeffery & Heber 1992). The model assumes hydrostatic, radiative and local thermodynamic equilibrium, as well as plane-parallel geometry. The radiative transfer equation is solved using Feautrier's scheme, and the temperature correction follows the Unsöld-Lucy procedure.

From 1990 to 2003 the treatment of the continuous opacities followed Kurucz (1979), with the addition of carbon and nitrogen opacities from Peach (1970). The line opacities were calculated using opacity distribution functions (ODF) computed for hydrogen-deficient mixtures from the Kurucz & Peytremann (1975) list of 265 000 lines.

Table 1. Opacity Project photoionization cross-sections used in the continuous opacity calculations.

Element	Ionization stage	Number of states
H	I	55
He	I, II	13, 55
Li	I, II, III	25, 53, 55
Be	I, II, III, IV	55, 25, 54, 55
B	I, II, III, IV	55, 55, 26, 53
C	I, II, III, IV	50, 21, 38, 24
N	I, II, III, IV	36, 50, 32, 39
O	I, II, III, IV	50, 29, 25, 36
F	I, II, III, IV	50, 50, 50, 50
Ne	I, II, III, IV	50, 50, 50, 50
Na	I, II, III, IV	32, 50, 50, 50
Mg	I, II, III, IV	50, 32, 50, 50
Al	I, II, III, IV	41, 50, 31, 50
Si	I, II, III, IV	50, 51, 50, 31
S	I, II, III, IV	50, 50, 50, 50
Ar	I, II, III, IV	50, 50, 50, 50
Ca	I, II, III, IV	50, 17, 50, 50
Fe	III, IV, V, VI	50, 50, 50, 50

2. METHODS

2.1. Continuous opacities

We focus the discussion on the continuous opacities due to bound-free transitions only, as the treatment of free-free absorption and scattering is preserved from the previous version of STERNE.

The Opacity Project (OP, The Opacity Project Team 1995, 1997) data used in the opacity calculations is shown in Table 1. The individual cross-sections must first be resampled on the model wavelength grid before the opacity calculations are carried out, and as a consequence the photoexcitation of the core (PEC) resonances of the cross-sections are not fully resolved. The resampling preserves the cross-sections to within an error of 10%.

The way in which the OP data are included in the model atmosphere code is sufficiently general that any combination of ions may be selected, once the necessary cross-sections have been downloaded from TOPbase (Cunto et al. 1993). Additional cross-sections may be added as they become available.

2.2. Line opacities

We have devised a procedure, loosely based on Sneden et al. (1976) to sample the line opacity directly at each wavelength grid point for all layers in a model atmosphere. Relevant lines are selected from a master list of atomic lines based on the temperature, pressures and abundances of the model at each wavelength and depth point. Approximately 500 000 lines are selected. For each grid point, the

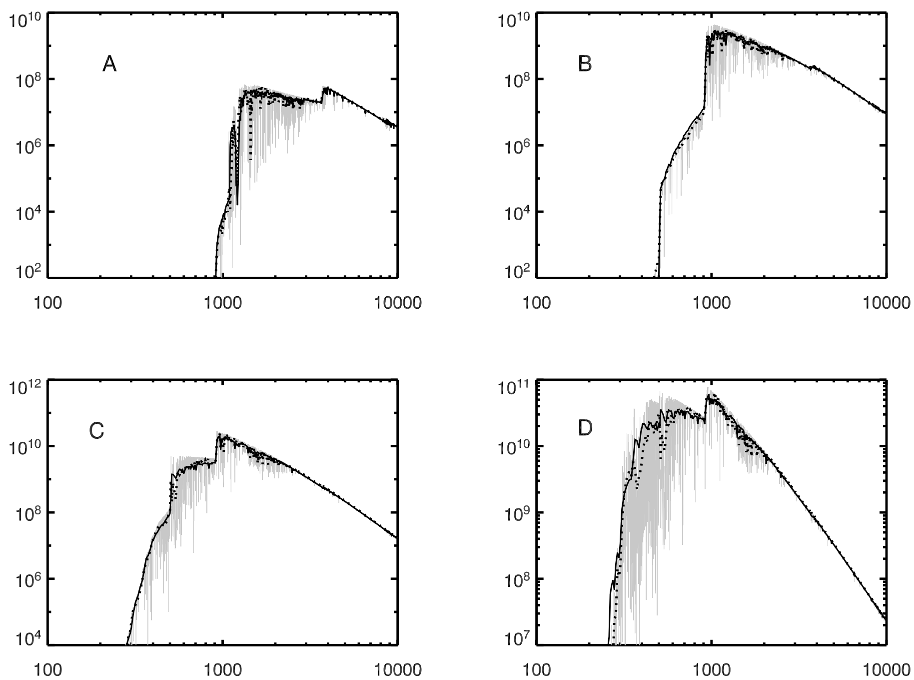

Fig. 2. Solar composition comparisons of the STERNE opacity sampled models to Kurucz's ATLAS9 models. The ATLAS9 models are shown by the black lines. The STERNE models are represented by the grey lines, and also shown resampled on the ATLAS9 grid by the dotted lines. The emergent flux is plotted as a function of wavelength for four $T_{\rm eff}$, log g pairs (see text).

contributions of all selected lines within prescribed search windows are included in the line opacity calculation. The line opacity is calculated using detailed line profiles for each selected spectral line. Computed in this fashion, the opacity sampling (OS) method is able to account for the depth dependence of the variation with wavelength of the line opacities. Lines are selected from the atomic line list compiled by Kurucz & Bell (1995).

2.3. Model verification

A comparison of the STERNE models with Kurucz's ATLAS9 models has been carried out using a solar composition and four effective temperature and gravity pairs. The results are shown in Figure 2.

The emergent flux is plotted as a function of wavelength for A: $T_{\rm eff} = 10\,000$ K, $\log g = 3.0$, B: $T_{\rm eff} = 20\,000$ K, $\log g = 3.0$, C: $T_{\rm eff} = 30\,000$ K, $\log g = 3.5$ and D: $T_{\rm eff} = 40\,000$ K, $\log g = 4.5$. The STERNE model has been resampled on the ATLAS9 grid to allow for comparison. Differences in the models can be accounted for by the different solar abundances used, and differences in the treatment of continuous and line opacities, which alter the model structure. We use the solar abundances of Grevesse & Sauval (1998), while Kurucz uses the abundances by Anders & Grevesse (1989).

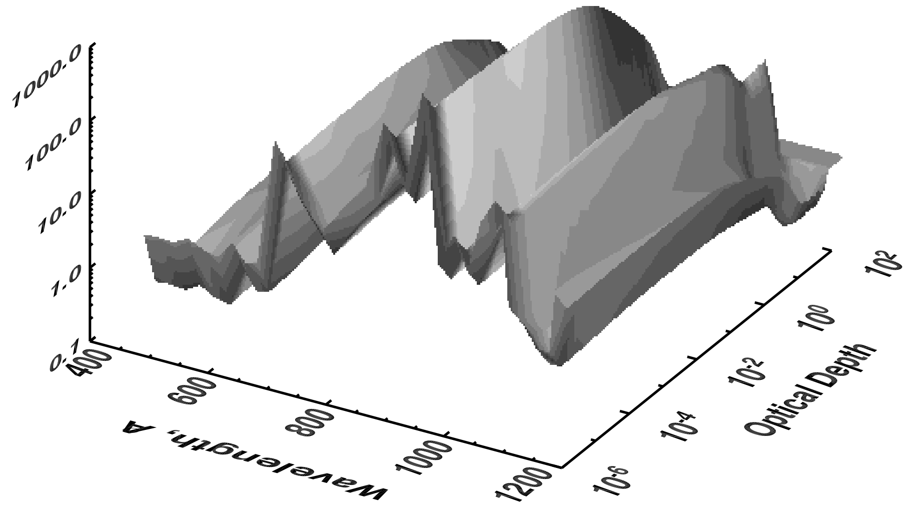

Fig. 3. The ratio of the OP C II continuous opacity to the Peach opacity in a model atmosphere with $T_{\rm eff}$ = 20 000 K and log g = 3.0.

3. RESULTS

We have compared hydrogen-rich and helium-rich models of the opacity sampled version of STERNE with new continuous opacities to the models computed using the ODF version of STERNE. Models have been computed with and without line opacity in order to compare the effect of changing the continuous opacities alone.

Looking at continuum-only models, we find general agreement between the models in the hydrogen-rich case. However, when comparing helium-rich models, we have found that the new opacities produce significant changes in the emergent flux distribution of the atmosphere, particularly in the region 500 Å $< \lambda <$ 1000 Å. The primary cause is the C II continuous opacity.

An increase in the opacity when using the OP cross-sections leads to an increase in the continuum opacity at $\lambda <$ 1000 Å, resulting in more UV flux with a steeper continuum at $\lambda >$ 1200 Å. A comparison of the C II opacity computed in both models is shown in Figure 3. The ratio of the opacity computed with the OP cross-sections to the opacity computed using the Peach tables (1970) is plotted as a function of optical depth in the atmosphere and as a function of wavelength.

When comparing continuum plus line models, we find that differences in the flux and temperature distributions are far more drastic for the helium-rich case than the hydrogen-rich case.

The plot on the left of Figure 4 shows the effects of the new opacities on the flux distribution of a hydrogen-rich atmosphere and the figure on the right for a helium-rich atmosphere with $T_{\rm eff}$ = 30 000 K and log g = 5.0. The ODF model is shown by the solid line, the OS model by the grey line and the OS model resampled on the ODF wavelength grid by the dotted line. The plots have been cropped to show regions of interest, the integral over the flux remains the same for both models.

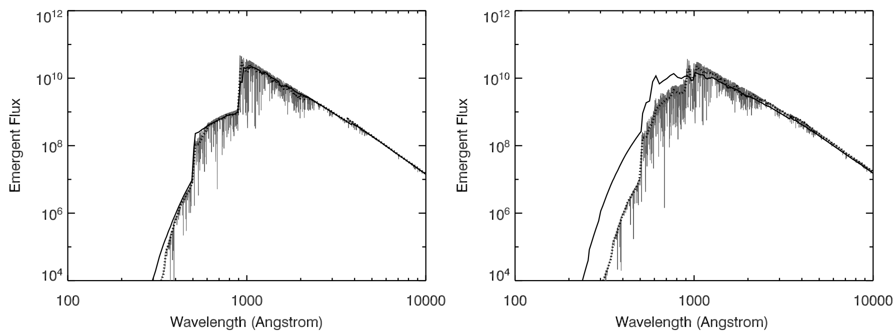

Fig. 4. Flux distributions of hydrogen-rich and helium-rich model atmospheres. The solid line represents the ODF model, and the grey line represents the new OS model, also shown resampled on the ODF grid (dotted line). Model parameters on the left: $T_{\rm eff} = 30\,000\,\rm K$, $log\, g = 5.0$, $n_{\rm H} = 0.911$ and $n_{\rm He} = 0.089$. Model parameters on the right: $T_{\rm eff} = 30\,000\,\rm K$, $log\, g = 5.0$, $n_{\rm H} = 0.0001$ and $n_{\rm He} = 0.99$, $n_{\rm C} = 0.0099$ and solar metallicity.

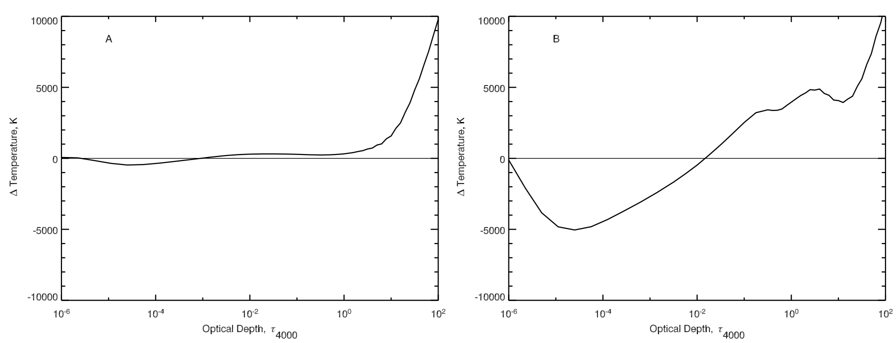

Fig. 5. Differences $(T_{\rm OS} - T_{\rm ODF})$ in the temperature distribution for the models as a function of optical depth. A – hydrogen-rich models from the left plot of Fig. 4, B – helium-rich models from the right plot of Fig. 4.

The effect of the new opacities on the temperature distribution of the atmosphere is shown in Figure 6. The temperature differences $(T_{\rm OS} - T_{\rm ODF})$, are plotted as a function of optical depth for both compositions. The differences in the temperature distribution translate into an approximate increase of up to 3000 K in the line forming region of the atmosphere for a hydrogen-deficient star with $T_{\rm eff} = 30\,000$ K. In the hydrogen-rich case we expect an increase of approximately 300 K.

Figure 6 shows the range of the approximate increase in temperature across the line forming region of both helium-rich and hydrogen-rich high-gravity stars at several effective temperatures. These results show that the new treatment of opacity will have implications in the effective temperature measurements of stars of all compositions and temperatures.

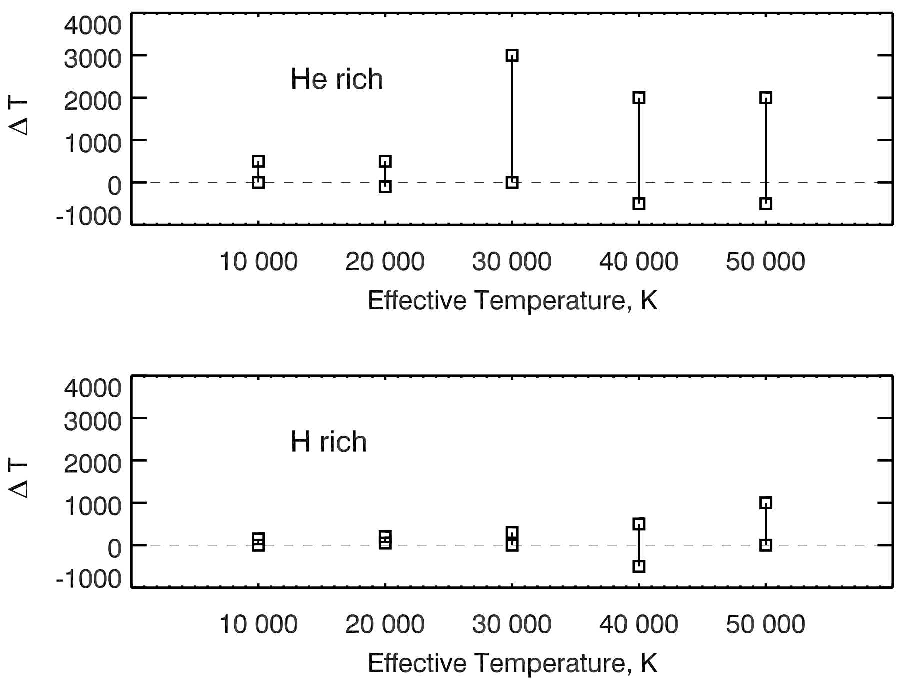

Fig. 6. Differences ($T_{\rm OS} - T_{\rm ODF}$) in the line forming region of the temperature distribution of helium-rich and hydrogen-rich model atmospheres with $(T_{\rm eff}, \log g) =$ (10 000, 3.0), (20 000, 4.0), (30 000, 5.0), (40 000, 6.0), (50 000, 6.0). The line forming region has been approximated as the range in optical depth 10^{-2} to 10^{0}.

4. SUMMARY

The treatments of continuous and line opacity in the model atmosphere code STERNE have been revised. Opacity Project cross-sections have been incorporated and an opacity sampling method has been implemented. Results show significant differences for chemically peculiar stars when compared to model atmospheres computed using Kurucz and Peach continuous opacities and an ODF treatment for line opacity. The principal results are that the C II continuous opacity computed using OP cross-sections substantially modifies the flux distribution of hydrogen-deficient atmospheres at $\lambda \sim 1000$ Å, and the new line opacity treatment significantly modifies the temperature distribution of these stars. Effects in the temperature distribution of hydrogen-rich stars of up to 300 K are also seen. These results will have consequences in the effective temperature measurements of stars of all compositions.

Several applications exist for these models. We intend to examine extreme helium stars, helium-rich sdB stars, chemically peculiar subdwarf B stars and hydrogen-deficient binaries.

ACKNOWLEDGMENTS. Research at Armagh Observatory is funded by the Department of Culture, Arts and Leisure, Northern Ireland.

REFERENCES

Anders E., Grevesse N. 1989, Geochim. Cosmochim. Acta, 53, 197

Cunto W., Mendoza C., Ochsenbein F., Zeippen C. J. 1993, A&A, 275, L5

Dudley R. E., Jeffery C. S. 1993, MNRAS, 262, 945

Grevesse N., Sauval A. J. 1998, Space Sci. Rev., 85, 161

Jeffery C. S., Heber U. 1992, A&A, 260, 133

Kurucz R. L. 1979, ApJS, 40, 1

Kurucz R. L., Bell B. 1995, Kurucz CD-ROM 23, Cambridge, SAO

Kurucz R. L., Peytremann E. 1975, SAOSR, 326, 1

Peach G. 1970, MNRAS, 73, 1

Schönberner D., Wolf R. 1974, A&A, 37, 87

Sneden C., Johnson H. R., Krupp B. M. 1976, ApJ, 204, 281

The Opacity Project Team. 1995 in *The Opacity Project*, Vol. 1, Institute of Physics Publishing, Bristol

The Opacity Project Team. 1997 in *The Opacity Project*, Vol. 2, Institute of Physics Publishing, Bristol

Baltic Astronomy, vol. 15, 123–126, 2006.

ATMOSPHERIC PARAMETERS FOR SUBDWARF B STARS: A CONSISTENCY CHECK BETWEEN THE BALMER LINES AND THE FAR-ULTRAVIOLET SPECTRUM

C. Pereira, F. Wesemael and P. Bergeron

Département de Physique, Université de Montréal, C.P. 6128, Succ. Centre-Ville, Montréal, Québec H3C 3J7, Canada; e-mail: pereira@astro.umontreal.ca

Received 2005 August 1

Abstract. The use of Balmer line profiles to determine atmospheric parameters of subdwarf B stars is a well-established method that relies on a comparison of spectroscopic observations with synthetic spectra generated from model atmospheres. This method allows us to determine parameters such as the effective temperature, surface gravity and photospheric helium abundance. The self-consistency of these parameters can be investigated by examining the Lyman lines covered by current far-ultraviolet observations. We discuss the results of a preliminary analysis of a sample of ten subdwarf B stars for which both optical and far-ultraviolet spectra were secured. At temperatures below 30 000 K we find good consistency between optical and ultraviolet spectra when some allowance is made for the metal-line blanketing present in the ultraviolet region. At higher effective temperatures, however, the consistency is not as satisfactory. Possible solutions to this puzzle are considered.

Key words: stars: atmospheres, subdwarfs

1. INTRODUCTION

The atmospheric parameters which characterize the subdwarf B (or sdB) stars are now routinely obtained from simultaneous fits to the Balmer line profiles with synthetic spectra generated from model atmospheres (see, e.g., Saffer et al. 1994). Over the years, this method has proved quite reliable, although systematic effects between various grids of models may still be present. The method can, in principle, be extended to the Lyman region of the spectrum, just as it has been for the DA (Barstow et al. 2001, 2003) and DAO white dwarfs (Good et al. 2004). However, in the case of the hot B subdwarfs, it is expected that the interpretation of the fits to the Lyman lines might be more complicated, since the far ultraviolet spectra of sdB stars are known to include hundreds of transitions from heavy elements (see, e.g., Ohl et al. 2000). The blocking effect of these numerous lines would have to be considered in any fit purporting to match the ultraviolet continuum level of hot B subdwarfs. This problem could be solved by fitting the ultraviolet continuum with fully blanketed synthetic spectra; however, this cannot be accomplished in a routine manner yet, as the abundance patterns of heavy elements which characterize sdB stars are still being documented (Edelmann et al. 2006; Fontaine et al.

2005). Thus, at this stage, it might be more appropriate to (i) determine the atmospheric parameters of hot B subdwarfs on the basis of optical spectroscopy and synthetic spectra as sophisticated as possible; (ii) calculate the ultraviolet continuum predicted at the values of $T_{\rm eff}$, log g and He/H derived in the optical; and (iii) investigate to what extent the predicted ultraviolet continuum is consistent with that observed with the FUSE satellite. We have undertaken such an exploratory study on a small sample of hot B subdwarfs and present here preliminary results from this investigation.

2. OBSERVATIONS, MODELS AND BALMER LINE FITS

Ten subdwarf B stars were selected for this analysis. The optical spectra were secured using the 2.3 m telescope at Steward Observatory, while the far-ultraviolet spectra were obtained through the FUSE satellite archives. We computed pure hydrogen and mixed helium and hydrogen (log He/H = -2.5), NLTE model atmospheres using version 200 of TLUSTY (Hubeny 1988) and the corresponding synthetic spectra using version 48 of SYNSPEC (Hubeny & Lanz 1995) with the Stark broadening tables of Lemke (1997). Our model grid extends over the following parameters: $T_{\rm eff}$ = 20 000 to 60 000 K spaced by 2000 K and log g = 5.0 to 6.5 spaced by 0.25 dex. We emphasize that our grid includes no heavy elements.

The technique used to fit the Balmer lines is standard and can be summarized as follows: the observed and theoretical Balmer line profiles (Hβ-H9) are normalized to a linear continuum set to unity. The observations are then compared to synthetic spectra and a chi-squared minimization technique is then applied until a best fit is achieved between the calculated model and the observations (see, e.g., Bergeron et al. 1992). All in all, the pure hydrogen models fit the optical spectra of our target stars quite satisfactorily.

3. THE FAR-ULTRAVIOLET CONTINUUM OF sdB STARS

As we emphasized earlier, a fit to the Lyman lines carried out in the same manner as the fit to the Balmer lines is not possible: while the optical spectra show few features besides the H I and He I lines, the FUSE observations reveal numerous lines of heavy elements that mar the ultraviolet spectrum. This prevents us from clearly determining the placement of the continuum, a crucial step in the standard fitting procedure. Thus, to verify the consistency of the parameters, we adopt the following approach. With the atmospheric parameters derived from the optical spectrum, we calculate the theoretical flux at 5458.7 Å associated with each star and, on the basis of existing Strömgren photometry, fix the solid angle. This allows us to normalize the emergent flux from our model atmospheres, and to predict the ultraviolet flux received at the Earth. For all but one star in our sample, no interstellar reddening was included, although the presence of small amounts of reddening cannot be excluded. In the case of PG 0823+466, however, reddening was required, and the color excess we determine, E_{B-V} = 0.10, is not unusual even for high-latitude PG stars. Unfortunately, there are no archival IUE observation of this object which would have provided a check on this measurement.

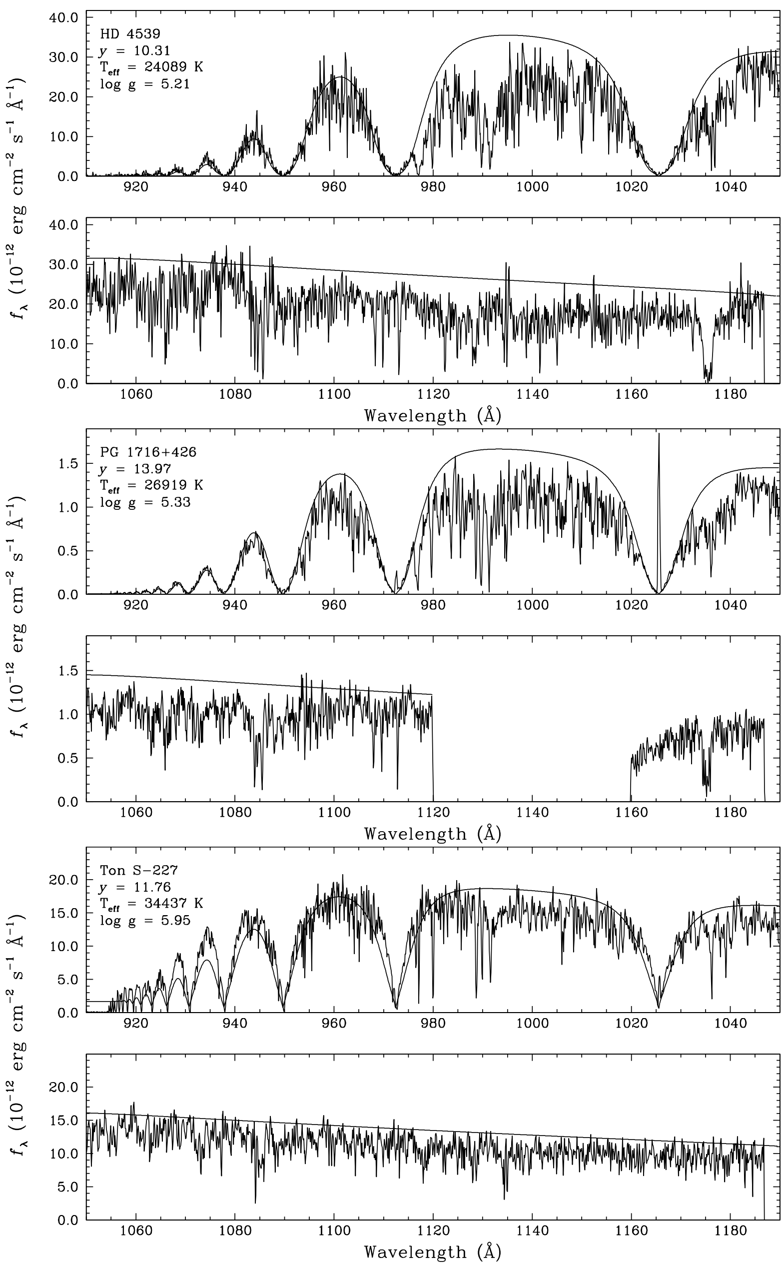

Fig. 1. Synthetic spectra calculated for three objects using the parameters derived from their optical spectrum (values are indicated in the top lefthand corner). These are superimposed onto the FUSE observations and are not fits, but rather provide a check on the consistency between the optical and ultraviolet ranges. The synthetic spectra are normalized using the y magnitude, as described in the text.

Our predictions of the ultraviolet flux are compared to the absolute flux measured by the FUSE satellite in Figure 1 for three objects in our sample. These include HD 4539, a cool and bright sdB star, PG 1716+426, the prototypical long-period sdB variable and Ton S-227, a well-studied sdB star at a somewhat higher effective temperature. The predicted fluxes are calculated on the basis of pure hydrogen or mixed hydrogen/helium models which do not include any heavy elements. For objects with $T_{\rm eff} < 30\,000$ K, our comparisons at ultraviolet wavelengths yield satisfactory results in the sense that, when some allowance is made for metal line blanketing, the synthetic spectra reproduce in a satisfactory manner the general shape of the continuum as well as the Lyman line profiles. This is shown in Figure 1 for HD 4539 and PG 1716+426. Interestingly, our procedure may provide us with a way to decide where the continuum level should be set in abundance analyses of FUSE spectra.

For objects with $T_{\rm eff} > 30\,000$ K, however, there appears to be a systematic discrepancy between the synthetic spectra derived from the optically determined parameters and the observed ultraviolet spectra. Ton S-227 provides us with a clear illustration of this situation: the predicted Lyman lines appear too wide, as if the surface gravity determined in the optical were too large, while the flux level in the interline region appears too low, in contrast to what it should be if line-blocking were the only significant omission in our models. Because some heavy elements are more abundant in hotter objects than in cooler ones, while the reverse is true for other elements, it is not possible, at this stage, to connect simply and unambiguously the trend we observe at high effective temperatures with the abundance of heavy elements. Moreover, it should be noted that Barstow et al. (2001, 2003) encountered similar discrepancies for DAs with $T_{\rm eff} > 50\,000$ K.

We are currently exploring other alternatives to account for the systematic discrepancy observed in the hotter sdB stars. Interstellar reddening, stratified H/He atmospheres, as well as homogeneous atmospheres incorporating large abundances (up to solar) of heavy elements, such as those considered by Heber (2006) and Behara & Jeffery (2006) at this conference, are currently being considered.

ACKNOWLEDGMENTS. We thank P. Chayer for useful discussions pertaining to this project. This work was supported in part by the NSERC Canada and by the Fund FQRNT (Québec)

REFERENCES

Barstow M. B., Good S. A., Burleigh M. R. et al. 2003, MNRAS, 334, 562

Barstow M. B., Holberg J. B., Hubeny I. et al. 2001, MNRAS, 328, 211

Bergeron P., Saffer R. A., Liebert J. 1992, ApJ, 394, 228

Fontaine M., Chayer P., Wesemael F. et al. 2005, in *Astrophysics in the Ultraviolet*, eds. G. Sonneborn, H. W. Moos & B.-G. Andersson, in press

Edelmann H., Heber U., Napiwotzki R. 2006, Baltic Astronomy, 15, ... (these Proceedings)

Good S. A., Barstow M. B., Holberg J. B. et al. 2004, MNRAS, 355, 1031

Hubeny I. 1988, Computer Physics Comm., 52, 103

Hubeny I., Lanz T. 1995, ApJ, 439, 875

Lemke M. 1997, A&AS, 122, 285

Ohl R. G., Chayer P., Moos H. W. 2000, ApJ, 538, 950

Saffer R. A., Bergeron P., Koester D., Liebert J. 1994, ApJ, 432, 351

Baltic Astronomy, vol. 15, 127–130, 2006.

IMPROVED HELIUM LINE FORMATION FOR EXTREME HELIUM STARS

N. Przybilla[1] K. Butler[2] U. Heber[1] and C. S. Jeffery[3]

[1] *Remeis-Sternwarte Bamberg, Sternwartstr. 7, D-96049 Bamberg, Germany*

[2] *Universitätssternwarte München, Scheinerstr. 1, D-81679 München, Germany*

[3] *Armagh Observatory, College Hill, Armagh BT61 9DG, Northern Ireland*

Received 2005 July 31

Abstract. Quantitative analyses of extreme helium stars to date face the difficulty that theory fails to reproduce the observed helium lines in their entirety, wings *and* line cores. Here, we demonstrate how the issues can be resolved using state-of-the-art non-LTE line formation for these chemically peculiar objects. Two unique B-type objects are discussed in detail, the pulsating variable V652 Her and the metal-poor star HD 144941. The improved non-LTE computations for helium show that analyses assuming LTE or based on older non-LTE model atoms can predict equivalent widths, for the He I 10 830 Å transition in particular, in error by up to a factor ∼3. Our modeling approach also succeeds in largely resolving the general mismatch for effective temperatures of EHe stars derived from ionization equilibria and from spectral energy distributions.

Key words: line: formation – stars: atmospheres – stars: fundamental parameters – stars: individual (V 652 Her, HD 144941)

1. INTRODUCTION

Extreme helium stars (EHes) are a rare class of low-mass H-deficient objects with spectral characteristics of B-giants. Most of the two dozen known EHes could be explained by post-AGB evolution, linking R CrB stars to Wolf-Rayet type central stars of planetary nebulae, see Heber (1986) and Jeffery (1996) for reviews.

LTE spectral analyses encounter two difficulties for EHe stars: (i) synthetic spectra have so far not succeeded in matching the observed helium lines in their entirety, and (ii) spectroscopic and spectrophotometric temperatures differ systematically. As inadequacies in the basic parameter determination can potentially hamper any further interpretation, the issue needs to be resolved. The necessary steps for improving the modeling will be discussed in the following for two test cases, V652 Her and HD 144941. Here, extreme helium stars turn out to be important testbeds for stellar atmosphere modeling. In particular, non-LTE model atoms for helium can be tested in more detail than in any other type of star, since all predicted transitions – including all forbidden components – can be measured. The sample stars are unique among the class members in several aspects. Both objects have gravities too large for post-AGB evolution and they show atypical surface abundances.

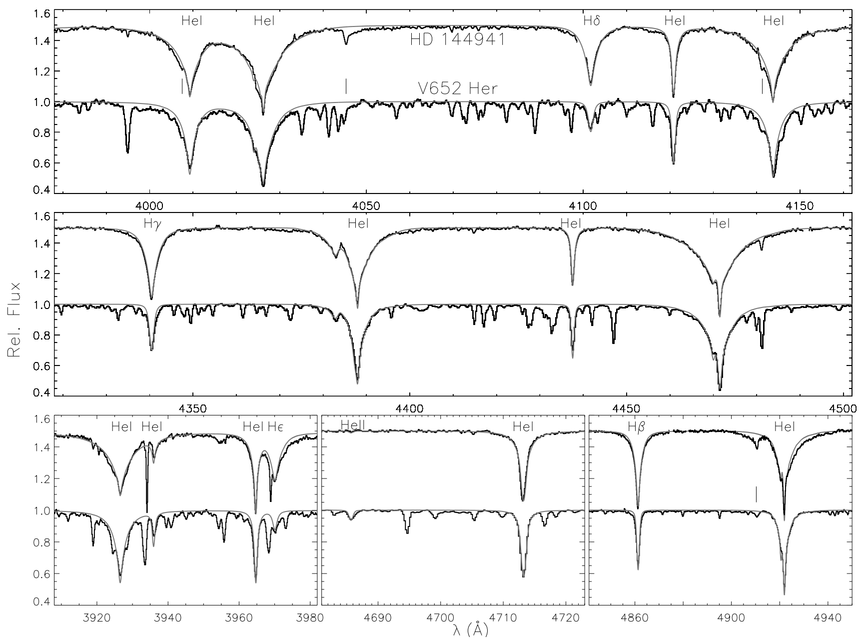

Fig. 1. Fits to He and H lines in the two sample stars.

2. MODEL CALCULATIONS AND OBSERVATIONAL DATA

The model calculations are carried out in analogy to the hybrid non-LTE approach chosen for sdB star analyses (Przybilla et al. 2006), but see also Przybilla et al. (2005) for further details. In brief, the atmospheric structure computations are carried out using the Atlas12 code (Kurucz 1996). Note that we have replaced the photoionization data for He I levels with principal quantum number $n = 2$ as used by Kurucz with data from the Opacity Project (Fernley et al. 1987). In particular the cross-sections for the $2p\,^3P^\circ$ level are increased by a factor $\sim$2 at the threshold, thus improving the fits of computed energy distributions with observation. Then, the restricted non-LTE problem is solved. State-of-the-art model atoms for He (Przybilla 2005) and H (Przybilla & Butler 2004) are utilised, and detailed line-broadening is accounted for in the spectrum synthesis (Barnard et al. 1969, 1974; Dimitrijević & Sahal-Bréchot 1990; Stehlé & Hutcheon 1999). For comparison, additional calculations are made using the He model atom of Husfeld et al. (1989). Details of the observations and the data reduction have been published elsewhere (Jeffery et al. 2001; Harrison & Jeffery 1997).

3. DISCUSSION

The stellar parameters are derived in a standard manner, using the He I/II ionization balance as $T_{\rm eff}$ and the Stark-broadened He I lines as $\log g$ indicators. Data for the final models (with estimated uncertainties) are summarised in Table 1, including microturbulence ξ and also H abundance $n_{\rm H}^{\rm NLTE}$ (by number). For V652 Her the atmospheric parameters agree very well with those found by Jeffery

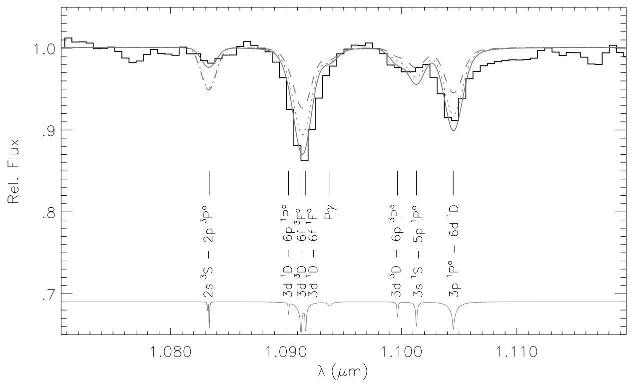

Fig. 2. Modeling of the J-band spectrum of V 652 Her.

Table 1. Stellar parameters.

	V652 Her ($R_{\rm max}$)	HD 144941
$T_{\rm eff}$ (K)	22 000±500	22 000±1000
$\log g$	3.20±0.10	4.15±0.10
ξ (km/s)	4±1	8±2
$n_{\rm H}^{\rm NLTE}$	0.005±0.0005	0.035±0.005

et al. (2001), except for the hydrogen abundance, which is reduced by a factor ~2 because of non-LTE strengthening of the Balmer lines. For HD 144941, however, the resulting parameters differ significantly from previous work of Harrison & Jeffery (1997), implying a reduction in $T_{\rm eff}$ by 1200 K and an increase in surface gravity by a factor ~2. The reduction in the hydrogen abundance is less pronounced in this star.

A comparison of our non-LTE spectrum synthesis for He and H (grey lines) with the observed spectra of V 652 Her and HD 144941 (histograms) is made in Figure 1. Excellent agreement for the entire line profiles – wings *and* line cores – is found. The great improvement achieved becomes obvious when comparing Figure 1 to Figure 2 of Harrison & Jeffery (1997) and Figure 5 of Jeffery et al. (2001). This resolves one of the most persistent inconsistencies in quantitative analyses of extreme helium stars. A few forbidden components of He I lines missing in our modeling are indicated by short vertical marks. The appropriate broadening data are unavailable to us.

The He I lines in the visual experience non-LTE strengthening, facilitated by the overpopulation of the $n = 2$ states relative to the levels of higher principal quantum number. This overpopulation occurs because of recombinations to levels of He I at higher excitation energies and subsequent de-excitation via downward cascades to the (pseudo-)metastable $2s$ states (the singlet resonance lines are close to detailed balance). Singlet lines are in general subject to larger non-LTE effects than the triplet lines. The level populations deviate by only a few percent from detailed equilibrium at the formation depths of the continua, indicating that the assumption of LTE for the model atmosphere computations is appropriate.

Analyses in the near-IR range are highly useful for constraining the atomic data input for the non-LTE computations because of amplified non-LTE effects in the Rayleigh-Jeans tail of the spectral energy distribution. The comparison of model calculations with the current He model (full grey line) and an old model by Husfeld et al. (1989, dotted line) with observation (histogram) for the He I 10 830 Å feature in Figure 2 demonstrates the superiority of the former. The old model predicts the line to be ~3 times stronger than observed, showing little deviation from detailed balance (dashed line). This success is facilitated by making use of accurate photoionization cross-sections in particular for the $2s\ ^3S$ state and a proper account of line blocking. Note that the line broadening is dominated by instrumental effects.

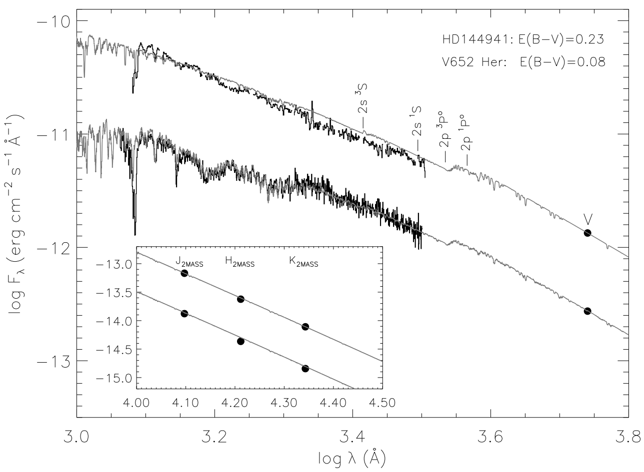

Fig. 3. SED fits for the sample stars.

High-resolution observations would be highly desirable for constraining the modeling even further.

The second major difficulty in the modeling of extreme helium stars is a general mismatch of effective temperatures derived from ionization equilibria and spectrophotometry. A comparison of the Atlas12 model fluxes (grey lines) for stellar parameters derived from the He I/II ionization equilibria (see Table 1) with IUE spectrophotometry and visual and near-IR photometry (black histograms and dots) is made in Figure 3. Excellent agreement is found for V 652 Her, and a reasonable match for HD 144941 when interstellar reddening is accounted for. We conclude that the hybrid non-LTE approach based on state-of-the-art model atoms as discussed here succeeds in solving the most persistent problems in the quantitative spectroscopy of extreme helium stars.

REFERENCES

Barnard A. J., Cooper L., Shamey L. J. 1969, A&A, 1, 28

Barnard A. J., Cooper L., Smith E. W. 1974, J. Quant. Spec. Rad. Transf., 14, 1025

Dimitrijević M. S., Sahal-Bréchot S. 1990, A&AS, 82, 519

Fernley J. A., Taylor K. T., Seaton M. J. 1987, J. Phys. B, 20, 6457

Harrison P. M., Jeffery C. S. 1997, A&A, 323, 177

Heber U. 1986, in *Hydrogen Deficient Stars and Related Objects*, eds. K. Hunger, D. Schönberner & N. Kameswara Rao, Reidel Publ. Co., Dordrecht, p. 33

Husfeld D., Butler K., Heber U., Drilling J. S. 1989, A&A, 222, 150

Jeffery C. S. 1996, in *Hydrogen-Deficient Stars*, eds. C. S. Jeffery & U. Heber, ASP Conf. Ser., 96, 152

Jeffery C. S., Woolf V. M., Pollacco D. L. 2001, A&A, 376, 497

Kurucz R. L. 1996, in *Model Atmospheres and Spectrum Synthesis*, eds. S. J. Adelman, F. Kupka & W. W. Weiss, ASP Conf. Ser., 108, 160

Przybilla N. 2005, A&A, 443, 293

Przybilla N., Butler K. 2004, ApJ, 609, 1181

Przybilla N., Butler K., Heber U., Jeffery C. S. 2005, A&A, 443, L25

Przybilla N., Nieva M. F., Edelmann H. 2006, Baltic Astronomy, 15, 107 (these proceedings)

Stehlé C., Hutcheon R. 1999, A&AS, 140, 93

Baltic Astronomy, vol. 15, 131–138, 2006.

FUSE OBSERVATIONS OF GERMANIUM, ZIRCONIUM AND LEAD IN SDB STARS

P. Chayer[1,2] M. Fontaine[3] G. Fontaine[3] F. Wesemael[3] and J. Dupuis[1]

[1] *Department of Physics and Astronomy, The Johns Hopkins University, 3400 N. Charles St., Baltimore, MD 21218, U.S.A.*

[2] *Primary affiliation: Department of Physics and Astronomy, University of Victoria, P.O. Box 3055, Victoria, BC, V8W 3P6, Canada*

[3] *Département de Physique, Université de Montréal, CP6128, Station Centre-ville, Montréal, QC H3C 3J7, Canada*

Received 2005 April 1

Abstract. We report the detection of the Ge III, Zr IV, Pb III and Pb IV resonance lines in Far Ultraviolet Spectroscopic Explorer (*FUSE*) spectra of hot subdwarf B stars (sdB). We analyze 18 stars that cover the effective temperature domain for this class of stars. We carry out an abundance analysis and demonstrate that Ge, Zr and Pb abundances are higher than the ones observed in the Sun's photosphere in almost every star. We perform radiative levitation calculations on Ge, Zr and Pb, and show that the theory predicts higher Ge and Zr abundances than the observations. Moreover, the large scatter of observed abundances cannot be explained by the radiative levitation alone. This suggests that other mechanisms must be taken into account for explaining the abundances of Ge, Zr and Pb in the atmospheres of sdB stars.

Key words: diffusion – spectroscopy – stars: abundances – subdwarfs

1. INTRODUCTION

The recent discovery of elements beyond the iron group in the atmospheres of hot subdwarf B stars (sdB) by O'Toole (2004) adds new pieces to the abundance anomaly puzzle observed at the surface of these relatively high gravity stars. O'Toole (2004) reported the detection of strong resonance lines of Ga III, Ge IV, Sn IV and Pb IV in the STIS and IUE spectra of many sdB and sdOB stars that cover a wide range of effective temperatures. Strong resonance lines of Ge III, Zr IV, Pb III and Pb IV are also formed in the far ultraviolet wavelength range. This is one of the last unexplored spectral windows in the study of sdB atmospheres. The Far Ultraviolet Spectroscopic Explorer (*FUSE*), which covers a spectral wavelength range of 905–1187 Å with a resolution of $R = \lambda/\Delta\lambda \simeq 18\,000$, is exploring in great details this important waveband. In this paper we present the results of an abundance analysis for the elements Ge, Zr and Pb observed in the atmospheres of 18 sdB stars. We also present results of radiative levitation calculations on Ge, Zr and Pb based on an approach developed by Michaud et al. (1976).

2. *FUSE* OBSERVATIONS

We retrieved the *FUSE* spectra from the Multimission Archive at STScI. All stars were observed through large apertures with exposure times of about 6000 s on average. The data were reduced using the program CALFUSE that processes the raw data into wavelength and flux calibrated 1-d spectra. Because each observation consists of several exposures, we co-added the individual exposures by cross-correlating them in order to remove any wavelength shifts. Figure 1 illustrates an example of merged *FUSE* spectra of the bright and cool sdB star HD 205805. The strongest lines observed in the spectrum are the hydrogen lines from Lyβ to the series limit, the He II 1084 and 992 Å lines, the C III 977 Å line and the C III 1175 Å multiplet.

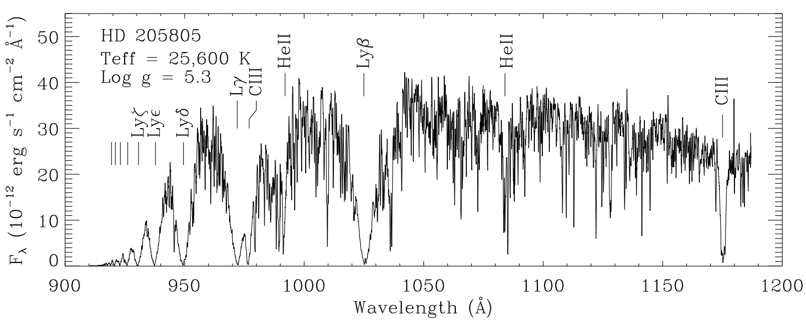

Fig. 1. *FUSE* spectrum of HD 205805.

The spectrum in Figure 1 seems noisy at this scale. In fact, this apparent noise is due to the huge number of photospheric and interstellar absorption lines that are observed in the *FUSE* spectra of almost all sdB stars. Interstellar lines such as H_2, C II, C III, N I, O I, Si II, P II and Fe II are observed along the lines of sight of many sdB stars. Photospheric lines come from elements such as C, N, O, Si, P, S, Cl and elements from the iron group such as V, Cr, Mn, Fe, Co and Ni. In addition to these elements, the *FUSE* wavelength range contains lines that are produced by elements beyond the iron group. Resonance lines from ions such as Ge III, Zr IV, Pb III and Pb IV are observed in the *FUSE* spectra of almost all sdB stars. Lines coming from excited levels of Pb III are also observed in a few stars. Table 1 summarizes the atomic properties of the Ge III, Zr IV, Pb III and Pb IV lines observed in the *FUSE* band.

Table 1. Atomic data for Ge, Zr and Pb.

Ion	Z	Wavelength (Å)	$\log gf$	g_l	E_l (cm^{-1})
Ge III	32	1088.463	0.264	1.0	0.0
Zr IV	40	1183.973	0.000	4.0	0.0
Pb III	82	1048.877	0.114	1.0	0.0
Pb IV	82	1028.611	0.086	2.0	0.0

3. ABUNDANCE ANALYSIS

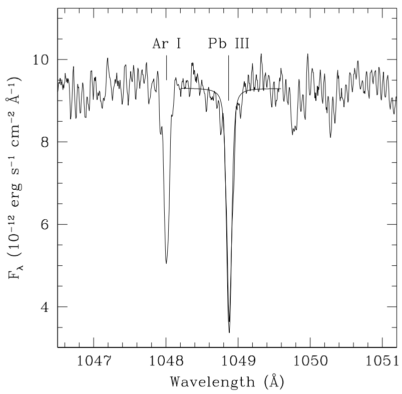

Fig. 2. *FUSE* spectrum of Feige 87 showing the Pb III 1048 Å line and our best fit.

We computed a set of LTE atmosphere models with the atmospheric parameters listed in Table 2 (the atmospheric parameters were derived by E. M. Green et al. 2006, in preparation; Edelmann 2003; M. Fontaine et al. 2006, in preparation; Kilkenny et al. 1987; Heber et al. 2002; Allard 1986 and Saffer et al. 1994). These models were computed for a hydrogen/helium chemical composition. We used two methods for determining the abundances of Ge, Zr and Pb. For stars that do not have numerous absorption lines and have a well defined continuum, we fitted each line by using a χ^2 minimization technique for which the abundance and a scaling factor are the free parameters. In this case we computed grids of LTE synthetic spectra by considering Ge, Zr and Pb as trace elements. The lines of Ge III, Zr IV, Pb III and Pb IV were computed for abundances ranging from $\log N(\mathrm{X})/N(\mathrm{H}) = -10.4$ to -6.0 in steps of 0.4 dex by assuming no microturbulent velocity. The calculations were performed by using the programs TLUSTY (Hubeny & Lanz 1995) and SYNSPEC (I. Hubeny 2004, private communication). The partition functions for the neutral, +1 and +2 ionization stages of Ge, Zr and Pb are calculated in the same manner as in the Kurucz's ATLAS9 code (Kurucz 1993; Proffitt et al. 2001). For the +4 ionization stage of Zr and Pb we adopted the ground-state statistical weights for the partition functions. The sdB star Feige 87 is a good example of a low-metallicity star for which this method gives excellent results (see Figures 2 and 3).

We cannot apply the χ^2 fitting technique for stars like the one illustrated in Figure 1 (see also Figure 1 of Blanchette et al. 2006). Instead we used the IDL (Interactive Data Language) program SYNPLOT developed by I. Hubeny. SYNPLOT is an interactive program that calculates and plots synthetic spectra using the program SYNSPEC. We can then overplot the observed spectrum and compare it to the model. If the model does not reproduce the observation, we can change the abundance and repeat the operation until the fit is acceptable, i.e., the comparison between the model and the observation is satisfactory. This is what we call fitting a spectrum by eye. The main difficulty encountered when fitting spectra with this method is the placement of the continuumm. For instance, Pereira et al. (2006) showed that LTE hydrogen-rich synthetic spectra computed in the *FUSE* band yielded continuum above the observed continuum. In their calculations they used T_{eff} and $\log g$ from a Balmer line analysis and normalized the synthetic spectra to the y magnitude. Their results indicate that the placement of the continuum may be one of the main sources of systematic error. When fitting a small portion of the spectrum we have a tendency to put the continuum close to what we believe is the real continuum. The study of Pereira et al. (2006) shows, however, that the continuum may be well above the one that we set for determining the abundances. Consequently, we may underestimate the abundances when fitting spectra that contain numerous absorption lines.

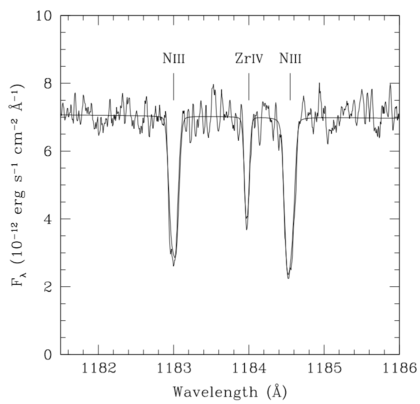

Fig. 3. *FUSE* spectrum of Feige 87 showing the Zr IV 1184 Å and N III 1183 and 1184 Å lines and our best fit.

In order to measure the zirconium abundance, we estimated the oscillator strength of the Zr IV 1184 Å line empirically, because no oscillator strength was available from the literature. We measured the Zr abundance in the atmosphere of the sdB star Feige 48 by using its ultraviolet spectrum obtained by the Space Telescope Imaging Spectrograph onboard HST (O'Toole et al. 2004). We analyzed the Zr III lines at 1790.113 Å, 1793.523 Å and 1798.048 Å and measured an abundance of $\log N(\mathrm{Zr})/N(\mathrm{H}) = -8.0$. Keeping this abundance constant, we fitted the Zr IV 1184 Å line observed in the *FUSE* spectrum by maximizing the oscillator strength gf in order to obtain the best fit for this line. This best gf value is given in Table 1. Because the Zr IV 1012 Å line is blended with the S III resonance line at 1012.498 Å, we only used the Zr IV 1184 Å line to estimate the Zr abundance. Figure 3 illustrates the best fit of the Zr IV 1184 Å and N III 1184 Å lines for the star Feige 87.

4. RESULTS

Table 2 summarizes the abundances for Ge, Zr and Pb observed in the atmospheres of our program stars. The first column is the name of the star. The second and third columns give the effective temperature in ascending order and the gravity, respectively. Columns 4, 6 and 8 are the measured abundances or upper limits ($\log[N(\mathrm{X})/N(\mathrm{H})]_\star$: $\star$ symbol). Columns 5, 7, and 9 are the observed abundances reported relative to the abundances in the Sun ($\log[N(\mathrm{X})/N(\mathrm{H})]_\star - \log[N(\mathrm{X})/N(\mathrm{H})]_\odot$: $\star - \odot$ symbol). The Ge, Zr and Pb abundances in the atmosphere of the Sun are −8.42, −9.41 and −10.00, respectively. They are taken from the review of Asplund et al. (2005). We estimate that the uncertainties (statistical and systematic) associated with the measured abundances vary from 0.1 dex to 0.3 dex. Table 2 shows that Ge, Zr and Pb are present in the atmospheres of almost all sdB stars. Although the average abundances relative to hydrogen are about the same for these three elements with a value of about $\log[N(\mathrm{X})/N(\mathrm{H})] \simeq -7.8$ and a dispersion of about 1.0 dex, the Ge, Zr and Pb abundances relative to the solar abundances are 0.62, 1.61 and 2.20 dex, respectively. The difference in the abundances relative to solar is due to the fact that

$$\log[N(\mathrm{Pb})/N(\mathrm{H})]_\odot < \log[N(\mathrm{Zr})/N(\mathrm{H})]_\odot < \log[N(\mathrm{Ge})/N(\mathrm{H})]_\odot. \tag{1}$$

Figure 4 illustrates the Ge, Zr and Pb abundances by number relative to hydrogen as a function of effective temperature. Filled circles and downward-pointing arrows correspond to abundances and upper limits. The horizontal dotted line in each panel is the solar abundance according to Asplund et al. (2005). The figure

Table 2. Abundance of Ge, Zr and Pb in the atmospheres of sdB stars compared to the Sun

Star	$T_{\rm eff}$	$\log g$	Ge		Zr		Pb	
	(10^3 K)	(cm s^{-2})	$\star$	$\star - \odot$	$\star$	$\star - \odot$	$\star$	$\star - \odot$
HD 4539	23.9	5.2	−7.7	0.7	−7.7	1.7	−8.1	1.9
JL 36	24.5	5.6	−7.8	0.6	−8.0	1.4	−7.7	2.3
HD 205805	25.6	5.3	−8.0	0.4	−7.4	2.0	−8.7	1.3
LB 1516	26.1	5.4	−8.0	0.4	−8.0	1.4	−8.7	1.3
Feige 48	29.6	5.5	−8.0	0.4	−8.0	1.4	−8.5	1.5
Feige 87	29.9	5.4	−10.3	−1.9	−8.4	1.0	−7.3	2.7
JL 236	29.9	5.7	−7.6	0.8	−7.5	1.9	−8.1	1.9
PG 0823+465	29.9	5.8	−9.0	−0.6	−7.4	2.0	<−9.0	<1.0
PG 1710+490	30.3	5.7	−7.9	0.5	−7.1	2.3	<−9.5	<0.5
PG 1206+165	30.5	5.6	−9.3	−0.9	−9.3	0.1	−6.7	3.3
PG 1610+529	31.0	5.8	−7.6	0.8	−7.1	2.3	−7.7	2.3
PG 1032+406	31.3	5.9	−6.7	1.7	−7.3	2.1	−7.1	2.9
Feige 91	31.3	6.0	−6.5	1.9	−7.3	2.1	−7.0	3.0
KPD2109+4401	31.4	5.6	−7.5	0.9	<−9.0	<0.4	−7.3	2.7
PG 1619+522	33.0	5.8	−6.7	1.7	−7.3	2.1	−7.2	2.8
PG 1538+401	33.5	5.9	−8.0	0.5	−8.8	0.6	−9.0	1.0
PG 1219+534	33.6	5.8	−6.6	1.8	−8.3	1.1	−7.0	3.0
PG 1255+547	33.9	5.8	−6.4	2.0	−7.1	2.3	−6.8	3.2

shows that the abundances are higher than the solar abundances in almost every star, and that these overabundances can reach 3 orders of magnitude in a few cases. The analysis of several stars provides the opportunity to uncover some trends in the abundance patterns. Can we observe such trends with the data that we have in hand? There may be a slight increase in the abundance as the temperature increases. The large scatter of the abundances, however, is really the most striking result. For instance, stars with $T_{\rm eff} \geq 29\,500$ K show a scatter of the abundances on a scale of 2 to 3 orders of magnitude for the three elements.

Three stars in our sample are EC 14026 pulsators: Feige 48, KPD 2109+4401 and PG 1219+534. The Ge, Zr and Pb abundances in Feige 48 are about the same and are close to the cooler stars. KPD 2109+4401 and PG 1219+534 display the same abundance pattern. Although they show relatively high Ge and Pb abundances, their Zr abundance is much lower. By comparison with other stars in general, the pulsators do not show any abundance enhancement. Two stars in our sample are out of the ordinary: Feige 87 and PG 1206+165. The two stars show low Ge and Zr abundances but high Pb abundance. Moreover, their *FUSE* spectra show very low abundances of iron peak elements, although their C, N and O abundances are relatively high. The hot PG1538+401 star is another interesting object. Its Ge, Zr and Pb abundances are systematically lower than the other hot stars.

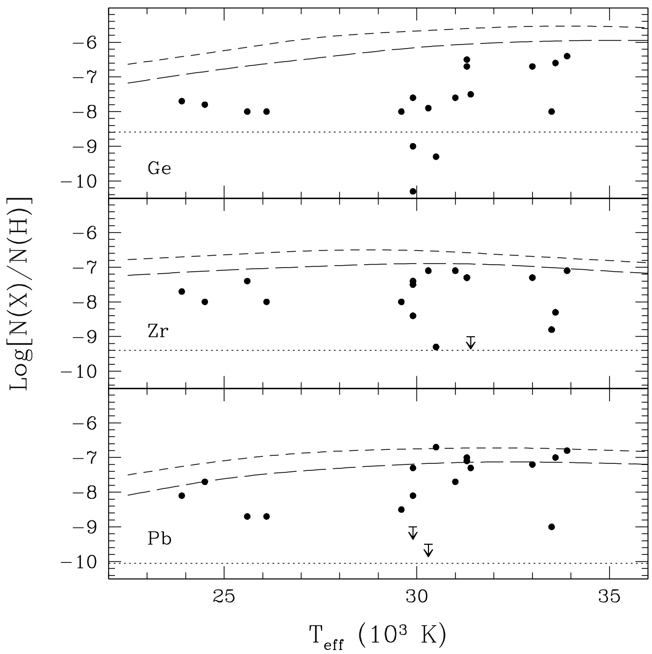

Fig. 4. Ge, Zr and Pb abundances (*filled circles*) and upper limits (*downward-pointing arrows*) observed in the *FUSE* spectra of sdB stars. The dotted line in each panel is the solar abundance according to Asplund et al. (2005). The dashed and long-dashed lines are predicted abundances computed within the framework of the radiative levitation theory according to Michaud et al. (1976) for models with $\log g = 5.5$ and 6.0, respectively.

5. RADIATIVE LEVITATION

In order to confirm the role of the radiative levitation for maintaining traces of heavy elements, we carried out radiative levitation calculations on Ge, Zr and Pb. Figure 4 illustrates radiative equilibrium abundances computed at $\tau_{\rm R} = \frac{2}{3}$ for models with $\log g = 5.5$ (dashed lines) and 6.0 (long-dashed lines). Because of lack of atomic data for Ge, Zr and Pb, we used the approximate method developed by Michaud et al. (1976) to compute the equilibrium abundances illustrated in Figure 4. Bergeron et al. (1988) showed that the approach of Michaud et al. (1976) yields good agreement with more detailed radiative levitation calculations carried out in sdB models for C, N and Si. Bergeron et al. (1988) added that this approximate formalism overestimates the radiative acceleration by no more than a factor of ~ 3 in the line-forming regions, and concluded that this method could be applied to other elements. Following the findings of Bergeron et al. (1988) and in order to better match the observed abundances, we reduced the radiative acceleration on Ge, Zr and Pb by a factor of 3. Figure 4 shows that the radiative levitation provides more than enough support for our elements of interest.

The predicted abundances are in general greater than the observed abundances. In a few cases the predictions are consistent with the observations. It is difficult to explain, however, the large scatter of the observed abundances. For instance, stars with $T_{\rm eff} \geq 29\,500$ K show abundances that vary over two to three orders of magnitude. According to the parameter-free diffusion model, which consists of a strict equilibrium between the gravitational and radiative accelerations, stars with similar atmospheric parameters should show similar abundances. The large scatter of the abundances for $T_{\rm eff} \geq 29\,500$ K cannot be interpreted only in terms of the atmospheric parameters.

6. DISCUSSION AND CONCLUSION

A weak stellar wind at the surface of sdB stars is one of the mechanisms that was proposed for opposing gravitational settling and at the same time affecting the equilibrium abundances predicted by the radiative levitation. Although the proposed mass loss rates are too low to be detected directly, their effect on the surface abundances may be quite important. Michaud et al. (1985) and Bergeron et al. (1988) put forward the wind hypothesis to explain the Si underabundance observed in a handful of sdB stars. Bergeron et al. (1988) demonstrated that detailed radiative levitation calculations predicted large Si abundances, even though observations showed that Si was underabundant as much as five orders of magnitude in stars with $T_{\rm eff} \geq 27\,000$ K. Michaud et al. (1985) suggested that an outward velocity field produced by a weak stellar wind could decrease the Si abundance at the surface of a sdB star.

By trying to explain the He underabundance in sdB stars, Michaud et al. (1989) demonstrated that the radiative forces were in fact too small to support the observed He abundance. This result prompted Fontaine & Chayer (1997) and Unglaub & Bues (1998) to compute time dependent diffusion calculations that included mass loss. Both groups showed that mass loss rates of the order of 10^{-13} to 10^{-14} $\mathrm{M}_\odot\,\mathrm{yr}^{-1}$ could maintain He abundances similar to those observed in the atmospheres of sdB stars. The wind hypothesis was also assumed by Chayer et al. (2004) to explain the presence of EC 14026 pulsators and non-pulsators in the empirical instability region. Chayer et al. (2004) showed that weak stellar winds could disrupt the Fe reservoir, which is responsible for driving the pulsations in EC 14026 stars, and explain why a star pulsates while another does not.

All the diffusion calculations that we have just reviewed involve weak stellar winds that assume an outward velocity that is provided by the continuity equation. This velocity depends on the mass loss rate, the density of matter, and the position where the velocity is calculated. This means that at a given radius all elements have the same outward velocity. This velocity is low in the deeper layers of the atmosphere, and is large in the upper layers. O'Toole (2004) proposed that this velocity could be different for elements with different atomic mass. He suggested that a fractionated wind could explain the Si underabundance and the presence of Ge, Sn and Pb in the atmospheres of sdB stars. O'Toole (2004) argued that Si, Ge, Sn and Pb should have similar susceptibility to absorb radiative momentum given that they occupy the same column of the periodic table and should have in principle similar atomic properties. He added that the atomic mass should be the parameter that could be involved in the separation of the elements in the wind. Consequently, a light element such as Si could be removed preferentially from the atmospheres of sdB stars in a fractionated stellar wind, while the heavier elements Ge, Sn and Pb should lag behind.

This interesting hypothesis can be tested by comparing the abundances of Si, Ge, Sn and Pb in a sample of stars with atmospheric parameters that cover the whole range of possible values for sdB stars. The present study is the first step in this direction. The *FUSE* observations provide the spectral window to identify not only Ge and Pb, but also Si. We are in the process of completing the Si abundance analysis and hope to test the hypothesis of the fractionated wind put forward by O'Toole (2004).

ACKNOWLEDGMENTS. P.C. is supported by CSA under a PWGSC contract. G.F. acknowledges the contribution of the Canada Research Chair Program. This work was supported in part by NASA grant NAG510647.

REFERENCES

Allard F. 1986, Master Thesis, Univ. Montréal

Asplund M., Grevesse N., Sauval A. J. 2005, in *Cosmic Abundances as Records of Stellar Evolution and Nucleosynthesis*, eds. F. N. Bash & T. G. Barnes, ASP Conf. Ser., in press (astro-ph/0410214)

Bergeron P., Wesemael F., Michaud G., Fontaine G. 1988, ApJ, 332, 964

Blanchette J. P. et al. 2006, Baltic Astronomy, 15, ... (these proceedings)

Chayer P. et al. 2004, Ap&SS, 291, 359

Edelmann H. 2003, Ph.D. Thesis Universität Erlangen-Nürnberg

Fontaine G., Chayer P. 1997, in *Third Conf. on Faint Blue Stars*, eds. A. G. D. Philip, J. Liebert & R. Saffer, Schenectady, L. Davis Press, p. 169

Heber U., Moehler S., Napiwotzki R., Thejll P., Green E. M. 2002, A&A, 383, 938

Hubeny I., Lanz T. 1995, ApJ, 439, 875

Kilkenny D., Heber U., Drilling J. S. 1987, in *Second Conf. on Faint Blue Stars*, IAU Colloq. 95, eds. A. G. D. Philip, D. S. Hayes & J. W. Liebert, L. Davis Press, p. 731

Kurucz R. L. 1993, CD-ROM 13, ATLAS9 Stellar Atmospheres Program and 2 km/s Grid, SAO, Cambridge

Michaud G., Bergeron P., Heber U., Wesemael F. 1989, ApJ, 338, 417

Michaud G., Bergeron P., Wesemael F., Fontaine G. 1985, ApJ, 299, 741

Michaud G., Charland Y., Vauclair S., Vauclair G. 1976, ApJ, 210, 447

Pereira C., Wesemael F., Bergeron P. 2006, Baltic Astronomy, 15, ... (these proceedings)

Proffitt C. R., Sansonetti C. J., Reader J. 2001, ApJ, 557, 320

Saffer R. A., Bergeron P., Koester D., Liebert J. 1994, ApJ, 432, 351

O'Toole S. J. 2004, A&A, 423, L25

O'Toole S. J., Heber U., Chayer P., Fontaine G., O'Donoghue D., Charpinet S. 2004, Ap&SS, 291, 427

Unglaub K., Bues I. 1998, A&A, 338, 75

Baltic Astronomy, vol. 15, 139–145, 2006.

CHEMICAL ABUNDANCES OF HELIUM-RICH SUBDWARF B STARS

A. Ahmad and C. S. Jeffery
Armagh Observatory, College Hill, Armagh BT61 9DG, U.K.

Received 2005 August 17

Abstract. Helium-rich subdwarf B (He-sdB) stars represent a small fraction of the population of hot subdwarfs. We report recent results of our spectral analysis of He-sdB stars including surface chemical abundance measurements of a bright He-sdB star – JL 87 – measured from its high-resolution optical spectrum using line-blanketed LTE model atmospheres. These measurements provide further insight into the formation mechanism(s) of these rare faint blue stars.

Key words: stars: chemically peculiar – stars: early-type - subdwarfs – stars: fundamental parameters – stars: abundances

1. INTRODUCTION

A very small fraction ($\leq 5\%$) of the subdwarf population comprises the so called helium-rich subdwarf B (He-sdB) stars. These are "cooler" subdwarfs with strong neutral helium lines in their optical spectrum. They are found in the field of our Galaxy (Green et al. 1986) and also in some globular clusters (Moehler et al. 1997, 2002, 2004).

He-sdB stars were originally identified as sdOD in the Palomar Green survey (Green et al. 1986) as subdwarfs showing strong He I lines plus weak He II lines but with no detectable hydrogen Balmer lines. From this spectral definition one would expect all sdOD stars to be extremely helium-rich and cooler than sdO stars. However, this is not the case as our spectral analysis (Ahmad & Jeffery 2003) showed that He-sdB stars exhibit a wide range in helium abundance and temperatures similar to both sdB and sdO stars.

Since "helium-rich" can be interpreted differently by different authors, it is vital that the label "He-sdB" is used homogeneously. The new MK-type classification scheme being developed by Drilling et al. (2000) would address this issue. For now we would use the He-sdB label for all subdwarfs that have previously been identified as such by other authors.

Two evolutionary models have been proposed for the formation of these He-sdB stars. The first, by Iben & Tutukov (1986), involves the merger of two white dwarfs (WD) to form a He-sdB star. The second, by Lanz et al. (2004), involves convective flash mixing of the atmosphere of a star on the white dwarf cooling track which has previously undergone high mass-loss.

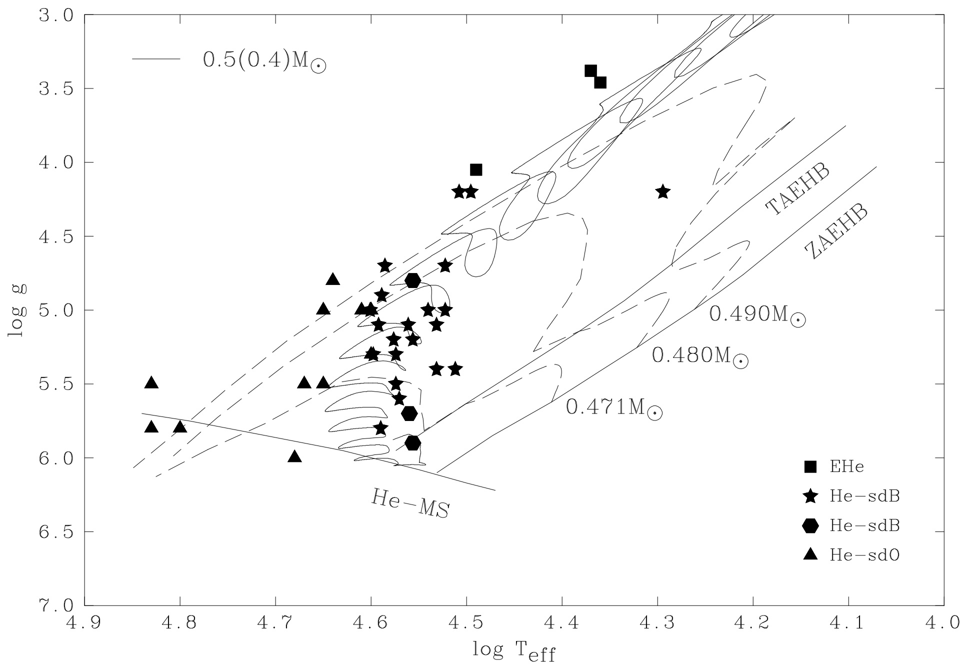

Fig. 1. Helium-rich stars on the $T_{\rm eff}$ vs. $\log g$ diagram plotted with evolutionary tracks. He-sdB stars from this study are plotted using the filled star symbol. He-sdB stars found in globular clusters (Moehler et al. 1997, 2002, 2004) are plotted with filled hexagonal symbol. Single star evolutionary tracks (dashed lines) are taken from Dorman et al. (1993) and merged He+He WD tracks (solid lines) are taken from Saio & Jeffery (2000). Adapted from Ahmad (2004).

Our aim is to establish whether either or both these models fit the observed properties of He-sdB stars. In this paper, we present physical parameters of additional He-sdB stars, new observations of the double-lined spectroscopic binary PG 1544+488, discuss preliminary abundance measurements of a He-sdB star JL 87, and discuss their possible evolution.

2. PHYSICAL PARAMETERS

In order to understand the evolution of He-sdB stars our first study involved determining the position of these stars on the $T_{\rm eff}$ vs. $\log g$ diagram. We measured atmospheric physical parameters of 22 He-sdB stars using LTE model atmospheres and the χ^2 fitting program SFIT2 (cf. Ahmad & Jeffery 2003) and plotted them on the $T_{\rm eff}$ vs. $\log g$ plane (Figure 1). In general, the effective temperatures ($T_{\rm eff}$) of He-sdB stars lie in the range 30 000–40 000 K, surface gravities ($\log g$) in the range 4.5–6.0 and helium abundance (by number, $n_{\rm He}$) in the range 0.10–0.99. Ten additional He-sdB stars appear to be hotter than 40 000 K. Since NLTE effects become increasingly important at such high temperature, these stars were not analyzed.

We have also divided our sample of He-sdB stars into carbon-rich and carbon-poor. Carbon-rich He-sdB stars show strong C II/III lines in their optical spectra and C III/IV lines in their ultraviolet (UV) spectra. It is likely that these two groups are produced by different evolutionary channels. To get some estimate of the carbon abundance in carbon-rich He-sdB stars we calculated a number of models with different carbon abundances and tried to match the strength of the carbon lines in the UV spectra. Preliminary results suggest that $n_{\mathrm{C}} \leq 0.01$ in carbon-rich He-sdB stars.

3. ABUNDANCES

The surface chemical abundances of a star provides further clues about its prior evolution. In our next study we carried out high-resolution spectroscopy of He-sdB stars to measure these abundances. Two bright ($V \sim 12$) He-sdB stars – PG 1544+488 and JL 87 – were selected for this study.

3.1. PG 1544+488

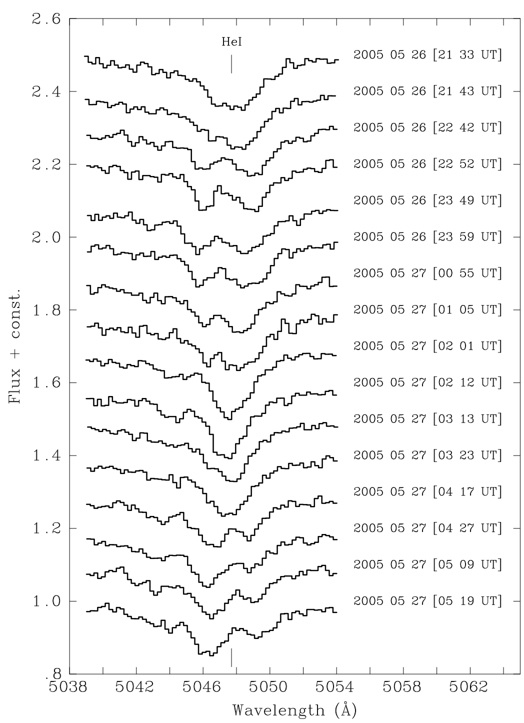

Fig. 2. One night's data from the 2005 WHT run of PG 1544+488 showing line profile variations in the He I 5047 Å absorption line.

We obtained optical blue spectra of the prototype PG 1544+488 with the William Herschel Telescope (WHT) in 2003 April. In total, seven spectra were obtained over two consecutive nights. While carrying out the spectral analysis we noticed that some of the neutral helium line profiles had an unusual shape seen here in Figure 2. On closer examination it became evident that this was due to line-doubling. It was suspected to be due to binarity. However to confirm this hypothesis, more data were required.

Coincidentally, PG 1544+488 had been observed twice with the Far Ultraviolet Spectroscopic Explorer (FUSE) satellite (PI: T.M. Brown) in 2002. At first, it was observed in 2002 March but since one of the detectors on FUSE failed during the observations it was re-observed in 2002 July. The FUSE observations were made in the timetag (TTAG) mode. In this mode, both the position and time of each photon event on the detector is recorded and therefore it was possible to re-extract the archival data and split them into short time-resolved spectra (∼900 s).

We then measured radial velocities from the WHT and FUSE spectra (for details, see Ahmad et al. 2004). The FUSE data showed similar velocity variations as the optical WHT data. We then combined the radial velocities from the FUSE spectra with those obtained from the WHT spectra and solved for the orbit. From the orbital solution we were able to demonstrate that PG 1544+488 is a short period binary with a period of ∼0.48 day, comprising two helium-rich hot subdwarfs and likely to be a product of close-binary evolution (cf. Ahmad et al. 2004). Some recent observations of PG 1544+88 from the 2005 WHT run are shown in Fig. 2.

No abundances could be measured for PG 1544+488 as line-doubling makes it impossible to measure the equivalent widths of the spectral lines. However in future, with better data it might be possible to deconvolve the spectra of the two components of the binary and measure their individual chemical abundances.

3.2. JL 87

A high-resolution optical spectrum of JL 87 was obtained at the Anglo-Australian Telescope (AAT) with the University College London Echelle Spectrograph (UCLES) in 1996. The spectrum was reduced using standard IRAF routines. Physical parameters of the star were measured from the optical spectrum using SFIT2 as described in section 2, and indicates that $T_{\rm eff} = 24\,000$ K and $\log g = 4.5$. Lanz et al. (2004) have measured $T_{\rm eff} = 29\,000$ K and $\log g = 5.5$ for JL 87 using far-ultraviolet spectrum of the star obtained with FUSE and NLTE model atmospheres. There is significant disagreement between the atmospheric parameters derived from the optical and far-ultraviolet spectra which cannot just be accounted for by NLTE effects.

Using our derived physical parameters, we measured the atmospheric chemical abundance listed in Table 1. There is some agreement between our preliminary measurement of hydrogen, helium and nitrogen abundances with those of Lanz et al. (2004).

There is a significant amount of hydrogen in the atmosphere of JL 87 ($n_{\rm H} \sim 0.80$). This is also evident from the strong hydrogen Balmer lines in the optical spectrum (Figure 3). Such a high hydrogen abundance is not typical for most He-sdB stars ($n_{\rm H} \leq 0.10$). Nitrogen is enriched while oxygen is depleted in JL 87 suggesting CNO processing. However carbon, which is destroyed in CNO cycle, is also enriched. The metal lines in the optical spectrum are quite sharp and can be reproduced with $v \sin i \leq 5\,{\rm km\,s^{-1}}$.

Table 1. Chemical abundances in JL 87 in mass fraction compared to Lanz el al. (2004) – L04 and solar values.

Element	this work	L04	Sun
H	0.5636	0.56 – 0.77	0.7054
He	0.4198	0.43 – 0.28	0.2758
C	0.0056	0.0140	0.0031
N	0.0031	0.0040	0.0011
O	0.0023	–	0.0096
Si	0.0003	0.0007	0.0007
S	0.0001	–	0.0004
Fe	0.0024	0.0013	0.0012

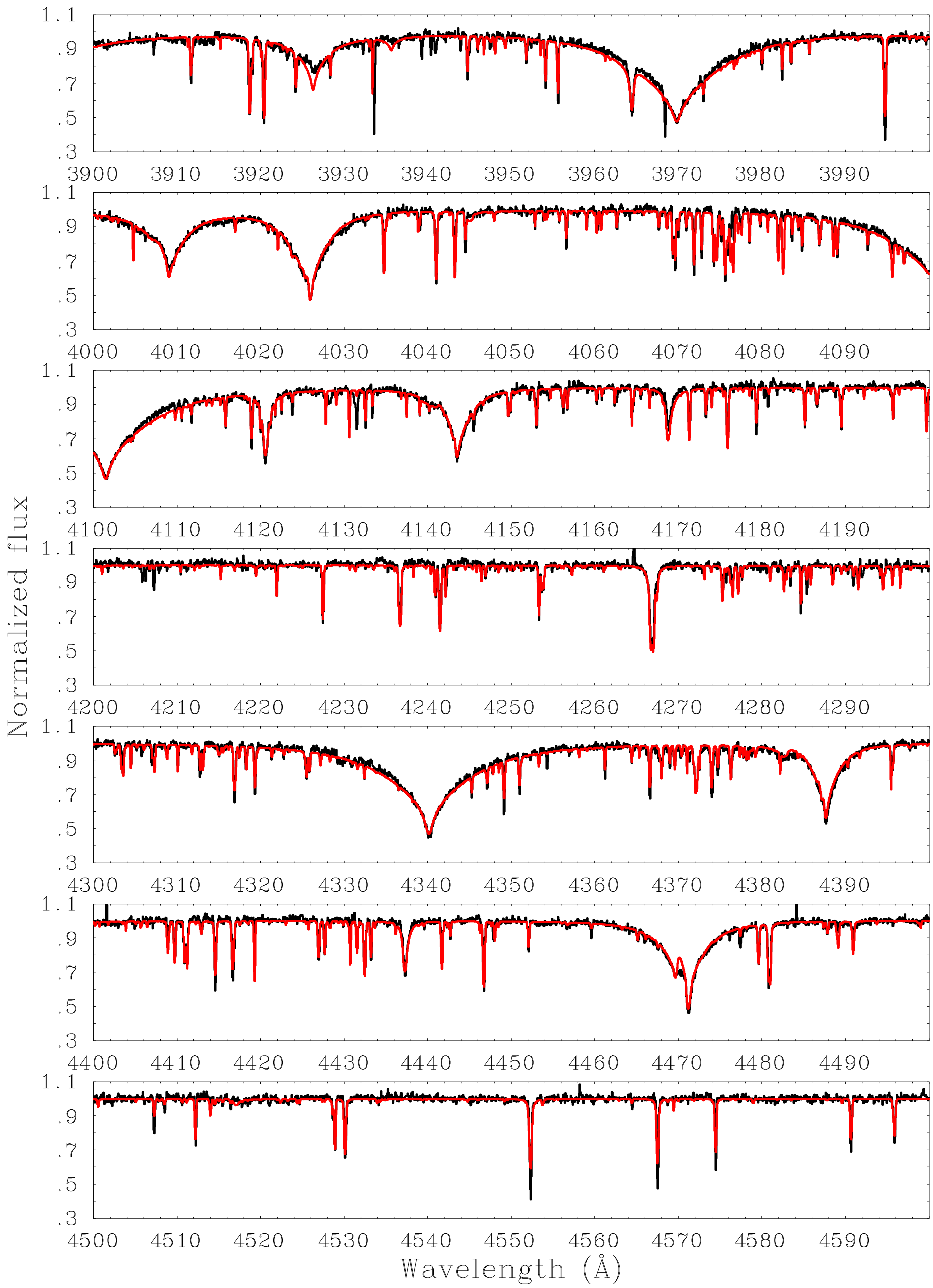

Fig. 3. A section (3900–4600 Å) of the high-resolution optical spectrum (3900–5000 Å) of JL 87 (dark line) along with best fit model.

It seems unlikely that JL 87 is the product of a white dwarf merger in which any remaining hydrogen is converted to helium resulting in an extremely helium-rich surface. It has been suggested that JL 87 is a product of shallow mixing (Lanz et al. 2004) as it can satisfactorily explain the surface abundances. However, our surface gravity measurement indicates that the star is too luminous to have been flash mixed. The atmospheric parameters and helium abundance of JL 87 are similar to those of chemically peculiar massive helium-rich stars known as intermediate helium stars (e.g., Zboril & North 1999). However, carbon is underabundant in these stars.

4. EVOLUTION

4.1. Late flash mixing model

It has been proposed by Lanz et al. (2004) that stars evolving with high mass-loss on the red giant branch undergo a late helium core flash on the white dwarf cooling track, leading to convective "flash mixing" of the envelope which then forms a helium and carbon rich hot subdwarf. All hot subdwarfs produced by this channel show carbon enrichment. Their recent analysis of the FUSE spectra of two He-sdB stars provide support for this evolutionary scenario.

4.2. Binary merger model

Iben & Tutukov (1986) on the other hand have suggested that the merger of two white dwarfs (WD) can produce a hot subdwarf with a depleted hydrogen atmosphere. More recently this has been modeled by Saio & Jeffery (2000) to explain the origin of extreme helium (EHe) stars. Some of these EHe stars are thought to evolve into He-sdB stars. The binary merger model can explain both carbon-rich and carbon-poor He-sdB stars. A merger of two helium WDs can produce a carbon-poor He-sdB star. A low-mass CO+He WD merger might produce a star which resembles a carbon-rich He-sdB during its evolution to the WD track. The analysis presented in section 2 (Ahmad & Jeffery 2003) and Fig. 1 lends general support to the white dwarf merger model for the formation of He-sdB stars.

4.3. Binary evolution

Both the existing evolutionary models for He-sdB stars assume a "single" star. The discovery that the prototype PG 1544+488 is a binary containing *two* He-sdB stars poses a challenge for both models. It is therefore likely that a close-binary evolution channel might be responsible for the formation of some He-sdB stars (see discussion in Ahmad et al. 2004).

4.4. Wind and magnetic field

None of the models discussed above satisfactorily accounts for all the observed parameters of JL 87. However, the observed properties of JL 87 are very similar to those of intermediate helium stars. These are massive young stars with stellar winds and magnetic fields. In normal B-type star atmospheres (assuming no wind), diffusion cannot lead to helium enrichment. However, it was shown by Vauclair (1975) that in the presence of stellar winds, diffusion can lead to helium overabundance. The intermediate helium stars normally show typical CNO abundances. However, peculiar CNO abundances patterns can also be produced depending on several parameters like magnetic field configuration and effective temperature. It is therefore possible that luminous He-sdB stars showing some helium enrichment like JL 87 are in fact intermediate helium stars.

5. SUMMARY

Spectral analysis of He-sdB stars shows that they are a very inhomogeneous group of hot subdwarfs. A fraction of these stars are misclassified (or cool) He-sdO stars. Their evolution is still under much debate. We have discovered that the prototype, PG 1544+488, is a short-period binary containing two low-mass hot helium subdwarfs which demonstrates that close binary evolution also plays an important role in their formation. The observed atmospheric parameters and abundances in JL 87 are similar to those of intermediate helium stars which are chemically peculiar massive young stars.

REFERENCES

Ahmad A., Jeffery C. S. 2003, A&A, 402, 335

Ahmad A., Jeffery C. S., Fullerton A. W. 2004, A&A, 418, 275

Ahmad A. 2004, Ph.D. thesis, Queens University, Belfast

Dorman B., Rood R. T., O'Connell R. W. 1993, ApJ, 419, 596

Drilling J. S., Moehler S., Jeffery C. S., Heber U., Napiwotzki R. 2000, in *The Kth Reunion*, ed. A. G. Davis Philip, p. 49

Green R. F., Schmidt M., Liebert J. 1986, ApJS, 61, 304

Iben I. J., Tutukov A. V. 1986, ApJ, 311, 742

Lanz T., Brown T. M., Sweigart A. V., Hubeny I., Landsman, W. B. 2004, ApJ, 602, 342

Moehler S., Heber U., Durrell P. R. 1997, A&A, 317, L83

Moehler S., Sweigart A. V., Landsman W. B., Dreizler S. 2002, A&A, 395, 37

Moehler S., Sweigart A. V., Landsman W. B., Hammer N. J. Dreizler S. 2004, A&A, 415, 313

Saio H., Jeffery C. S. 2000, MNRAS, 313, 671

Vauclair S. 1975, A&A, 45, 233

Zboril M., North P. 1999, A&A, 345, 244

Baltic Astronomy, vol. 15, 147–150, 2006.

MULTICOMPONENT WINDS IN SDB STARS?

K. Unglaub
Remeis Sternwarte Bamberg, Sternwartstrasse 7, D-96049 Bamberg, Germany

Received 2005 April 1

Abstract. In previous diffusion calculations with mass-loss a steady outflow of all elements has been assumed. However, the existence of a chemically homogeneous wind requires an efficient momentum transfer via Coulomb interactions from the heavy elements to hydrogen and helium. For the example $T_{\rm eff} = 35\,000$ K and $\log g = 6.0$ it will be shown that hydrogen and helium would fall back onto the star if the mass-loss rate is below about $10^{-12} M_\odot$/yr. This effect may change the predicted surface compositions.

Key words: stars: hot subdwarfs – stars: mass-loss – stars: winds, outflow – stars: diffusion

1. INTRODUCTION

In previous papers (Unglaub & Bues 2001 and Unglaub 2005) it has been shown that the effects of diffusion and weak winds with mass-loss rates $\dot{M} \approx 10^{-13} M_\odot$/yr may explain the helium abundances in sdB stars with number fractions H/He between about solar and 10^{-4}. However, the abundance anomalies of heavy elements can hardly be explained simultaneously, at least if a solar initial composition is assumed. In contrast to many observational results helium should always be more deficient than each of the elements C, N and O. A possible reason for this discrepancy may be the decoupling of metals on the one hand and H+He on the other hand in the wind region. This may happen if the momentum redistribution via Coulomb interactions between H, He and the metals is not sufficiently effective.

Vink & Cassisi (2002) calculated mass-loss rates for sdB stars with the assumption of a fixed velocity law. For "luminous" sdB stars with $5.0 \le \log g \le 5.5$ they obtain $10^{-11} M_\odot/\mathrm{yr} \le \dot{M} \le 10^{-10} M_\odot$/yr for solar composition and, for example, $\dot{M} \approx 10^{-12} M_\odot$/yr for $T_{\rm eff} = 35\,000$ K and $\log g = 6.0$. Our own hydrodynamical calculations, which will be published elsewhere (A&A, in preparation), are in good agreement with these results (within a factor of two). For the "compact" sdB stars with $\log g > 5.5$, however, $\dot{M}$ may be clearly lower especially if the CNO elements are deficient.

Possible wind signatures (Hα lines with a central line emission) have been detected by Heber et al. (2003) in four of the more luminous sdB stars. The spectral synthesis of Hα by Vink (2004) with $\dot{M} \approx 10^{-11} M_\odot$/yr showed a similar behavior of the line core. Insofar theoretical predictions seem to be in agreement with observational results. In the present paper, for the example $T_{\rm eff} = 35\,000$ K, $\log g = 6.0$ and a stellar mass $M_\star = 0.5 M_\odot$ it will be investigated for which mass-loss rates a one component wind solution may be consistent.

2. METHOD OF ANALYSIS

In the following the elements H and He, for which the radiative acceleration is assumed to be zero, will be denoted as "element" 1, whereas the metals are denoted as "element" 2. As in the supersonic region the gradient of the gas pressure can be neglected, the momentum equation for "element" 1 (H+He) reads:

$$g_{\mathrm{coll}} = g_{(r)} + v_1 \frac{dv_1}{dr} \ , \tag{1}$$

g_{coll} is the collisional acceleration on H and He due to Coulomb interactions with the metals and $g_{(r)}$ is the gravitational acceleration as a function of radius. The existence of a supersonic wind with increasing velocity in outward direction requires that the acceleration term $v_1 dv_1/dr$ is larger than zero. Thus this equation can only be valid if:

$$g_{\mathrm{coll}} > g_{(r)}. \tag{2}$$

H and He cannot be accelerated if this condition is violated. Then the assumption of a steady outflow of all elements is inconsistent. As derived by Burgers (1969) g_{coll} can be written as:

$$g_{\mathrm{coll}} = \frac{\rho_2}{m_1 m_2} \frac{4\pi q_1^2 q_2^2}{kT} (\ln \Lambda)\, G_{(x)} \ , \tag{3}$$

m_1 and m_2 are the mean masses of "elements" 1 and 2, respectively, and $\ln \Lambda = -1/2 + \ln\left(3kTR_{\mathrm{D}}/\left(q_1 q_2\right)\right)$, where R_{D} is the Debye radius. From Eq. (3) it can be seen that (apart from the weak dependence via $\ln \Lambda$) g_{coll} is proportional to the squares of the mean charges q_1 and q_2 of both "elements" and to the inverse of the temperature T. As g_{coll} is proportional to the density ρ_2 of the metals, it decreases if the metal abundances in the wind region are reduced.

In order to accelerate H and He via collisions with the heavy elements, the mean velocity in radial direction of the metals must be larger than the one for H and He. If this velocity difference is denoted with Δv, then x is defined as

$$x = \frac{\Delta v}{\alpha}, \tag{4}$$

where $\alpha = \sqrt{2kT/\mu}$ if μ is the reduced mass of both "elements". For $T = 35\,000$ K it is $\alpha = 22$ km/s. The Chandrasekhar function $G_{(x)}$ is defined as in Krtička et al. (2003) and as it is plotted, e.g., in Krtička & Kubát (2005). The important point is that $G_{(x)}$ increases with x for $x < 1$, reaches a maximum value for $x \approx 1$ and decreases for $x > 1$. Thus for given temperature, mean charges of the elements and density of the metals, g_{coll} cannot exceed some maximum value. If this maximum value is smaller than the gravitational acceleration, no velocity difference exists for which condition (2) is fulfilled.

The density of the metals ("element" 2) as a function of radius and velocity can be obtained from the equation of continuity $\eta_2 \dot{M} = 4\pi r^2 \rho_2 v_2$ where η_2 is the mass fraction of the metals. From this equation ρ_2 can be inserted into Eq. (3) so that

$$g_{\mathrm{coll}} = \frac{1}{m_1 m_2} \frac{\eta_2 \dot{M}}{4\pi r^2 v_2} \frac{4\pi q_1^2 q_2^2}{kT} (\ln \Lambda)\, G_{(x)} \tag{5}$$

As both $g_{\rm coll}$ and $g_{(r)}$ scale with r^{-2}, we calculate $g_{\rm coll}$ for $r = R_\star$ and compare this with the surface gravity of the star. For the velocity of the metals $v_2 = 1000$ km/s is assumed, which is of the same order of magnitude as the surface escape velocity of 1260 km/s. If with these values condition (2) is violated for all values of x, H and He decouple from the metals before the wind is accelerated to the surface escape velocity.

3. RESULTS

The collisional acceleration on H and He is calculated for solar abundances of the metals (represented by the CNO elements). So we obtain mean masses $m_1 = 2.13 \times 10^{-24}$ g for H and He and $m_2 = 2.44 \times 10^{-23}$ g for the heavy elements. The mass fraction of the metals is $\eta_2 = 0.0133$. To maximize $g_{\rm coll}$, the maximum value of $G_{(x)}$ at $x \approx 1$ is inserted, it is $G_{(1)} = 0.214$. The mean charges have been calculated with the LTE assumption for $T = 35\,000$ K and an electron density $n_{\rm e} = 5 \times 10^{14}$ cm^{-3}. We obtain $q_1 = 1.0 q_{\rm p}$ (where $q_{\rm p}$ is the proton charge) for H and He and $q_2 = 2.6 q_{\rm p}$ for the CNO elements. As in the outer parts of the wind region the electron density is much lower, the mean charge of the metals may be larger. Thus the results for $q_2 = 5.0 q_{\rm p}$ are presented in addition.

Table 1. $g_{\rm coll}^{\rm max}$ for several values of mass-loss rates, mean charges $q_2/q_{\rm p}$ ($q_{\rm p}$ = proton charge) of the metals and temperatures.

$\log \dot{M}$ $[M_\odot/{\rm yr}]$	–11.0			–12.0			–13.0		
$q_2/q_{\rm p}$	2.6	5.0	5.0	2.6	5.0	5.0	2.6	5.0	5.0
T [kK]	35	35	350	35	35	350	35	35	350
$\log g_{\rm coll}^{\rm max}$ [cgs]	6.7	7.3	6.4	5.7	6.3	5.4	4.8	5.3	4.4

In Table 1 the maximum values of $g_{\rm coll}$ (denoted with $g_{\rm coll}^{\rm max}$) are given for several mass-loss rates, temperatures and mean charges of the metals. $g_{\rm coll}^{\rm max}$ may be compared with the surface gravity of the star ($\log g = 6.0$).

For $\log \dot{M} = -11.0$ it is $g_{\rm coll}^{\rm max} > g$ in all cases. Thus for this mass-loss rate a steady outflow of all elements may exist.

For $\log \dot{M} = -12.0$ the situation is less clear. For $T = 35\,000$ K and $q_2 = 2.6 q_{\rm p}$ it is $\log g_{\rm coll}^{\rm max} = 5.7$ only. Thus H and He would fall back onto the star so that a one component wind solution is inconsistent. For $q_2 = 5.0 q_{\rm p}$ and the same temperature we obtain $\log g_{\rm coll}^{\rm max} = 6.3$, which is larger than the surface gravity. In this case the elements could be coupled. If, however, frictional heating (due to the velocity difference of the elements) increases the temperature, then the elements could decouple again. For $T = 350$ kK (instead of $T = 35$ kK) it is $\log g_{\rm coll}^{\rm max} = 5.4$ only. Thus for $\log \dot{M} = -12.0$ more detailed calculations are necessary.

Finally, for $\log \dot{M} = -13.0$ in all cases $g_{\rm coll}^{\rm max}$ is lower than $\log g$ by a factor of the order of ten at a distance where the velocity is 1000 km/s. This means that metals decouple from H and He clearly before the wind is accelerated to the surface escape velocity.

4. CONCLUSIONS

For the case $T_{\rm eff} = 35\,000$ K and $\log g = 6.0$ it has been shown that a one component description of winds is clearly inconsistent for a mass-loss rate of the order

$10^{-13} M_\odot$/yr as required from diffusion theory to explain the helium abundances. The Coulomb coupling between H, He and the metals in the supersonic region of the wind is not sufficient to accelerate or at least to levitate H and He. Thus these elements would fall back onto the star. This result is in agreement with the predictions of Krtička & Kubát (2005).

The decoupling of elements in the wind region probably will lead to surface compositions which are different from those predicted with the assumption of chemically homogeneous winds. So it seems to be possible that fractionated winds exist and lead to the large deficiencies of Si in some sdB stars as suggested by O'Toole (2004). Fontaine et al. (2006) suggested that weak winds of the order $10^{-15} M_\odot$/yr are responsible for the coexistence of pulsating and non-pulsating sdB stars with the same stellar parameters. As the actual mass-loss rate in a multicomponent wind is unclear, this may be a viable explanation.

ACKNOWLEDGMENTS. I thank I. Bues for careful reading of the manuscript and for financial support.

REFERENCES

Burgers J. M. 1969, *Flow Equations for Composite Gases*, Academic Press, New York

Fontaine G., Green E. M., Chayer P. et al. 2006, Baltic Astronomy, 15, 211 (these proceedings)

Heber U., Maxted P. F. L., Marsh T. R., Knigge C., Drew J. E. 2003, in *Stellar Atmospheres Modeling*, eds. I. Hubeny, D. Mihalas & K. Werner, ASP Conf. Ser., 288, 251

Krtička J., Owocki S. P., Kubát J., Galloway R. K., Brown J. C. 2003, A&A, 402, 713

Krtička J., Kubát J. 2005, in *14th European Workshop on White Dwarfs*, eds. D. Koester & S. Moehler, ASP Conf. Ser., 334, 337

O'Toole S. 2004, A&A, 423, L25

Unglaub K. 2005, in *14th European Workshop on White Dwarfs*, eds. D. Koester & S. Moehler, ASP Conf. Ser., 334, 297

Unglaub K., Bues I. 2001, A&A, 374, 570

Vink J. S. 2004, in *Extreme Horizontal Branch Stars and Related Objects*, Ap&SS, 291, 239

Vink J. S., Cassisi S. 2002, A&A, 392, 553